

FILE COPY

Circulate _____

File No. 19.30A

**DEVELOPING A COAL QUALITY EXPERT:
COMBUSTION AND FIRESIDE PERFORMANCE
CHARACTERIZATION FACTORS**

TOPICAL REPORT ON COALS FROM
PUBLIC SERVICE OF OKLAHOMA'S
NORTHEASTERN STATION

JULY 1992

PREPARED BY

COMBUSTION ENGINEERING, INC.

WINDSOR, CT 06095

PREPARED FOR

CQ Inc./U.S. DEPARTMENT OF ENERGY

UNDER CONTRACT NUMBER: DE-FC22-90PC89663

ABB
ASEA BROWN BOVERI

DEVELOPING A COAL QUALITY EXPERT: COMBUSTION AND FIRESIDE PERFORMANCE CHARACTERIZATION FACTORS

**TOPICAL REPORT ON COALS FROM
PUBLIC SERVICE OF OKLAHOMA'S
NORTHEASTERN STATION**

Project Manager

Richard W. Borio

Principal Investigator

David E. Thornock

Investigators ABB-CE

Loraine S. Miemiec

Nsakala ya Nsakala

Benjamin R. Pease

Ramesh L. Patel

Investigators EERC-UND

Sean E. Allan

Steve A. Benson

Chris Ziygarlicke

EXECUTIVE SUMMARY

The overall objective of the Coal Quality Expert (CQE) Clean Coal I Program is the development and validation of a comprehensive PC-based expert system for evaluating the impacts of coal quality on total power plant generating costs. This system will allow assessment of overall plant economics and support in developing the most economical coal cleaning, blending and switching options, based upon emissions control strategies.

A key part of the CQE program is the development of sub-models to predict the effects of coal quality on boiler performance under various operating conditions. Existing correlations between fuel properties and boiler performance are weak in several areas. These weaknesses are being addressed in this program through a combination of comprehensive bench-, pilot- and full-scale testing. Performance and validation data for a series of coals fired in selected utility boilers are being generated by laboratory and field tests.

Included in ABB Combustion Engineering's (ABB CE's) work scope is the generation of information to facilitate the formulation of a sub-model to predict ash slagging and fouling and subsequent impacts on boiler performance. This is an area of primary importance because of the poor reliability of current predictive indices, and the strong influence which ash deposition can have on overall boiler performance and power generating costs. In order to predict slagging and fouling, modeling efforts will apply a more fundamental approach which subdivides the ash deposition process to focus on ash formation, transport and deposition, deposit strength development and response to soot blowing, and deposit heat transfer effects. Pilot-scale testing is used to facilitate the quantification of these phenomena by providing a highly controlled combustion environment that allows isolation of the effects of boiler operating conditions. This high level of control also provides a means to directly measure key performance parameters for development of cause-and-effect relationships. The correlation of measured fuel properties to physical and thermal properties of ash deposits is an essential element of the slagging/fouling algorithm development.

Similarly, combustion performance, specifically carbon burnout, cannot be reliably predicted directly from conventional fuel analyses. A more fundamental approach is being pursued that applies fuel combustion kinetic information in conjunction with boiler operating conditions to model the combustion process. Fuel reactivity parameters will be measured during small-scale combustion testing to form a data base from which combustion predictions can be made.

This report summarizes the bench- and pilot-scale test results along with results from the boiler performance modeling (combustion reactivity as well as computational boiler performance modeling) which was conducted at ABB Combustion Engineering (CE) for coals burned at Public Service of Oklahoma's (PSO's) Northeastern station, Unit 4. These fuels included a Wyoming subbituminous coal and blends of this coal with an Oklahoma high-volatile bituminous coal. Additionally, a sample of the Oklahoma coal was cleaned at CQ, Inc.'s coal cleaning facility and blended with the Wyoming coal for testing and analysis. Results from field testing at Unit 4 were used to assess and substantiate findings from bench- and pilot-scale tests as well as results from the boiler performance model. The primary purpose of this report is to summarize key information required for further sub-model development efforts.

Detailed fuel property characterization was conducted by ABB CE and University of North Dakota's Energy and Environmental Research Center (EERC). In general, Wyoming subbituminous and Oklahoma bituminous coals were found to differ significantly in chemical characteristics (volatility contents, calorific values, ash loadings, etc.) and in mineralogy. The coals are, however, fairly similar in ash chemistry (compositions, fusibility temperatures, etc.), indicating that blending should not create major problems.

Bench-scale and drop tube furnace combustion tests at ABB CE indicated that the Wyoming coal char is much more reactive than the Oklahoma coal char. All PSO chars prepared from the parent coals and coal blends are much higher in reactivity than a char prepared from a West Virginia medium volatile bituminous coal, which is used as a marginal coal reactivity bench-mark at ABB CE, and is successfully burned

in pulverized form in a tangentially-fired utility boiler. Reaction kinetic parameters determined by bench-scale tests imply the Wyoming coal char is much less sensitive to temperature than the Oklahoma coal char; i.e., at relatively lower temperatures, it would react more rapidly and completely than the Oklahoma coal char.

Pilot-scale testing at ABB CE defined ash performance characteristics and allowed in-depth analysis of furnace deposits during and after formation. Deposit formation, growth and thermal effects were measured in both radiant and convective sections. The effects of key boiler operating conditions were determined and continuous operation limitations were established for each test coal. A blend of 70% Wyoming coal and 30% cleaned Oklahoma coal (70% WY/30% CLN) exhibited better slagging performance than the other test fuels. This fuel produced deposits in the lower furnace which remained cleanable at temperatures up to 2975 to 3000 °F. The 100% Wyoming fuel (100% WY) and 70% Wyoming/30% Oklahoma (uncleaned) fuel (70% WY/30% OK), by contrast, produced lower furnace deposits which were cleanable only up to 2800 to 2850°F. Average thermal conductances ($k/\Delta x$), as measured during pilot-scale testing, were significantly higher for deposits from a 90% Wyoming/10% Oklahoma blend (90% WY/10% OK) as compared to the 100% WY and 70% WY/30% OK deposits. This is consistent with field testing; the 90% WY/10% OK coal blend, for example, resulted in the lowest furnace outlet temperature, implying that heat transfer (through the ash deposits) was best in this case.

Low excess air was shown to have a more significant effect on the nature of lower furnace deposits in the 100% WY case; this was corroborated by field data. Specifically, low excess air reduced the critical temperature for adequate deposit cleanability to a greater extent in the 100% WY case than for the other fuel blends tested.

Boiler performance modeling results corroborated pilot-scale conclusions that Northeastern Unit 4 should be capable of typical cycling operation while firing the 90% WY/10% OK fuel and the 70% WY/30% OK fuel. "Cycling operation," which is standard procedure for this unit, involves a load drop of about 40% during off-peak

periods when electricity demand is low, and is usually accompanied by shedding of the slag that has accumulated on waterwall sections in areas of low wall blower effectiveness.

Pilot-scale studies also included examination of the fouling tendencies of the subject fuels. Deposit-to-tube bonding strengths in the convective pass generally increased with increasing concentrations of the OK coal. However, only with the 70% WY/30% OK and the 70% WY/30% OK cleaned coal blends did the deposit bonding strength clearly begin to exceed the ability of conventional soot blowers to remove deposits; such conditions generally occurred at gas temperatures of 2250°F or higher.

In general, the composition and particle size distribution of ash deposit inner layers (measured by CCSEM) indicated that small particle/vapor phase diffusion and thermophoresis dominate the inner layer formation and growth. Analytical data on ash deposit outer layers indicated that the inertial impaction of large particles dominates deposit growth after the initial layer has been formed.

Convective tube erosion rates due to fly ash impingement were evaluated for the subject fuels during pilot-scale testing. Though erosion rates of fly ashes from the 90% WY/10% OK fuel were three times that of the 70% WY/30% OK cleaned fuel, both blends showed very low erosion relative to most other U.S. coals.

Overall, a great deal of detailed, quantitative fuel and performance data were collected during these series of PSO Northeastern coal tests. Ash slagging and fouling data were obtained over a range of utility boiler operating conditions. At conditions representative of the Northeastern unit, pilot-scale results were generally consistent and compared very favorably with field test results. Fuel property and performance results detailed in this report, along with those results from the fuels still to be tested under this project, should provide a sound basis for development of key sub-models for the Coal Quality Expert.

ACKNOWLEDGMENTS

The authors appreciatively acknowledge the following ABB CE/KDL employees for their invaluable efforts in running the tests, proof reading the many drafts of this report, and providing helpful insight in to this investigation:

Stanley Bohdanowicz

Gregory A. Burns

Oscar K. Chow

James F. Durant

V. R. Garimella

Peter J. Grandia

Bruce F. Griffith

Rudy A. Jacobek

Armand A. Levasseur

Dana R. Raymond

Gary M. Tessier

The authors also gratefully acknowledge the staffs of the ABB CE Chemical Systems group and the Energy and Environmental Research Center at the University of North Dakota who have provided the chemical analyses for all of the coals/coal bends, furnace deposits and ashes. Without their help the advanced analyses offered in this report would not have been possible. Joni Miller, Carylon Miller, and Kay Nadeau are gratefully acknowledged for their assistance with graphics and typing.

The field testing crews and personnel of the Electric Power Technologies Inc., Energy and Environmental Research Corp., and Fossil Energy Research Corp. also provided a significant amount of data and discussion which was extremely helpful in writing this report.

Table of Contents

Section 1

1.0 INTRODUCTION	1
1.1 PROGRAM OVERVIEW	1
1.2 BACKGROUND	4
1.2.1 Ash Particle Size and Composition Evolution	4
1.2.2 Transport Mechanisms	5
1.2.3 Growth/Strength Development	7

Section 2

2.0 BENCH-SCALE TESTING	8
2.1 CHARACTERISTICS OF TEST FUELS	8
2.1.1 Sources of Test Fuels	8
2.1.2 Standard Analyses	10
2.1.3 Special Analyses	13
2.1.3.1 <u>Weak Acid Leaching (WAL)</u>	13
2.1.3.2 <u>Computer Controlled Scanning Electron Microscopy (CCSEM)</u> <u>And Chemical Fractionation</u>	14
2.1.3.3 <u>Mill Erosion/Abrasion Potential</u>	19
2.2 REACTIVITIES OF TEST FUELS	21
2.2.1 Ignitibility /Reactivity Characteristics	21
2.2.2 Drop Tube Furnace System-1 (DTFS-1) Combustion Kinetic Parameters of PSO's Northeastern Fuels	27
2.2.2.1 <u>Facility Description</u>	27
2.2.2.2 <u>Swelling Factors of Coals</u>	29
2.2.2.3 <u>Typical Test Matrix</u>	30
2.2.2.4 <u>Combustion Kinetic Parameters of Chars</u>	30
2.2.2.5 <u>Combustion Kinetic Data Base for Algorithm Development</u>	40

2.3 ASH DEPOSITION/DEPOSIT FORMATION	44
2.3.1 Deposit Description	46
2.3.2 Determination of Deposit Strengths	47
2.3.3 Physical and Chemical Examination of Deposits and Substrate Materials	51

Section 3

3.0 PILOT-SCALE TESTING	56
3.1 TEST FUELS	57
3.2 FIRESIDE PERFORMANCE CHARACTERISTICS	58
3.2.1 Test Conditions	60
3.2.2 Characterization of Pilot-Scale In-Flame Solids	65
3.2.3 Furnace Slagging	69
3.2.3.1 <u>Simulated Waterwall Heat Absorptions</u>	70
3.2.3.2 <u>Description of Waterwall Slag Deposition and Deposits</u>	94
3.2.3.3 <u>Sacrificial Probe Evaluations</u>	101
3.2.3.4 <u>Lower Furnace Deposit Thermal Conductance</u>	106
3.2.3.5 <u>Effects of Excess Air</u>	108
3.2.4 Convective Pass Fouling	110
3.2.4.1 <u>Description of Super Heater Fouling Deposition and Deposits</u>	127
3.2.5 Fly Ash Characterization and Erosion	134

Section 4

4.0 BOILER PERFORMANCE MODELING	138
4.1 DESCRIPTION OF NORTHEASTERN UNIT 4	139
4.2 BOILER OPERATION	140
4.3 COAL SOURCE	142
4.4 BOILER PERFORMANCE PROGRAM DESCRIPTION	144
4.5 BOILER PERFORMANCE PROGRAM CALIBRATION PROCEDURE	147
4.5.1 Calibration of Northeastern Unit 4	151

4.6 BOILER PERFORMANCE WITH BLENDED FUELS	156
4.6.1 Performance Prediction Procedure	156
4.6.2 Boiler Island Performance of the 90% WY/10% OK and 70% WY/30% OK Fuels	163
4.6.3 Evaluation of Full-Scale and Pilot-Scale Data for the Blended Fuels	167

Section 5

5.0 CONCLUSIONS	174
------------------------------	-----

Bibliography

Appendix A - Facility Descriptions

Appendix B - UND SEM Procedure

Appendix C - Detailed CCSEM and Chemical Fractionation Results

Appendix D - CE Pilot-Scale (FPTF) Data

List of Figures

Figure 1.1 Slagging and Fouling Algorithm Development Schematic	2
Figure 2.1 Coal Particle Size Distribution for PSO Coals and Coal Blends	12
Figure 2.2 Mineral Matter Particle Size Distributions for PSO Coals and Coal Blends	19
Figure 2.3 Flammability Apparatus	22
Figure 2.4 Coal/Char Preparation and TGA/BET Evaluation	24
Figure 2.5 TGA Burn-Off Curves in Air at 700°F for PSO and Reference DTFS Coal Chars	25
Figure 2.6 Schematic of Drop Tube Furnace System - 1 (DTFS-1)	28
Figure 2.7 DTFS-1 Determination of Coal Chars' Combustion Kinetic Parameters .	31
Figure 2.8 DTFS-1 Combustion Efficiency Plots of Various 200x400 Mesh PSO Coal/Coal Blend Chars	32
Figure 2.9 Effect of Fuel Type on DTFS Combustion Efficiencies of Various 200 x 400 Mesh PSO Coal/Coal Blends at Two Gas Temperatures	34
Figure 2.10 Arrhenius Plot for 200x400 Mesh PSO Coal Char Combustion in the DTFS-1	36
Figure 2.11 Comparison of Arrhenius Lines of Three PSO Fuels	37
Figure 2.12 Relationship Between Surface Reactivity Coefficient and Surface Temperature for the Present Study and Selected Literature Data	39
Figure 2.13a Boiler Dimensional/Operating Data Required for ABB CE's LFP-SKM Inputs	41
Figure 2.13b Flow Diagram for ABB CE's LFP-SKM Simulation	41
Figure 2.14 Procedure for Choosing Surrogate Coal Combustion Kinetic Parameters for Modeling Purposes	42
Figure 2.15 Schematic of EERC Drop Tube Furnace	45
Figure 2.16 Deposit Strength Measurement Apparatus	50
Figure 2.17 Strength Curves for PSO Coal and Coal Blend Deposits Generated in the DTF	52
Figure 2.18 Ash Sticking Fraction vs. Time for the PSO Test Fuels as Generated in the DTF	52
Figure 2.19 Viscosity Distribution in DTF Base Deposits	54
Figure 2.20 Viscosity Distribution in DTF Main Deposits	55
Figure 3.1 Coal Particle Size Distributions For PSO Coals And Coal Blends	58
Figure 3.2 Fireside Performance Test Facility	59

Figure 3.3	Typical FPTF Variation of Temperature Profiles with Distance During Test Firing of the Northeastern Fuels	62
Figure 3.4	Typical Radial and Axial Gas Temperatures in the FPTF While Firing Northeastern Fuels	62
Figure 3.5	Heat Flux Comparison Between the FPTF and the Northeastern Unit 4 ..	63
Figure 3.6	Comparison of Bulk Gas Residence Times at Similar Loads for all Fuels Tested	64
Figure 3.7	Comparison of L1 In-flame Solids Particle Size Distributions	68
Figure 3.8	In-flame Solids Sample Viscosity Distribution	69
Figure 3.9	Schematic of Waterwall Panel and Deposit	71
Figure 3.10	FPTF Waterwall Panel Heat Flux While Testing 100% WY	72
Figure 3.11	FPTF Waterwall Panel Heat Flux While Testing 100% WY	73
Figure 3.12	FPTF Waterwall Panel Heat Flux While Testing 90% WY/10% OK	74
Figure 3.13	FPTF Waterwall Panel Heat Flux While Testing 90% WY/10% OK	75
Figure 3.14	FPTF Waterwall Panel Heat Flux While Testing 70% WY/30% OK	76
Figure 3.15	FPTF Waterwall Panel Heat Flux While Testing 70% WY/30% OK	77
Figure 3.16	FPTF Waterwall Panel Heat Flux While Testing 70% WY/30% OK CLN	78
Figure 3.17	100% WY Heat Flux Summary	81
Figure 3.18	90% WY/10% OK Heat Flux Summary	81
Figure 3.19	70% WY/30% OK Heat Flux Summary	82
Figure 3.20	70% WY/30% OK CLN Heat Flux Summary	82
Figure 3.21	Lower Furnace Deposit Buildup - Time Sequencing (100% WY Test 6)	84
Figure 3.22	Lower Furnace Deposit Buildup - Time Sequencing (90% WY/10% OK Test 2)	85
Figure 3.23	Lower Furnace Deposit Buildup - Time Sequencing (90% WY/10% OK Test 3)	86
Figure 3.24	Lower Furnace Deposit Buildup - Time Sequencing (70% WY/30% OK Test 1)	87
Figure 3.25	Lower Furnace Deposit Buildup - Time Sequencing (70% WY/30% OK Test 2)	88
Figure 3.26	Lower Furnace Deposit Buildup - Time Sequencing (70% WY/30% OK CLN Test 1)	89
Figure 3.27	Lower Furnace Deposit Buildup - Time Sequencing (70% WY/30% OK CLN Test 2)	90

Figure 3.28	Lower Furnace Deposit Buildup - Time Sequencing (70% WY/30% OK CLN Test 2, Panel 3)	91
Figure 3.29	Lower Furnace Deposit Buildup - Time Sequencing (70% WY/30% OK CLN Test 3)	92
Figure 3.30	Cleanability Comparison Between the Four Fuels at Similar Loads ...	94
Figure 3.31	Comparison of In-Flame Solids (L5-3) with Waterwall Panel 5 Inner layer (100% WY)	97
Figure 3.32	Viscosity Distribution Comparison -- Waterwall Panel 1 Inner Layers .	98
Figure 3.33	Viscosity Distribution -- Waterwall Panel 1 Outer Layer	98
Figure 3.34	A Comparison of Furnace Outlet Gas Temperatures Under Similar Furnace Loads for the Coal/Coal Blends Tested in the Field (EER) ...	99
Figure 3.35	Schematic Elevational View of Northeastern Unit 4 Showing the Location of the Furnace Outlet Temperature Measurements	100
Figure 3.36	A Simplified Schematic of the Sacrificial Probe	101
Figure 3.37	Pictures of the Sacrificial Probe After Deposit Accumulation	103
Figure 3.38	Panel Deposit Heat Balance and Thermal Conductance Measurement Technique	107
Figure 3.39	Effects of Excess Air -- 100% WY	109
Figure 3.40	Effects of Excess Air -- 90% WY/10% OK	109
Figure 3.41	Effects of Excess Air -- 70% WY/30% OK	109
Figure 3.42	Furnace Outlet Temperatures as a Function of Excess Air for Fuels Tested in Northeastern Unit 4 (EER)	110
Figure 3.43	Convection Pass Deposit Bonding Strength Summary	111
Figure 3.44	Typical Superheater Tube Initial Deposition for Two Fuels	113
Figure 3.45	Superheater Tube Deposit Buildup Rates - 100% WY - Test 4	114
Figure 3.46	Superheater Tube Deposit Buildup Rates - 100% WY - Test 5	115
Figure 3.47	Superheater Tube Deposit Buildup Rates - 90% WY/10% OK - Test 1	116
Figure 3.48	Superheater Tube Deposit Buildup Rates - 90% WY/10% OK - Test 1	118
Figure 3.49	Superheater Tube Deposit Buildup Rates - 90% WY/10% OK - Test 3	119
Figure 3.50	Superheater Tube Deposit Buildup Rates - 90% WY/10% OK - Test 5	120
Figure 3.51	Superheater Tube Deposit Buildup Rates - 70% WY/30% OK - Test 5	121
Figure 3.52	Superheater Tube Deposit Buildup Rates - 70% WY/30% OK - Test 5	122
Figure 3.53	Superheater Tube Deposit Buildup Rates - 70% WY/30% OK CLN - Test 1	123

Figure 3.54	Superheater Tube Deposit Buildup Rates - 70% WY/30% OK CLN - Test 2	124
Figure 3.55	Superheater Tube Deposit Buildup Rates - 70% WY/30% OK CLN - Test 3	125
Figure 3.56	Superheater Tube Deposit Buildup Rates - 70% WY/30% OK CLN - Test 3	126
Figure 3.57	Comparison Between Compositions of Inner Deposit, In-flame and ASTM Ash Samples for 100% WY Coal	131
Figure 3.58	Comparison of Outer Deposit, In-flame and ASTM Ash Samples for 100% WY Coal	132
Figure 3.59	Comparison of Viscosity Distributions For Superheater Probe 1A Deposit Inner Layers	133
Figure 3.60	Comparison of Fly Ash Particle Size Distributions	136
Figure 3.61	Erosion Comparison between PSO Northeastern Unit 4 Coal Blends and Other Coals/Coal Blends	137
Figure 4.1	Northeastern Unit 4 Side Elevation View	141
Figure 4.2	Northeastern Unit 4 Wall and Soot Blower Locations	143
Figure 4.3	Boiler Performance Program Domain	146
Figure 4.4	Boiler Performance Program Flowchart for 100% WY Coal Calibration . .	149
Figure 4.5	Bonding Strength Measurements vs. Gas Temperature for FPTF and Field Data (100% WY)	153
Figure 4.6	Comparison of Field Test Data: Model of Generated vs. Measured Heat Flux Radiation at the Furnace Wall	154
Figure 4.7	Northeastern Unit 4 - Port Arrangement and Radiation Heat Flux Values	155
Figure 4.8	Thermal Conductance vs. Gas Temperature for 100% WY	156
Figure 4.9	Boiler Performance Program Flowchart for Boiler Performance Prediction	159
Figure 4.10	Thermal Conductance vs. Gas Temperature for 90% WY/10% OK Blend FPTF Tests	161
Figure 4.11	Thermal Conductance vs. Gas Temperature for 70% WY/30% OK Blend FPTF Tests	161
Figure 4.12	Thermal Conductance vs. Gas Temperature for the 90% WY/10% OK Fuel	170
Figure 4.13	Thermal Conductance vs. Gas Temperature for 70% WY/30% OK Fuel in FPTF and Field Tests	173

List of Tables

Table 2.1	Characterization of PSO'S Northeastern Power Station Fuels	9
Table 2.2	ASTM Standard Analyses of Northeastern Coals	11
Table 2.3	Weak Acid Leaching Data for PSO's Northeastern Fuels	13
Table 2.4	Mineralogical Characteristics of Northeastern Unit 4 Fuels as Determined by CCSEM	16
Table 2.5	Organically Associated Mineral Contents in Northeastern Unit 4 Fuels as Determined by Chemical Fractionation	16
Table 2.6	Particle Size Distributions of Inorganic Components for the Northeastern Fuels Using CCSEM and Chemical Fractionation	18
Table 2.7	Quantities of Excluded Minerals in Northeastern Fuels	20
Table 2.8	Alpha-Quartz Contents in Ash Samples From PSO Northeastern Fuels and Reference Coals	20
Table 2.9	Flammability Indices of Northeastern Coals and Reference Coals	21
Table 2.10	BET Surface Areas of Chars Prepared from PSO'S Northeastern Fuels and Reference Coals	26
Table 2.11	Kinetic Data From DTFS-1 Combustion of 200X400 Mesh PSO Coal Chars in 0.03 ATM. O ₂ and 1285-1760 °K Particle Surface Temperature Range	38
Table 2.12	Combustion Kinetic Parameters of PSO Northeastern Coals/Chars ...	40
Table 2.13	Combustion Kinetic Information Database of DOE- and EPRI- Sponsored Work	43
Table 3.1	FPTF Firing Conditions Test Matrix	61
Table 3.2	CCSEM Comparisons of Radiant Section In-flame Solids at L1	65
Table 3.3	Radiant Section In-flame Solids - SEMPC and XRD at L1	66
Table 3.4	Chemical Formula definitions for Crystalline Phase Detected by XRD ...	67
Table 3.5	FPTF Critical Thermal Conditions	83
Table 3.6	Compositions of Panel 1 Water Wall Slag Deposits	96
Table 3.7	SEMPC Compositions of L1 Sacrificial Probe Deposits	105
Table 3.8	Thermal Conductance of Deposits Generated at Various Elevations in the FPTF (Btu/hr-ft ² °F)	107
Table 3.9	Comparisons of Superheater Probe 1A Deposit Composition	130
Table 3.10	SEMPC and XRD Comparisons of Fly Ash (Dust Loading Samples) ...	135
Table 4.1	Analyses of PSO Field-Tested Fuels	144
Table 4.2	Northeastern Unit 4 - Calibration of Field Test Data for 100% WY Coal ..	150

Table 4.3	Northeastern Unit 4 Surface Effectiveness Factors (SEF's)	153
Table 4.4	Bench and Pilot-Scale Coal Quality Indicators	158
Table 4.5	Northeastern Unit 4 Comparison of 90% WY/10% OK and 70% WY/30% OK Blends to Calibrated 100% WY Results	164
Table 4.6	Projected Efficiency Losses (Based on Reverse Calibration of 100% WY) for 90% WY/10% OK and 70% WY/30% OK Fuels	165
Table 4.7	Northeastern Unit 4 90% WY/10% OK Boiler Performance Results	168
Table 4.8	Data Summary for the 90% WY/10% OK Fuel	169
Table 4.9	Northeastern Unit 4 70% WY/30% OK Fuel Performance Results	171
Table 4.10	Data Summary for the 70% WY/30% OK Fuel	172

Section 1

INTRODUCTION

1.1 PROGRAM OVERVIEW

The overall objective of the Coal Quality Expert (CQE) Clean Coal I Program is the development of a Coal Quality Expert -- a comprehensive PC-based expert system for evaluating the potential for coal cleaning, blending and switching options to reduce emissions while producing the lowest cost electricity. A key part of the CQE program is the development of sub-models to predict the effects of coal quality on boiler performance under various operating conditions. Included in ABB Combustion Engineering's work scope is the generation of information to facilitate the formulation of a sub-model to predict slagging and fouling and its subsequent effect on boiler performance, and to predict combustion performance, specifically carbon burnout. In order to predict slagging and fouling, ash deposition processes must be defined and modeled. Ash formation, transport and deposition, deposit strength development and response to soot blowing and effect on heat transfer are the key processes which will be modeled. The correlation of measured fuel properties to physical and thermal properties of ash deposits is an essential element of the slagging/fouling algorithm development. The overall slagging and fouling algorithm development scheme is presented in Figure 1.1. Similarly, fuel reactivity parameters will be measured to form a database from which combustion predictions can be made. The generation of required information was obtained from a combination of bench-, pilot-, and full-scale testing which has been carried out on a series of coals and coal blends which were of interest to Public Service of Oklahoma (PSO) at their Northeastern Station.

This report summarizes the bench- and pilot-scale test results along with results from the boiler performance modeling (combustion reactivity as well as computational boiler performance modeling) which was conducted at ABB Combustion Engineering (CE) for the coals obtained from PSO's Northeastern Unit 4. Results from field testing at Unit 4 were used to substantiate findings from bench- and pilot-scale tests as well as results from the boiler performance model.

Bench-scale testing was used to characterize combustion kinetic properties and ash deposition propensities of fuels burned in both full-scale and pilot-scale units. These fuels included a Wyoming subbituminous coal and blends of this coal with an Oklahoma high-volatile bituminous coal. Additionally, a sample of the Oklahoma coal was cleaned at CQ, Inc.'s coal cleaning facility and blended with the Wyoming coal for testing and analysis. Standard ASTM analyses were performed on these fuels, as were special analyses, including Weak Acid Leaching (WAL), Computer Controlled Scanning Electron Microscopy (CCSEM), and Chemical Fractionation (CF). Special analyses were necessary to provide specific fuel and ash information on mineral size, associations and abundance not obtained through conventional ASTM analyses. Ignitibility and reactivity characteristics for selected coal/coal blends and their respective chars were measured to provide input necessary for the combustion performance computational models as well as for carbon burnout algorithm development.

Pilot-scale tests, performed in Combustion Engineering's Fireside Performance Test Facility (FPTF), were designed to closely match field unit furnace conditions. Pilot-scale testing allowed in-depth analysis of furnace deposits during and after formation under well-controlled conditions. Deposit formation, growth and thermal effects were characterized in both the radiant and convective sections of the FPTF; this information will be the basis of slagging and fouling-related algorithm development. Coal, deposit and ash samples generated in the FPTF were analyzed at the Energy & Environmental Research Center (EERC-UND) of the University of North Dakota using advanced methods of coal and coal ash analysis. The key objectives of the FPTF testing was to address cause and effect relationships of slagging and fouling deposition, and to quantify slagging and fouling for correlation with coal properties. Thermal and physical characteristics were to be separately analyzed and correlated to deposit strength and growth.

The boiler performance models, which can use bench-, pilot- and full-scale information, were applied to predict the performance of the various coal/coal blends in PSO's Northeastern Unit 4. Calibration of the computational models with known

baseline data allowed the prediction of boiler performance when firing alternate fuels. Computational models were used to supplement field data and provide more complete boiler performance information. This boiler performance data, used in conjunction with the lab-scale data, provides the foundation for algorithm development.

1.2 BACKGROUND

Fundamental to the development of algorithms which will predict fireside boiler performance is an understanding of coal specific fouling and slagging tendencies and how it is related to boiler operation for optimal heat transfer and boiler cleanliness. The purpose of this section is to describe some mechanisms of ash formation and deposition, and provide insight into fireside ash transformation phenomena. Specific pilot-scale and bench-scale results are presented and discussed in the body of the report.

1.2.1 Ash Particle Size and Composition Evolution

The inorganic components associated with coal undergo a complex series of chemical and physical transformations during coal combustion. These transformations lead to the formation of ash intermediates (inorganic vapors, liquids, and solids). The intermediate ash components range from vapors to solid particles with a bimodal (modes at ≈ 0.1 and $\approx 12 \mu\text{m}$) final ash particle-size distribution, and have a wide range of chemical compositions.

A significant portion of the submicron particles form in the combustion gas stream as a result of homogeneous condensation of flame-volatilized species. Other particles form as a result of submicron minerals and ash particles shedding from the surface of chars. The flame-volatilized species may also condense heterogeneously on the surfaces of larger particles. Larger particles, sometimes referred to as residual ash, are largely derived from mineral grains. The composition and size distribution of larger particles result from transformations or interactions between discrete mineral grains in higher-rank coals. In lower-rank coals, the interaction of organically associated elements with

mineral grains occurs concurrently with mineral-mineral interactions. Processes such as ash mineral coalescence, partial coalescence, ash shedding, and char fragmentation during char combustion and mineral fragmentation, all play important roles in the size and composition of the final fly ash. Loehden et al. (ref. 6) and Zygarlicke et al. (ref. 7) indicate that three potential modes for fly ash generation can be used to describe fly ash particle size and composition evolution. The first, "fine limit," assumes that each mineral grain forms a fly ash particle and that the organically associated elements form fly ash particles less than 2 μm in diameter. The second, "total coalescence," assumes one fly ash particle forms per coal particle. The third, "partial coalescence," suggests that the fly ash composition and particle size evolve due to partial coalescence.

1.2.2 Transport Mechanisms

The transport of intermediate ash species (i.e., inorganic vapors, liquids, and solids) is a function of the state and size of the ash species and system conditions such as gas flow patterns, gas velocity, and temperature. Several processes are involved in the transport of ash particles.

Small particles ($<1 \mu\text{m}$) and vapor phase species are transported by small particle and vapor phase diffusion. These species are characteristically flame-volatilized and condense upon gas cooling in the bulk gas or in the gas boundary layer next to the tube. The diffusion mechanisms that are important with respect to the transport of vapor species and small particles include:

1. Fick diffusion - molecular level.
2. Brownian diffusion - particles suspended by a host liquid.
3. Eddy diffusion - turbulent systems.

A mechanism of ash particle transport in the $<10 \mu\text{m}$ size range of particles is thermophoresis. Thermophoresis is a transport force that is produced as a result of a temperature gradient in the direction from hot to cold. Electrophoresis is another transport mechanism that may be important with respect to the formation of deposits.

The transport mechanisms account for the formation of initial deposit layers in both the radiant and convective sections.

The initial deposition layer typically forms on all exposed tube surfaces and consists of particles less than 5 μm in diameter. These initial layers are abundant and form rapidly when firing coals that produce high levels of intermediate and small sized particles. Coals which characteristically produce high levels of intermediate and small sized particles contain low-levels of mineral grains and high levels of organically associated inorganic components.

Outer deposits which form on lower furnace walls and the leading surfaces of convection pass tubes result from particles greater than 5-10 μm transported to the surface by inertial impaction. The initial deposit layer, typically, consists of condensed flame-volatilized species, which provides a sticky surface that traps inertially impacting larger non-sticky particles. As the outer surfaces become more insulated from the water cooled steel surface, the temperature of the exposed deposit surface increases. Increasing surface temperature results in increasing the quantity of liquid phase components. These liquid phase components act as efficient collectors and increase the collection of ash particles impacting the deposit surface. Inertial impaction accounts for the bulk of the deposit growth. Particles that inertially impact have sufficient inertial momentum to leave gas streamlines and impact the tube. For small particles, the drag effect will be great enough to change the direction of the particles, allowing them to flow past the tube/deposit surfaces. The chances of a particle impacting a surface and sticking depend upon inertial momentum, particle drag force, the ability of the surface to absorb the particle kinetic energy, and particle surface liquid phase characteristics. Gas velocity has a significant effect on the size of the ash particles which will impact the surface. For example, in a gas turbine with a gas velocity on the order of 100 m/s, particles with diameters greater than 1 μm will impact. In typical utility boilers, the gas velocity is 10-25 m/s, and particles with diameters of 5-10 μm or greater will impact.

1.2.3 Growth/Strength Development

Strength development in deposits can be explained through sintering theory. A good description of sintering theory can be found in Kingery et al. (ref. 30). Briefly, sintering of a material is defined as a densification process resulting from heat treatment. Sintering mechanisms involve solid-state and viscous flow. In solid-state sintering, the densification process is a result of the decrease in surface area and a reduction in free energy by eliminating the porosity. The solid-state sintering mechanisms include vaporization and condensation, bulk diffusion transfer, and surface diffusion. Viscous flow or plastic flow occurs as two particles begin to sinter. The liquid phase component is the primary contributor to deposit strength development. The abundance and viscosity of the liquid phases, therefore, are the primary factors needed to assess deposit sintering potential. The liquid phase can be described as being reactive or nonreactive to the other solid components in the melt. A reactive liquid readily dissolves the solid particles, and a nonreactive liquid contains insoluble solids. The physical characteristics of the liquid phase can be changed appreciably by crystallization or decomposition. In nonreactive viscous flow, sintering of the liquid phase does not dissolve the solid components. (For example, in low-temperature sulfate-based deposits, the sulfates bond the silicate particles together with little or no reaction occurring between the silicate or sulfate phases.) In reactive viscous flow, sintering of the liquid phase dissolves the solid components and results in the formation of additional liquid. Strength development in ash deposits is, therefore, a dynamic and complex process which is largely dependent on furnace thermal conditions throughout all phase of deposit growth.

Specific mineral matter transformations to inflame solids and eventual deposit formation for the coal/coal blends fired in the Public Service of Oklahoma's Northeastern Unit 4 are presented in this report. The combined results presented are derived from bench-, pilot-, and full-scale testing. Existing computational models have been used take advantage of the bench- and pilot-scale data to fill in the gaps in the full-scale data set and to provide new insight into the full-scale boiler operation.

Section 2

BENCH-SCALE TESTING

The purpose of this section is to describe the bench-scale analytical techniques used to determine CQE test fuel and ash properties and to present the results of these analyses. The analyses conducted have been comprehensive in that they include bench-scale fuel, ash and deposit characterization, as well as, bench-scale characterization of fuel and ash samples generated in the pilot- and commercial-scale. Bench-scale characterization, performed on both bench-scale and pilot-scale fuel/ash samples, can be substantiated with concurrent full-scale testing. The ultimate goal in conducting these analyses is to develop fundamental relationships which can be used to formulate algorithms describing combustion and fireside characteristics of a range of fuels. Ideally, the input necessary for execution of the CQE model will be obtainable through bench-scale analysis of the coal.

Fuel testing entailed ASTM standard analyses, special tests and advanced techniques conducted in drop tube furnace systems, to derive information such as: (1) standard fuel analyses and deposit structures; (2) ignitibilities and reactivity characteristics; (3) combustion kinetic parameters of coals/coal chars; and (4) ash deposit formation characteristics. The objective of the bench-scale testing is to provide fundamental data for use in developing CQE algorithms to predict coal and coal ash performance in commercial pulverized coal-fired boilers. The testing procedures used and results obtained are discussed in the following sections.

2.1 CHARACTERISTICS OF TEST FUELS

2.1.1 Sources of Test Fuels

Six fuels have been characterized using ASTM standard and special analyses. They consist of the Wyoming subbituminous coal from Wyodak Seam (WY), Oklahoma high

volatile bituminous coal from Croweburg Seam (OK), CQ Inc.-cleaned Croweburg coal (OK CLN), and three mixtures thereof, as specified in Table 2.1.

Table 2.1 Characterization of PSO'S Northeastern Power Station Fuels

FUEL	EVALUATION LEVEL				
	BENCH-SCALE			PILOT-SCALE (FPTF)	FULL-SCALE (NORTHEASTERN UNIT 4)
	STD./SPECIAL ANALYSES	DTFS-1 KINETICS	EERC DTF ANALYSES		
100% WY*	X	X	X	X	X
90% WY/10% OK **	X		X	X	X
70% WY/30% OK	X		X	X	X
70% WY/30% OK (CLN)	X	X	X	X	
100% OK	X	X			
100% OK(CLN)***	X				

* WY = Wyoming Coal from Wyodak Seam

** OK = Oklahoma Coal from Croweburg Seam

*** CLN = Clean Northeastern Unit 4

Three of these fuels (100% WY, 90% WY/10% OK and 70% WY/30% OK) were obtained during the full-scale testing at the Public Service of Oklahoma's Northeastern Power Station Unit 4. These three fuel samples were subsequently test fired, along with the 70% WY/30% OK CLN blend, in CE's pilot-scale Fireside Performance Test Facility (FPTF) (See Section 3). Three fuels (100% WY, 100% OK and 70% WY/30% OK CLN) were also tested in CE's Drop Tube Furnace System-1 (DTFS-1) to derive their combustion kinetic parameters. The Oklahoma cleaned coal was obtained from CQ, Inc. and then blended with the Wyoming coal prior to pulverization in preparation for the pilot-scale testing; an aliquot of this sample was used for bench-scale testing. Testing the same fuel samples in bench-, pilot- and full-scale equipment enables the establishment of a common link for deriving correlation factors, which can be used for boiler performance prediction purposes, as well as for algorithm formulation.

2.1.2 Standard Analyses

The chemical analyses of the fuels tested for this portion of the CQE project are reported in Table 2.2. Wyoming subbituminous and Oklahoma bituminous coals differ significantly in their properties (volatile contents, calorific values, ash loadings, etc.). The coals are, however, fairly similar in ash compositions and fusibility temperatures. The impact of coal quality is also evident, when comparing the Oklahoma coal with its CQ Inc. cleaned counterpart. The calorific value of the cleaned product is 10% higher than that of its run-of-mine counterpart, and its ash loading is reduced by a factor of three. The coal properties and ash characteristics of the WY/OK and WY/OK CLN blends are commensurate with the various mixture ratios of the two parent coals. Because of the similarity in the ash composition, the bulk ash chemistry is virtually unaffected by blending the Wyodak and Croweburg coals.

These fuel ashes are typical of "Western" coal ashes in which the iron contents are lower than the sums of alkali and alkaline earth contents. The relatively low iron contents in these ashes are fluxed by the relatively high alkaline earth contents (principally CaO), as indicated by the low $\text{Fe}_2\text{O}_3/\text{CaO}$ ratios. This fluxing action of alkaline earths is known to cause low coal ash fusibility temperatures, as indicated in Table 2.2. However, because of the low iron contents of these fuels, this fluxing phenomenon was of limited significance. For these fuels, fluxing of the silicate matrix by calcium may be of greater significance.

Experimental experience testing of similar types of fuels in the FPTF indicates each of these coals and coal blends have relatively high furnace slagging/fouling potentials. Such potentials could cause problems which would be exacerbated by firing these fuels at high thermal loadings in a tightly designed boiler.

Test fuels were pulverized during pilot-scale testing with the target of matching pulverization levels achieved during field testing. Figure 2.1 shows the mean particle sizes and the typical particle size distributions for each of the fuels. The 100% OK fuel, which was not field or pilot-scale tested, was pulverized at EERC in a small ball mill.

Table 2.2 ASTM Standard Analyses of Northeastern Coals

Analysis	100% WY		90% WY/ 10% OK		70% WY/ 30% OK		70% WY/ 30% OK CLN		100% OK	
	As Fired	Dry	As Fired	Dry	As Fired	Dry	As Fired	Dry	As Rec.	Dry
Proximate, wt.%										
Moisture	13.4	-	11.5	-	8.5	-	8.0	-	8.9	-
Volatile Matter	43.8	50.5	43.0	48.6	40.2	43.9	41.4	45.0	28.8	31.6
Fixed Carbon	35.9	41.4	38.2	43.2	43.2	47.2	44.0	47.8	51.0	56.0
Ash	6.9	7.9	7.3	8.2	8.1	8.9	6.6	7.2	11.3	12.4
HHV, Btu/lb	10225	11807	10552	11923	11332	12385	11484	12482	11803	12956
Ultimate, wt.%										
Moisture	13.4	-	11.5	-	8.5	-	8.0	-	8.9	-
Hydrogen	4.4	5.0	4.4	4.9	4.4	4.8	4.7	5.1	4.3	4.7
Carbon	57.9	66.9	59.8	67.6	64.5	70.5	65.5	71.2	65.4	71.8
Sulfur	0.5	0.6	0.6	0.6	0.6	0.7	0.6	0.6	0.6	0.7
Nitrogen	0.9	1.0	1.0	1.1	1.3	1.4	1.2	1.3	1.6	1.7
Oxygen	16.0	18.6	15.4	17.6	12.6	13.7	13.4	14.6	7.9	8.7
Ash	6.9	7.9	7.3	8.2	8.1	8.9	6.6	7.2	11.3	12.4
Ash Loading, lb/MBtu	6.7	-	6.9	-	7.1	-	5.7	-	9.6	-
Forms of Sulfur, wt.%										
Sulfate (dry)	0.02		0.01		0.01		0.04		0.03	
Pyritic (dry)	0.13		0.14		0.16		0.10		0.19	
Organic (dry)	0.45		0.45		0.53		0.46		0.48	
Ash Fusibility, °F (Reducing Atmosphere)										
I.T.	2108		2120		2115		2100		2138	
S.T.	2131		2169		2147		2165		2210	
H.T.	2140		2186		2170		2184		2258	
F.T.	2158		2203		2194		2224		2320	
Temp. Diff. (F.T. - I.T.)	50		83		79		124		182	
Ash Composition, wt.%										
SiO ₂	31.7		35.3		37.7		35.4		48.5	
Al ₂ O ₃	15.8		16.2		15.6		16.3		17.6	
Fe ₂ O ₃	5.6		5.8		5.8		6.7		7.2	
CaO	19.5		18.1		16.0		16.5		12.3	
MgO	4.3		3.9		2.8		3.5		1.5	
Na ₂ O	0.8		0.8		0.7		0.7		0.6	
K ₂ O	0.5		0.8		1.6		1.1		3.0	
TiO ₂	1.2		1.2		1.0		1.2		0.8	
P ₂ O ₅	0.4		0.6		0.5		0.6		0.1	
SO ₃	19.0		16.4		17.8		15.1		7.9	
Ratios										
Base/Acid	0.63		0.56		0.50		0.54		0.37	
Fe ₂ O ₃ /CaO	0.29		0.32		0.36		0.41		0.59	
SiO ₂ /Al ₂ O ₃	2.01		2.18		2.42		2.17		2.76	

Table 2.2 (Cont'd) ASTM Standard Analyses of PSO's Northeastern Coals

Analysis	100% OK		100% OK CLN	
	As Fired	Dry	As Fired	Dry
Proximate, wt.%				
Moisture	8.9	-	12.8	-
Volatile Matter	28.8	31.6	29.4	33.7
Fixed Carbon	51.0	56.0	53.7	61.6
Ash	11.3	12.4	4.1	4.7
Ultimate, wt.%				
Moisture	8.9	-	12.8	-
Hydrogen	4.3	4.7	4.7	5.4
Carbon	65.4	71.8	70.7	81.1
Sulfur	0.6	0.7	0.6	0.7
Nitrogen	1.6	1.7	1.9	2.2
Oxygen	7.9	8.7	5.2	5.9
Ash	11.3	12.4	4.1	4.7
HHV, Btu/lb	11803	12956	12392	14211
Ash Loading, lb/MBtu	9.6	-	3.3	-

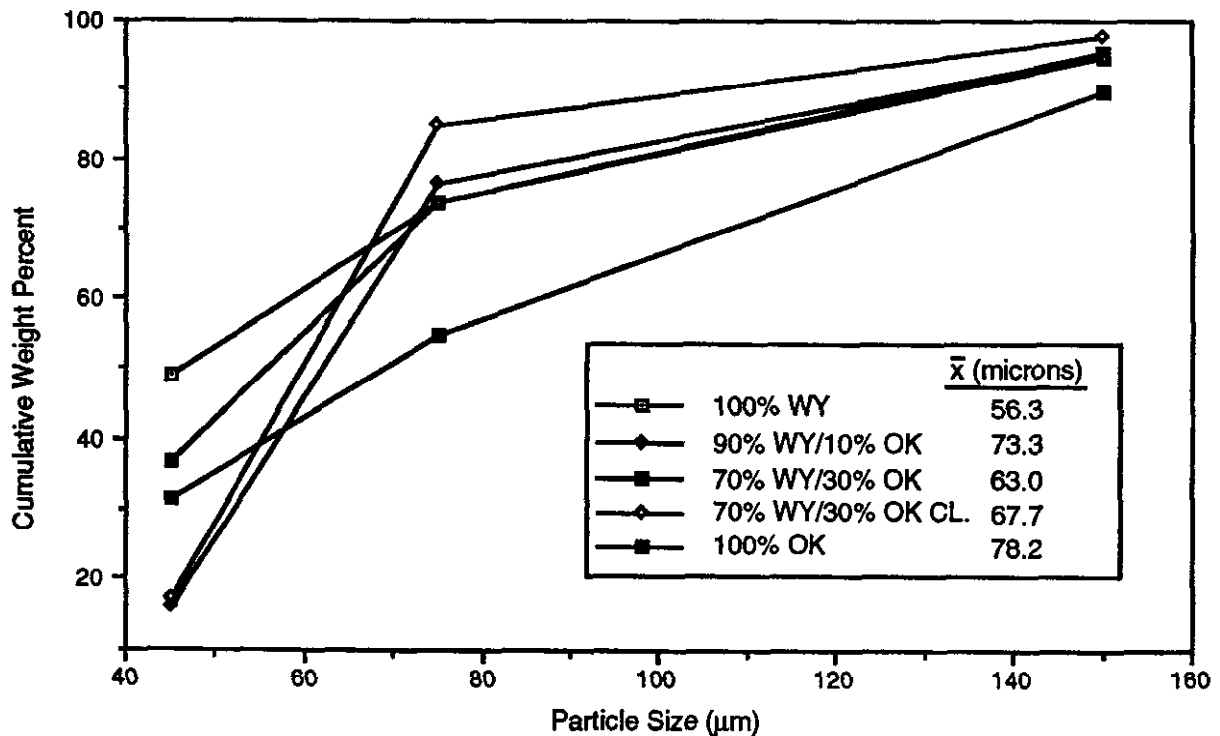


Figure 2.1 Coal Particle Size Distribution for PSO Coals and Coal Blends

2.1.3 Special Analyses

2.1.3.1 Weak Acid Leaching (WAL)

Weak acid leaching testing is designed to determine the concentrations of volatile alkali metals in a coal sample, which are leachable by a weak acid (acetic acid solution with a pH of 2.9). The volatilizable alkali metals are known to play a major role in the ash fouling phenomenon and, as such, the knowledge of their concentrations for a wide range of fuels can provide necessary input to CQE fouling algorithm development.

Results of the Weak Acid Leaching are reported in Table 2.3 along with those obtained by the ASTM method. The WAL results show that most of the sodium, in particular, is in a volatilizable form. These values would in themselves not be indicative of high ash fouling potentials, since the alkali contents of these ashes are so low. However, these values, evaluated in conjunction with the low ash fusibility temperatures (given in Table 2.1), indicate the test fuels possess moderate potential to produce ash fouling-related problems.

Table 2.3 Weak Acid Leaching Data for PSO's Northeastern Fuels

Fuels	Alkali Metals, Wt.% of Ash				Volatilizable	
	ASTM Method		WAL Method		Alkali Metals, %**	
	Na ₂ O	K ₂ O	Na ₂ O	K ₂ O	Na ₂ O	K ₂ O
100% WY	0.8	0.5	0.84	0.15	105	30
90% WY/10% OK	0.8	0.8	0.74	0.13	93	16
70% WY/30% OK	0.7	1.6	0.53	0.11	76	7
70% WY/30% OK CLN	0.7	1.1	0.69	0.26	99	24
100% OK	0.6	3.0	0.11	0.08	18	3

** The percent of alkali metals volatilized, based on WAL and ASTM measurements (e.g., for 100% WY, $\text{Na}_2\text{O} = (0.84/0.8)100 = 105\%$)

2.1.3.2. Computer Controlled Scanning Electron Microscopy (CCSEM) And Chemical Fractionation

Computer-controlled scanning electron microscopy (CCSEM) analysis was carried out by the Energy and Environmental Research Center of the University of North Dakota (EERC-UND) to determine compositions, size distributions and abundance of minerals in the test fuels. The CCSEM information is used to elucidate the mechanisms of ash transformation and as input data to the slagging and fouling algorithms. In addition, the information generated by CCSEM is particularly useful in determining the effectiveness of coal-cleaning processes.

The CCSEM data is used to quantify and size discrete mineral grains in the coal or individual particles in fly ash. Approximately 2000 grains, ranging in diameter from 1 to 100 μm , are analyzed in a polished section of the coal or ash sample. The average diameter, area, and energy dispersive elemental composition for each mineral are recorded, and the mineral is classified according to its chemistry. Unclassified minerals are usually the result of SEM beam effects. Adjacent minerals or mineral associations, within the excitation volume, may produce an energy dispersive spectrum which is a mixture of the associated mineral grains; in these instances, the CCSEM program is unable to classify the particle based on chemistry alone (for a more detailed explanation, see Appendix B). Back-scattered electron imaging (BEI) and energy dispersive spectrum (EDS) detection are used to analyze the minerals. Since the mineral or ash particles appear brighter in BEI relative to the lower atomic number background of the matrix, a distinction can be made between coal, epoxy, and mineral grains. Using the Tracor-Northern particle recognition and characterization program, the electron beam is programmed to scan over the field of view to locate bright inclusions that correspond to mineral or ash species. On finding a bright inclusion, the beam performs eight diameter measurements on the inclusion, finds the center of the inclusion, and collects an EDS for 5 seconds. The system is set up to analyze for 12 elements: Na, Mg, Al, Si, P, S, Cl, K, Ca, Fe, Ba, and Ti. Data from the CCSEM analysis is transferred simultaneously to a personal computer where it is stored on disk. The CCSEM technique is described in detail by Zygarlicke and Steadman (1990).

Chemical Fractionation was also used at EERC to quantify the distributions of major and minor elements in coal (Benson and Holm, 1985). The procedure is based on the differences in solubilities of coal inorganic constituents in stirred solutions of deionized water (H₂O), 1 M ammonium acetate (NH₄OAc) and 1 M hydrochloric acid. A 25-gram sample of 100% minus 200 mesh, vacuum dried coal is used to perform the analysis. After each extraction, the coal mixture is filtered, dried, and a portion of the residue is analyzed for ash content using standard ASTM proximate and x-ray fluorescence (of the ASTM ash) analyses. Chemical data for the original coal, residues, and leachates and residue ash contents are utilized in mass balance calculations to determine the elemental losses from each extraction. The elements removed by H₂O are primarily associated with water-soluble minerals such as halite (NaCl). Elements associated with salts of organic acids are removed by NH₄OAc. HCl removes elements associated with acid-soluble minerals (e.g., carbonates) and organic coordination complexes. Elements remaining in the final residue are presumably associated with insoluble minerals such as clays, quartz, and pyrite.

Analysis of the coal minerals using CCSEM revealed major differences between the Wyoming and Oklahoma coals (Table 2.4). The major minerals in the Wyoming coal were kaolinite, quartz, montmorillonite, and Ca-Al-phosphate minerals, while the major minerals in the Oklahoma coal were quartz, calcite, and illite (K Al-silicate). The 90% WY/10% OK and 70% WY/30% OK blends show intermediate mineral quantities between the mineral contents of the parent coals. The 70% WY/30% OK CLN blend was similar to the uncleaned 70% WY/30% OK blend, except it had a lower level of illite.

Chemical Fractionation (CF) results (Table 2.5) were used to determine the weight percent of ash constituents that are organically bound in each of the fuels. The Wyoming coal, as expected, had the most organically associated inorganics (2.2%, coal basis), the blends had lower levels (1.0-1.6%, coal basis) and the Oklahoma coal had virtually no organically bound inorganic elements (0.15%, coal basis). Calcium

was primarily present as calcite in the Oklahoma coal. The cleaning process had little effect on the organically bound inorganics, since both the 70% WY/30% OK blend and the 70% WY/30% OK cleaned blend had similar total organically bound contents (~1%, coal basis). Detailed chemical fractionation results for each of the coals are given in Appendix C.

Table 2.4 Mineralogical Characteristics of Northeastern Unit 4 Fuels as Determined by CCSEM

MINERAL, Wt.%	100%WY	90%WY/10%OK	70%WY/30%OK	70%WY/30%OK CLN	100%OK
Quartz	24.4	24.1	22.2	23.1	9.3
Iron Oxide	1.1	0.7	0.4	1.7	0.5
Calcite	0.0	1.7	5.5	5.1	15.1
Kaolinite	17.8	16.3	13.8	15.3	4.9
Montmorillonite	11.0	9.2	4.5	6.2	1.4
K Al-Silicate	3.5	10.0	22.1	11.6	40.3
Aluminosilicate	6.8	3.1	1.2	2.2	5.1
Pyrite	5.2	8.5	7.0	8.0	2.8
Ca Al-Phosphate	14.2	7.6	2.8	4.4	0.0
Silicon Rich	6.5	6.9	4.7	3.7	4.9
Total	6.2	5.7	6.6	3.8	13.6

Table 2.5 Organically Associated Mineral Contents in Northeastern Unit 4 Fuels as Determined by Chemical Fractionation

ORG.-BOUND MIN. WT.% OF COAL	100%WY	90%WY/10%OK	70%WY/30%OK	70%WY/30%OK CL	100%OK
Silicon	0.00	0.00	0.00	0.00	0.00
Aluminum	0.37	0.23	0.03	0.00	0.00
Iron	0.14	0.03	0.04	0.03	0.09
Titanium	0.03	0.00	0.00	0.00	0.00
Phosphorus	0.00	0.00	0.00	0.00	0.00
Calcium	1.15	0.73	0.61	0.49	0.00
Magnesium	0.43	0.27	0.26	0.24	0.06
Sodium	0.04	0.03	0.03	0.03	0.01
Potassium	0.00	0.00	0.00	0.00	0.02
Total Org. Bound Mineral	2.16	1.29	0.97	0.79	0.18

Particle size distributions (PSD) of the mineral particles in the fuels (Table 2.6 and Figure 2.2) showed the Oklahoma coal to have the largest PSD, followed by both 90% WY/10% OK and 70% WY/30% OK CLN blends, which were fairly similar. The 70%WY/30% OK blend and 100% WY were at the finer end of the spectrum and also fairly similar. The minerals in the Oklahoma coal that had the larger sizes were illite, calcite and kaolinite. More excluded minerals, those not associated with coal particles, were observed for the 100% OK coal and the WY/OK blends using CCSEM and image analysis (Table 2.7). Appendix C contains the detailed particle sizes and composition distributions of the major minerals in each of the fuels.

Interestingly, the particle size distributions of these test fuels also show that the Oklahoma coal had the largest particle size distribution (Figure 2.1). However, with the possible exception of excluded minerals, there is no reason to expect coal particle size to affect mineral particle size. Each of the fuels were blended and then pulverized independently. The particle size generated is more a function of mill settings rather than coal/mineral matter properties.

Table 2.6 Particle Size Distributions of Inorganic Components
for the Northeastern Fuels Using CCSEM and Chemical Fractionation

FUEL	Weight Percent					
	<2.2 μm	2.2-4.6 μm	4.6-10 μm	10-22 μm	22-46 μm	> 46 μm
CCSEM Data (Mineral Basis)						
100% WY	14.6	26.7	28.9	16.4	11.8	1.6
90% WY/10% OK	15.0	24.0	24.0	13.0	12.0	12.0
70% WY/30% OK	21.0	29.5	27.6	15.0	6.5	0.4
70% WY/30% OK CLN	16.0	23.0	20.0	16.0	17.0	9.0
100% OK	8.5	17.7	21.7	17.3	24.1	10.8
CCSEM/CF Data (Coal Basis)						
100% WY	3.07**	1.66	1.79	1.02	0.73	0.10
90% WY/10% OK	2.00	1.35	1.39	0.74	0.70	0.67
70% WY/30% OK	2.59	2.19	2.05	1.12	0.48	0.03
70% WY/30% OK CLN	1.62	0.87	0.76	0.60	0.63	0.32
100% OK	1.34	2.41	2.95	2.35	3.28	1.47
CCSEM/CF Data (MM Basis)						
includes inorganic and organically associated minerals						
100% WY	37.0	19.8	12.1	21.3	8.7	1.2
90% WY/10% OK	29.2	19.7	20.3	10.8	10.2	9.8
70% WY/30% OK	30.6	25.9	24.2	13.2	5.7	0.4
70% WY/30% OK CLN	33.7	18.2	15.8	12.6	13.1	6.7
100% OK	8.5	17.7	21.7	17.3	24.1	10.8
Weight Percent Less Than						
		2.2 μm	4.6 μm	10 μm	22 μm	46 μm
CCSEM/CF Data (MM Basis)						
100% WY		37.0	56.8	78.1	90.2	98.8
90% WY/10% OK		29.2	48.9	69.2	80.0	90.2
70% WY/30% OK		30.6	56.5	80.7	93.9	99.6
70% WY/30% OK CLN		33.7	51.8	67.6	80.2	93.3
100% OK		8.5	26.1	47.8	65.1	89.2

** Corrected by multiplying CCSEM data by the total coal mineral content (Table 2.4) and adding organically-bound inorganics (Table 2.5) to the <2.2 μm fraction only.

Example: $3.07 = 14.6 * 0.062 + 2.16$

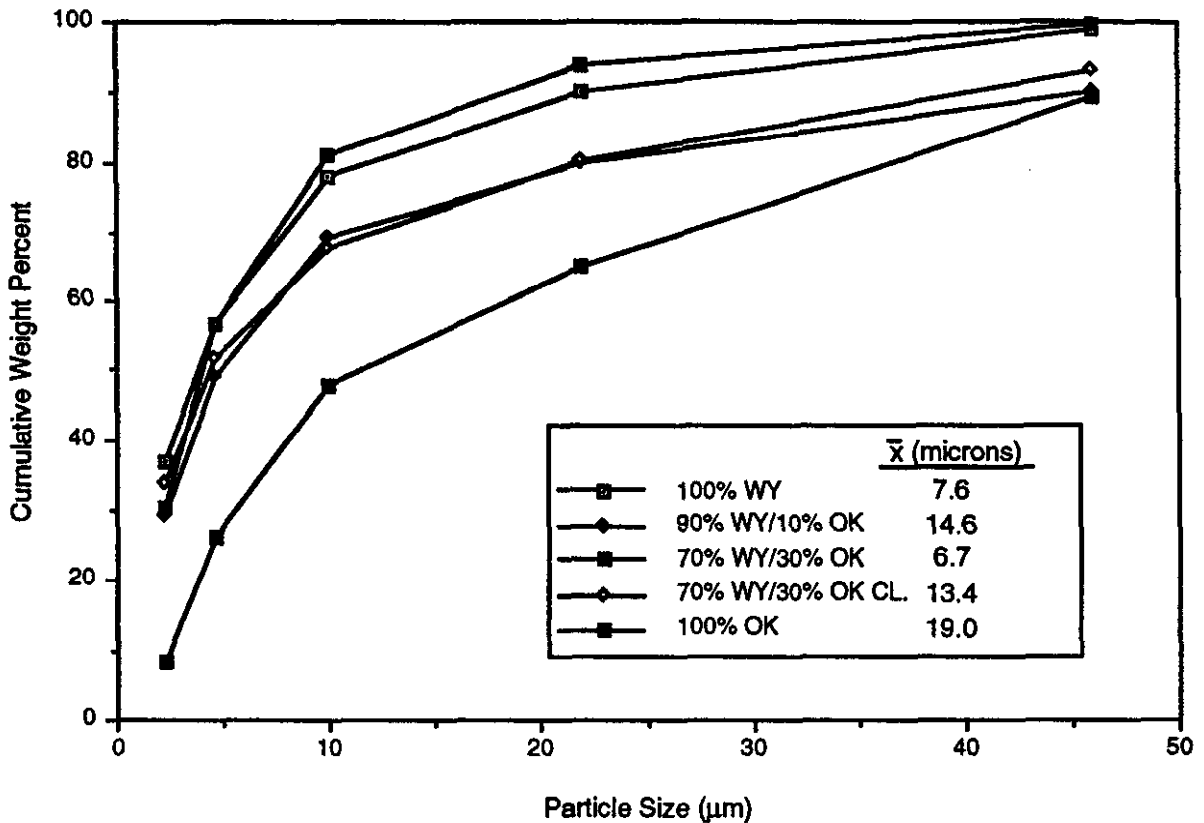


Figure 2.2 Mineral Matter Particle Size Distributions for PSO Coals and Coal Blends

2.1.3.3 Mill Erosion/Abrasion Potential

CE has developed a procedure for assessing coal erosion/abrasion potential in a mill, based on the alpha-quartz content of an ASTM ash sample. The procedure involves generating an ash sample from pulverized coal in a muffle furnace at 1380 °F (750° C), consistent with the ASTM protocol for coal ash content determination. This ASTM ash sample is subsequently analyzed quantitatively by X-Ray Diffraction (XRD) for total alpha-quartz content. This result is then compared with results obtained from coal ash samples with which CE has field experience to assess its mill erosion potential.

Generally, the alpha-quartz content in coal is one of the key factors affecting mill wear. This type of information is, therefore, useful for developing a mill erosion/abrasion algorithm. The alpha quartz values found for the test fuels fall in a narrow range of 19-20%, compared with database numbers which vary from 8-24% (Table 2.8). These results indicate that all the Northeastern Unit 4 coal samples tested have moderate to high mill erosion/abrasion potentials.

Size distributions quartz and pyrite contents obtained through CCSEM analyses also yields much information about a given coal/coal bend's potential to cause mill erosion/abrasion. The amount of excluded quartz and pyrite, with their particle size distributions should correlate directly to mill wear. Once a significant database can be established on coal/coal bends that includes CCSEM and mill wear information, an algorithm can be initiated which will correlate the properties of the coal minerals with the mill erosion/abrasion performance.

Table 2.7 Quantities of Excluded Minerals in Northeastern Fuels

LIB. MINERAL (Wt. % of Individual Mineral)	100%WY	90%WY/10%OK	70%WY/30%OK	70%WY/30%OK CLN	100%OK
Quartz	53	52	47	45	48
Calcite	0	82	76	100	83
Kaolinite	33	38	51	52	71
K Al-Silicate	50	50	55	34	54
Aluminosilicate	33	53	60	40	49
Pyrite	75	50	53	61	57
Ca Al-Phosphate	16	55	33	38	0
Wt.% of Total Mineral Excluded	29	35	35	35	46

Table 2.8 Alpha-Quartz Contents in Ash Samples From PSO Northeastern Fuels and Reference Coals

Fuel	ALPHA-QUARTZ IN ASTM ASH, Wt. %
<u>PSO Fuels</u>	
100% WY	20
90% WY/10% OK	20
70% WY/30% OK	19
70% WY/30% OK CLN	20
<u>Reference Coals</u>	
Sub-bituminous:	
Coal A	8
Coal B	16
Coal C	24
High-Vol. Bituminous:	
Coal D	15
Coal E	17
Coal F	22

2.2 REACTIVITIES OF TEST FUELS

2.2.1 Ignitibility /Reactivity Characteristics

A parameter called Flammability Index (FI) was used as a measure of the ignitibility characteristics of each fuel. This test entails firing 0.2 gram of 200x0 mesh fuel in an oxygen atmosphere through a preheated furnace. The temperature of the furnace is raised incrementally until a point is reached where the fuel ignites, as shown in Figure 2.3. This temperature is called Flammability Index. Comparing this value with those of coals in the data bank indicates its relative ignition and turndown (ignition stability) characteristics.

The Flammability Indices (FIs) of the test fuels are given in Table 2.9 The FI values of these coals fall in a narrow range of 780 to 830°F. Comparatively, the FI results in the CE data bank are as follows: 800-1050°F for lignites and subbituminous coals, 1050-1250°F for bituminous coals and 1450-1700+°F for anthracites. Results for the PSO coals indicate that each of the test coals has good ignitibility and ignition stability characteristics. Hence, none of these coals should cause ignitibility or turndown problems if suspension-fired under reasonable operating conditions (fuel fineness, excess air, load, temperature/time history, etc.).

Table 2.9 Flammability Indices of Northeastern Coals and Reference Coals

COALS	FLAMMABILITY INDEX (°F)
<u>PSO Fuels</u>	
100% WY	800
90% WY/10% OK	780
70% WY/30% OK	815
70% WY/30% OK CLN	830
100% OK	1000
<u>Reference Coals</u>	
Lignites-Subbituminous Coals	800 - 1050
Bituminous Coals	1050 - 1250
Anthracites	1450+



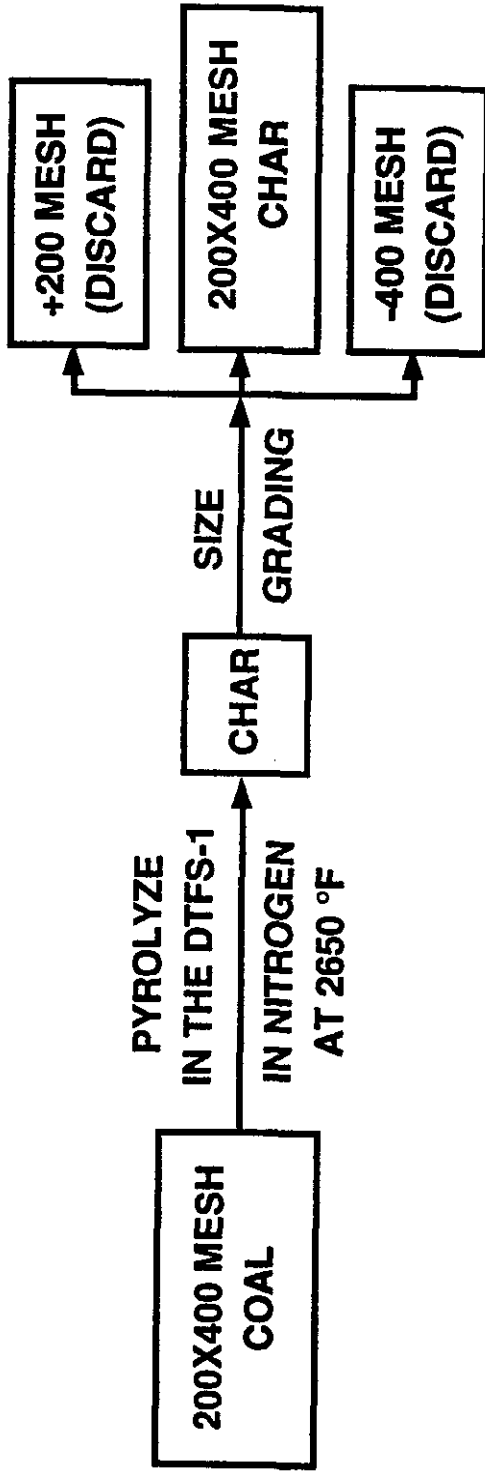
Figure 2.3 Flammability Apparatus

A CE two-step standard procedure for evaluating the reactivities of chars was carried out as follows: (1) a 200x400 mesh size fraction of the solid fuel under study is pyrolyzed in DTFS-1 (See description in Appendix A) in a nitrogen atmosphere at 2650 °F to drive off the volatile matter under appropriate rapid heating conditions, and the resulting char is size-graded to 200x400 mesh; and (2) this 200x400 mesh char is subsequently subjected to thermo-gravimetric analysis (TGA) reactivity testing in air at 1290 °F (700 °C) and BET surface area measurement in nitrogen at -321°F (-196 °C). The char preparation, TGA and BET procedures are depicted schematically in Figure 2.4. The rationale for carrying out these studies on volatile matter-free chars is that char burnout, rather than volatile matter release and burnout, constitutes the rate-determining step in the overall scheme of pulverized coal combustion. While the TGA data give a direct measure of char reactivity, the BET data are used to explain the char reactivity information.

The TGA burn-off curves for the 200x400-mesh chars are given in Figure 2.5 along with those from reference data base coal chars. Results indicate that: (1) The Wyoming coal char is much more reactive than the Oklahoma coal char; (2) the reactivities of the coal blend chars fall in a narrow band, situated between those of the Wyoming and Oklahoma coal chars; (3) the reactivities of the run-of-mine and CQ Inc.-cleaned Oklahoma coal chars are close to one another; (4) The reactivity of both Oklahoma coal chars are slightly lower than that of the West Virginia high volatile A bituminous coal char (from Pittsburgh #8 Coal Seam); and (5) most importantly, all PSO chars prepared from the parent coals and coal blends are much higher in reactivity than a char prepared from a West Virginia medium volatile bituminous coal, which is used as a marginal coal reactivity benchmark, but which is also successfully burned in a CE tangentially-fired utility boiler.

The BET specific pore surface areas of the same 200x400-mesh coal chars are given in Table 2.10 The values for the Wyoming and Oklahoma coal chars are 85 and 13 m²/g [dry-ash-free basis (daf)], respectively, and those of blends from both coals fall in between; the value for the Oklahoma cleaned coal char is 27 m²/g. Comparatively, the BET specific pore surface areas of reference 200x400-mesh chars prepared from a

CHAR PREPARATION (STEP 1)



CHAR EVALUATION (STEP 2)

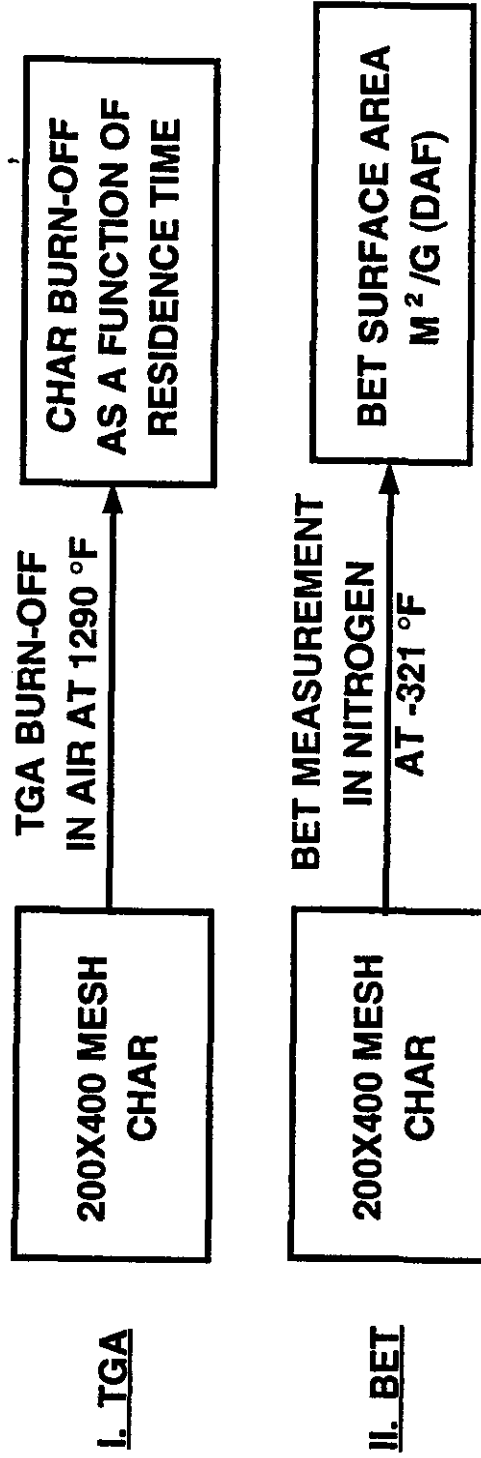


Figure 2.4 Coal Char Preparation and TGA/BET Evaluation

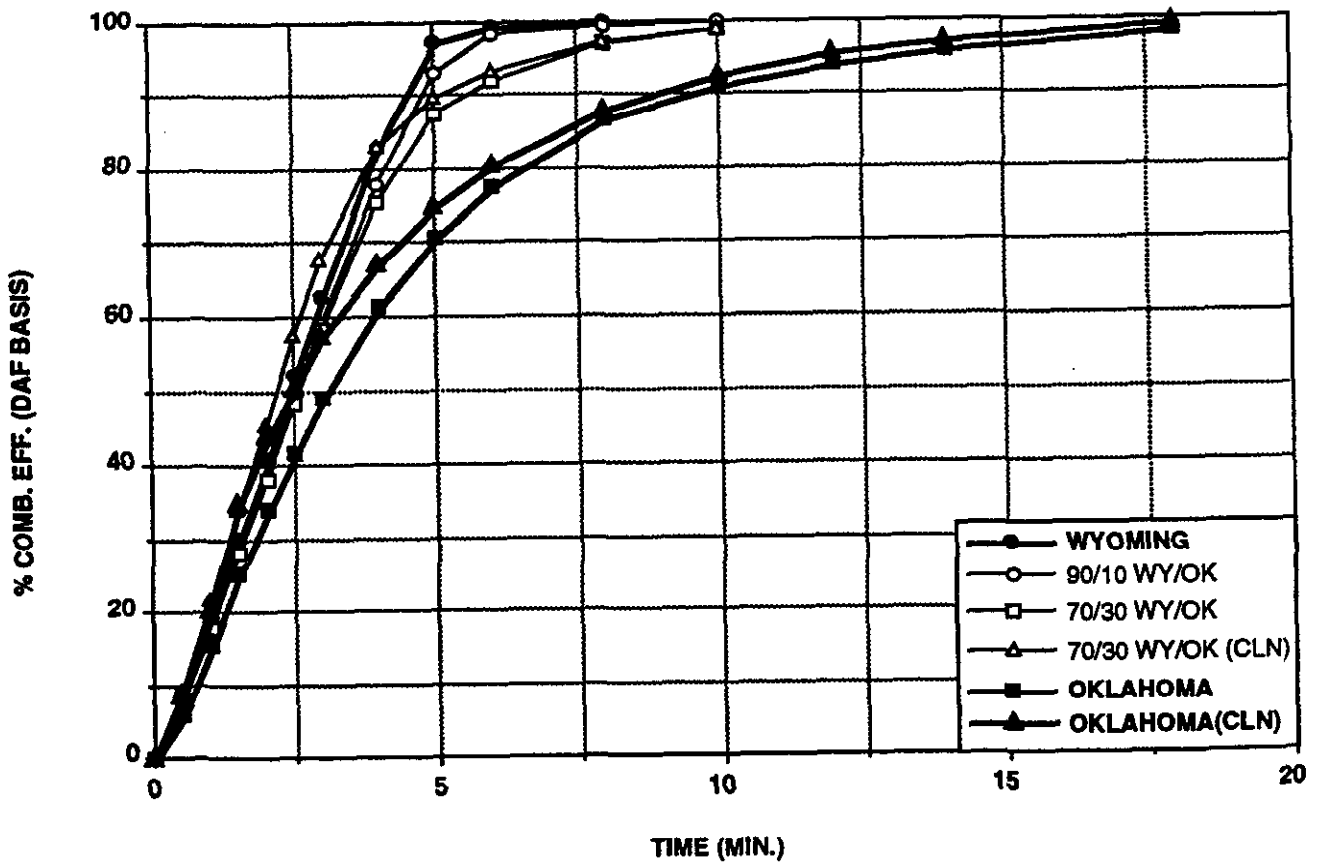
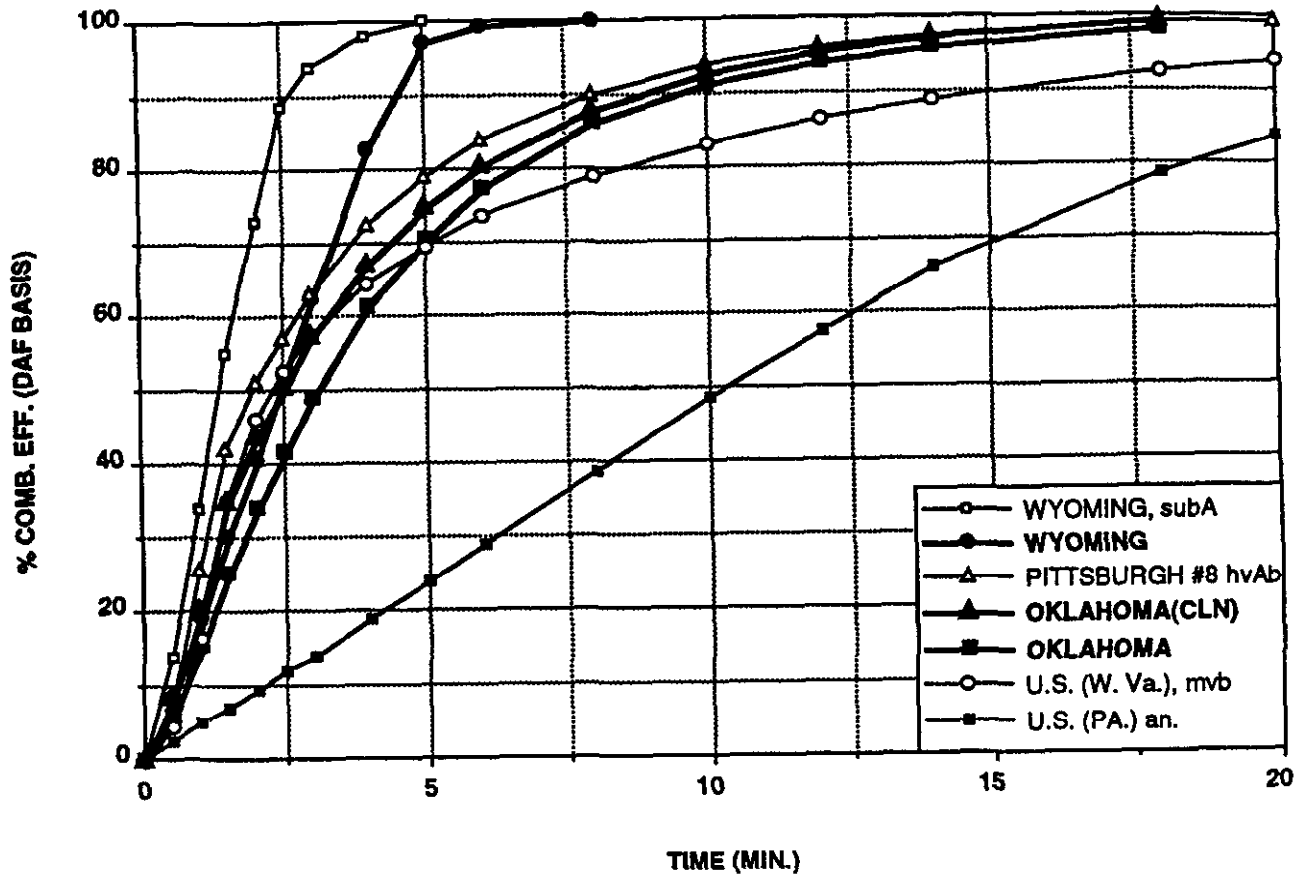


Figure 2.5 TGA Burn-Off Curves In Air at 700°F for PSO and Reference DTFS Coal Chars

Wyoming subbituminous A (subA) coal, a West Virginia high volatile A bituminous (hvAb) coal, a West Virginia medium volatile bituminous (mvb) coal and a Pennsylvania anthracite are 64, 29, 12 and 3 m²/g (daf), respectively.

Table 2.10 BET Surface Areas of Chars Prepared from PSO'S Northeastern Fuels and Reference Coals

COALS	BET SURFACE AREAS (m ² /g)
<u>PSO Fuels</u>	
100% WY	85.3
90% WY/10% OK	77.1
70% WY/30% OK	45.5
70% WY/30% OK CLN	51.5
100% OK	13.3
100% OK(CLN)	27.0
<u>Reference Coals</u>	
Wyoming subA	64.2
W.Va. (Pitts. #8) hvAb	29.0
W.Va. mvb	11.9
Pennsylvania Anthracite	2.6

These results show that the BET surface areas of the PSO coal char samples, like the TGA results, fall in a wide range. The trend exhibited by the BET surface areas is similar to the TGA trend, indicating the role pore structure plays during char reactivity. It is important to note that BET values for all test fuels are higher than the value for a char prepared from the West Virginia medium volatile bituminous coal, which is the marginal reactivity bench-mark.

Inasmuch as char burnout, rather than volatile matter release and burnout, constitutes the rate-determining step in the overall scheme of pulverized fuel combustion, these results indicate that burning the Wyoming subbituminous coal, Oklahoma high volatile bituminous coals or blends thereof in a tangentially-fired utility boiler, should not cause serious carbon loss-related problems, under typical operating conditions (coal fineness, excess air, temperature/time history, load, etc.). A more quantitative assessment of the impact of coal quality and boiler design and operating conditions on carbon loss in the PSO's Northeastern Unit 4 is illustrated in Section 4.

2.2.2 Drop Tube Furnace System-1 (DTFS-1) Combustion Kinetic Parameters of PSO's Northeastern Fuels

CE's DTFS-1 was used to generate a char sample from each coal/coal blend under study and to burn it under specific conditions. The char combustion data were subsequently used to derive its kinetic parameters (apparent activation energy and frequency factor). This facility was also used to derive swelling factors for each coal, which is important for combustion modeling purposes. The DTFS-1 facility, testing procedures and program are briefly described below.

2.2.2.1 Facility Description

The Drop Tube Furnace System-1 (DTFS-1) is comprised of a 1-inch inner diameter horizontal tube gas pre-heater and a 2-inch inner diameter vertical tube test furnace (Figure 2.6) for providing controlled temperature conditions to study devolatilization, gasification and/or combustion phenomena. This entrained flow reactor, which is electrically heated with silicon carbide elements, is capable of heating reacting particles to temperatures of up to 2650 °F and sustaining particle residence times of up to about one second to simulate the rapid heating, suspension firing conditions encountered in pulverized coal-fired boilers.

The DTFS-1 testing procedure entails the following: (1) the fuel is fed at a precisely known rate through a water-cooled injector into the test furnace reaction zone; (2) the fuel and its carrier gas are allowed to rapidly mix with a pre-heated down-flowing secondary gas stream; (3) devolatilization, gasification or combustion is allowed to occur for a specific time (dictated by the transit distance); (4) reactions are rapidly quenched by aspirating the mixture into a water-cooled sampling probe; (5) the solids are separated from gaseous products in a filter medium; and; (6) an aliquot of the effluent gas stream is sent to a dedicated gas analysis system for on-line determination of NO_x, SO₂, O₂, CO₂, CO, and THC (total hydrocarbons) concentrations. A data acquisition system records, on demand, all relevant test data for subsequent retrieval and processing.

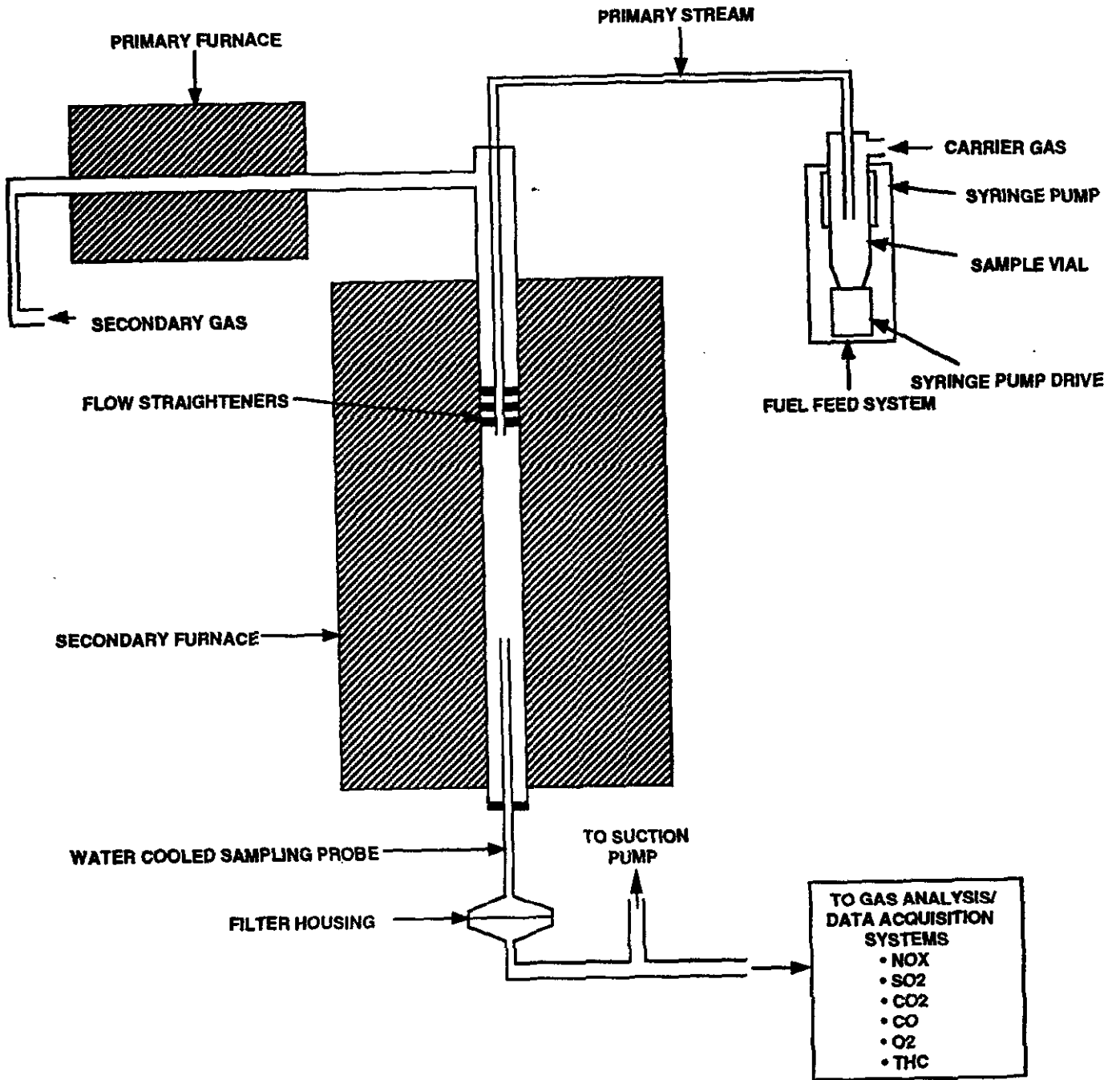


Figure 2.6 Schematic of Drop Tube Furnace System (DTFS-1)

An ash tracer technique (Badzioch and Hawksley, 1970; Nsakala, et al., 1977) is used in conjunction with the proximate analyses of feed samples and chars subsequently generated in the DTFS-1 test furnace to calculate the devolatilization, gasification or combustion efficiency as a function of operational parameters (particle temperature, particle residence time, fuel fineness, reaction medium, etc.). A proprietary software package can, alternatively, use the information on concentrations of CO₂, CO and THC (if available) in the effluent gas streams to calculate carbon conversion rates under prevailing conditions.

The DTFS-1 testing to derive the swelling factors and combustion kinetic parameters of PSO's Northeastern coals/coal chars, and results obtained, are described below.

2.2.2.2 Swelling Factors (α) of Coals

The swelling factors (α) were measured on the test fuels (100% WY, 100% OK and 70% WY/30% OK CLN) which were tested in the DTFS-1 to derive their combustion kinetic parameters. This parameter is important from a combustion modeling standpoint, because it dictates the particle size distribution of a char right after complete devolatilization of its parent fuel.

The procedure for measuring α entails pyrolyzing the test fuel in the DTFS-1 in nitrogen atmosphere at 2650 °F, and collecting chars at various reaction zones (I). The swelling factor is subsequently computed as follows:

$$\alpha = \frac{1}{X_0} \frac{1}{N} \sum_{i=1}^N X_i \quad 2.1$$

where **N** is the number of data points taken (**i** = 1, 2, 3, ... **N**, where points 1, 2, 3, 4 may, for example, stand for 4-, 8-, 12-, and 16-inch reaction zones), and **X_i** are the Rosin-Rammler mean weight particle sizes (Field, et al., 1967) of chars obtained at various reactions zones, and **X₀** is the mean weight particle size of the feedstock.

The swelling factors of the PSO coals are 1.00, 1.25 and 1.20 for Wyoming subbituminous coal, Oklahoma high volatile bituminous coal and 70% WY/30% OK CLN, respectively. These values indicate a narrow, but significant, variability between the test fuels. They are consistent with the chemical natures of their respective fuels. That is: (1) the Wyoming subbituminous coal is a non-swelling (i.e., thermosetting) coal and, as such, has a swelling factor of 1.00; (2) the Oklahoma bituminous coal is of a swelling (i.e., thermoplastic) nature and, hence has a swelling factor which is greater than 1.00. The values found in the CE data bank range from 1.0 to 1.7 (Nsakala, et al., 1986 and 1991).

2.2.2.3 Typical Test Matrix

The typical test matrix used in the present study is depicted in Figure 2.7. Essentially, the 200x400-mesh, volatile matter-free char, generated in the DTFS-1 in nitrogen atmosphere at 2650 °F, is burned in 0.03 atmosphere O₂ (with nitrogen as the balance) at four temperatures (1900, 2150, 2400 and 2650 °F) and data are collected in each case at various transit distances (e.g., 4, 8, 12 and 16 inches from the tip of the solid sample injector), to vary the particle residence times from about 0.1 to 0.8 sec. The rationale for using a volatile matter-free char is that it enables one to study the C-O₂ heterogeneous reaction without interference from burning volatile species. The data from this study were subsequently used to derive the combustion kinetic parameters of interest.

2.2.2.4 Combustion Kinetic Parameters of Chars

The char combustion efficiency results obtained by means of the test matrix shown previously in Figure 2.7 are given in Figure 2.8 as a function of both particle temperature (Nsakala, et al., 1985) and time.

These results clearly show that both temperature and time play major roles in char combustion efficiency; the higher the temperature and/or the longer the time, the higher the combustion efficiency. The nature of a char also plays a major role in its combustion efficiency, given a prescribed temperature/time history. The DTFS-1 data reproducibility is quite good (compare T1 with T1R and T4 with T4R cases).

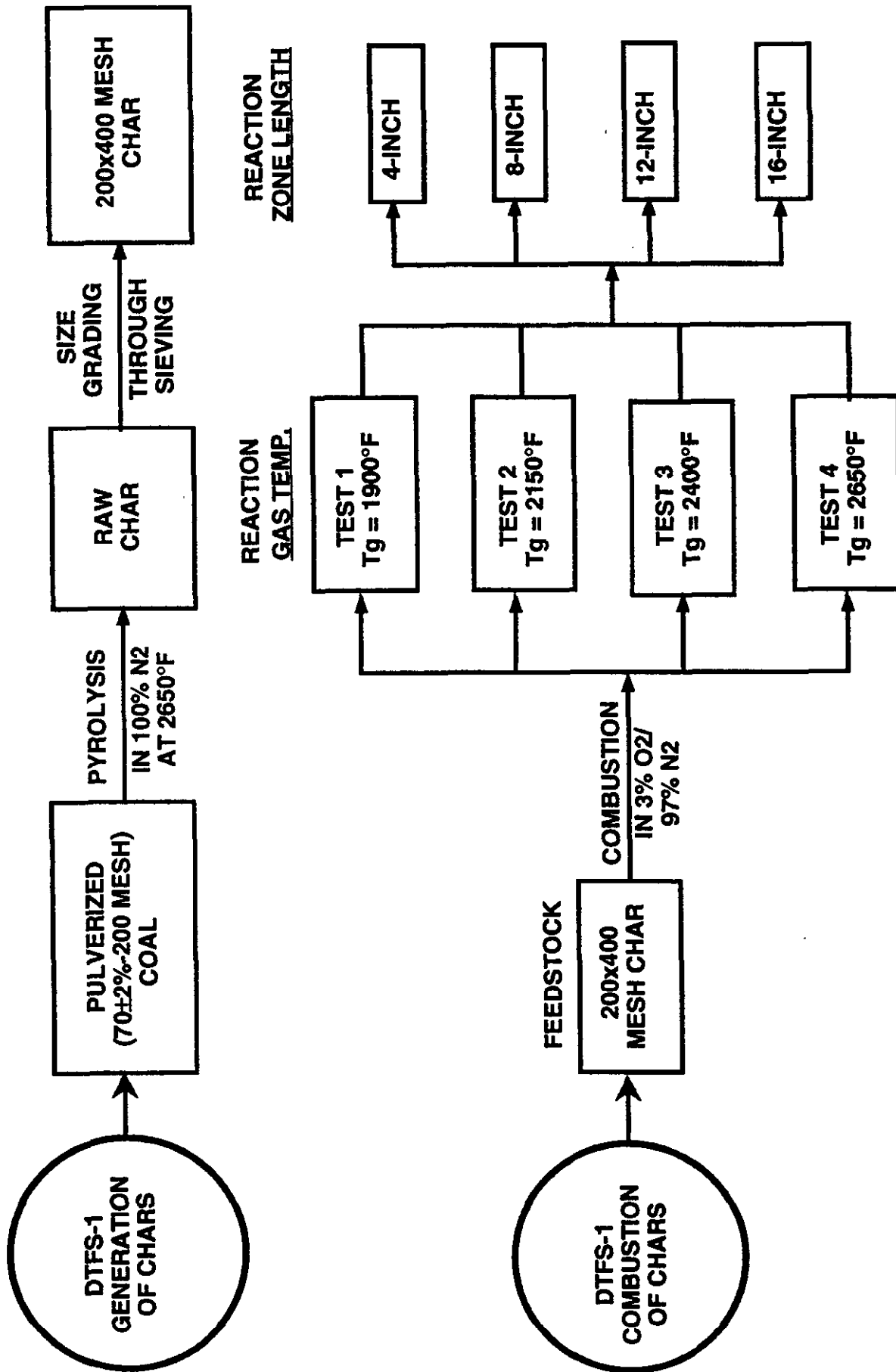


FIGURE 2.7 DTFS-1 DETERMINATION OF COAL CHARS' COMBUSTION KINETIC PARAMETERS

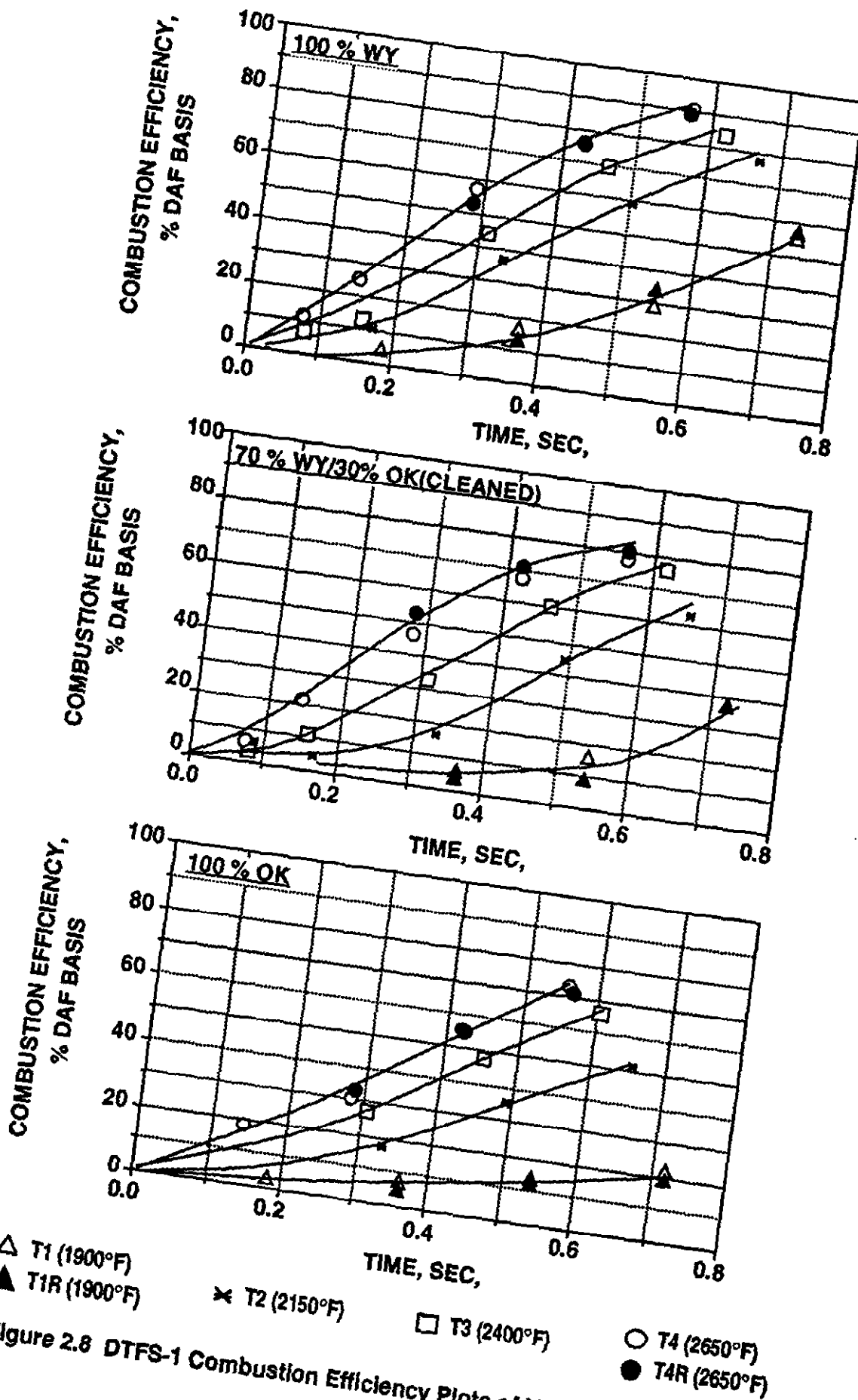


Figure 2.8 DTFS-1 Combustion Efficiency Plots of Various 200x400 Mesh PSO Coal/Coal-Blend Chars

To put the total picture in perspective, all the combustion efficiency curves for 2650 and 1900 °F are re-plotted in Figure 2.9. These results clearly show that: (1) for the 2650 °F case a char combustion efficiency trend of $\eta_{100\% \text{ WY}} > \eta_{70\% \text{ WY}/30\% \text{ OK CLN}} > \eta_{100\% \text{ OK}}$ emerges, where η stands for char combustion efficiency (expressed as a percentage of the original dry-ash-free char) and the subscripts describe the fuel-types used; and (2) for the 1900 °F case, while the combustion efficiency of the 100% WY char is still the highest, those of 70% WY/30% OK CLN and 100% OK chars are roughly equivalent. These apparent disparities are simply due to differences in temperature sensitivities of the chars under study. This is actually one of the technical arguments used by the authors in stipulating that it is prudent to measure, rather than to assume, the apparent activation energies and frequency factors of unknown chars, especially if subsequent combustion performance modeling studies of their parent fuels require high confidence levels.

The combustion efficiency results given in Figure 2.8 were used to determine the overall rates of carbon removal per unit external surface areas (K), assuming the following:

- The carbon-oxygen reaction proceeds by a shrinking-core mechanism (it is recognized that chars resulting from thermoplastic and thermosetting coals will have different shapes), and;
- CO is the primary surface reaction product, which is oxidized to CO₂ in the boundary layer.

The diffusional reaction rate coefficients (K_D) were computed using the classical relationship (Field, et al., 1967):

$$K_D = 24 \frac{D\emptyset}{XRT_g} \quad 2.2$$

where \emptyset is the mechanism factor (a value of 2 indicating that CO is the primary reaction product), D is the binary diffusion coefficient of oxygen through the nitrogen gas carrier (cm²/sec.), X is the fuel particle size (cm), R' is the gas constant (82.06 atm. cm³/mole °K) and T_g is the gas temperature in the boundary layer (°K).

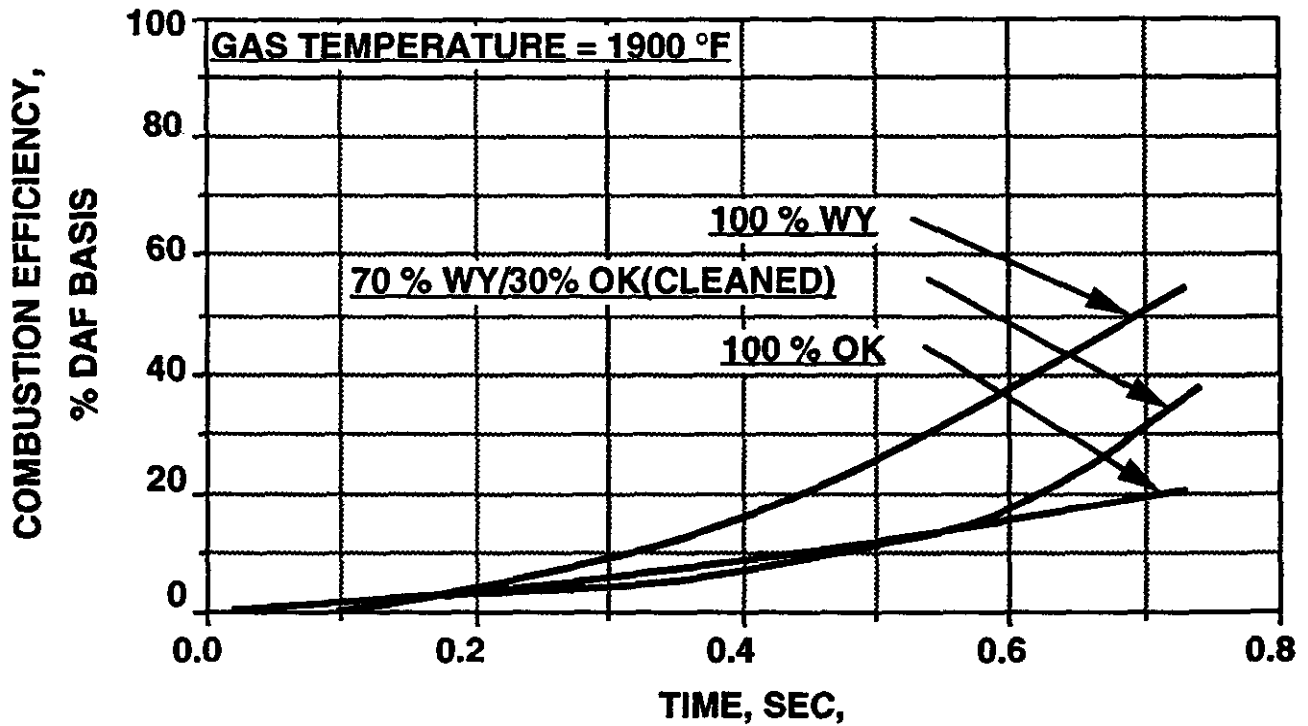
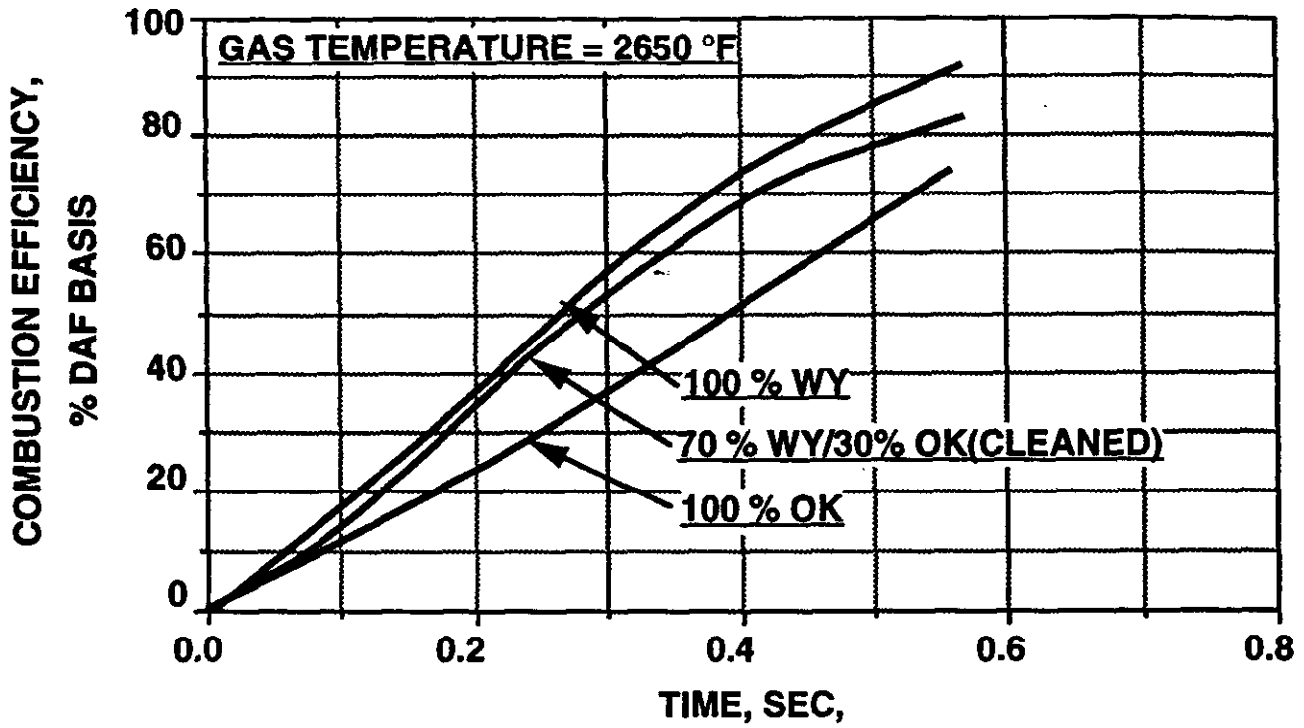


Figure 2.9 Effect of Fuel Type on DTFS-1 Combustion Efficiencies of Various 200X400 Mesh PSO Coals/Coal Blends at Two Gas Temperatures

The values of K were used in conjunction with corresponding K_D values to derive the surface reaction rate coefficients (K_s) according to the relation:

$$\frac{1}{K} = \frac{1}{K_D} + \frac{1}{K_s} \quad 2.3$$

which can be rearranged to:

$$K_s = \frac{KK_D}{K_D - K} \quad 2.4$$

A first order, with respect to oxygen partial pressure, Arrhenius Equation is applied to the data as follows:

$$K_s = A \exp \left(- \frac{E}{RT_p} \right) \quad 2.5$$

where E, A, R and T_p are, respectively, the apparent activation energy, frequency factor, universal gas constant and calculated particle surface temperature (Nsakala, et al., 1985). The experimental conditions are such that $K \ll K_D$ in all cases, ensuring that the external diffusion of oxygen to the particle surface does not constitute a rate-determining step in the K_s derivations.

Plotting K_s vs. $1/T_p$ (Table 2.11) yields straight lines (Figure 2.10) from which the values of E and A can be obtained from the slopes and intercepts of the least squares fits. The least squares fit lines of Figure 2.10 are placed in one single frame in Figure 2.11 to show the variabilities in their slopes, hence, in their apparent activation energies.

The combustion kinetic parameters obtained from this study are summarized in Table 2.12 along with other relevant data (swelling factors of fuels and mercury densities and of chars). The apparent activation energies are 19.2, 22.9 and 24.3 kcal/mole for the Wyoming, 70% Wyoming/30% Oklahoma CLN and Oklahoma coal chars, respectively. The corresponding frequency factors are 17.7, 55.6 and 70.1 g/cm² sec.

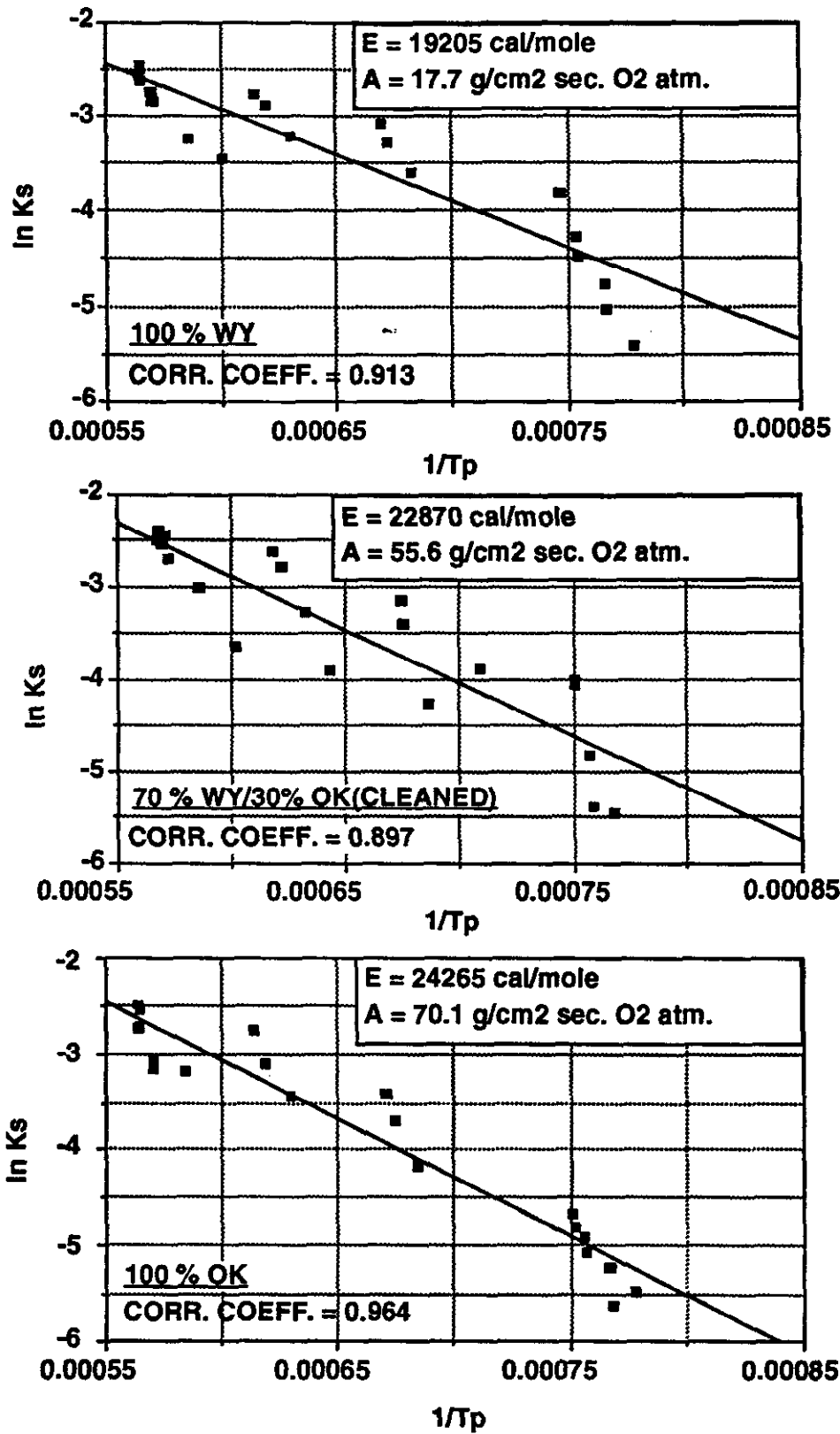


FIGURE 2.10 ARRHENIUS PLOT FOR 200X400 MESH PSO'S COAL CHARS' COMBUSTION IN THE DTFS-1

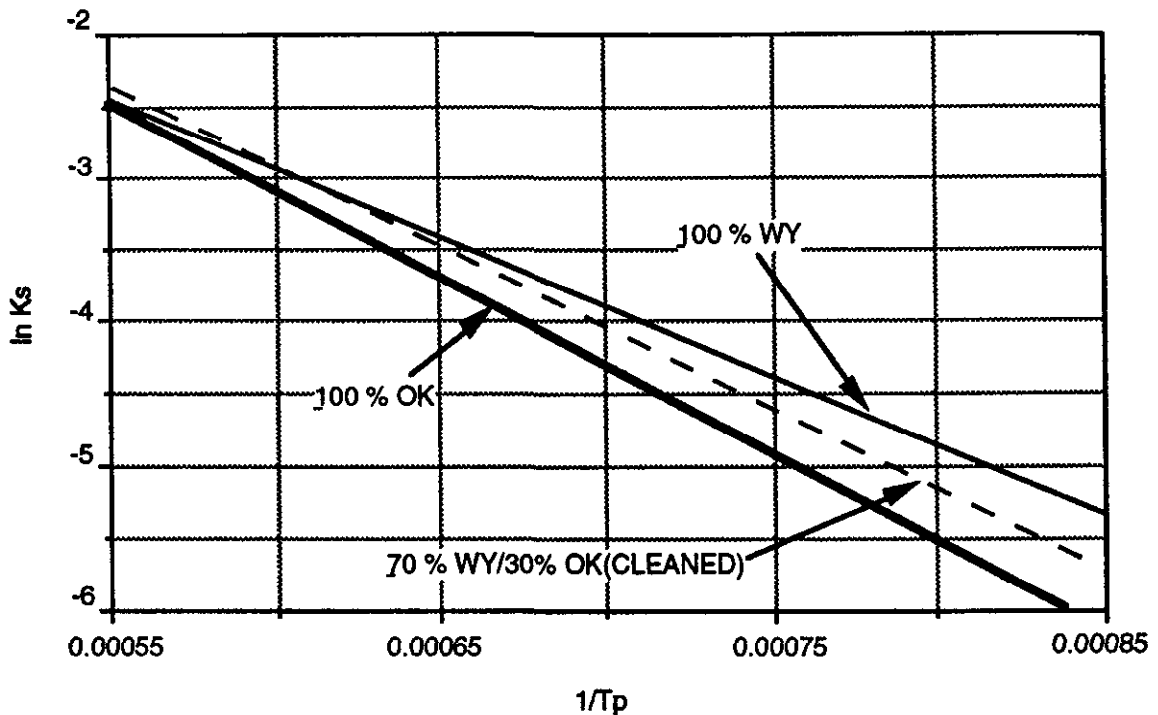


Figure 2.11 Comparison of Arrhenius Lines of Three PSO Fuels

(O₂ atm.) These results indicate a significant variability in temperature sensitivity between the three coal chars. The Wyoming coal char is much less sensitive to temperature than the Oklahoma coal char; i.e., at relatively lower temperatures, it would react more efficiently than the Oklahoma coal char.

The combustion kinetic parameters from this study are plotted as K_s vs. $1/T_p$ in Figure 2.12 along with some selected literature values obtained by the present and other investigators (Beer, et al., 1961; Field, et al., 1967; Nsakala, et al., 1985; Mitchell, 1987). While the present results are of the same order of magnitude as those obtained previously by the present authors, the variabilities in surface reactivities of the various chars given in Figure 2.12 extend over orders of magnitudes. These differences are due to actual differences in char reactivities and in experimental techniques used. Differences in reaction rates are manifested as a functions of pore structure, char density, swelling and the assumed reaction order. Significant variance in reaction rate can result from variations in a single parameter or a combination of small changes in several parameters. These differences clearly indicate that using char combustion

kinetic parameters from the open literature for modelling purposes could lead to spurious results. This practice should, therefore, only be used with utmost circumspection.

Table 2.11 Kinetic Data From DTFS-1 Combustion of 200X400 Mesh PSO Coal Chars in 0.03 ATM. O₂ and 1285-1760 °K Particle Surface Temperature Range

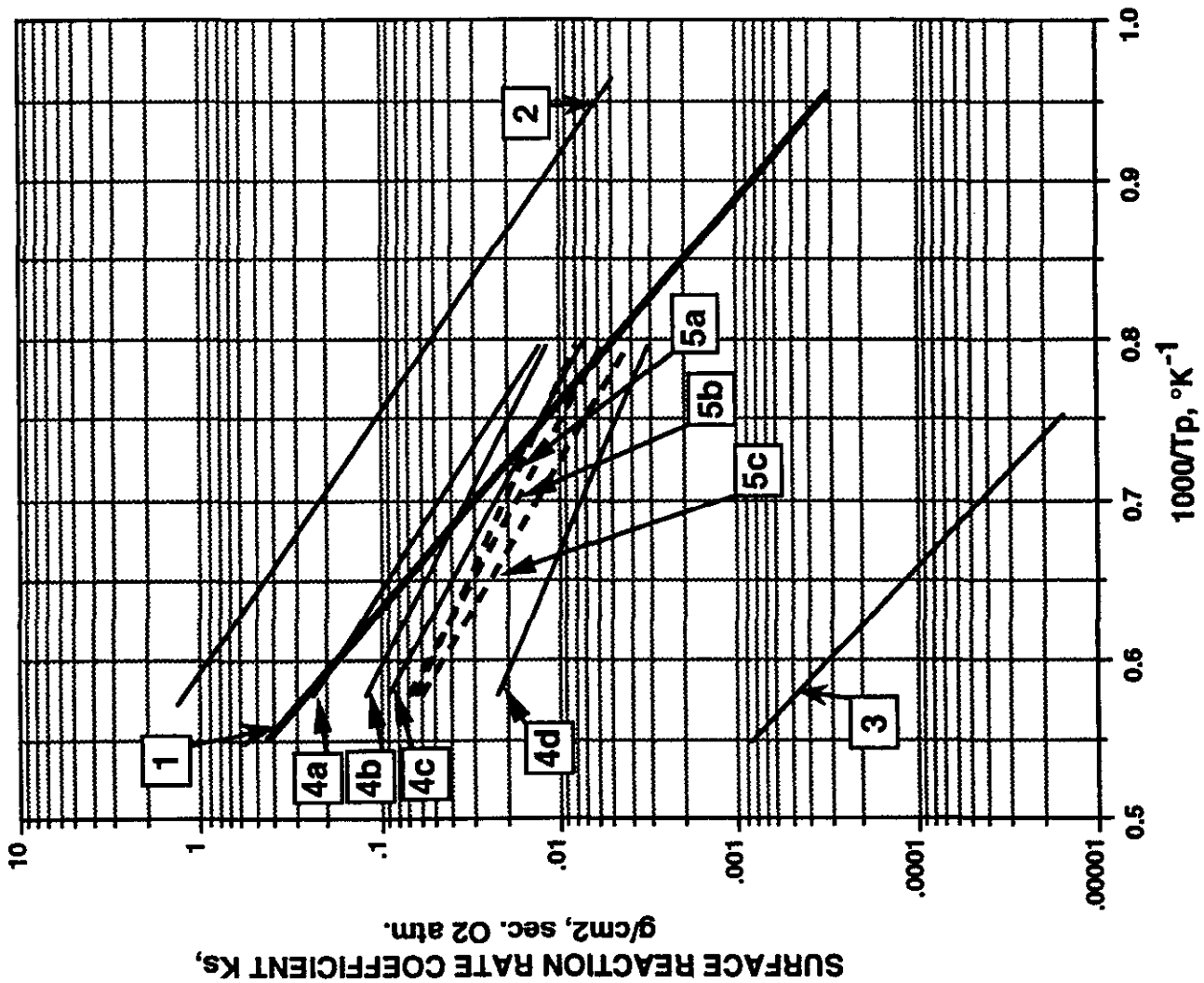
100% WY		70% WY/30% OK CLN		100% OK	
T _p	K _s	T _p	K _s	T _p	K _s
1285	0.0045	1302	0.0042	1286	0.0041
1304	0.0086	1321	0.0081	1303	0.0053
1322	0.0112	1333	0.0174	1321	0.0072
1332	0.0212	—	—	1330	0.0094
—	—	—	—	—	—
1303	0.0066	1317	0.0046	1302	0.0036
1323	0.0136	1333	0.0182	1321	0.0063
1332	0.0214	—	—	1329	0.0083
—	—	—	—	—	—
1461	0.0267	1410	0.0205	1459	0.0153
1487	0.0355	1457	0.0140	1480	0.0244
1479	0.0420	1481	0.0333	1484	0.0319
—	—	1484	0.0432	—	—
—	—	—	—	—	—
1581	0.0385	1556	0.0201	1582	0.0315
1603	0.0520	1582	0.0383	1608	0.0430
1610	0.0558	1609	0.0621	1618	0.0579
—	—	1617	0.0725	—	—
—	—	—	—	—	—
1666	0.0313	1662	0.0264	1709	0.0410
1704	0.0382	1709	0.0497	1745	0.0413
1745	0.0600	1750	0.0674	1762	0.0603
1755	0.0649	1761	0.0825	1758	0.0741
1748	0.0716	1756	0.0792	—	—
—	—	—	—	—	—
1743	0.0554	1752	0.0862	1747	0.0446
1755	0.0691	1762	0.0907	1761	0.0619
1748	0.0692	1756	0.0836	1757	0.0701
<u>Kinetic Parameters</u>		<u>Kinetic Parameters</u>		<u>Kinetic Parameters</u>	
E =	19205	E =	22870	E =	24265
A =	17.7	A =	55.6	A =	70.1
y =	-0.913	y =	-0.897	y =	-0.964

T_p = Particle Surface Temperature, °K

K_s = Surface Reaction Rate Coefficient, g/cm² sec. O₂ atm

E = Apparent Activation Energy, cal/mol

A = Frequency Factor, g/cm² sec. O₂ atm



- 1 VARIOUS CARBONS, FIELD ET AL. (1967)
- 2 SANDIA, MITCHEL ET AL. (1987)
- 3 ANTHRACITE, BEER ET AL. (1961)

- 4a subB
 - 4b ligA
 - 4c hvAb
 - 4d anthracite
- NSAKALA, ET AL. (1985)

THIS DOE/CQE PROGRAM
NORTHEASTERN'S COALS

- 5a 100% WYOMING (WY)
- 5b 70% WY/30% OK
- 5c 100% OKLAHOMA

FIGURE 2.12 RELATIONSHIP BETWEEN SURFACE REACTIVITY COEFFICIENT AND SURFACE TEMPERATURE FOR PRESENT STUDY AND SOME LITERATURE DATA

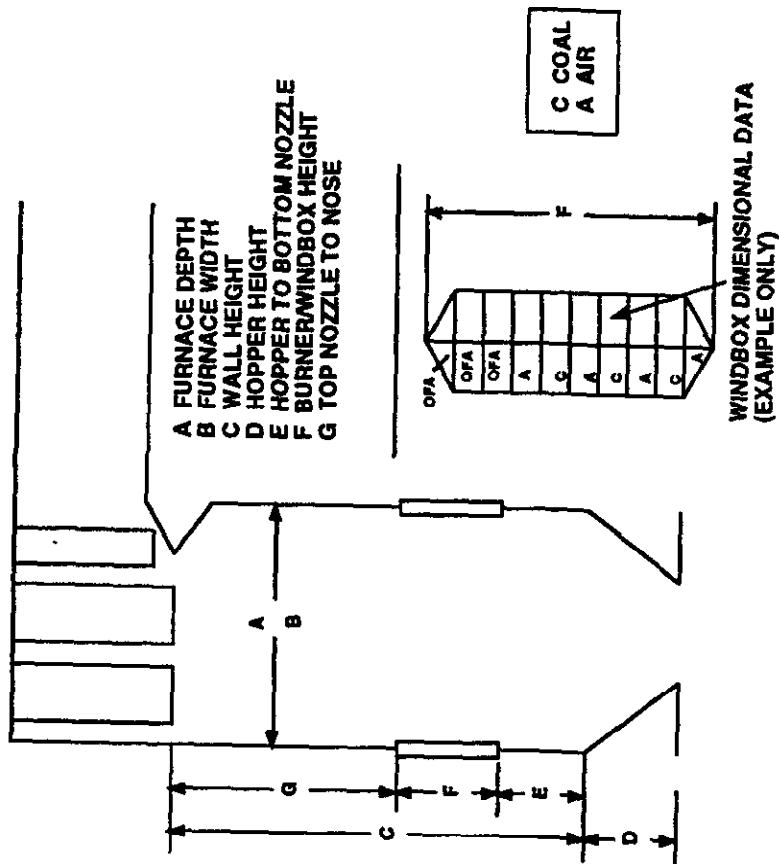
Table 2.12 Combustion Kinetic Parameters of PSO Northeastern Coals/Chars

Coal	α	ρ (g/cm ³)	A (g/cm ³ sec. O ₂ atm)	E (cal/mole)
100% WY	1.00	0.62	17.7	19205
70% WY/30% OK (CLN)	1.20	0.88	55.6	22870
100% OK	1.25	0.86	70.1	24265

2.2.2.5 Combustion Kinetic Data Base for Algorithm Development

To model the combustion performance of a fuel in a given boiler, key information, needed includes: (1) the physical and chemical characteristics of the fuel concerned; (2) the combustion kinetic parameters of the char produced from the coal; and (3) the boiler design and operating specifications. Details of this data requirement and methodology are presented in Figures 2.13a and 2.13b. A methodology for predicting, principally, carbon heat losses, is shown in Section 4 (Combustion Performance Modeling).

It is, however, important to note that the combustion kinetic information on specific coals are not readily available. Combustion kinetic information can, therefore, be cautiously used on a surrogate basis; in such a case a database is needed from which to obtain the kinetic information. The kinetic information derived so far from this work is presented in Table 2.13 along with the kinetic information derived previously in this laboratory, under the DOE/PETC and EPRI auspices (Goetz, et. al., 1983; Nsakala, et. al., 1985, 1987 and 1991). This methodology has been successfully applied, as illustrated in Figure 2.14, for predicting combustion performance in commercial pulverized coal-fired boilers. Key to the success or failure of this prediction procedure is the accuracy to which the fuel parameters are defined (i.e., kinetics, carbon content, ash content, swelling factors etc.). It is the combination of these variables which produces an accurate simulation. ABB CE is in the process of developing (following the guidelines given in Figures 2.13 (a&b)) an algorithm geared towards the proper selection of combustion kinetic information on a surrogate basis.



- 0 % EXCESS AIR
- 0 % OVER FIRE AIR (% OFA) (IF ANY)
- 0 % GAS RECIRCULATION (IF ANY)
- 0 COAL FEED RATE
- 0 COAL FINENESS (% ON 50 OR 100 MESH AND % - 200 MESH)
- 0 COAL ANALYSIS

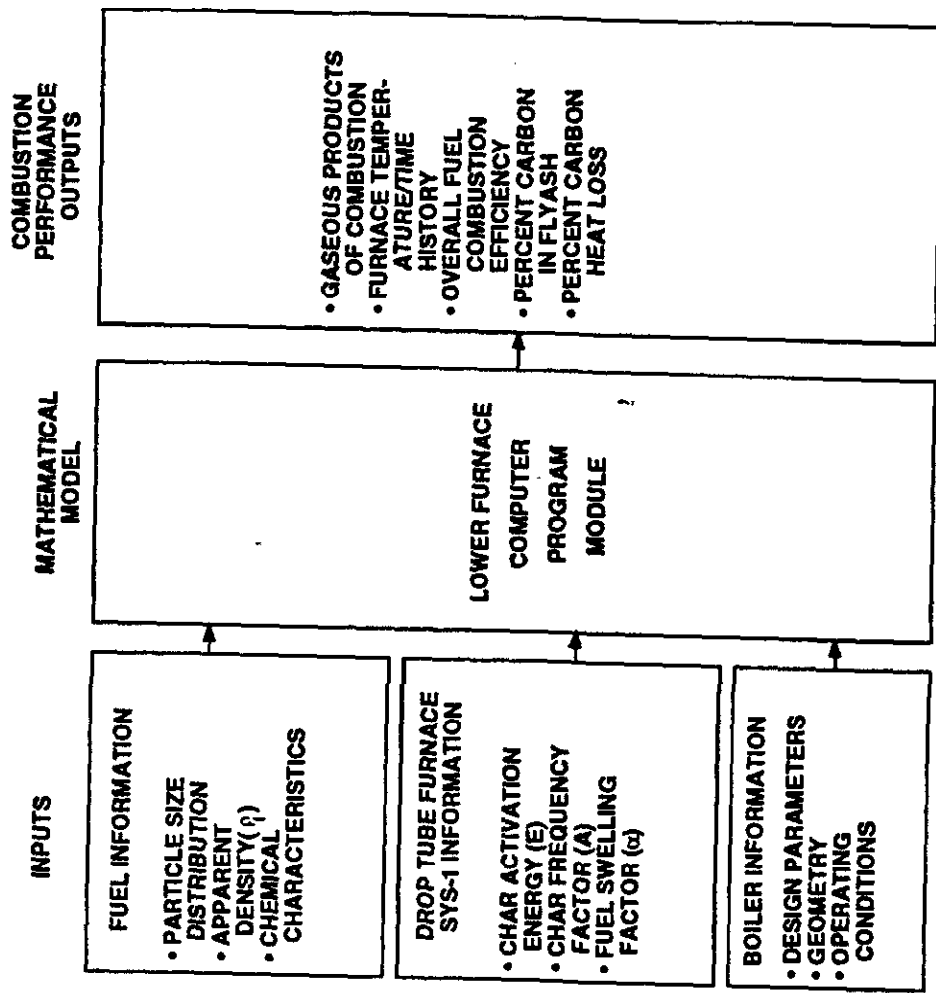


FIGURE 2.13a BOILER DIMENSIONAL/OPERATING DATA REQUIRED FOR ABB CE'S LFP-SKM INPUTS

FIGURE 2.13b FLOW DIAGRAM FOR ABB CE'S LFP-SKM SIMULATION

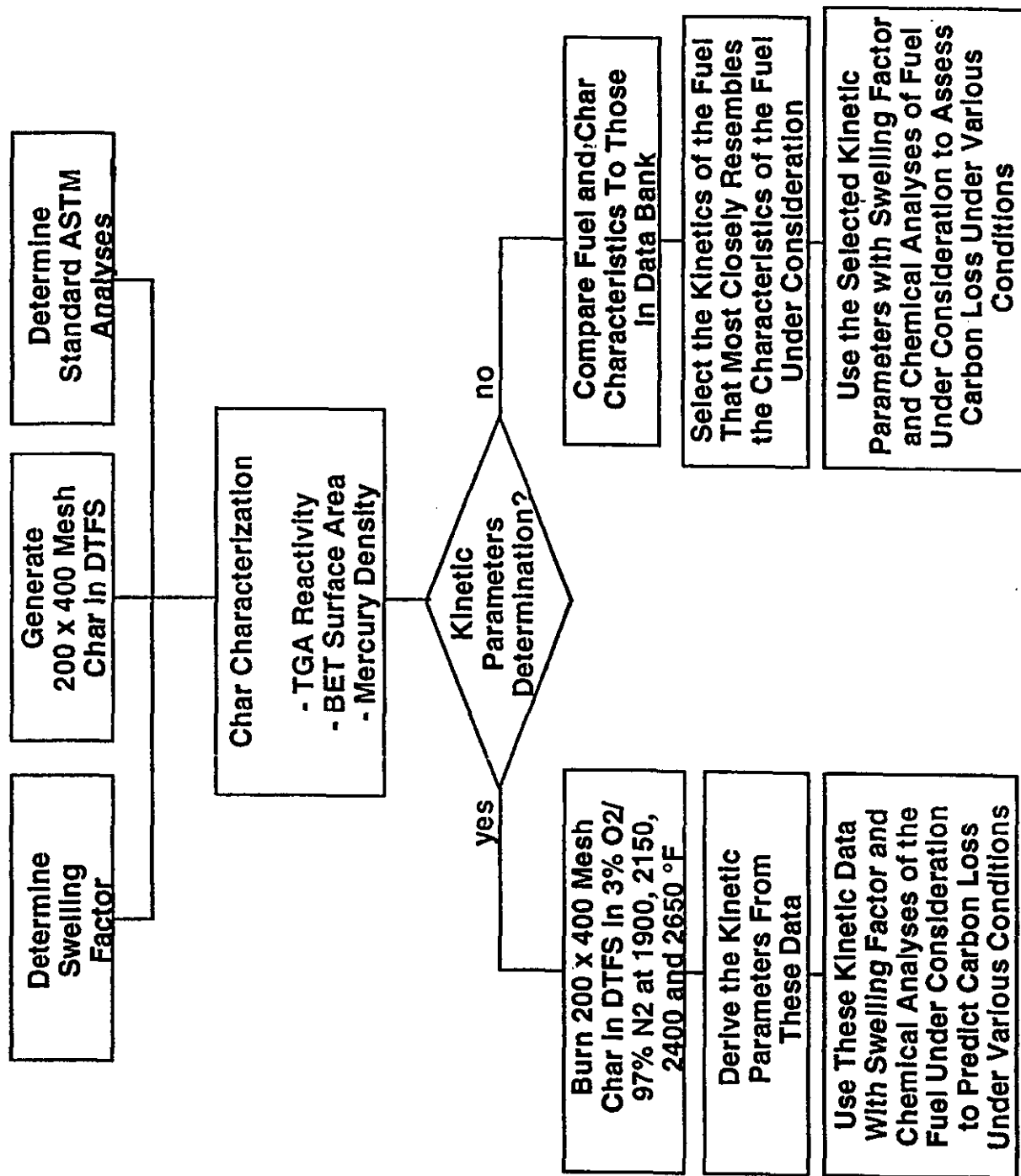


FIGURE 2.14 PROCEDURE FOR CHOOSING SURROGATE COAL COMBUSTION KINETIC PARAMETERS FOR MODELING PURPOSES

Table 2.13 COMBUSTION KINETIC INFORMATION DATABASE OF DOE- AND EPRI-SPONSORED WORK

SPONSOR	FUEL TYPE	σ	S_{set} m ² /g(daf)	ρ (g/cm ³)	A (g/cm ² sec. O ₂ atm.)	E (kcal/mole)
DOE/CQE	100% WY	1.00	85.3	0.62	17.7	19.2
	90% WY/10% OK	"	77.1	"	"	"
	70% WY/30% OK	"	45.5	"	"	"
	70% WY/30% OK (CLN)	1.20	51.5	0.88	55.6	22.9
	100% OK	1.25	13.3	0.86	70.1	24.3
	100% OK (CLN)	"	27.0	"	"	"
DOE/BCF	Ill. #6 hvCb	1.19	33.1	"	"	"
	Ill. #6 MFP ^a	1.00	31.0	0.66	0.47	10.9
	Ill. #6 SOAP ^b	1.30	42.0	0.66	25.4	23.2
	Pitts. #8 hvAb	1.67	44.8	"	"	"
	Pitts. #8 MFP	1.20	37.4	0.53	0.79	12.6
	Pitts. #8 SOAP	1.28	31.9	0.49	5.00	18.0
	Upper Freeport mvb	1.54	23.6	"	"	"
	Upper Freeport MFP	1.33	17.8	0.59	2.17	14.2
	Upper Freeport SOAP	1.25	35.4	0.33	17.0	24.8
		Texas Ilg. A	1.00	191.3	0.79	57.0
	Montana subB	1.00	89.9	0.69	563.0	26.7
	Alabama hvAb	1.34	16.4	0.86	80.0	23.3
	Pa. anthracite	1.00	2.6	1.62	4.3	18.0
EPRI ^c	Wyoming subC	1.00	97.4	"	145.0	20.0
	Ill. #6 hvCb	"	54.4	"	60.0	17.2
	Pitts. #8 hvAb	"	12.9	"	66.0	20.4
	Texas Ilg. EDS Residue	"	44.0	0.83	25.5	19.3
	Wyodak subB EDS Residue	"	47.0	0.78	21.5	18.3
	Ill. #6 hvCb EDS Residue	"	48.0	0.67	64.	22.4
	Lurgi Pyrolysis Char	"	26.0	1.00	648.0	33.0
			"			

a. MFP = Microbubble Flotation Process (Hervol and Feeley, Ill, 1987)

b. SOAP = Spherical Oil-Agglomeration Process (Schaal and Lippsmeyer, 1990)

c. Nsakala, et al., 1985

d. Goetz, et al., 1983; Chow and Nsakala, 1983; and Nsakala, et. al., 1987

2.3. ASH DEPOSITION/DEPOSIT FORMATION

The objective of EERC's Drop Tube Furnace work (Figure 2.15, description in Appendix A) was to produce fundamental, bench-scale ash deposits under highly-controlled conditions in order to determine the critical temperatures and conditions under which deposits form and develop strength. State-of-the-art analytical methodologies were used to identify key components in the deposits that are responsible for ash deposit formation as a function of selected boiler operating conditions. The ultimate goal is to use these results along with those from the pilot-scale and field units to develop a framework for fouling and slagging algorithms that will enhance the CQE program.

PSO coal samples generated in the FPTF were tested in the drop-tube furnace to evaluate deposit collection efficiencies, initial slagging temperatures, deposit crushing strengths and deposit compositions. Particle residence times and gas cooling rates can be varied to simulate specific slagging/fouling within pilot-scale and full-scale boilers. For tests performed on the PSO coals, furnace conditions were used to study the slagging behavior of each coal or blend to develop fundamental understanding of the deposits formed in the FPTF and the field unit.

Temperatures at which slagging initiates were determined by monitoring the gas temperature and character of the deposit. Constant feed rates and excess oxygen levels were maintained as consistent as possible for all tests. The 100% WY coal was burned in the drop-tube furnace at a furnace temperature that produced a molten deposit after approximately 1-2 mm growth in height from the substrate. The substrate temperatures were kept at approximately 350 °C (660 °F). The furnace temperature was increased until deposits showed signs of the sintered ash just starting to fuse as the deposits grew; fused ash formed towards the top to the deposits when they were grown to a height of about 10 mm. Furnace temperatures were adjusted according to the ash fusion results for the four field-tested PSO coal samples (Table 2.1). Minor adjustments were made in the furnace temperature until the deposits grown from the blends appeared to have the same degree of ash fusion as the Wyoming coal. For all deposits grown, an excess air of approximately 40% was used. One (1) actual liter per

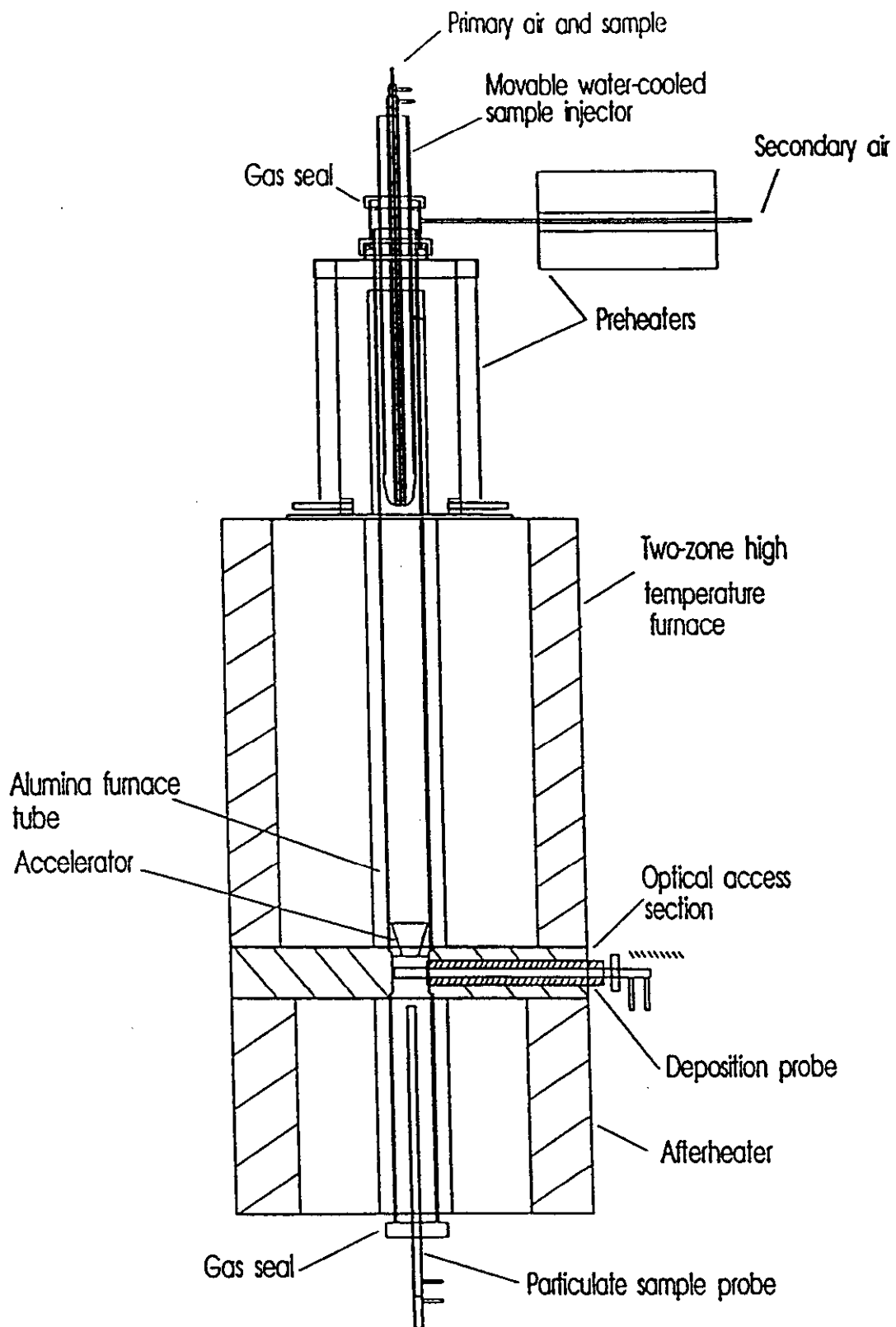


Figure 2.15 Schematic of EERC Drop Tube Furnace

minute of air was used as the primary air to carry the coal into the furnace. Three (3) actual liters per minute of N₂ was used as the secondary gas to provide the laminar flow in the furnace. Due to the small amount of air used in the DTF, a slight variation of the feed rate has a great influence on the excess air level. For all coals tested, the sticking fractions of the deposits (ash deposited/ash fired) were determined. The combustion parameters used are given in Table 2.14. Initial slagging temperatures for the fuels are listed as 1450-1475 °C for 100% WY, 1456-1483°C for 90% WY/10% OK, 1455-1480 °C for 70% WY/30% OK blend, and 1465-1485 °C 70% WY/30% OK CLN blend. Under normal conditions, therefore, it is hypothesized that the 100% WY coal would be the worst of the four fuels with regard to slagging. These results are in general agreement with ash slagging performance established during pilot-scale and field testing.

2.3.1 Deposit Description

Each deposit produced was megascopically examined to provide a general morphological description. These descriptions provide a basis for general comparisons with other deposits by experienced EERC personnel.

The base (initial) part of the 100% WY deposit was tan-white in color and had a very fine grain texture. The main (bulk) portion was light tan in color nearest the base and darker tan-brown at the deposit tip (furthest point facing into the gas stream). The bulk deposit was 12 mm high, 1.5 mm wide at its midpoint, and 6 mm wide at its base; the top 2 mm consisted of beaded slag.

The initial ash deposit of the 90% WY/10% OK fuel was tan-white fine ash with darker tan-brown, larger particles scattered throughout. The bulk deposit was tan in color, 12 mm high and 1.5 mm wide at its midpoint. A larger amount of slag was formed at the tip of the deposit compared to the 100% WY deposit sample.

The 70% WY/30% OK initial deposit sample was tan-white in color, was fine-grained, and had darker, tan-brown larger particles scattered throughout, similar to the 90%

WY/10% OK deposit sample. The 70% WY/30% OK deposit had a length of 9-11 mm (slightly shorter than those of the other deposit samples) and a midpoint width of 1.5 mm. The bulk deposit was darker tan in color toward its tip.

The initial deposit of the 70% WY/30% OK CLN fuel showed a fine light gray ash covered with a more prevalent tan-colored fine ash. The bulk deposit was tan-colored nearer the base and increasingly gray in color toward the tip. This deposit was 10 mm long and 2 mm wide.

2.3.2 Determination of Deposit Strengths

Deposits formed in the drop-tube furnace were removed from the coupons and measured for strength at ambient temperature. The apparatus used to determine the crushing strength of these ash deposits is shown in Figure 2.16. It consists of a miniature horizontal translator and a miniature pressure transducer. The translator (Ealing Electro Optics Model 37-0254) has a range of travel of 25 mm, a resolution of 0.1 μm , and a maximum translational speed of 15 mm/min. The pressure transducer (Precision Measurement Company Model 156) is a diaphragm strain gauge design with one active sensing face. The pressure range is 0-1000 psi. The transducer output is attached to a strain transducer indicator (Precision Measurement Company Model X). The transducer is mounted in a slot on top of an aluminum block and attached to the horizontal translator. A rod inserted in the side of the block meets the sensing face of the transducer and transmits the force exerted on the deposit as the translator moves.

Table 2.14 Drop Tube Furnace (DTF) Test Matrix for Ash Deposit Generation

100% WY

	<u>Test 1</u>	<u>Test 2</u>	<u>Test 3</u>	<u>Test 4</u>	<u>Test 5</u>
Gas Flow Rates (l/min)					
Primary Air	1	1	1	1	1
Secondary Air	3	3	3	3	3
Vacuum	4.2	4.2	4.2	4.2	4.2
Temperatures (°C)					
Injector	amb	amb	amb	amb	amb
Secondary Air	1104	1139	1104	1103	1102
Furnace 1 Upper	1473	1539	1470	1470	1470
Furnace 1 Lower	1455	1545	1466	1465	1466
Run Duration (min)	30.0	30.0	15.0	10.0	5.0
Residence Time (sec)	2	2	2	2	2
Coal Burned (g)	3.73	3.40	1.21	0.86	0.38
Coal Feed Rate (g/min)	0.12	0.11	0.08	0.09	0.08
Ash Collected (g)	0.13	0.12	0.04	0.03	0.01
Coal Ash (%)	7.9	7.9	7.9	7.9	7.9
Ash Fed (g)	0.29	0.27	0.1	0.07	0.03
Sticking Fraction	0.44	0.43	0.42	0.40	0.39

90% WY/10% OK

	<u>Test 1</u>	<u>Test 2</u>	<u>Test 3</u>	<u>Test 4</u>	<u>Test 5</u>	<u>Test 6</u>
Gas Flow Rates (l/min)						
Primary Air	1	1	1	1	1	1
Secondary Air	3	3	3	3	3	3
Vacuum	4.2	4.2	4.2	4.2	4.2	4.2
Temperatures (°C)						
Injector	amb	amb	amb	amb	amb	amb
Secondary Air	1106	1106	1110	1106	1104	1106
Furnace 1 Upper	1482	1482	1492	1481	1482	1484
Furnace 1 Lower	1459	1464	1477	1463	1466	1463
Run Duration (min)	30.0	30.0	20.0	15.0	10.0	5.0
Residence Time (sec)	2	2	2	2	2	2
Coal Burned (g)	2.96	3.18	2.03	1.78	1.08	0.53
Coal Feed Rate (g/min)	0.10	0.11	0.10	0.12	0.11	0.11
Ash Collected (g)	0.11	0.12	0.08	0.07	0.04	0.02
Coal Ash (%)	7.1	7.1	7.1	7.1	7.1	7.1
Ash Fed (g)	0.21	0.23	0.14	0.13	0.08	0.04
Sticking Fraction	0.53	0.53	0.54	0.54	0.52	0.52

Table 2.14 Cont. Drop Tube Furnace (DTF) Test Matrix for Ash Deposit Generation

70% WY/30% OK

	<u>Test 1</u>	<u>Test 2</u>	<u>Test 3</u>	<u>Test 4</u>	<u>Test 5</u>	<u>Test 6</u>
Gas Flow Rates (l/min)						
Primary Air	1	1	1	1	1	1
Secondary Air	3	3	3	3	3	3
Vacuum	4.2	4.2	4.2	4.2	4.2	4.2
Temperatures (°C)						
Injector	amb	amb	amb	amb	amb	amb
Secondary Air	1103	1103	1103	1103	1103	1102
Furnace 1 Upper	1477	1477	1475	1477	1475	1475
Furnace 1 Lower	1462	1450	1466	1450	1463	1463
Run Duration (min)	30.0	30.0	30.0	20.0	10.0	5.0
Residence Time (sec)	2	2	2	2	2	2
Coal Burned (g)	NA	3.33	3.22	2.04	1.08	0.55
Coal Feed Rate (g/min)	NA	0.11	0.11	0.10	0.11	0.11
Ash Collected (g)	0.16	0.15	0.15	0.09	0.05	0.02
Coal Ash (%)	8.9	8.9	8.9	8.9	8.9	8.9
Ash Fed (g)	NA	0.30	0.29	0.18	0.10	0.05
Sticking Fraction	NA	0.49	0.51	0.49	0.51	0.49

70% WY/30% OK CLN

	<u>Test 1</u>	<u>Test 2</u>	<u>Test 3</u>	<u>Test 4</u>	<u>Test 5</u>
Gas Flow Rates (l/min)					
Primary Air	1	1	1	1	1
Secondary Air	3	3	3	3	3
Vacuum	4.2	4.2	4.2	4.2	4.2
Temperatures (°C)					
Injector	amb	amb	amb	amb	amb
Secondary Air	1104	1105	1104	1106	1106
Furnace 1 Upper	1483	1483	1481	1485	1483
Furnace 1 Lower	1464	1466	1465	1464	1462
Run Duration (min)	32.0	32.0	20.0	10.0	5.0
Residence Time (sec)	2	2	2	2	2
Coal Burned (g)	3.62	3.65	2.10	1.22	0.58
Coal Feed Rate (g/min)	0.11	0.11	0.11	0.12	0.12
Ash Collected (g)	0.12	0.12	0.07	0.04	0.02
Coal Ash (%)	6.5	6.5	6.5	6.5	6.5
Ash Fed (g)	0.24	0.24	0.14	0.08	0.04
Sticking Fraction	0.52	0.52	0.51	0.51	0.47

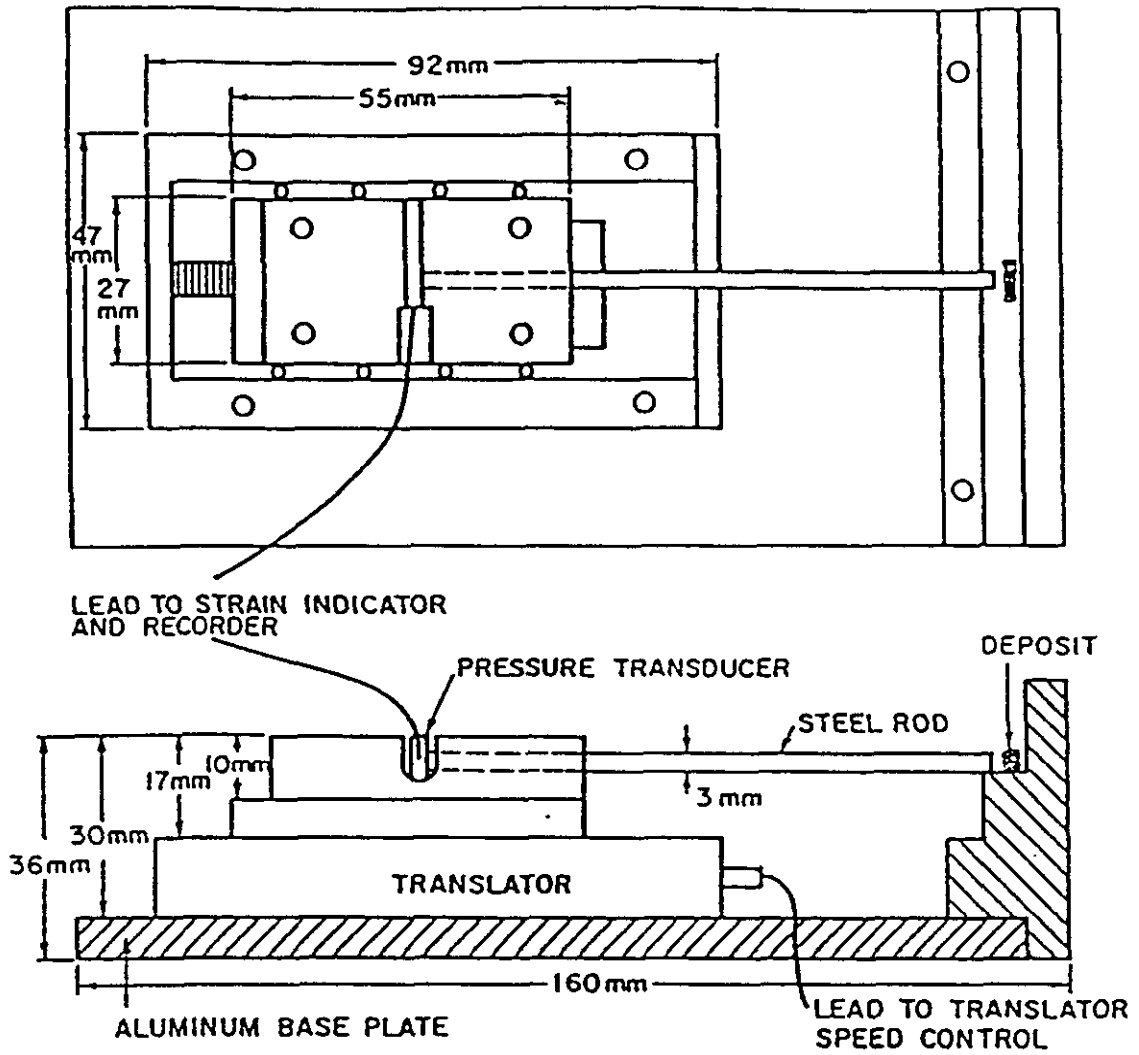


Figure 2.16 Deposit Strength Measuring Apparatus

Strength curves for deposits generated under slagging conditions, i.e., at the initial slagging temperatures, (Figure 2.17) show the 70% WY/30% OK blend to have the greatest overall crushing strength and the 70% WY/30% OK cleaned blend to have the greatest tip strength. Greater strength at the highest point (tip) of the deposit may be indicative of greater slagging potential, since molten deposits are known to have higher crushing strengths than sintered deposits.

Ash sticking fraction versus time for the PSO fuels is displayed in Figure 2.18. A higher percentage of ash was sticking for the 90% WY/10% OK and 70% WY/30% OK blends as compared to the 100% WY; however, the deposit growth rate (sticking fraction) for the 100%WY coal increased with time.

2.3.3 Physical and Chemical Examination of Deposits and Substrate Materials

The deposits generated in the EERC drop tube furnace were analyzed using SEM techniques. Both the main (bulk) deposit and the base (initial) layer were analyzed. XRD analysis was performed on all of these same samples before SEM analysis. SEM morphologic analysis was performed on each of the deposits to observe the physical and chemical characterization of the bonding matrix in the deposits.

Deposit chemistries and phase compositions were determined using SEMPC analysis on the initial and bulk deposits. (The SEMPC method is described in detail in Appendix B.) Since the SEMPC mineral classifications are based on strictly chemical composition data, x-ray diffraction (XRD) is used to verify the presence of major crystalline phases. This provides the corroborating evidence needed, since the XRD determines the mineral phases directly based on their crystal structure. X-ray fluorescence analysis (XRFA) is also used routinely to verify the SEMPC results because it determines a bulk chemical analysis.

Table 2.15 lists the elemental and inorganic phase compositions for the deposits. Viscosity distributions for the liquid silicate phases in the base deposits are given in Figure 2.19. The 90% WY/10% OK blend had the largest quantity of low viscosity liquid phases, followed by the 70% WY/30% OK cleaned blend, 100% WY, and 70%

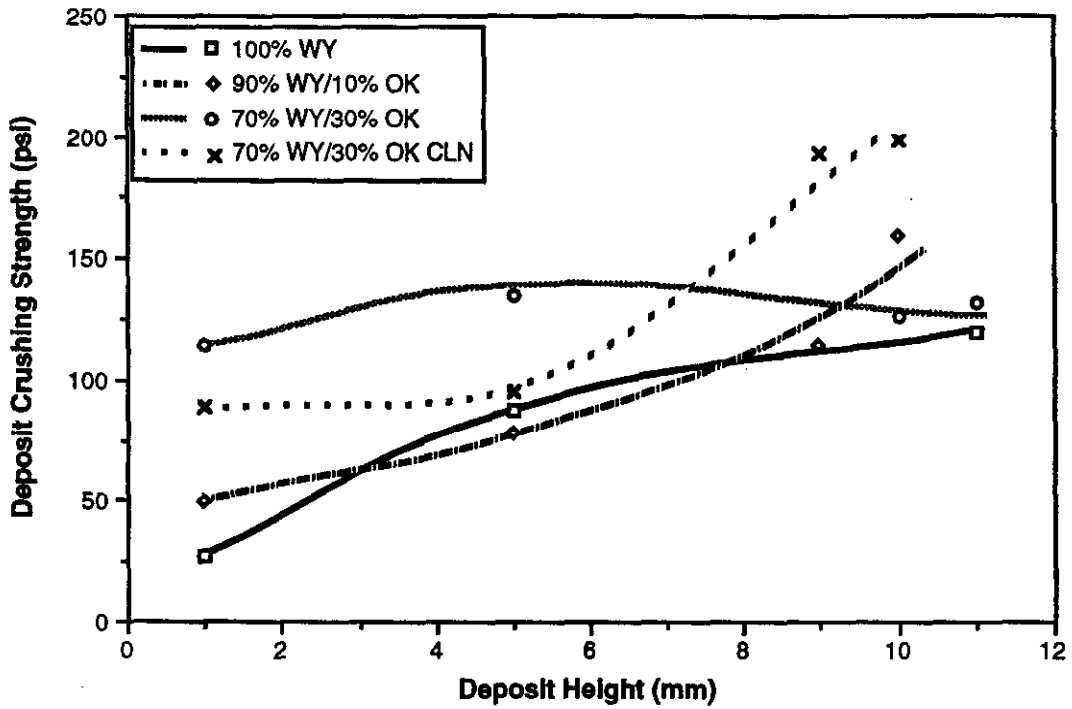


Figure 2.17 Strength Curves for PSO Coal and Coal Blend Deposits Generated in the DTF

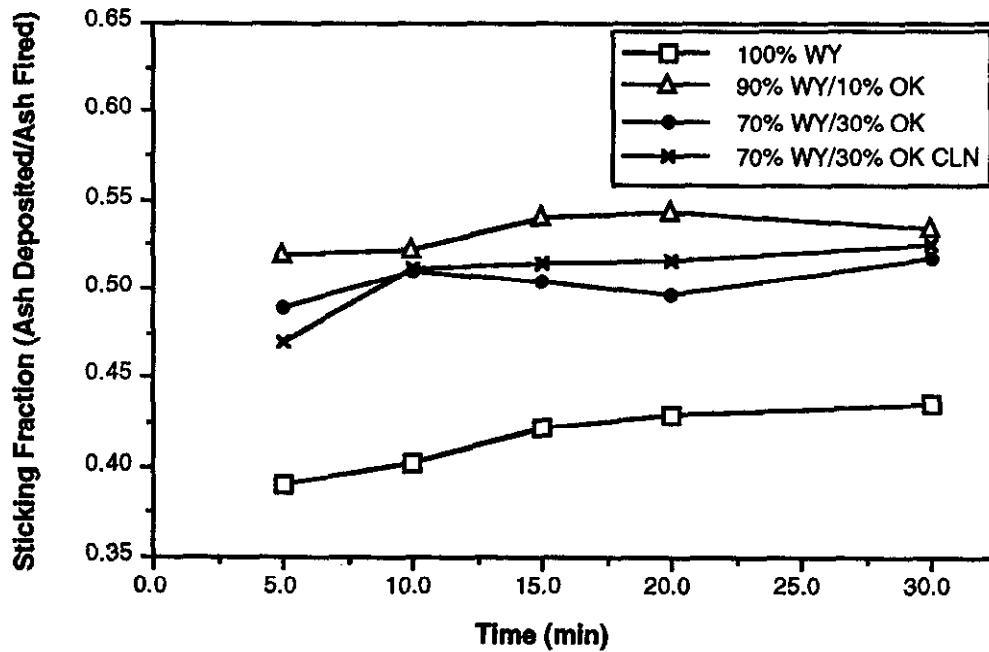


Figure 2.18 Ash Sticking Fraction vs. Time for the PSO Test Fuels as Generated in the DTF

Table 2.15 SEMPC Analyses of Drop Tube Furnace Deposits

Mineral Phases (SEMPC Wt. %)	100% WY		90% WY/10% OK		70% WY/30% OK		70% WY/30% OK CLN	
	Initial	Bulk	Initial	Bulk	Initial	Bulk	Initial	Bulk
Gehlenite	7.0	0.0	6.4	0.0	4.0	0.0	6.0	0.0
Anorthite	8.4	42.4	3.6	32.4	2.0	35.2	4.4	26.0
Albite	0.0	0.0	0.0	0.0	0.4	0.0	0.0	0.0
Pyroxene	0.4	0.0	0.4	0.0	0.4	0.0	0.0	0.0
Pure Kaolinite	7.0	4.0	5.2	1.6	5.2	0.4	7.2	0.8
Kaolinite-Derived	5.3	3.2	5.6	0.8	4.4	0.4	6.8	3.2
Illite (Amorphous)	0.9	0.0	3.6	0.0	3.6	0.8	3.6	0.0
Montmorillonite	9.7	15.2	8.0	39.2	4.0	36.8	7.2	32.8
Bulk Oxide Comp. (Wt. %)								
SiO ₂	45.7	57.9	45.1	57.9	47.1	58.0	42.9	57.4
Al ₂ O ₃	23.9	19.6	24.6	20.3	26.4	15.1	24.7	18.4
Fe ₂ O ₃	3.7	5.1	5.3	5.6	5.7	7.6	5.4	9.0
TiO ₂	1.8	2.3	1.7	1.4	1.4	1.9	1.8	1.2
P ₂ O ₅	0.7	0.5	0.3	0.6	0.8	0.2	0.6	0.2
CaO	19.2	10.7	17.7	10.2	13.2	12.8	19.5	9.6
MgO	3.4	3.3	3.3	2.3	2.7	2.5	3.5	2.1
Na ₂ O	0.8	0.3	0.6	0.5	0.7	0.5	0.5	0.7
K ₂ O	0.7	0.6	1.2	1.1	1.8	1.4	1.2	1.4
ClO	0.0	0.0	0.0	0.0	0.0	0.0	0.0	0.0
Cr ₂ O ₃	0.1	0.1	0.1	0.1	0.1	0.1	0.1	0.1
SO ₃ (Added for Comparison)	0.8	0.2	0.7	0.0	1.8	0.0	0.6	0.0
Major Minerals (XRD)								
	Quartz	Quartz Plagioclase	Quartz	Quartz Plagioclase	Quartz	Quartz Plagioclase	Quartz	Quartz Plagioclase
Minor Minerals (XRD)								
	Doipside Lime Hullite Fe Spinel Hematite	Hematite	Hematite Fe Spinel Lime Hullite Anhydrite	Hematite	Hullite Lime Hematite Fe Spinel	Hematite	Fe Spinel Lime Hullite Hematite	Hematite Fe Spinel

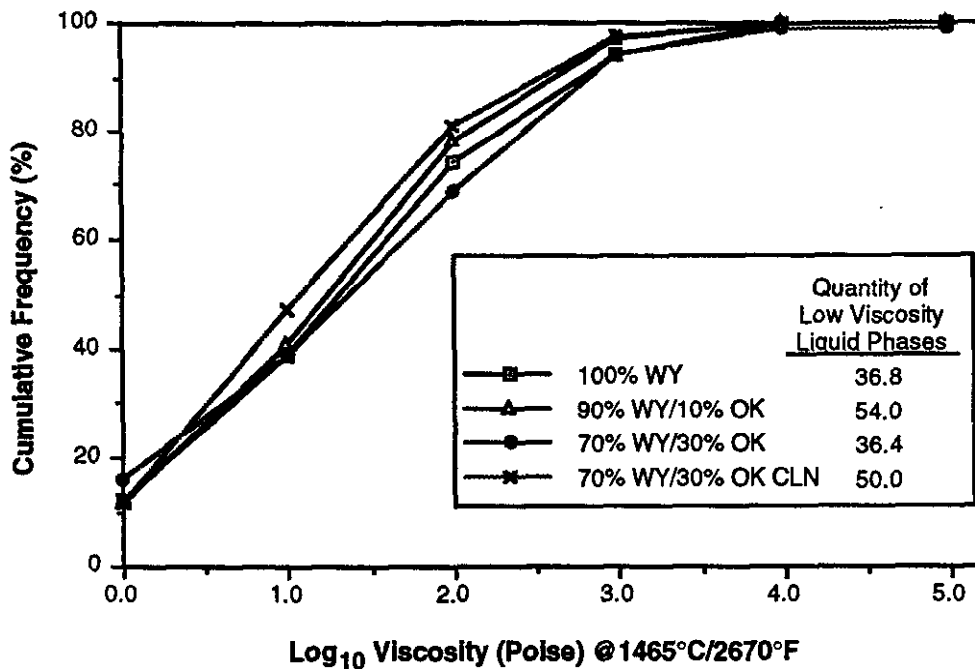


Figure 2.19 Viscosity Distribution in DTF Base Deposits

WY/30% OK blend. The 70% WY/30% OK blend main deposit shows the largest quantity of low viscosity liquid phase material (Figure 2.20) with the 90% WY/10% OK blend, 100% WY, and 70% WY/30% OK cleaned having successively smaller quantities of low viscosity liquid phases. The main deposit is the part of the deposit that will appear molten when slagging occurs. The degree to which a deposit will form abundant molten material can be ascertained by calculating the amount of low viscosity silicate liquid phases. In the case of Figures 2.19 and 2.20, the low viscosity phase amounts are defined as the volume percent of material having a viscosity of less than 250 poise. The reason the 70% WY/30% OK blend fuel had a higher propensity to form a liquid phase in the main deposit is the lower level of aluminum in the liquid phase. The aluminum acts to buffer the effects of other components in the melt phase. The deposits contain a lower level of kaolinite and kaolinite-derived materials, and the silica-to-aluminum ratio in the 70% WY/30% OK blend is 3.9, compared to 2.9 for the 90% WY/10% OK and 100% WY deposits. The clay mineralogy with respect to the alkali and alkaline earth aluminosilicates is a key to liquid phase formation.

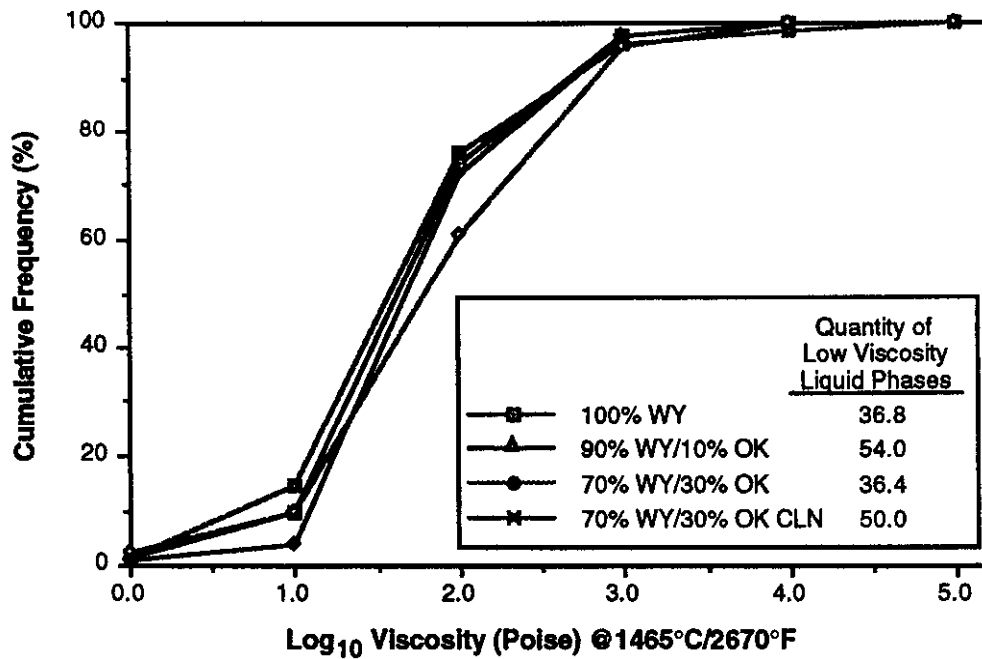


Figure 2.20 Viscosity Distribution in DTF Main Deposits

In summary, based on initial slagging temperatures and liquid phase viscosity distributions, and crushing strength of the deposits, the 70% WY/30% OK and WY 100% fuels seem to show higher propensities for slag formation. The 70% WY/30% OK cleaned blend may be considered a likely slagging fuel also, but the ash loading is considerably lower than the other fuels.

Section 3

PILOT-SCALE TESTING

Pilot-scale tests were designed to evaluate the fireside performance of the test fuels in an environment where the unit-specific effects (such as boiler design, upper furnace convective pass tube spacing, and firing arrangement) could be eliminated, allowing an evaluation based on fuel property differences and boiler operating conditions. Maintaining the same, or very similar firing conditions, heat absorption and temperature profiles in a full-scale unit to evaluate fuel performance while switching fuels is virtually impossible and can be very expensive. However, the pilot scale facility allows for better control over the temperature profiles and heat fluxes, and is capable of modeling full-scale boiler phenomena in a controlled environment. The pilot-scale also allows an evaluation over a broader range of furnace conditions allowing extrapolation to more units and establishing limits in various performance areas. It should be quickly added, however, that the combination of pilot-scale and field data is the ideal situation.

Comprehensive tests were conducted in CE's Fireside Performance Test Facility (FPTF) to evaluate the combustion, furnace slagging, convective pass fouling and fly ash erosion characteristics of the fuels tested at the Northeastern Unit 4. Representative in-flame solids and ash deposit samples were collected and analyzed in detail to enhance fundamental understanding of mineral matter transformation and ash deposition. Pilot-scale testing is designed to investigate the relationships between parent fuel characteristics (e.g., mineral contents and particle size distributions) and ash and deposit characteristics in the radiant section as well as in the convective pass section of a furnace. The ultimate results of the pilot-scale data gathering and analysis shall aid in algorithm development and verification for fouling and slagging routines which are able to model ash deposition, growth, thermal properties and cleanability under specific boiler conditions.

3.1 TEST FUELS

Four test fuels were evaluated for combustion and fireside performance in the FPTF. These fuels were: 100% WY, 90% WY/10% OK, 70% WY/30% OK and 70% WY/30% OK CLN (cleaned). All of the fuels except the 70% WY/30% OK CLN were part of the field testing performed at the Northeastern Unit 4. Coal samples were obtained during the full-scale testing through a coal handling system which permitted on-line fuel sampling to ensure that the coal samples obtained (for the bench- and pilot-scale studies) were representative of those burned in the field tests. The coal samples were collected in 55-gallon barrels and then shipped to CE for pilot- and bench-scale testing.

Problems were experienced with coal handling in that often the content of OK coal in the blend varied from day to day. This meant that barrels of coal collected on a given day had a different OK coal concentration than barrels filled on other days. To alleviate these fluctuations in coal mixtures, prior to testing, all of the coal to be used for a test was dumped from the barrels into a common pile and then thoroughly mixed. This was done to ensure that the coal properties tested in the pilot-scale were specific to the overall coal mixture and not subject to fluctuations in the coal blending process.

The crushed coal obtained from the field (1/2" to 1" top size) was fed from a storage hopper to a CE Model 271 bowl mill where it was pulverized to the desired fineness. The small, deep-bowl, single-journal (roller) mill was equipped with a direct gas-fired air heater to provide mill drying air. The pulverized coal was pneumatically transported to a cyclone collector where most of it was dropped into a storage hopper. Fines in the cyclone effluent were collected in a bag filter and returned to the storage hopper. Pulverized coal was fed into the FPTF with a belt-type gravimetric feeder combined with a rotary air lock which allowed the coal to be injected pneumatically at the burner front.

Coal samples were systematically taken from the FPTF feeder system to supply representative coal samples for the bench-scale analyses. These highly

representative samples were used for bench-scale analysis as reported in Section 2 of this report. Coal particle size distributions for each of the fuels fired in the FPTF are shown in Figure 3.1. The pulverizer was set to produce a particle size distribution that was representative of the particle size distribution during field testing.

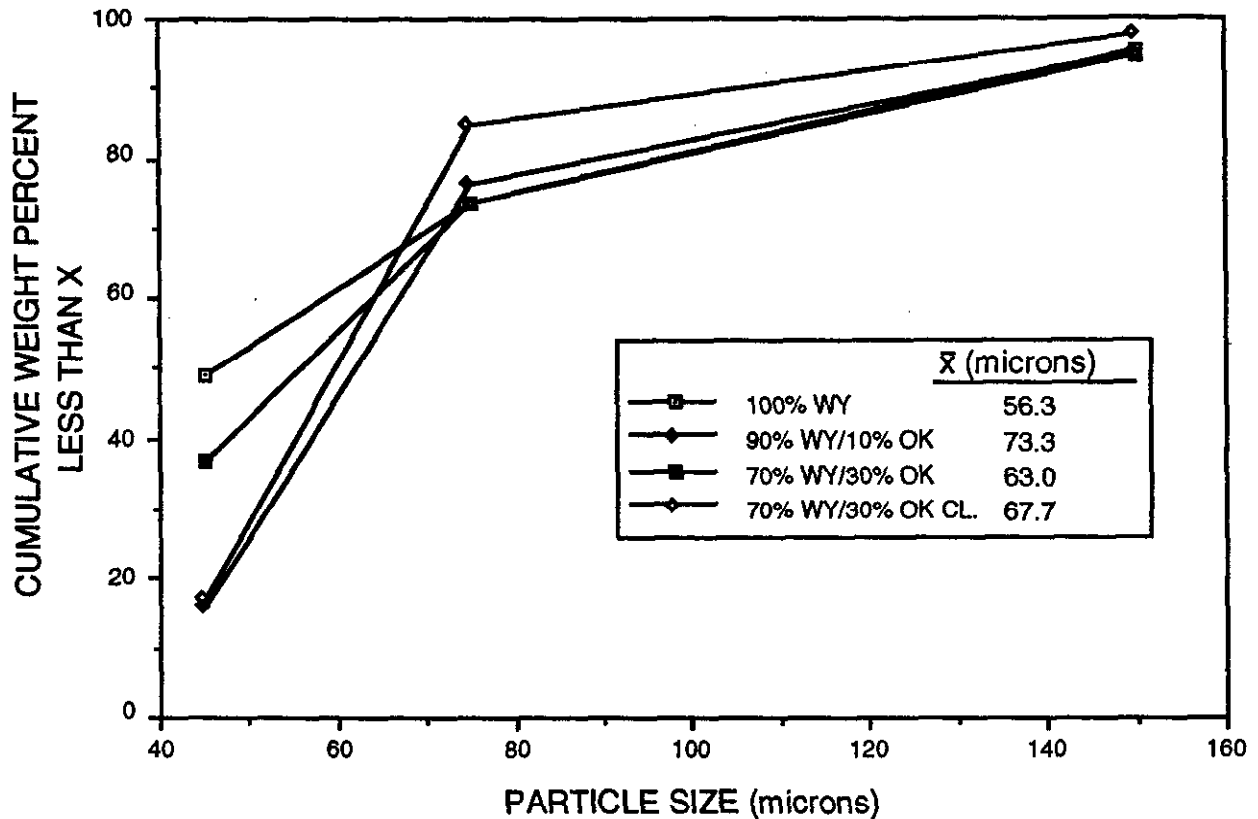


Figure 3.1 Coal Particle Size Distributions For PSO Coals And Coal Blends

3.2. FIRESIDE PERFORMANCE CHARACTERISTICS

The fireside performance characteristics of the fuels tested, specifically the deposits they formed, were evaluated in the lower and upper furnace sections of the FPTF. A simplified schematic of the FPTF is shown in Figure 3.2. In the lower furnace section, four elevations of panels simulating waterwall tube surfaces have been inserted to evaluate slag deposition. Probe banks have been inserted in the convective pass

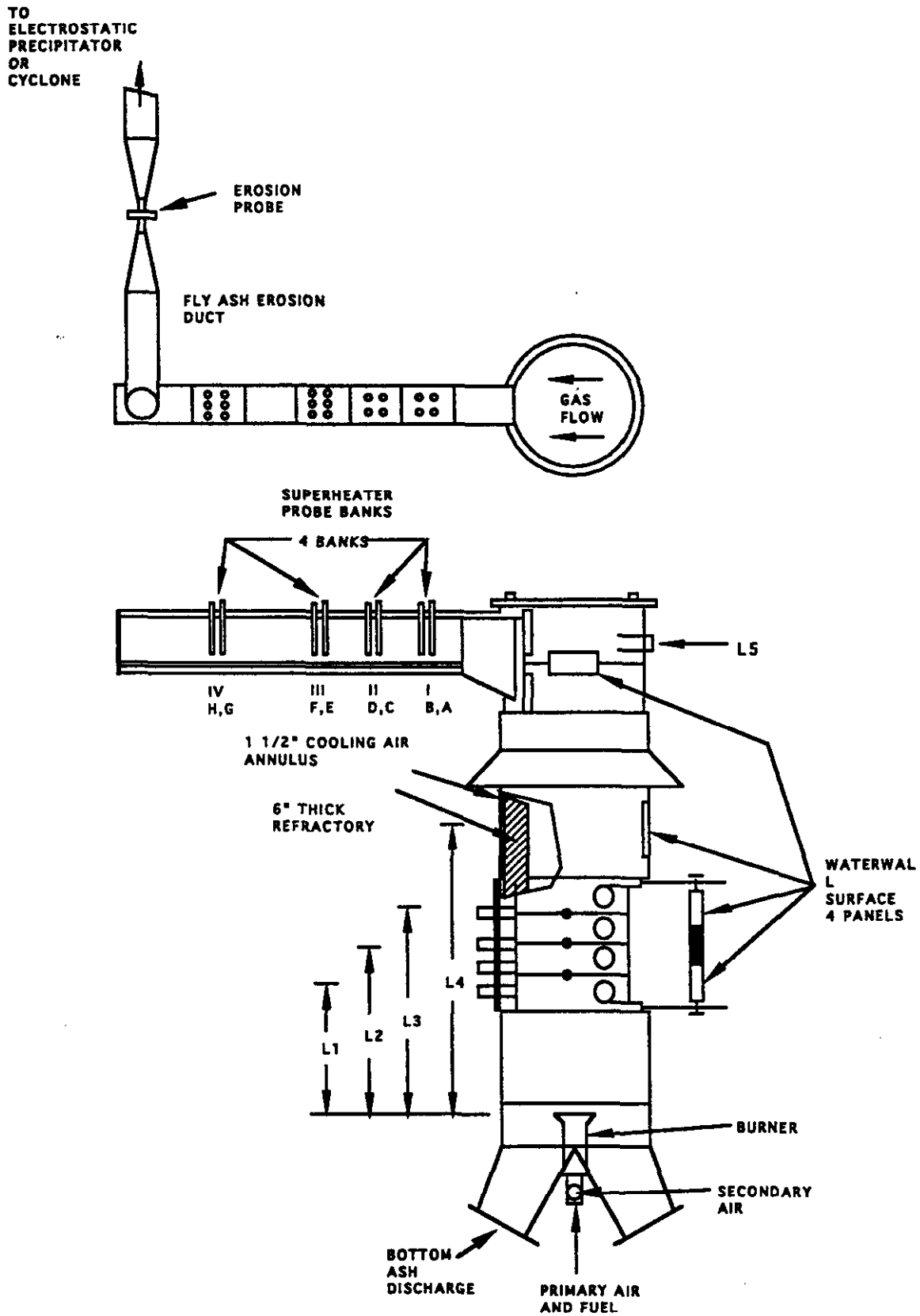


FIGURE 3.2
FIRESIDE PERFORMANCE TEST FACILITY

section of the upper furnace for an evaluation of fouling deposition. From the convective section of the furnace, the flue gas is introduced into a high-velocity duct section where an irradiated coupon is exposed to the entrained ash particles as a measure of erosion wear.

The overall combustion characteristics of all four of the fuels tested in the FPTF were good. Good, stable flames were obtained and very few sparklers (glowing, incompletely burned carbon particles) were observed during most of the tests. Chemical analyses of the isokinetically-collected fly ash samples indicated that in every case the carbon contents were very low, and the carbon conversion efficiencies were greater than 99.9% for all fuels tested.

3.2.1 Test Conditions

The combustion test matrix was designed to assess fuel performance characteristics over a range of boiler operating conditions. Emphasis was placed on establishing the maximum temperature and thermal input allowable for controllable ash formation/deposition in the lower furnace; specifically, a determination of those parameters which would lead to the establishment of load-limiting firing conditions in full-scale utility boiler applications.

The test matrix used to evaluate the four fuels is shown in Table 3.1. Coal firing rates between 3.0 and 4.0 MBtu/hr combined with varied degrees of secondary air preheat were used to control gas temperature and permit assessment of deposit formation as a function of gas temperature at each panel elevation in the furnace. As shown in the table, the first three tests on each fuel were used to determine critical thermal conditions for the fuels at 20% excess air. Once the critical thermal conditions were established, two additional tests were performed at those same thermal conditions with a low and a high excess air level. A sixth, repeat test was performed at critical conditions for 20% excess air for the purpose of waterwall panel deposit collection, since the deposits from earlier tests had been removed during soot blower effectiveness evaluations.

Table 3.1 FPTF Firing Conditions Test Matrix

Test No.	Duration (hrs)	Firing Rate (MBtu/hr)	Avg. Operating Temperature (°F)	Excess Air (%)
100% WY				
1	12	3.6	2900-2925	20
2	12	3.4	2850-2875	20
3	12	3.2	2800-2825	20
4	12	3.3	2825-2850	12.5
5	12	3.3	2825-2850	30
6	12	3.3	2825-2850	20
90% WY / 10% OK				
1	12	3.3	2825-2850	20
2	12	3.7	2925-2950	20
3	9	4.0	3000-3025	20
4	12	3.8	2950-2975	12.5
5	12	3.8	2950-2975	30
6	12	3.7	2925-2950	20
70% WY / 30 % OK				
1	12	3.7	2925-2950	20
2	12	3.3	2825-2850	20
3	12	3.0	2700-2725	20
4	12	3.2	2800-2825	12.5
5	12	3.2	2800-2825	30
6	12	3.2	2800-2825	20
70 % WY / 30 % OK CLN				
1	12	3.2	2800-2825	20
2	12	3.6	2900-2925	20
3	12	4.0	3000-3025	20

Figure 3.3 presents typical FPTF gas temperatures, as a function of distance from the burner, for the four test fuels fired at similar loads. Temperatures were measured with shielded, high velocity suction pyrometers at the first eight furnace locations, and the ninth was measured with a bare thermocouple located where the isokinetic dust sample is collected. Figure 3.4 depicts typical radial and axial gas temperatures at the four panel elevations in the FPTF. As can be seen in this figure, temperature profiles

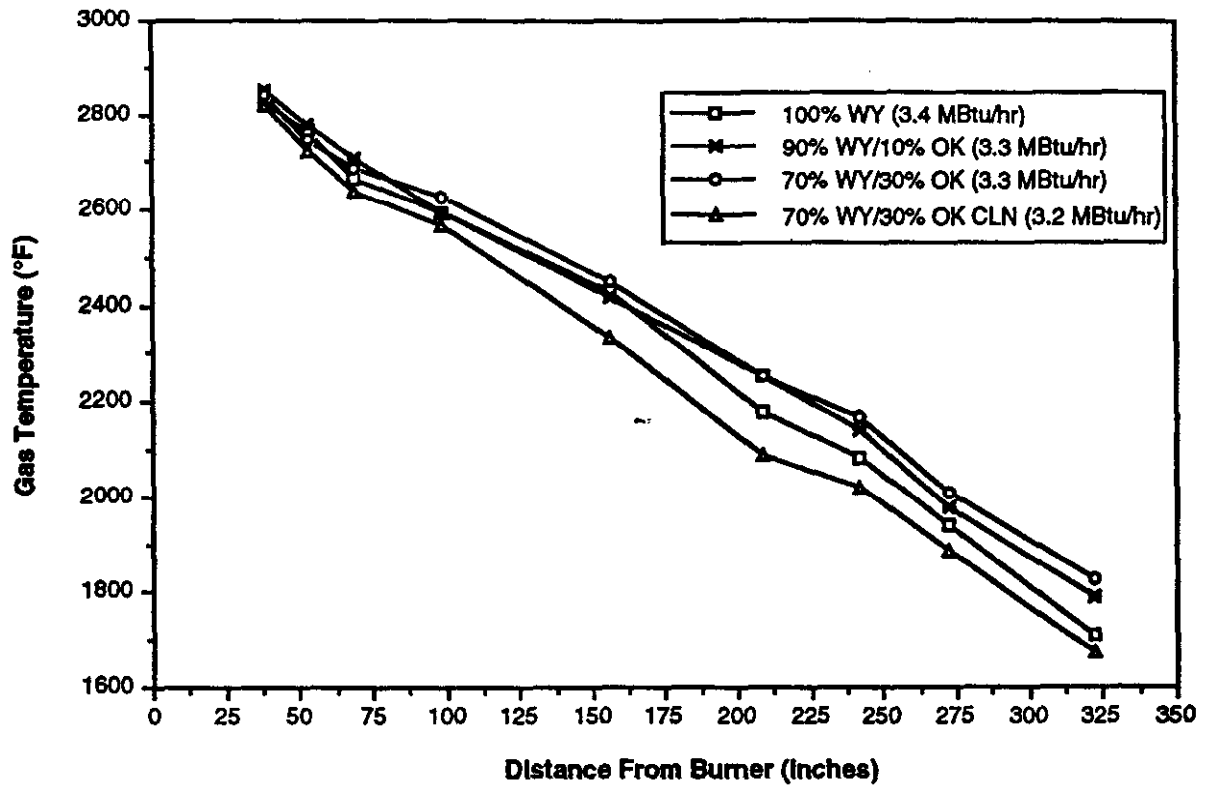


Figure 3.3 Typical FPTF Variation of Temperature Profiles with Distance During Test Firing of Northeastern Fuels

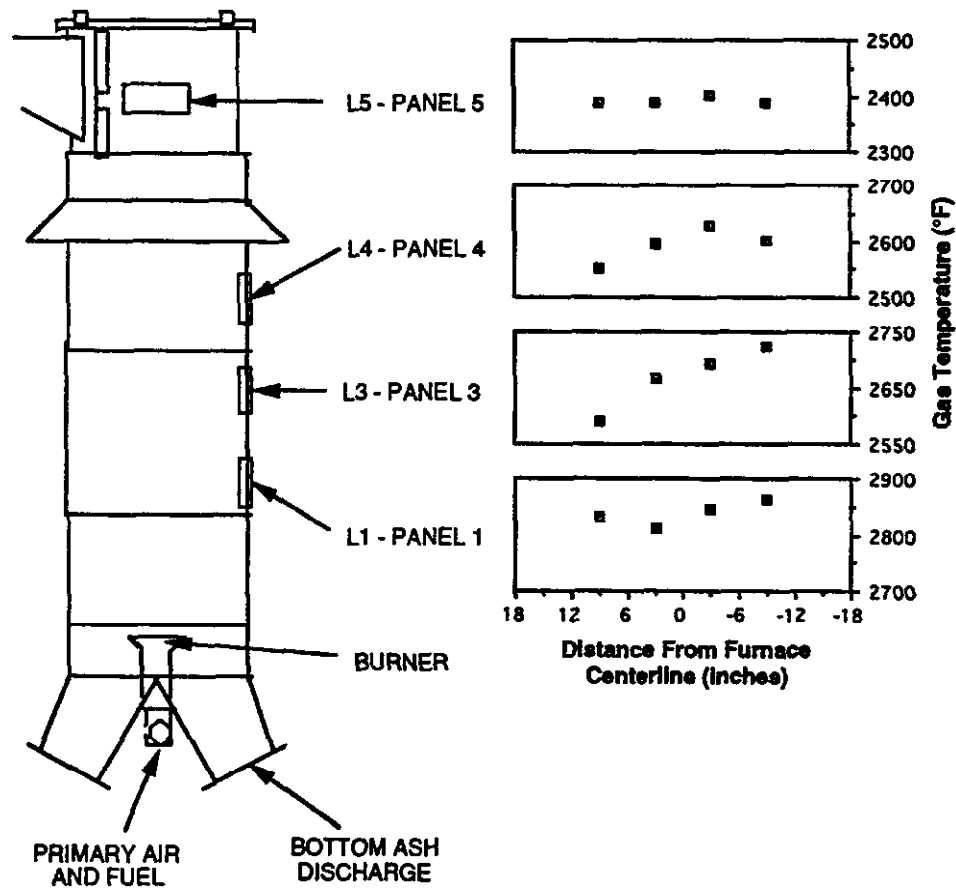


Figure 3.4 Typical Radial and Axial Gas Temperatures in the FPTF While Firing Northeastern Fuels

were reasonably uniform at each elevation. Radial variations in temperature which did occur may be attributed to irregularities in flame shape and to turbulence in the gas flow.

A major objective in setting up the test conditions was to match localized total heat fluxes between the FPTF and those measured in the Northeastern Unit 4. As can be seen in Figure 3.5, heat fluxes measured in Northeastern's unit 4 and those measured in the FPTF show that the total heat flux seen by the FPTF as deposition panels match full-scale boiler local waterwall heat flux conditions rather closely. Total heat fluxes, for both the field and the FPTF, were measured with a water-cooled total heat flux meter.

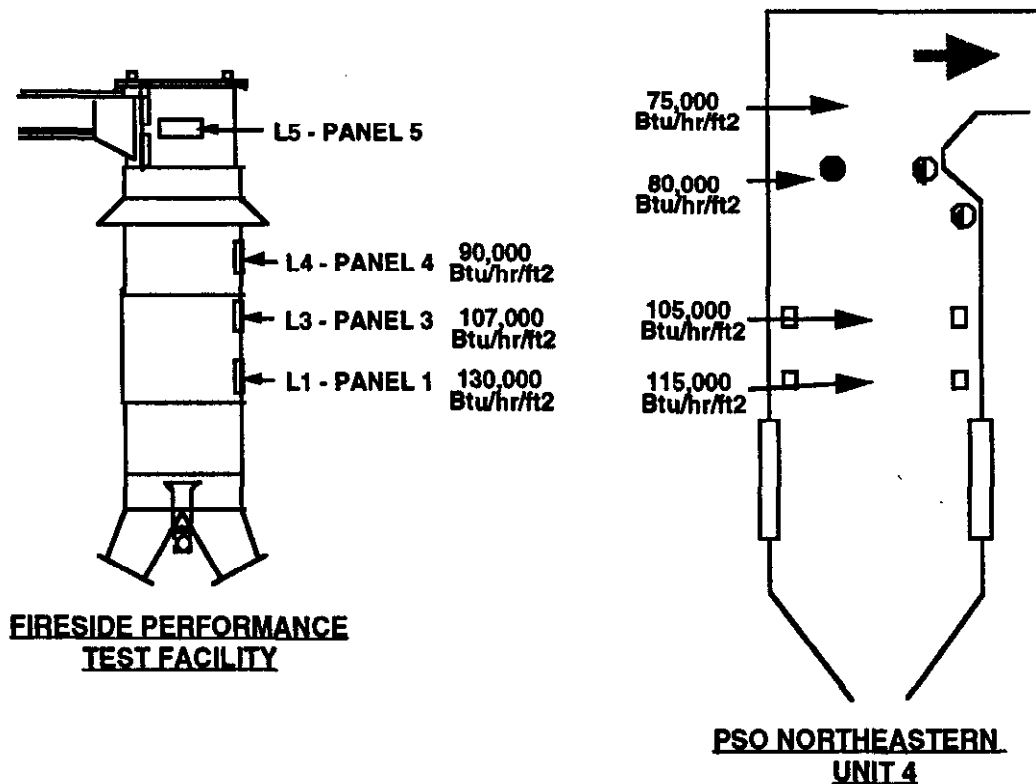


Figure 3.5 Heat Flux Comparison Between the FPTF and the Northeastern Unit 4

Residence time of the bulk gas as a function of distance from the burner was calculated from a bulk flow mass-energy balance. Figure 3.6 illustrates this relationship for the four test fuels at similar loads. Both the residence times and temperatures were controlled such that, when tested at similar thermal loads, the four test fuels had very similar time-temperature histories during combustion. Complete residence time and temperature data for each combustion test are found in Appendix D.

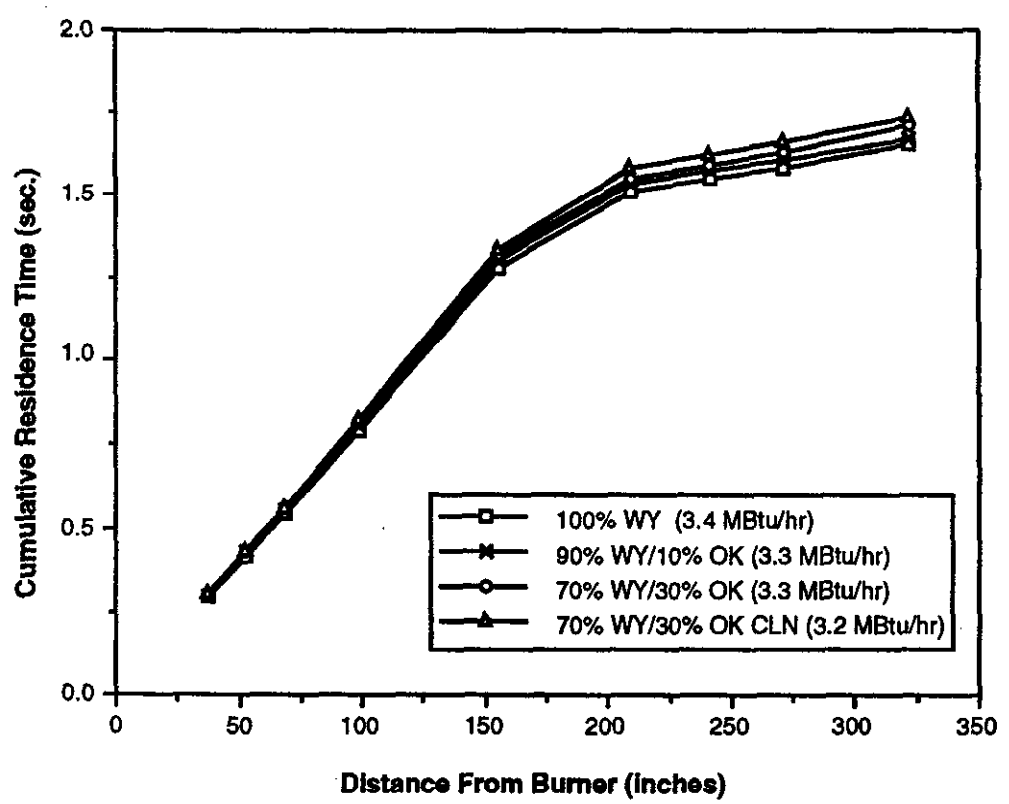


Figure 3.6 Comparison of Bulk Gas Residence Times at Similar Loads for all Fuels Tested

3.2.2 Characterization of Pilot-Scale In-Flame Solids

In-flame solid samples were taken at each of the four panel elevations in the radiant section of the FPTF. The samples were taken three inches in front of the panels to obtain a representative sample of the material impinging on the panel surfaces. Tables 3.2 and 3.3 show comparisons of the mineral constituents and mineral phases of the samples taken at L1 (the first panel elevation) for all of the fuels tested. Comparisons have been made using CCSEM, SEMPC, and XRD measurement techniques. Table 3.4 provides the chemical formulae for the mineral phases defined by XRD. All of the fuels show some production of calcium aluminosilicate or illite-derived phase still remaining in the fly ash. The original unblended OK coal had high quantities of illite and calcite, and remnants of these minerals, probably in the form of fused or molten particles, were part of the 70% WY/30% OK inflame solids.

Table 3.2 CCSEM Comparisons of Radiant Section In-flame Solids at L1

Minerals, (Wt%)	100% WY	90% WY/10% OK	70% WY/30% OK	70% WY/30% OK CLN
Quartz	3.6	5.5	9.5	6.6
Calcium Oxide	0.1	0.0	2.0	0.0
Kaolinite	1.5	1.1	2.9	5.7
Montmorillonite	0.3	1.4	1.9	4.0
K Al-Silicate	0.0	1.0	1.1	0.5
Fe Al-Silicate	0.0	0.0	1.1	0.5
Ca Al-Silicate	19.0	29.1	18.1	28.9
Mixed Al-Silicate	0.5	1.6	5.1	1.9
Ca Silicate	1.8	2.1	1.0	1.3
Ca Aluminate	4.7	5.1	4.6	7.7
Gypsum/Al-Silic.	2.2	2.2	2.2	2.1
Si-Rich	2.4	1.3	2.5	3.1
Ca-Rich	3.2	2.7	2.5	0.4
Ca-Si Rich	0.6	1.6	0.4	0.8
LOI	0.56	N/A	4.30	N/A

Table 3.3 Radiant Section In-flame Solids - SEMPC and XRD at L1

Minerals, (Wt%)	100% WY	90% WY/10% OK	70% WY/30% OK	70% WY/30% OK CLN
Gehlenite	25.2	18.4	14.4	11.6
Anthorite	6.8	10.0	7.6	9.6
Albite	0.4	0.0	0.0	0.0
Pyroxene	0.8	0.0	0.0	0.4
Calcium Silicate	0.0	0.0	0.4	0.0
Spurrite	0.4	0.0	0.0	0.4
Calcium Aluminate	1.6	0.8	0.8	1.6
Quartz	2.0	3.6	4.4	5.2
Iron Oxide	0.0	0.0	0.4	0.0
Calcium Oxide	0.0	0.0	0.4	0.4
Ankerite	0.0	0.0	0.4	0.0
Anhydrite	0.0	0.0	0.8	0.8
Pure Kaolinite	0.8	0.0	1.6	1.2
Kaolinite Derived	4.0	1.6	12.4	9.6
Illite (Amorp)	0.4	0.0	2.0	0.8
Montmorillonite	4.0	2.4	7.6	4.4
Unclassified	53.6	63.2	46.8	53.6
Bulk Oxide Composition (Wt%)				
SiO ₂	28.0	32.3	40.7	35.3
Al ₂ O ₃	21.9	21.0	24.2	23.0
Fe ₂ O ₃	6.0	6.1	5.4	5.9
TiO ₂	1.5	1.7	1.0	2.3
P ₂ O ₅	1.3	1.4	0.6	1.1
CaO	31.8	29.0	19.5	24.8
MgO	6.4	6.1	4.2	5.3
Na ₂ O	1.7	1.4	1.5	1.1
K ₂ O	0.6	0.9	2.2	1.2
ClO	0.0	0.0	0.0	0.0
BaO	0.7	0.0	0.4	0.0
SO ₃	1.5	2.2	1.8	2.5
Major Minerals (XRD)				
	Lime, Periclase Dicalcium Silicate, C ₃ A, Quartz	Lime, Periclase, C ₃ A, Quartz, Bassanite	Quartz	Quartz Periclase, C ₃ A Calcite, Hematite
Minor Minerals				
	Magnesioferrite	Ferrite Spinel	Lime, Periclase	Anhydrite

Table 3.4 Chemical Formula definitions for Crystalline Phase Detected by XRD

<u>Mineral/Compound</u>	<u>Chemical Formula</u>
Anhydrite	CaSO ₄
Aluminous Diopside	Ca(Mg,Fe,Al)(Si,Al) ₂ O ₆
Augite	Ca(Mg,Fe)Si ₂ O ₆
Bassanite	CaSO ₄ · ¹ / ₂ H ₂ O
Cristobalite	SiO ₂
Dicalcium Silicate	Ca ₂ SiO ₄
Diopside	CaMg(SiO ₃) ₂
Ferrite Spinel	Mg(Al,Fe) ₂ O ₄
Hematite	Fe ₂ O ₃
Lime	CaO
Magnesioferrite	MgFe ₂ O ₄
Melilite	(Ca,Na) ₂ [(Mg,Al,Fe,Si) ₃ O ₇]
Gehlenite	Ca ₂ (Al ₂ SiO ₇)
Akermanite	Ca ₂ (Mg,Si) ₂ O ₇
Periclase	MgO
Plagioclase	(Ca,Na)(Al,Si) ₄ O ₈
Anorthite	CaAl ₂ Si ₂ O ₈
Albite	NaAlSi ₃ O ₈
Quartz	SiO ₂

The 100% WY had the smallest in-flame solids particle size distribution followed by the 70% WY/30% OK CLN blend, the 90% WY/10% OK blend, and the 70% WY/30% OK blend (Figure 3.7). These distributions agree with the minerals particle size distribution which showed the 100% WY having the smallest minerals and the 100% OK having the largest minerals. The high amount of small ash particles may aggravate deposit formation and growth in both radiant and convective pass furnace sections. The reason for the smaller entrained ash for the Wyoming coal is due to the abundance of organically associated inorganic elements that formed smaller-sized fly ash grains, especially calcium-rich ash particulate. The Wyoming coal contained little

calcite; therefore, the primary source of the calcium in the calcium-rich ash was organically bound calcium. The 90% WY/10% OK and 70% WY/30% OK blends showed progressively larger in-flame particle-size distributions, as expected, because the added Oklahoma coal increased the amounts of larger-sized mineral grains.

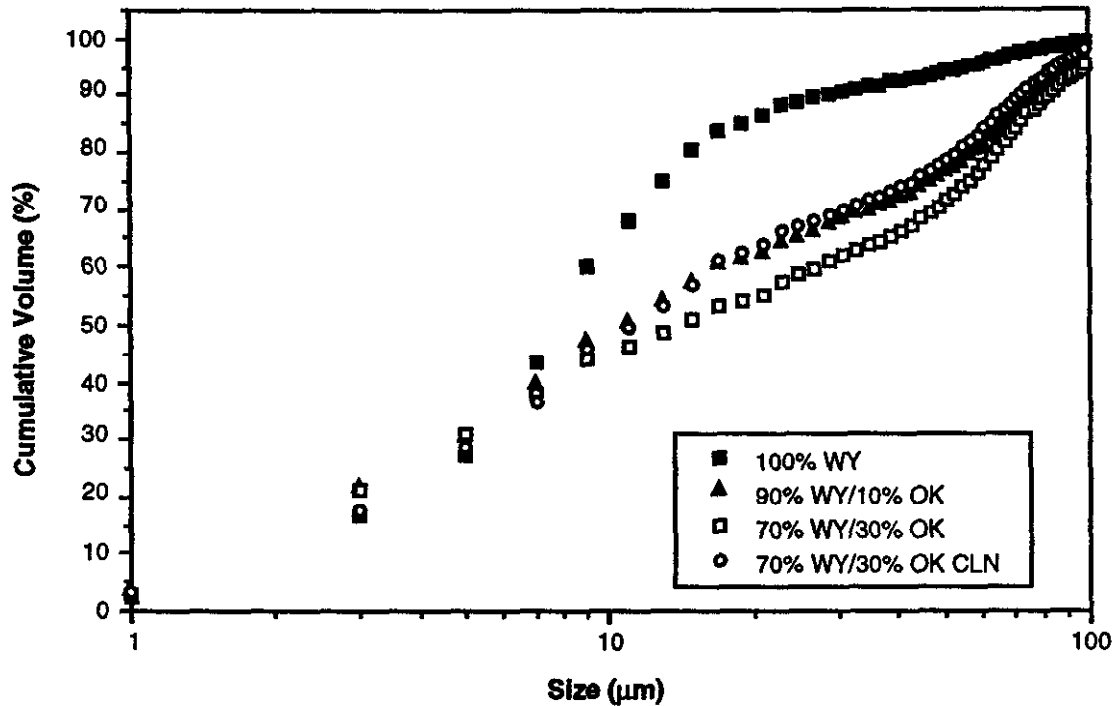


Figure 3.7 Comparison of L1 In-flame Solids Particle Size Distributions

Some clear trends are obvious from the SEMPC and XRD data, which include: 1) less CaO and MgO with increasing OK coal content, which ultimately influenced the amount of gehlenite ($\text{Ca}_2\text{Al}_2\text{SiO}_7$) that was able to form, 2) increasing quartz content with increasing OK coal content, probably due to the added silica content from the abundant illite clay in the OK coal, or to the added quartz content, 3) increased CaO or lime for the 100% WY than for the blends. SEMPC classified much of this fine Ca-rich material as gehlenite or anorthites because of SEM beam effects, whereby smaller ($<1\mu\text{m}$) ash particles give overlapping x-ray spectra instead of a distinct spectrum for each individual grain, and 4) increased kaolinite-derived mineral phases in the 70% WY/30% OK and the 70% WY/30% OK CLN blends, possibly derived from the abundant clays in the OK coal.

Viscosity distributions of what were deemed liquid silicate phases in the in-flame solids are displayed in Figure 3.8. The importance of the viscosity distributions is that they allow assessment of the sticking potential of the entrained ash. A relationship between viscosity and sticking is a good example of the type of relationship that must be developed for the slagging and fouling algorithms.

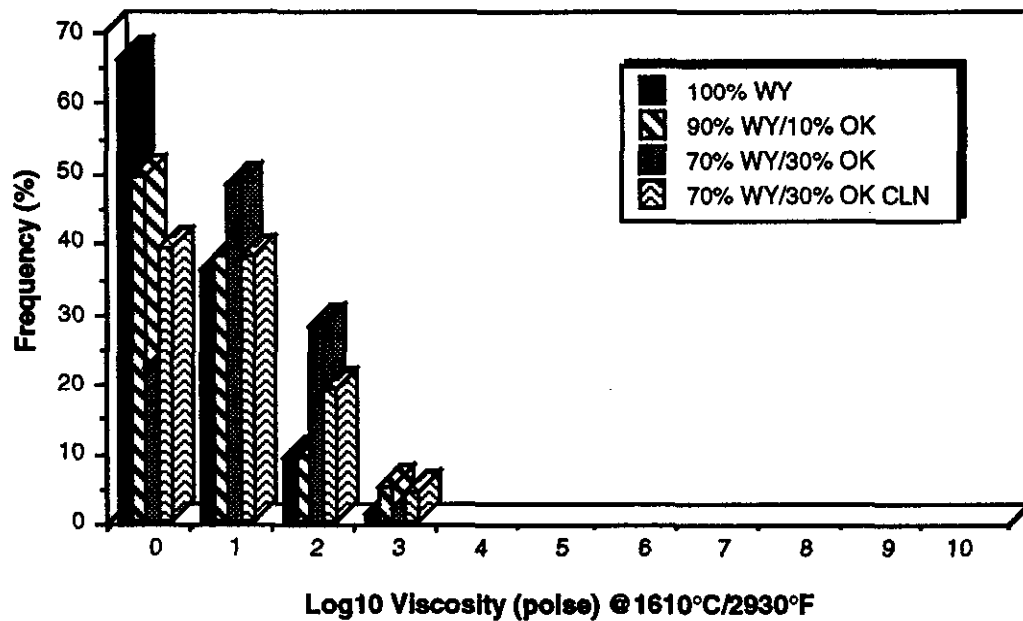


Figure 3.8 In-flame Solids Sample Viscosity Distribution

The 100% WY in-flame solids have the lowest viscosity values, followed by the 90% WY/10% OK blend, the 70% WY/30% OK CLN blend and the 70% WY/30% OK blend, respectively. The amount of liquid phase with low viscosity values was similar for all four fuels. This information implies that the 100% WY and the 90% WY/10% OK fuels have greater tendencies to adhere to surfaces in the radiant section of the boiler and initiate or enhance slag deposition.

3.2.3 Furnace Slagging

Furnace slagging characteristics were determined by the ease of deposit removal (deposit cleanability) in response to wall blower cleaning, and by the thermal properties of deposits formed on simulated waterwall surfaces.

3.2.3.1 Simulated Waterwall Heat Absorptions

As shown previously in Figure 3.2, simulated waterwall panels have been mounted flush with the refractory fireside surface. At the different elevations in the FPTF, each panel has a 15" x 15" surface (ribbed to model a boiler waterwall surface as shown in Figure 3.9). The panels in the lower sections of the FPTF are surrounded by a water-cooled frame to reduce interference from slag generated on adjacent hot refractory surfaces. Fireside panel surface temperatures are controlled through heat exchangers, using Syltherm, a high boiling point organic liquid, to extract the heat required to maintain a surface temperature of 700 °F. Panel heat absorption rates are continuously monitored by recording the coolant (Syltherm) flow rate and the fluid temperature increase from the panel inlet to outlet.

For each of the test runs described in Table 3.1, the heat flux passing through the panel surface was recorded as a function of time and is reported for Panels 1 and 3 in Figures 3.10 to 3.16. Heat flux plots for each of the individual tests show a large drop in the heat transferred through the panels in the first one to two hours of the test. During the initial buildup stages of the deposit formation, a thin powdery layer of deposit was formed on the panel surfaces. The initial steep drop in heat flux can be attributed to two major effects on heat transfer: 1) the powdery initial layer typically has a lower emissivity/absorptivity than that of the iron oxide panel surface, causing more of the incident radiation to be reradiated, and 2) inter-particle bonds which form the initial deposition layer act as a thin, insulative layer which limits conduction from the outermost exposed surface to the metal panel surface increasing the deposit outer layer surface temperature.

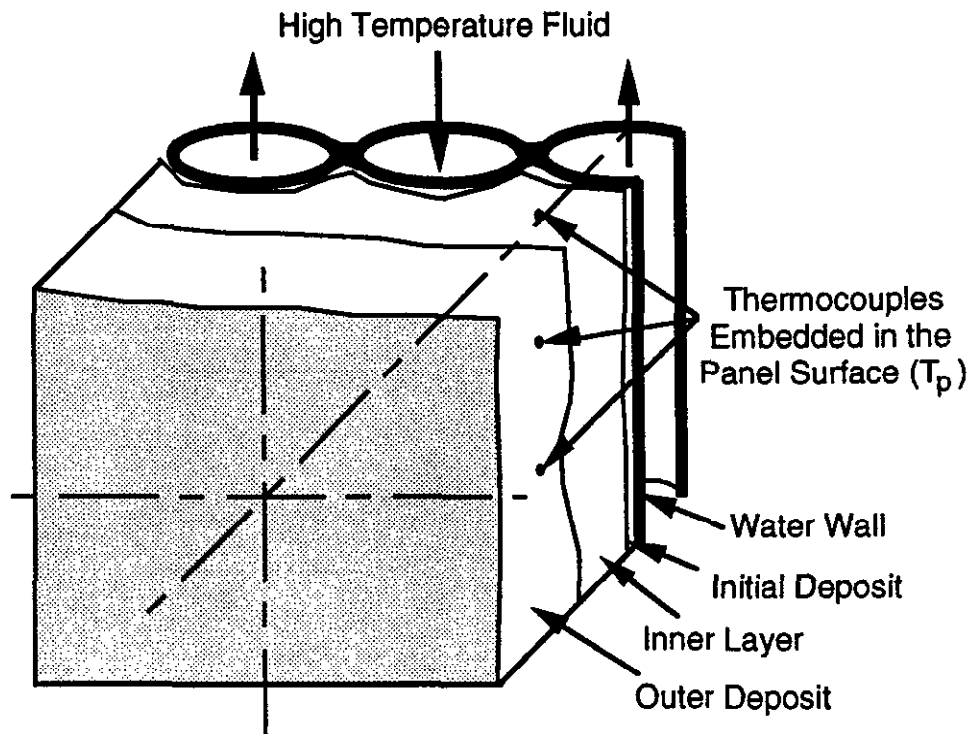


Figure 3.9 Schematic of Waterwall Panel and Deposit

Changes in heat flux through the panel after the initial buildup (during which time the clean panel surface develops a powdery initial deposit layer) were not as dramatic from hour to hour as initial changes in heat flux starting with a clean panel. As lower furnace deposits continue to grow, changes in deposit emissivity and thermal conductivity diminish. However, significant changes in deposit thermal properties (emissive and conductive) can be found as deposits transform from a powdery state into a sintered state and then into a molten state. Typically, deposits initially formed as sintered particle agglomerations in the ribbed depressions between the convex tube surfaces of the simulated waterwall panels. As the deposits grow and protrude further into the furnace, they are exposed to higher temperatures and develop a “sticky” or tacky surface. Impacting particles are retained on this surface, and the deposits grow out of the webs to cover the tube surfaces as well. As the deposits continues to accumulate, the surface may partially or completely transformed to a molten state. Molten deposits, if temperatures are sufficiently high, could run down the crown of the

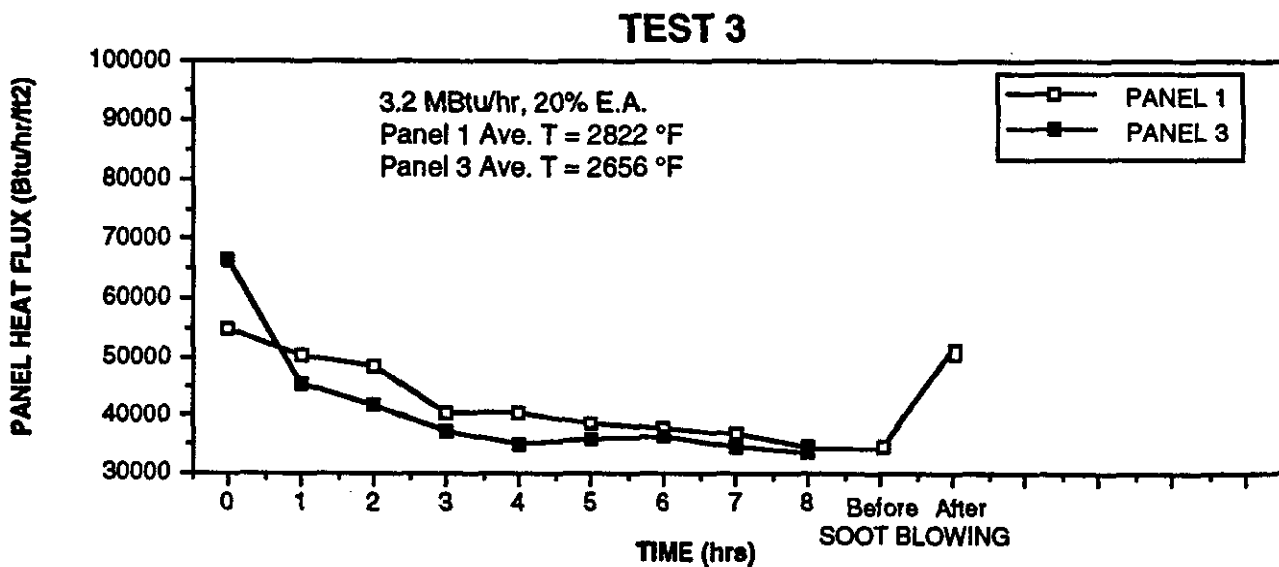
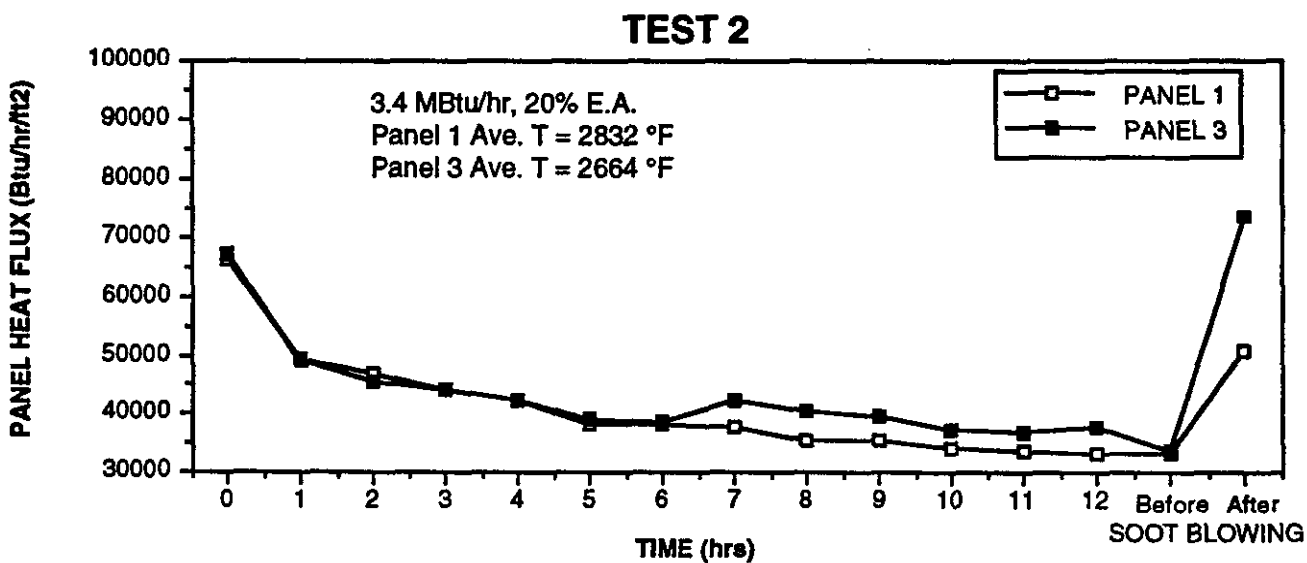
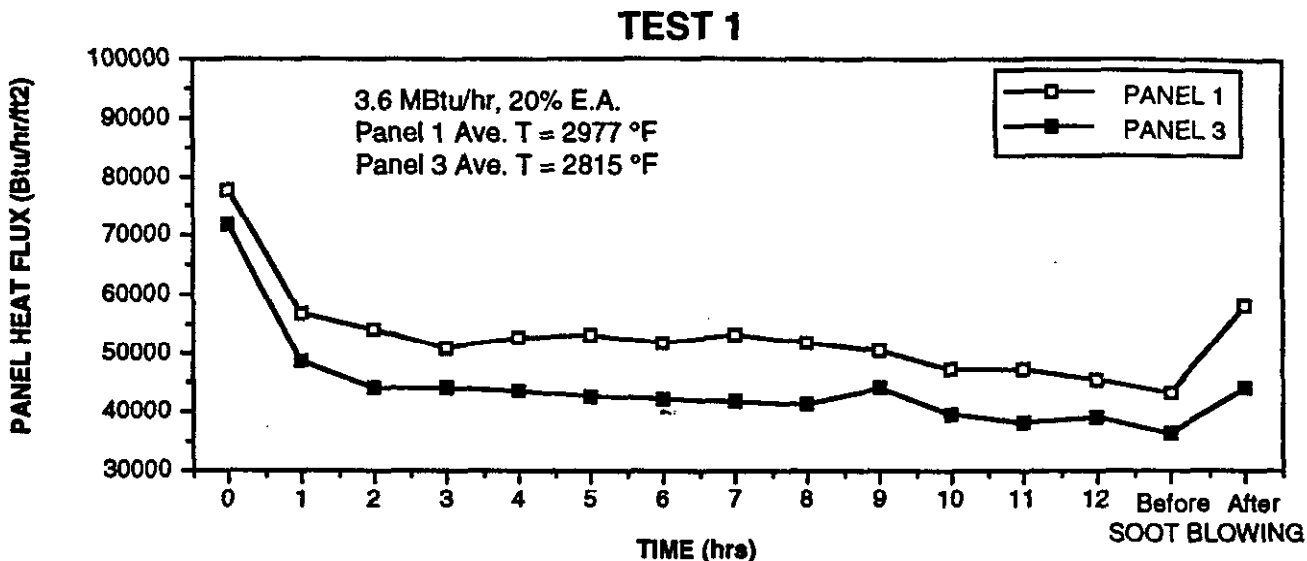
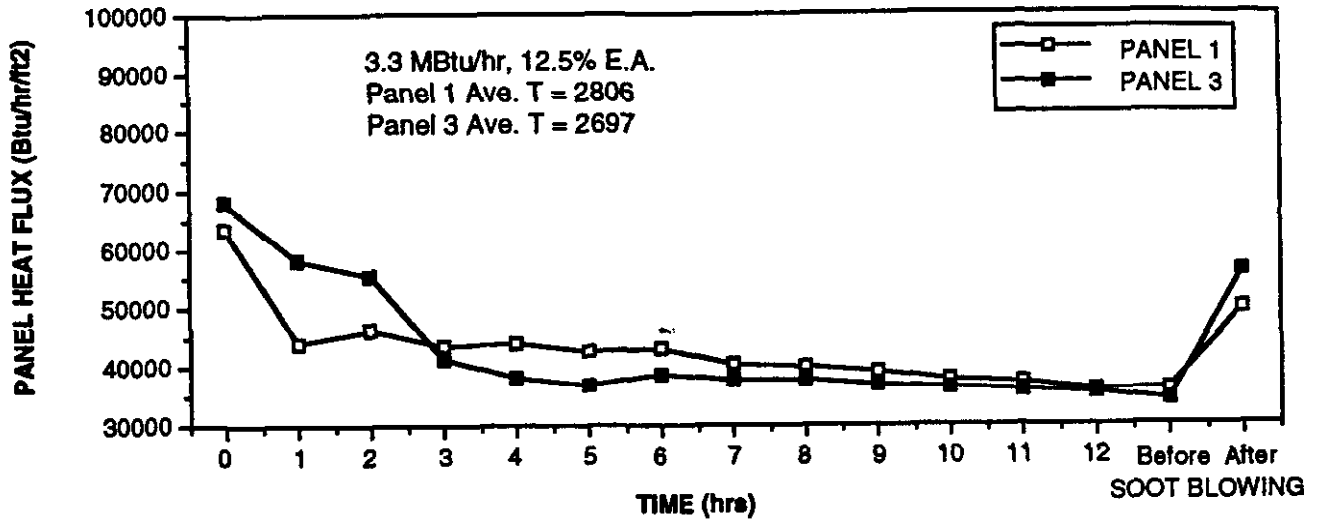
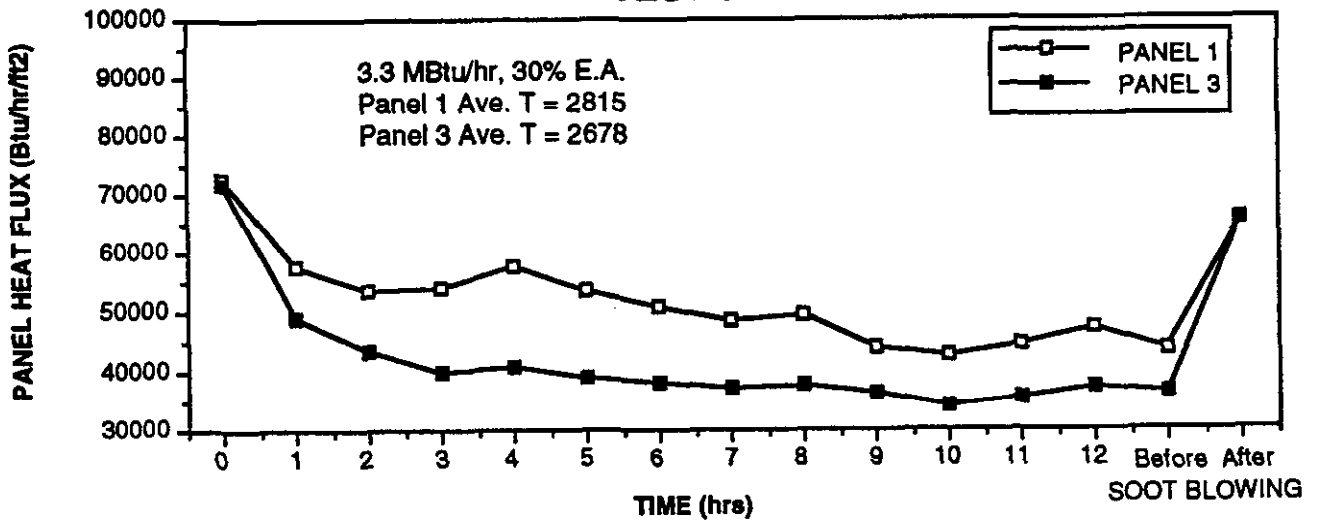


Figure 3.10 FPTF Waterwall Panel Heat Flux While Testing
100% WY Coal

TEST 4



TEST 5



TEST 6

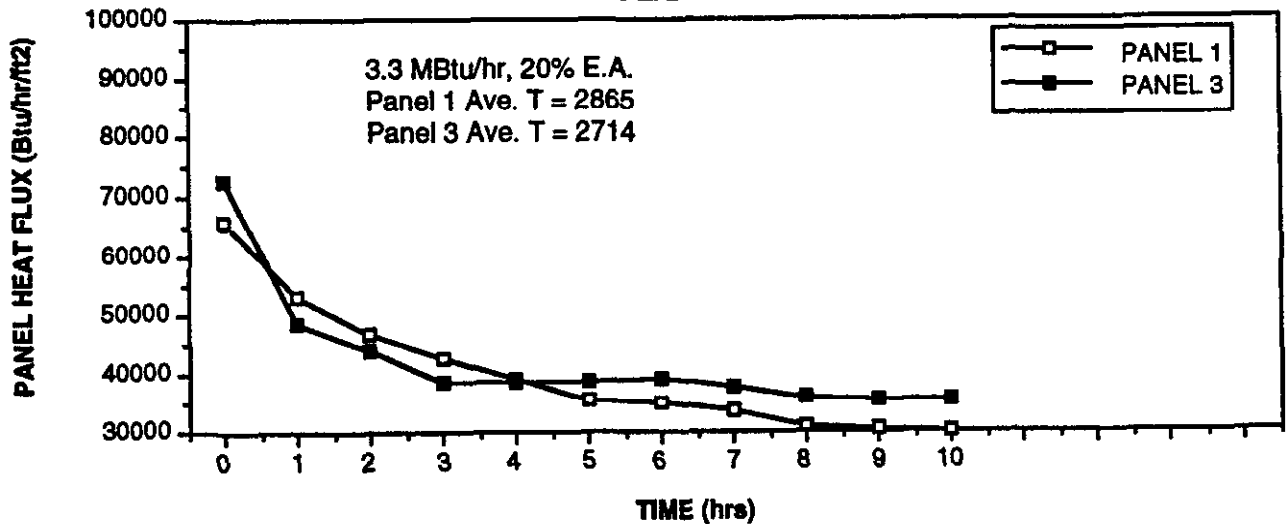
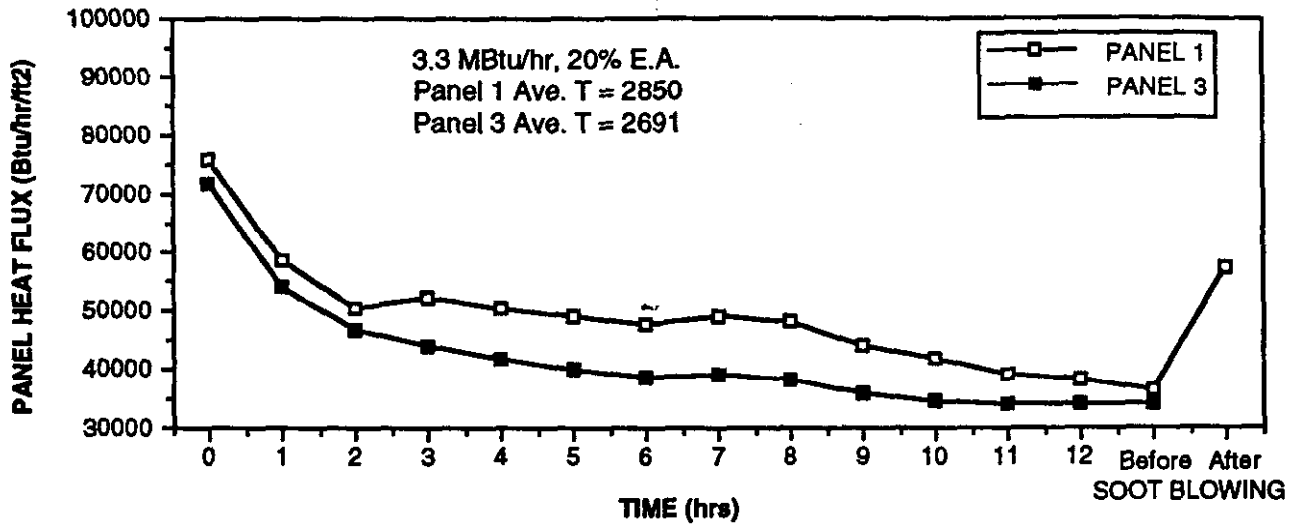
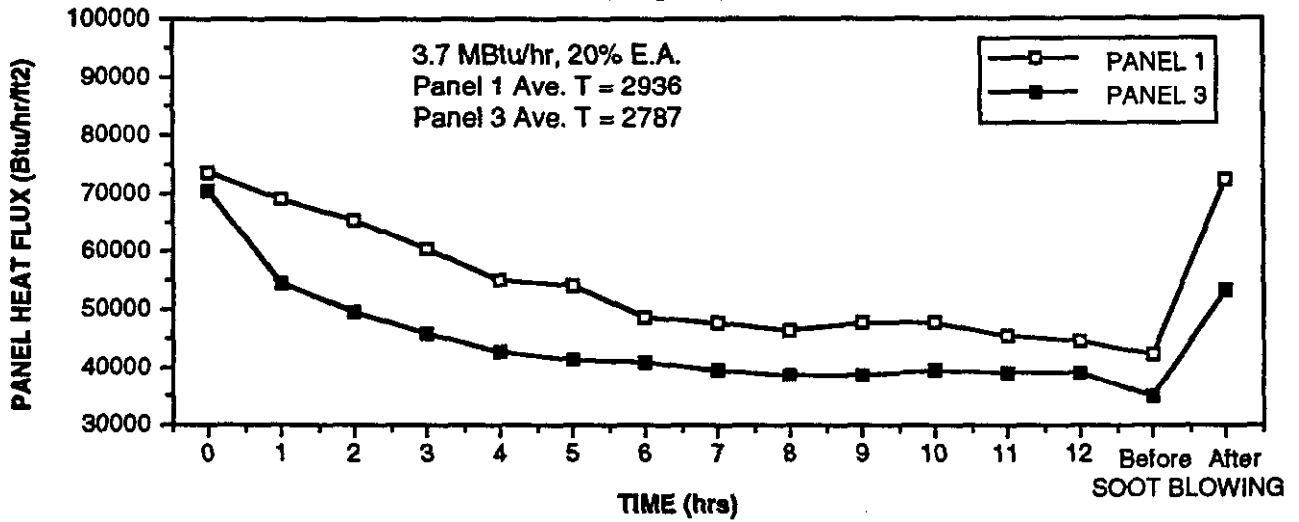


Figure 3.11 FPTF Waterwall Panel Heat Flux While Testing
100% WY Coal

TEST 1



TEST 2



TEST 3

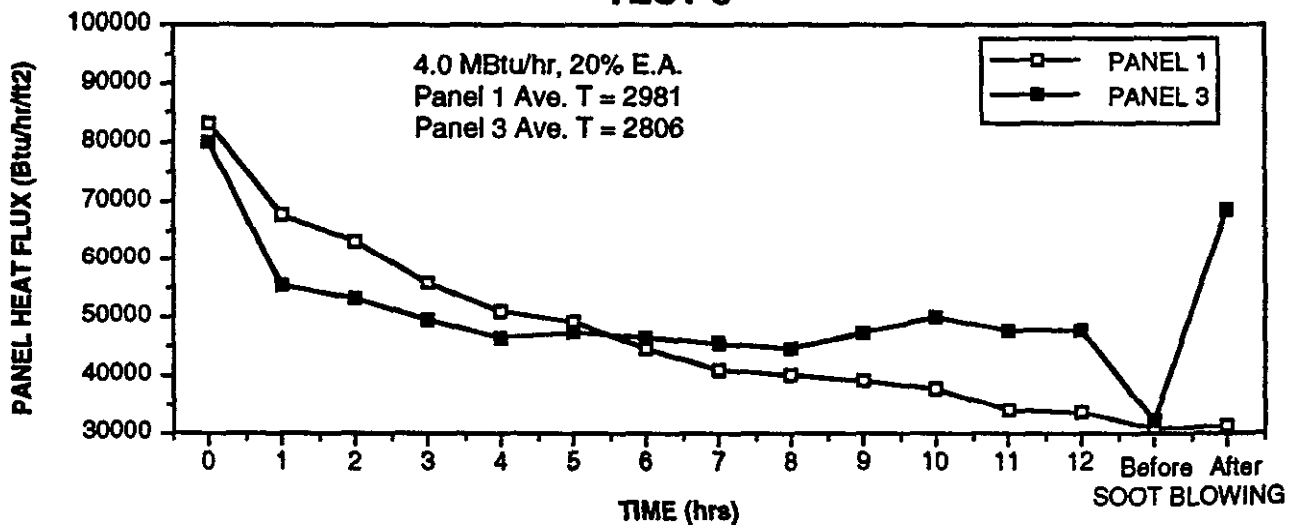


Figure 3.12 FPTF Waterwall Panel Heat Flux While Testing
90% WY/10% OK Coal Blend

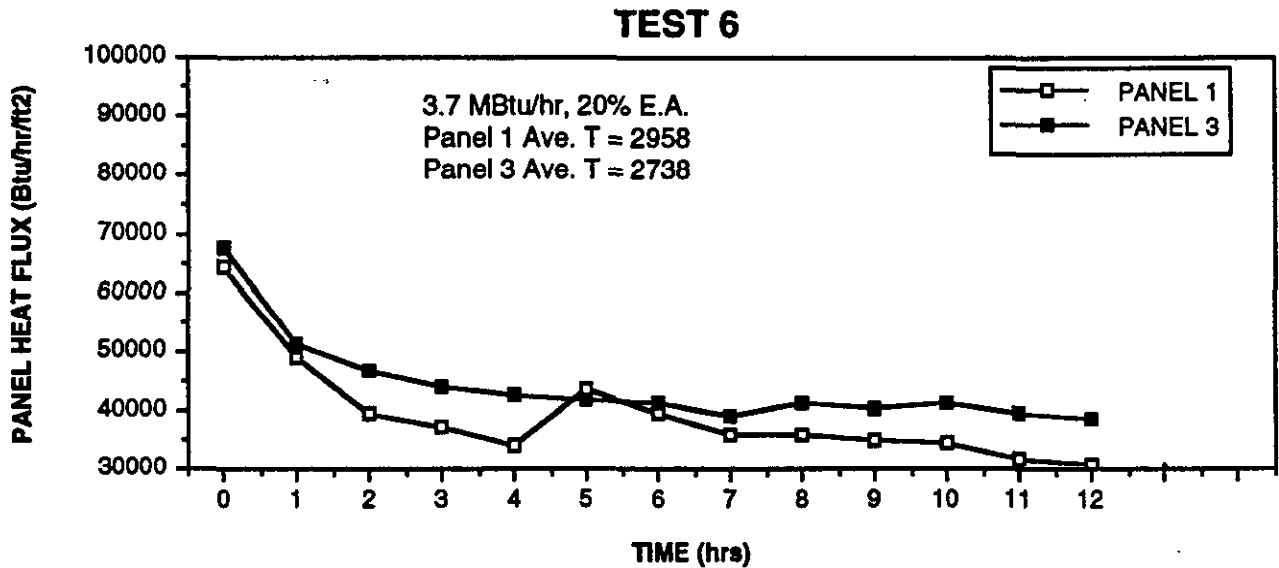
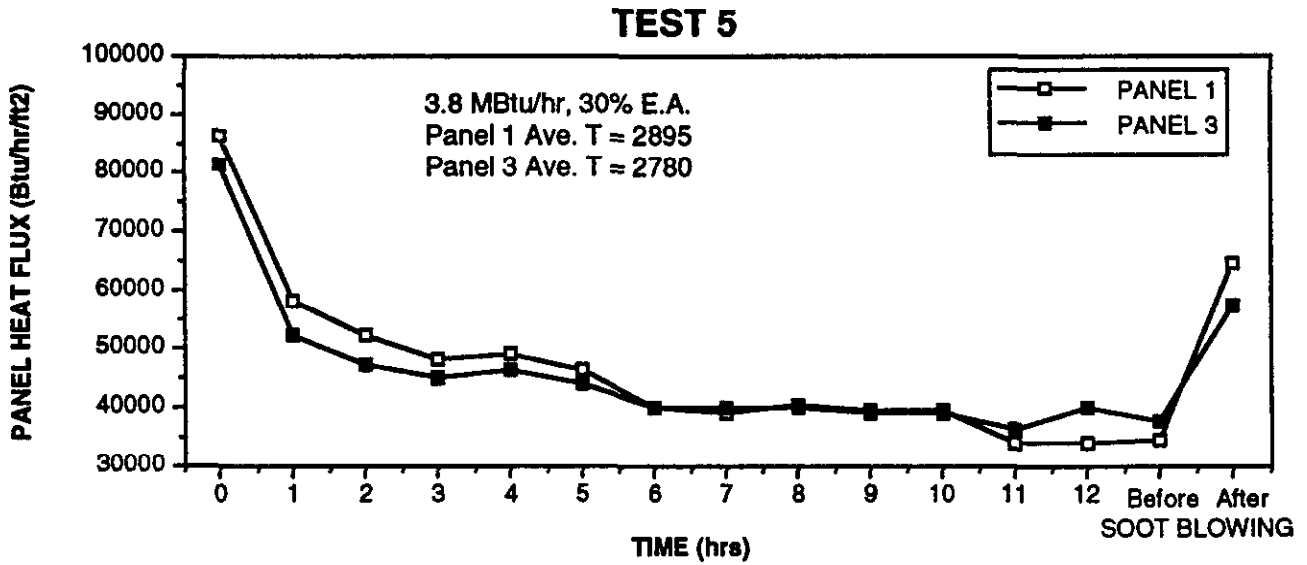
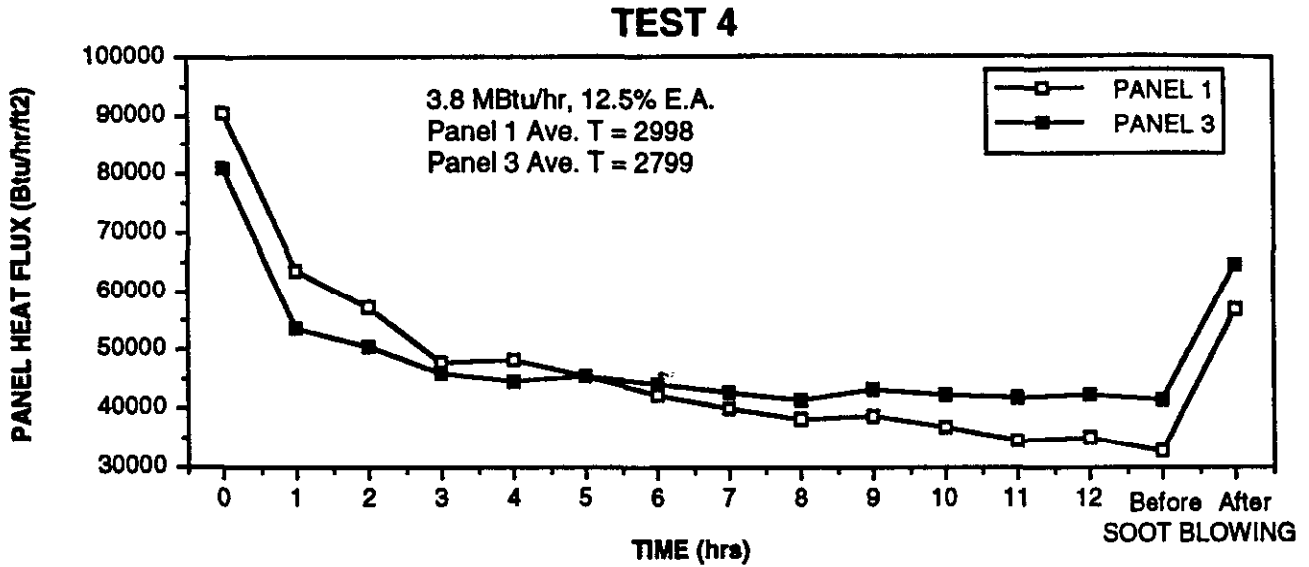


Figure 3.13 FPTF Waterwall Panel Heat Flux While Testing
90% WY/10% OK Coal Blend

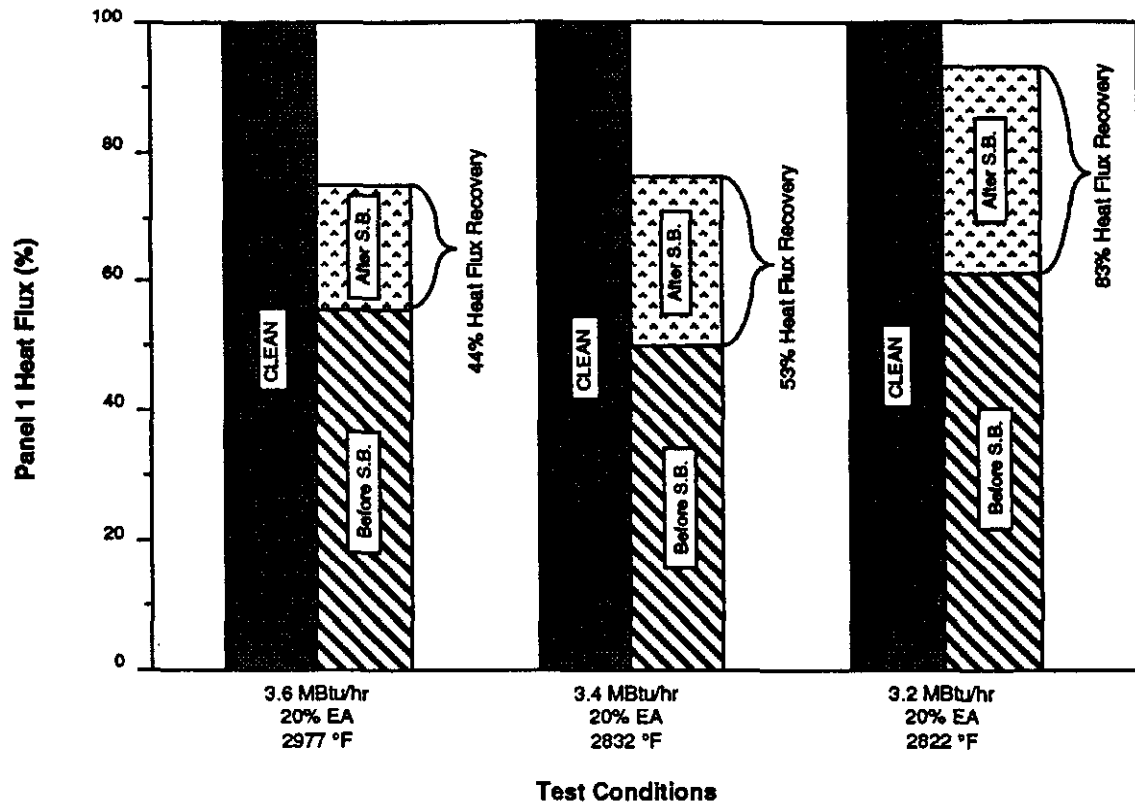


Figure 3.17 100% Wyoming Coal Heat Flux Summary

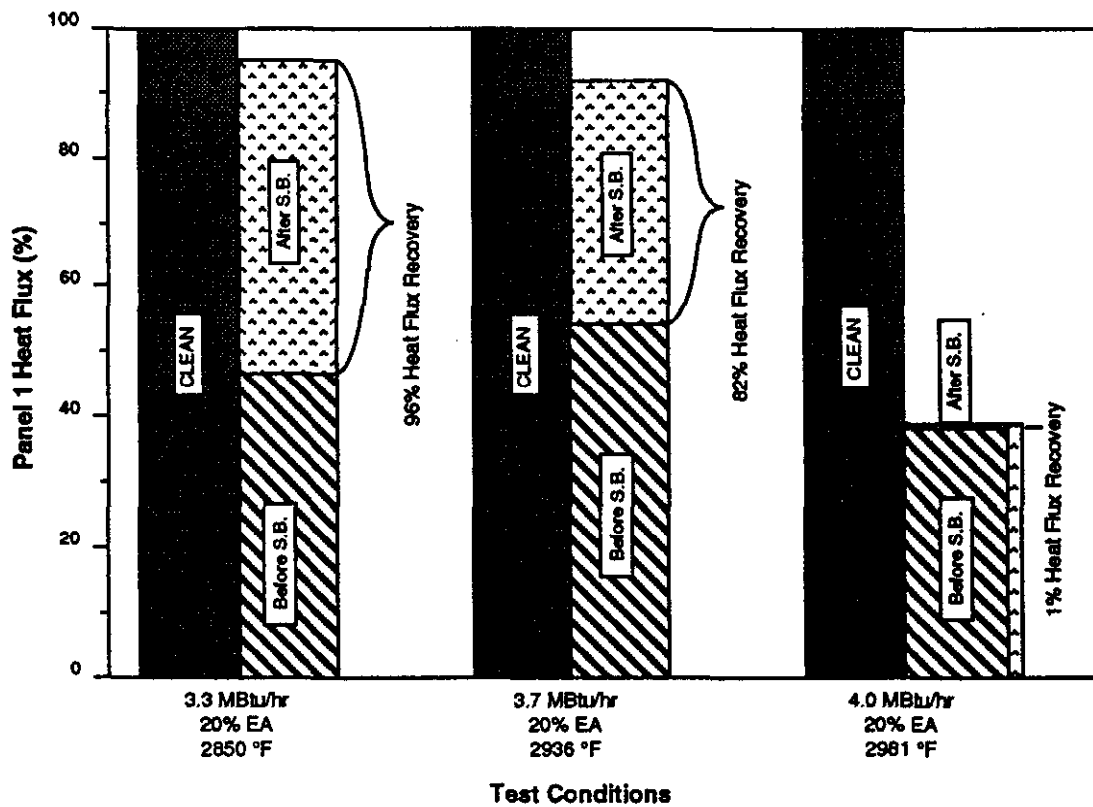


Figure 3.18 90% Wyoming / 10% Oklahoma Coal Blend Heat Flux Summary

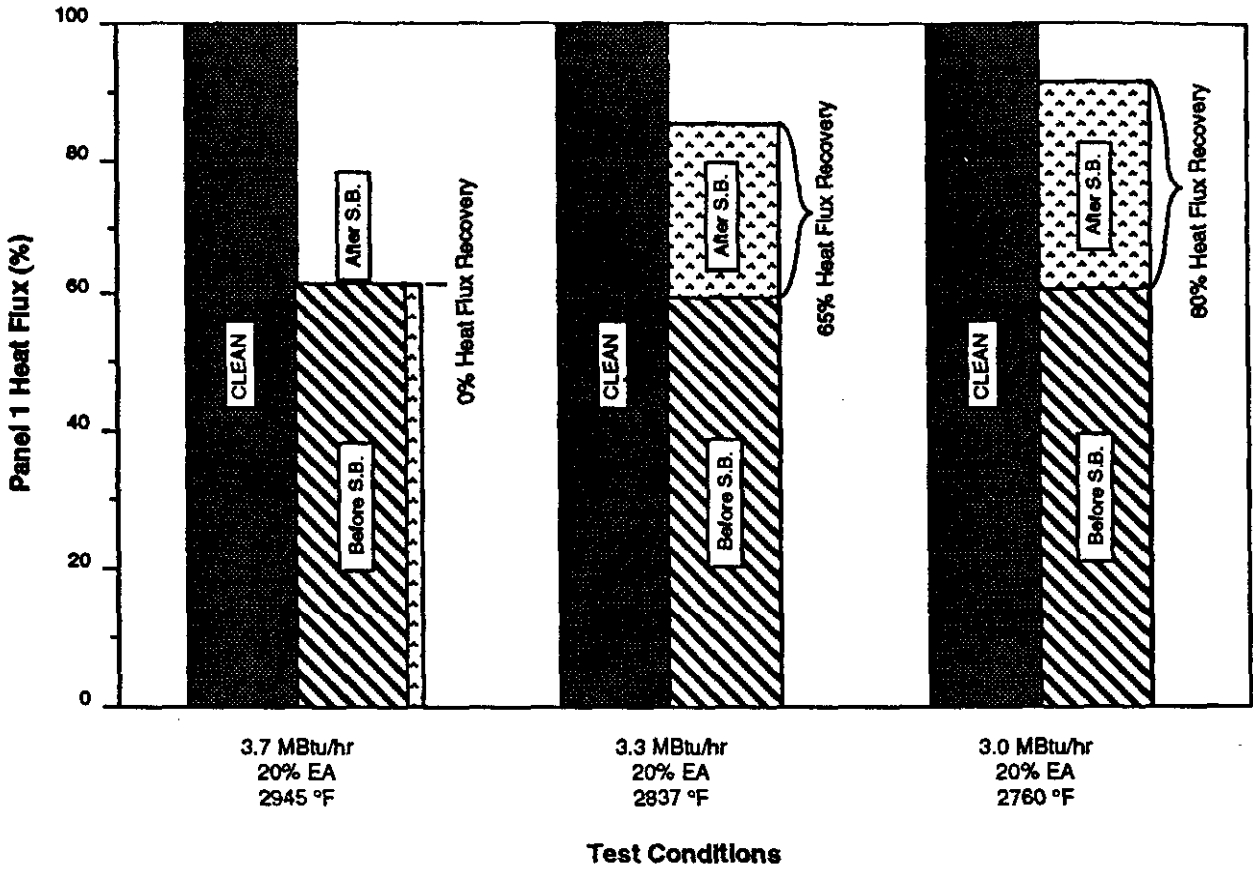


Figure 3.19 70% Wyoming / 30% Oklahoma Coal Blend Heat Flux Summary

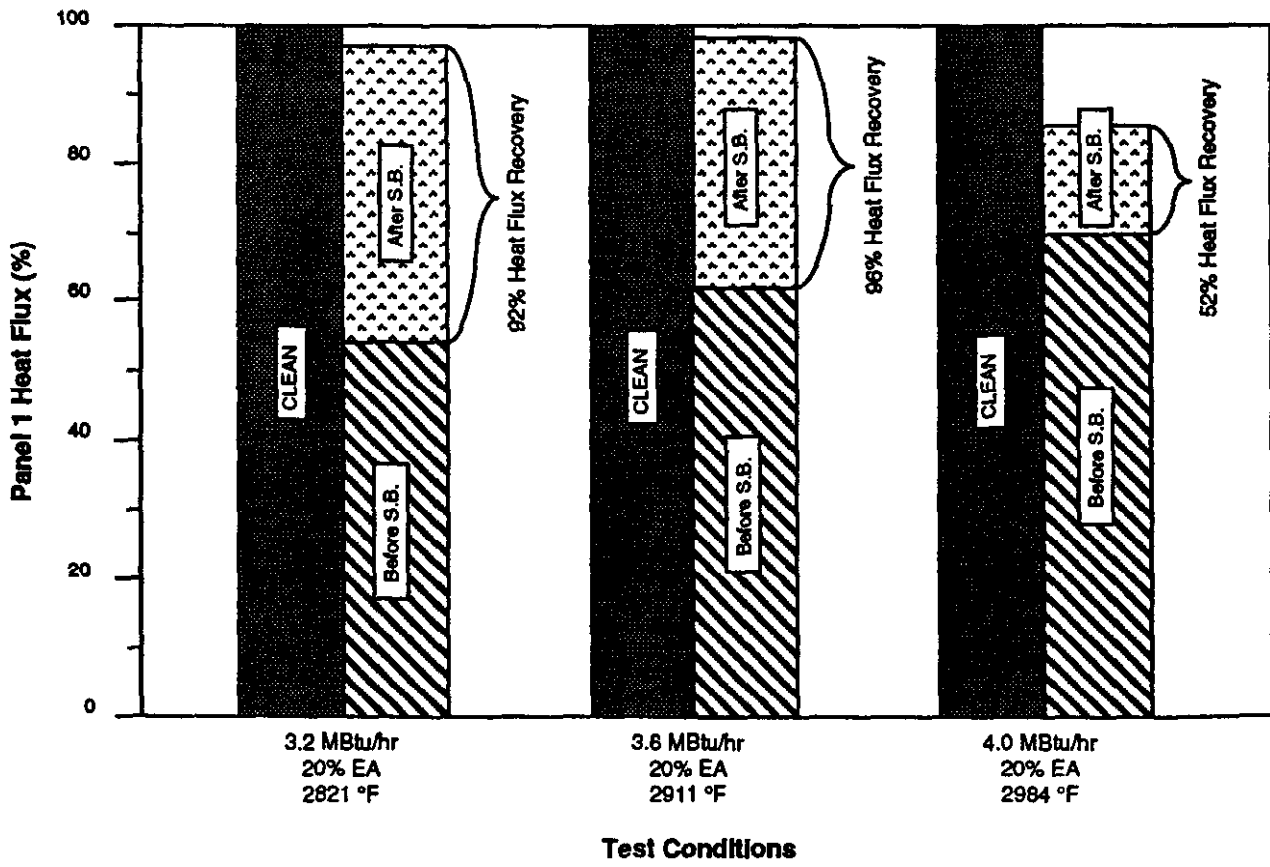


Figure 3.20 70% Wyoming / 30% Oklahoma Cleaned Coal Blend Heat Flux Summary

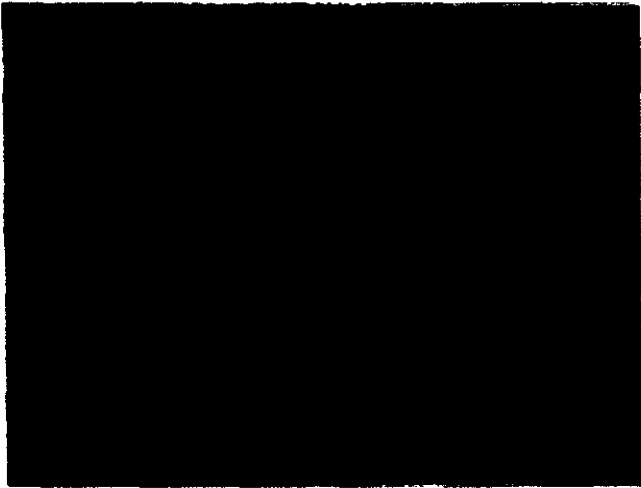
Table 3.5 FPTF Critical Thermal Conditions

<u>Fuel Description</u>	<u>Firing Rate (MBtu/hr)</u>	<u>Ave. Gas Temp at Level 1(°F)</u>
100% WY	3.3	2825-2850
90% WY/10% OK	3.8	2950-2975
70% WY/30% OK	3.2	2800-2825
70% WY/30% OK CLN	3.9	2975-3000

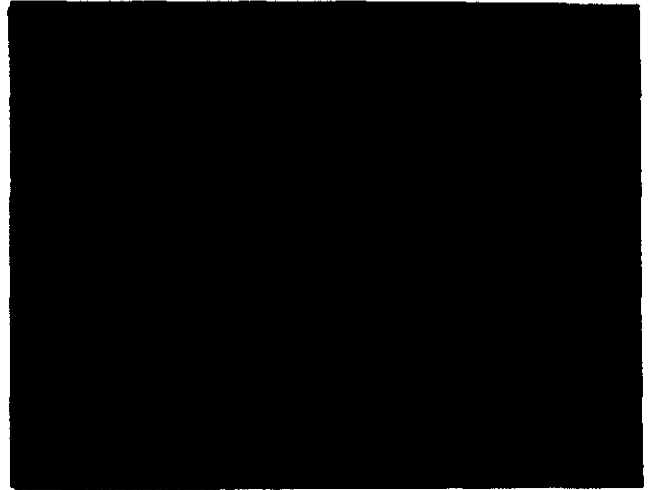
During the twelve-hour deposit buildup tests, the simulated waterwall panels were photographed at regular intervals to document the nature and rate of lower furnace wall deposition. Figures 3.21 to 3.29 present time-sequenced series of Panel 1 and Panel 3 photographs. Figures 3.22 to 3.27, and Figure 3.29 include end-of-test photographs of the panel after soot blowing, providing qualitative visual validation of the heat flux recovery data. Test conditions, including local (panel) gas temperatures, are provided for each series of photographs. Figure 3.21 shows the deposition history of the 100% WY fuel fired at critical thermal conditions (3.3 MBtu/hr), and illustrates typical deposit formation, growth and transition to the molten state.

Figures 3.22 and 3.23 depict the contrast between the deposition phenomena of thermal loadings below and above critical conditions, in this case for the 90% WY/10% OK fuel. In the test in which deposits were cleanable (Fig. 3.22), sintered deposits formed in the depressions between the tubes, or "webs", grew at a relatively slow rate, and became partially molten after about ten hours; soot blowing was effective and visibly removed almost all of the deposits. In the test in which deposits were not cleanable (Fig. 3.23), the deposits grew at a much greater rate, and became almost completely molten within eight hours; after twelve hours, the panel was almost entirely blanketed with molten deposit, and soot blowing was ineffective.

Figures 3.24 and 3.25 illustrate two 70% WY/30% OK tests, and show that in these tests the deposits formed were quite different from those formed in the 100% WY and the 90% WY/10% OK tests. In the 70% WY/30% OK tests, less molten deposit was



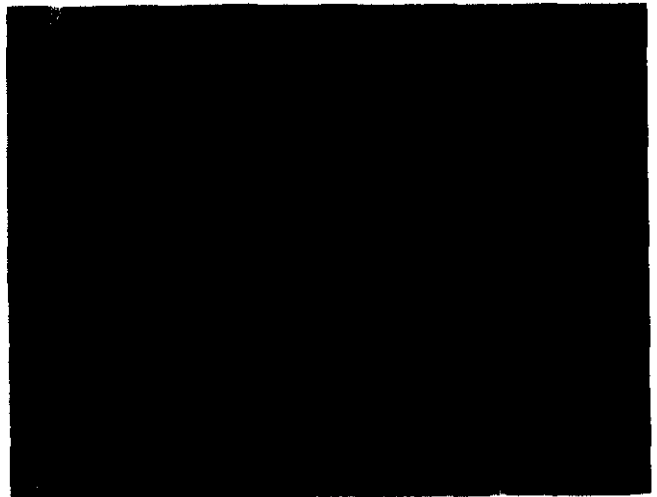
2 HOURS



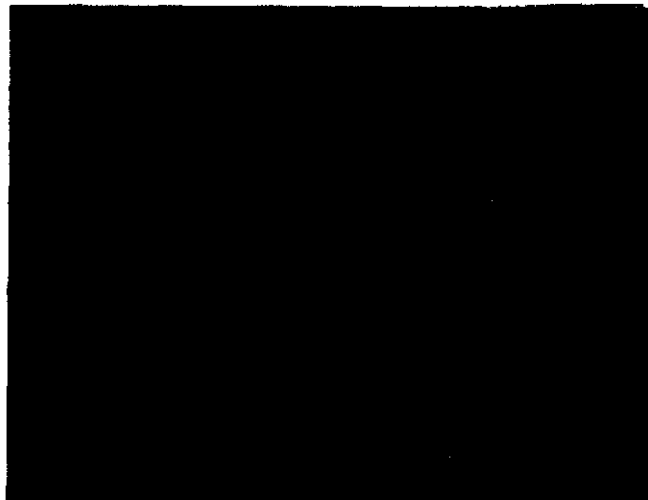
4 HOURS



6 HOURS



8 HOURS



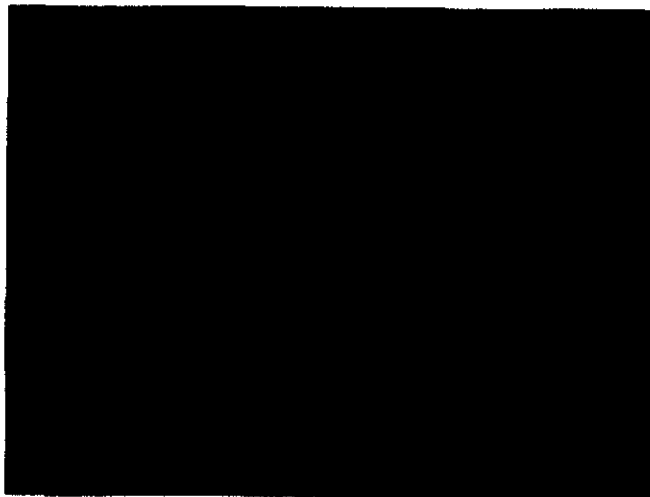
10 HOURS

PANEL 1

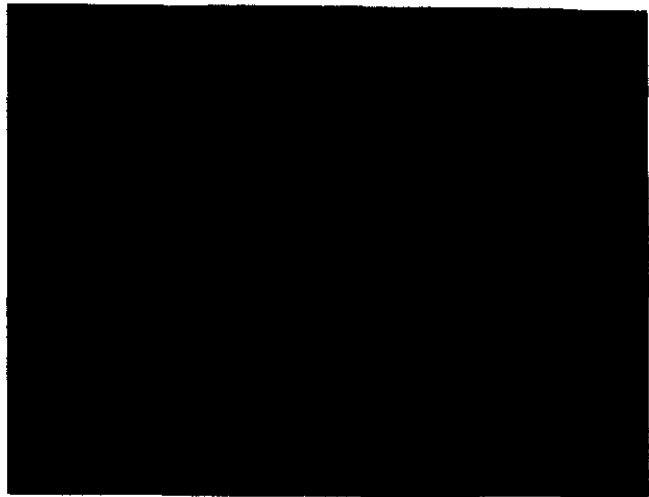
100% WY - TEST 6

3.3 MBtu/hr, 20% E.A., 2860 °F

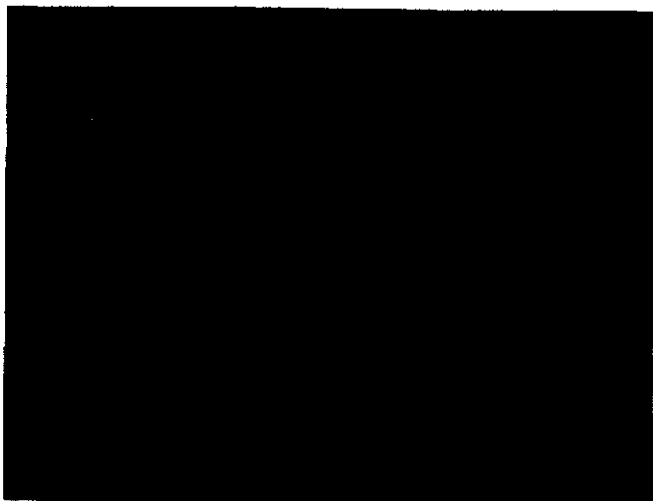
Figure 3.21 Lower Furnace Deposit Buildup - Time Sequencing



2 HOURS



4 HOURS



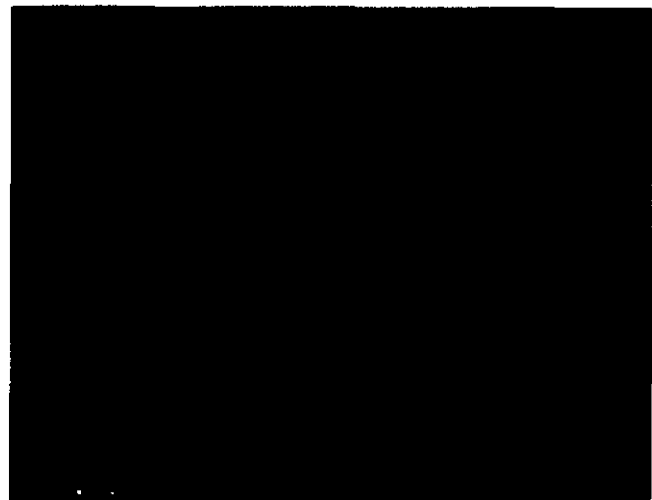
6 HOURS



10 HOURS



12 HOURS



After Blowing Soot -- 82% Recovery

PANEL 1

90% WY/10% OK - TEST 2
3.7 MBtu/hr, 20% E.A., 2935 °F

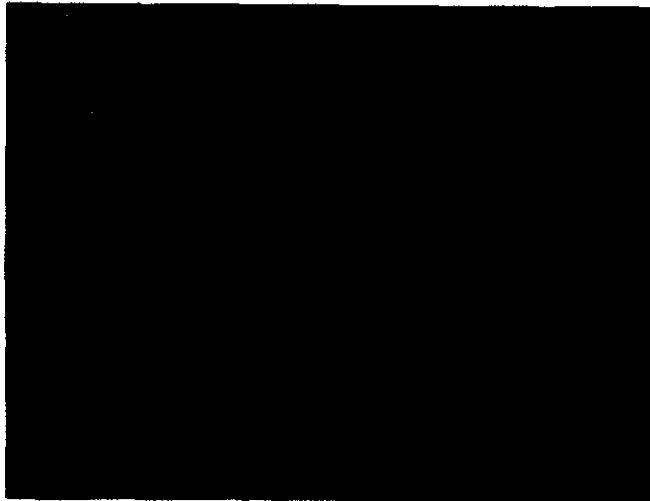
Figure 3.22 Lower Furnace Deposit Buildup - Time Sequencing



2 HOURS



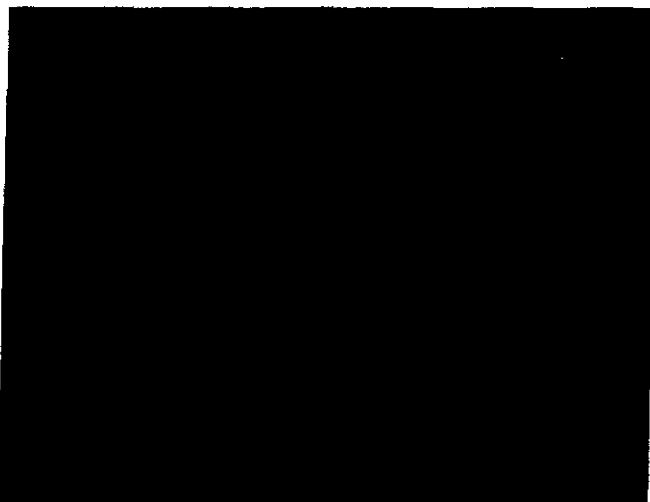
4 HOURS



8 HOURS



10 HOURS



12 HOURS

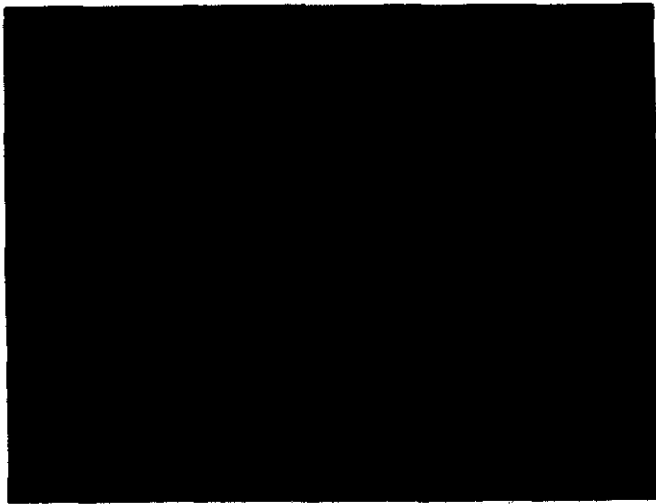


After Blowing Soot -- 1% Recovery

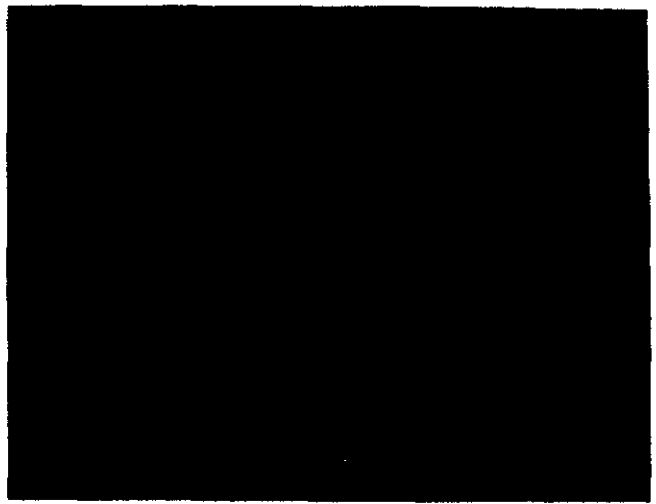
PANEL 1

90% WY/10% OK - TEST 3
4.0 MBtu/hr, 20% E.A., 2981 °F

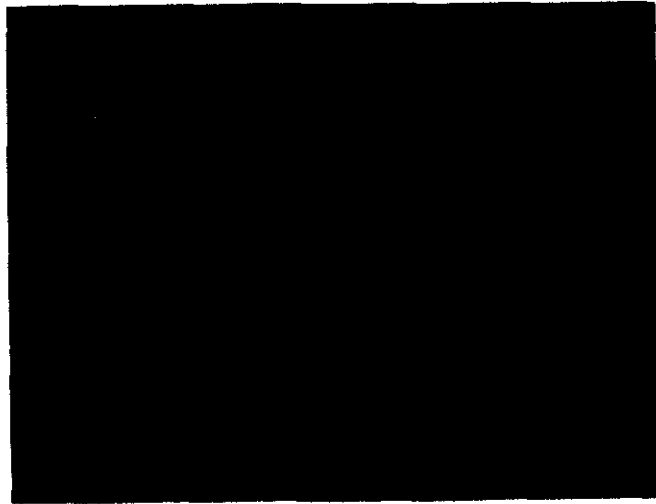
Figure 3.23 Lower Furnace Deposit Buildup - Time Sequencing



INITIAL



2 HOURS



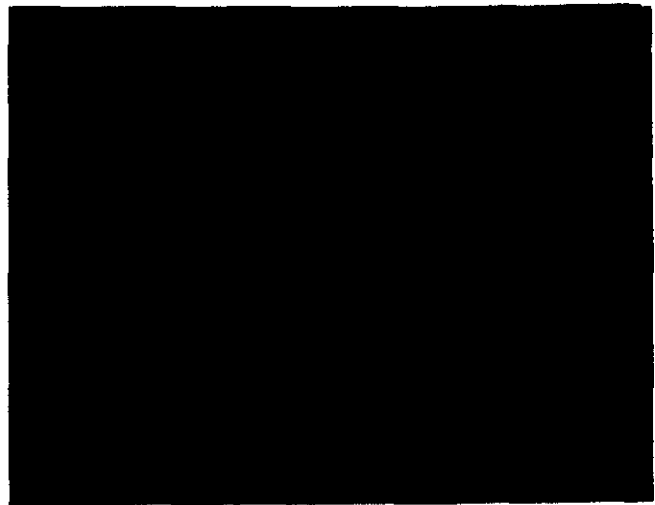
4 HOURS



8 HOURS



12 HOURS



After Blowing Soot -- 0% Recovery

PANEL 1

70% WY/30% OK - TEST 1
3.7 MBtu/hr, 20% E.A., 2945 °F

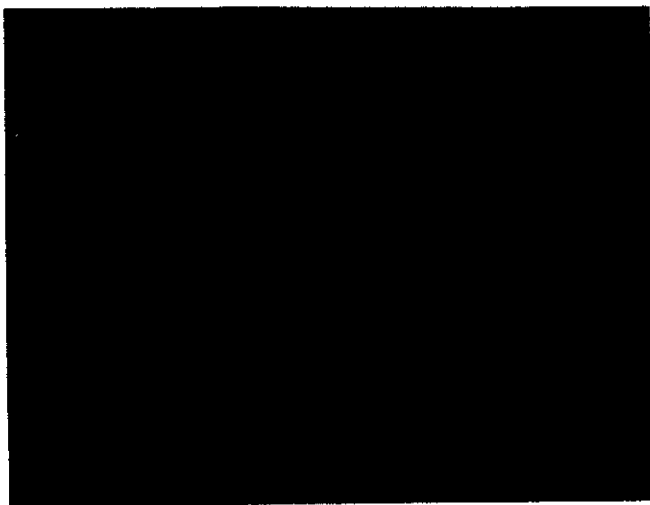
Figure 3.24 Lower Furnace Deposit Buildup - Time Sequencing



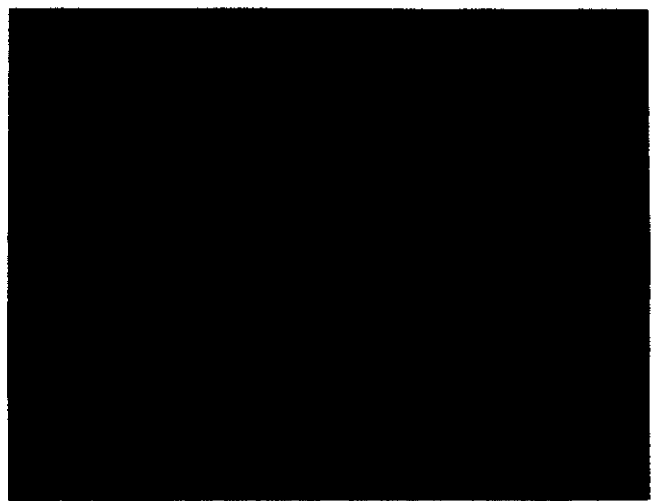
INITIAL



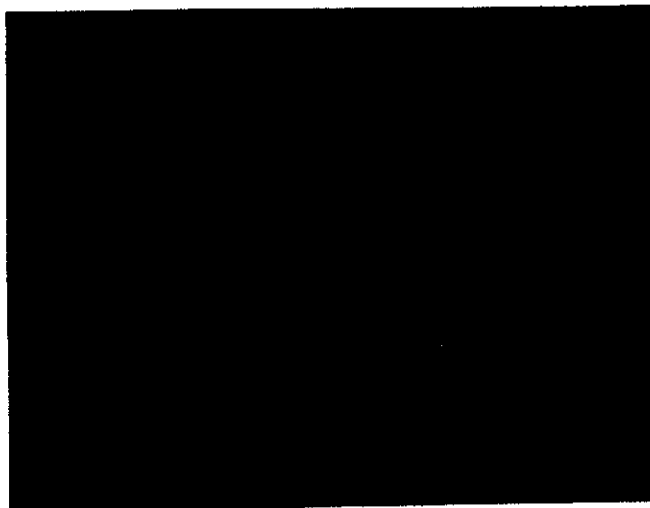
2 HOURS



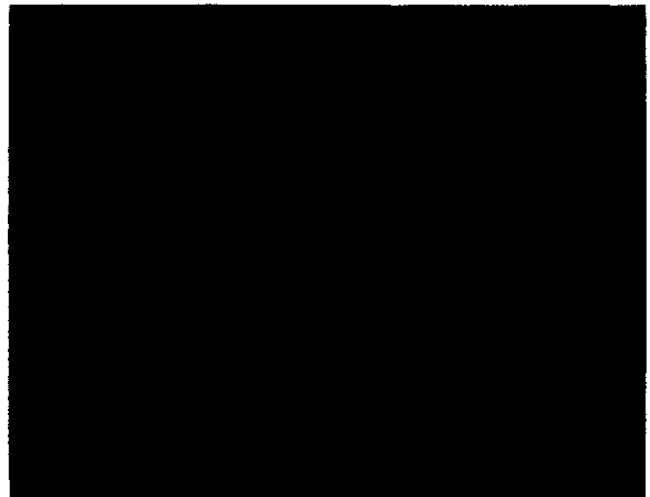
4 HOURS



8 HOURS



12 HOURS



After Blowing Soot -- 65% Recovery

PANEL 1

70% WY/30% OK - TEST 2
3.3 MBtu/hr, 20% E.A., 2837 °F

Figure 3.25 Lower Furnace Deposit Buildup - Time Sequencing



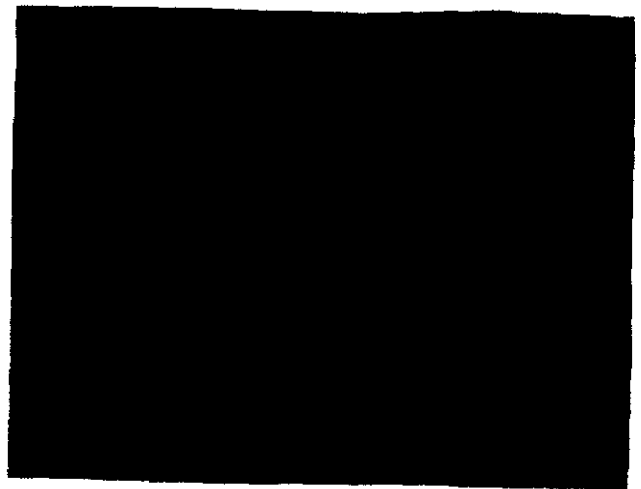
INITIAL



2 HOURS



4 HOURS



8 HOURS



12 HOURS

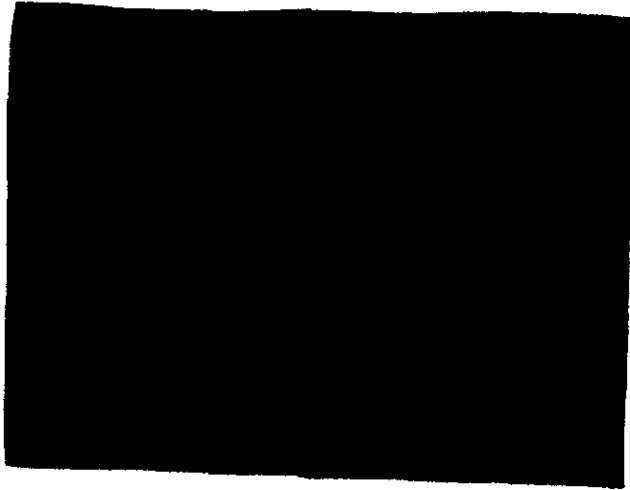


After Blowing Soot -- 92% Recovery

PANEL 1

70% WY/30% OK CLN - TEST 1
3.2 MBtu/hr, 20% E.A., 2821 °F

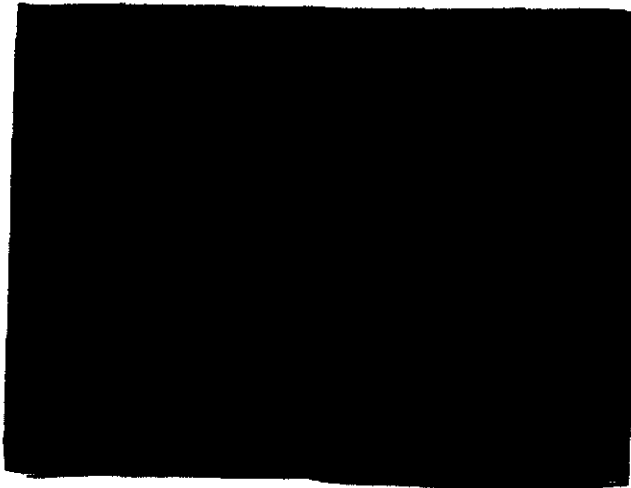
Figure 3.26 Lower Furnace Deposit Buildup - Time Sequencing



2 HOURS



4 HOURS



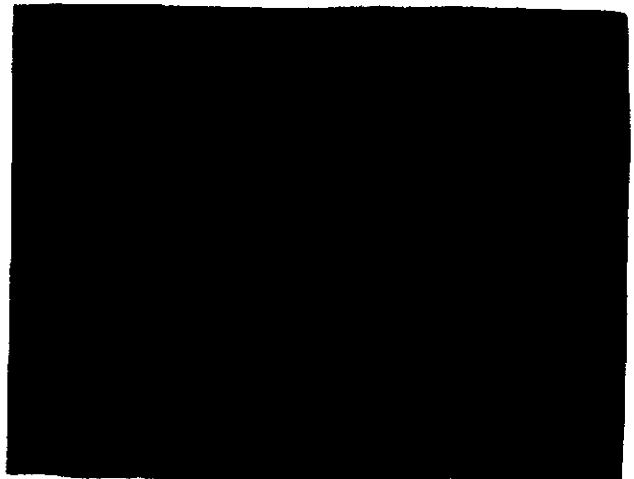
6 HOURS



8 HOURS



12 HOURS



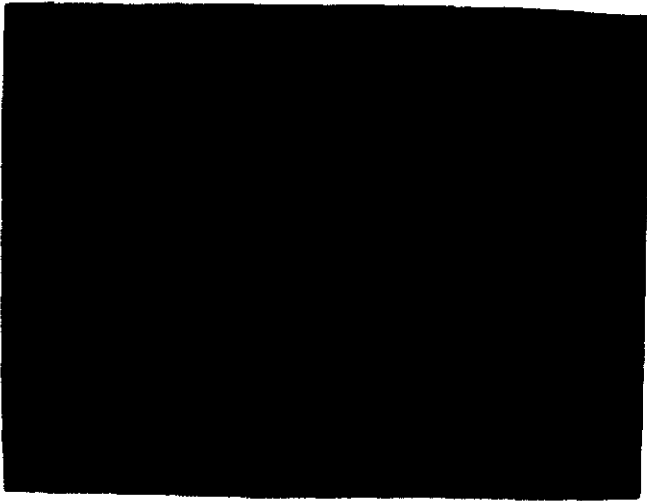
After Blowing Soot -- 96% Recovery

PANEL 1

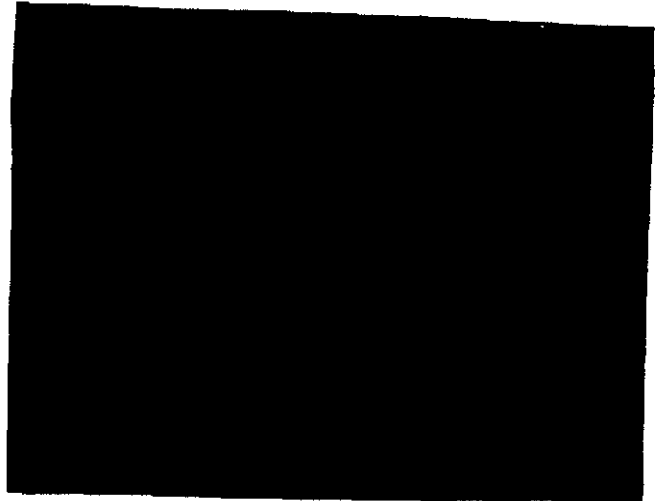
70% WY/30% OK CLN - TEST 2

3.6 MBtu/hr, 20% E.A., 2911 °F

Figure 3.27 Lower Furnace Deposit Buildup - Time Sequencing



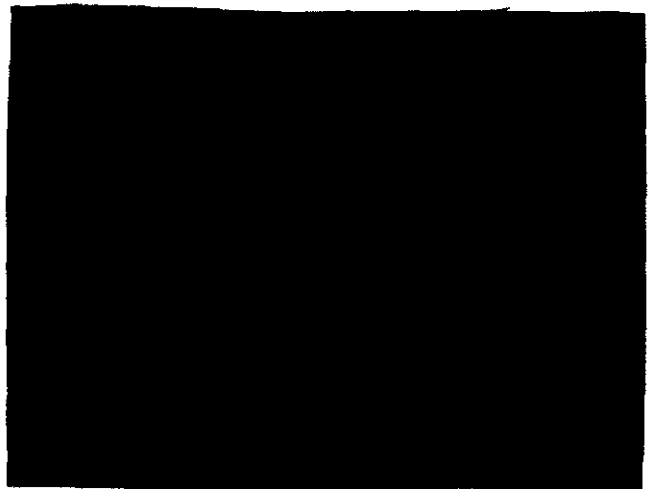
2 HOURS



4 HOURS



6 HOURS



8 HOURS



10 HOURS

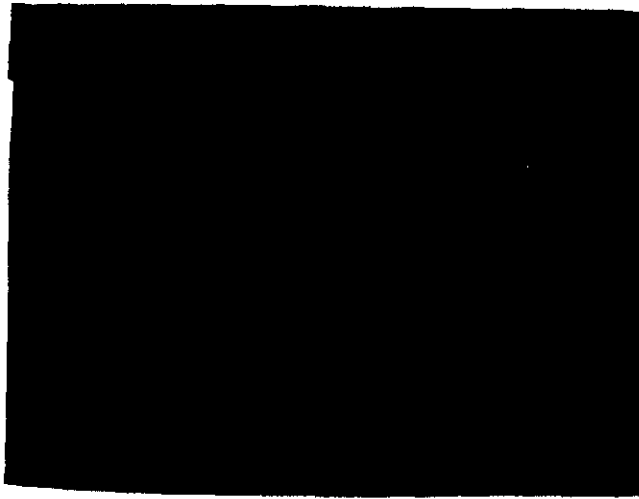


12 HOURS

PANEL 3

70% WY/30% OK CLN - TEST 2
3.6 MBtu/hr, 20% E.A., 2722 °F

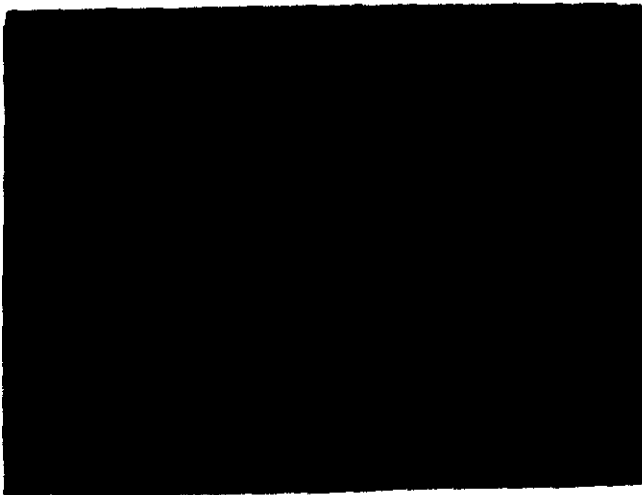
Figure 3.28 Lower Furnace Deposit Buildup - Time Sequencing



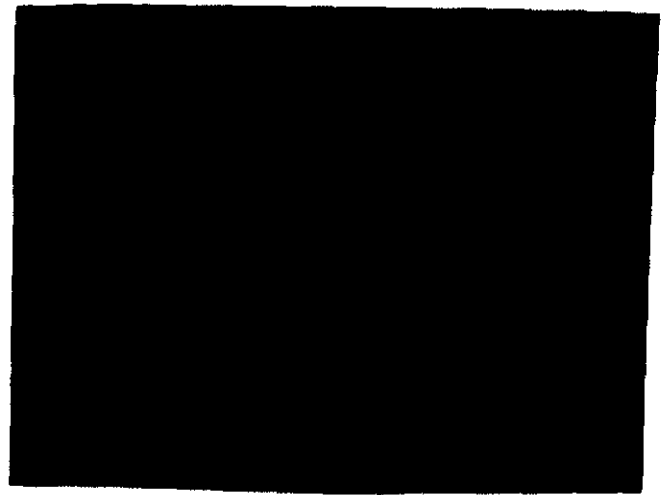
4 HOURS



6 HOURS



8 HOURS



12 HOURS



After Blowing Soot -- 51% Recovery

PANEL 1

70% WY/30% OK CLN - TEST 3

4.0 MBtu/hr, 20% E.A., 2984 °F

Figure 3.29 Lower Furnace Deposit Buildup - Time Sequencing

formed; instead, a tenacious sintered deposit layer more uniformly covered the entire panel, resulting in the lowest critical thermal conditions for the four fuels tested (3.2 MBtu/hr).

Figures 3.26 through 3.29 illustrate the waterwall panel deposit characteristics of the 70% WY/30% OK CLN fuel. Figures 3.26 and 3.27 depict tests conducted at thermal loadings below critical conditions, and show that even when soot blowing was very effective (>90% heat flux recovery for these tests), there remained a tenacious initial deposit layer, as evidenced by the photographs and the incomplete heat flux recoveries. Panel 3 deposition characteristics are shown in Figure 3.28 for the 3.6 MBtu/hr test, corresponding to the Panel 1 photographs shown in Figure 3.27. Local gas temperatures at Panel 3 were nearly 200 °F lower than those at Panel 1; consequently, deposition on Panel 3 was much less severe. During the course of combustion testing of all four fuels, it was found that in every case in which Panel 1 was cleanable (>75% heat flux recovery), Panel 3 was cleanable as well. Figure 3.29 illustrates a test for the 70% WY/30% OK CLN fuel, conducted at a thermal loading above critical conditions. The final photograph shows that during soot blowing, deposits were not removed uniformly across the panel, and emphasizes that in field operation deposit cleanability is a function not only of deposit characteristics, but also of soot blower placement and aerodynamics.

Figure 3.30 provides a lower furnace cleanability comparison between all four fuels tested at the same excess air and very similar Level 1 (L1) gas temperatures (L1 is the first panel elevation). Heat flux recoveries on the 90% WY/10% OK and the 70% WY/30% OK CLN were notably higher than those resulting from the 100% WY and the 70% WY/30% OK fuels.

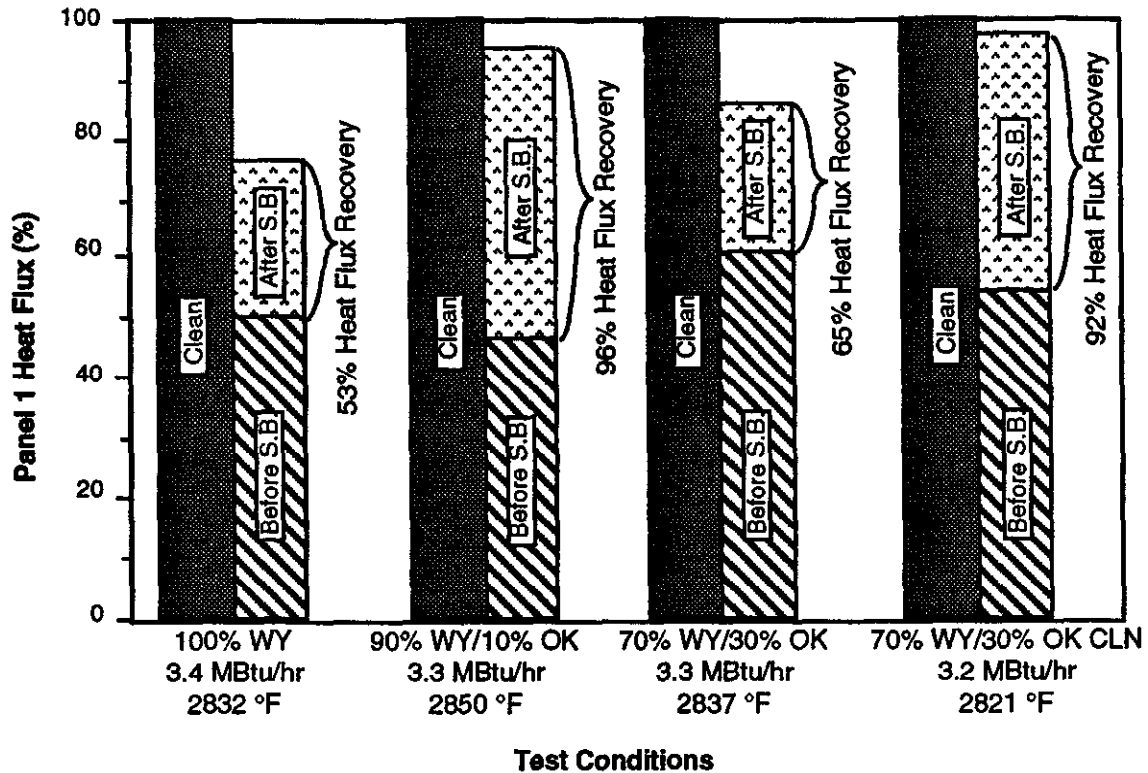


Figure 3.30 Cleanability Comparison Between the Four Fuels at Similar Loads

3.2.3.2 Description of Waterwall Slag Deposition and Deposits

Slag deposits range in consistency from being lightly sintered to molten flowing material. These lower furnace deposits reduce heat transfer. The decrease in heat transfer is the result of a combination of radiative properties (emissivity) and thermal resistance (thermal conductivity) of a deposit. The physical state of the deposit has a significant effect on the heat-transfer properties. For example, a molten deposit will have higher emissivity than a sintered deposit. In some cases, heat transfer can be significantly reduced by the formation of a highly reflective ash layer in the radiant section. This reflective ash layer is a result of the transport of small particles to the heat-transfer surface and is characteristic of coals that produce an abundance of small particles. Molten deposits may be more difficult to remove than sintered deposits. Therefore, the physical state of the deposit must be predicted as a function of coal composition, firing conditions, geometry, and location in the boiler.

Key factors contributing to the formation of slag deposits include (1) gas flow patterns resulting in impacting and sticking particles; (2) high levels of fine particulate that are thermophoretically deposited; (3) low-excess air conditions, causing localized reducing conditions which increase the quantity of low melting point phases; (4) a molten captive deposit surface forming that becomes an efficient collector of impacting particles; and (5) decrease in heat transfer, causing increases in deposit temperatures and aggravation of slagging and fouling problems.

Slag deposits are usually dominated by silicate liquid phases, but may also contain moderate to high levels of reduced iron phases. The initial layers of slag deposits are usually rich in small, lightly-sintered particles along with larger particles that have impacted the surface and adhered. These initial layers are composed of simple oxides, such as CaO, MgO, FeO, Fe₂O₃, and Fe₃O₄, and complex silicate phases that are stable in the radiant section of the boiler. The initial layer produces a captive liquid surface that is necessary for rapid deposit growth.

Analyses of outer and inner layers of slag collected on water wall panel 1 for each fuel are given in Table 3.6. The analyses used were scanning electron microscopy point count analysis (SEMPC) and X-ray diffraction (XRD). The inner layers show enrichment in quartz, anhydrite, and amorphous material. These phases are all typical of the fine ash particulate or vaporized oxides and sulfates that adhere or condense on clean steel surfaces, forming the white initial deposit layer. The inner layer deposits showed increased anhydrite with increased Oklahoma coal in the blend. Greater sulfur content in the Oklahoma coal from pyrite may have contributed to the enhanced calcium sulfate production.

The inner layers of the slag deposits are composed of very fine ash particulate and condensed vapor species from selective deposition of the fine (< 5µm) the in-flame solids as shown in Figure 3.31. The initial deposits formed during the testing of the PSO fuels The Wyoming coal contains more smaller-sized, Ca-rich reflective ash species such as calcium oxide (lime) and calcium silicate, which may tend to drive up the furnace outlet gas temperature (FOT).

Table 3.6 Compositions of Panel 1 Water Wall Slag Deposits

Minerals Phases	100% WY		90%WY/10% OK		70%/30%OK		70/30 CLN Blend	
	Outer	Inner	Outer	Inner	Outer	Inner	Outer	Inner
Gehlenite	0.0	4.0	0.0	0.8	0.4	1.6	0.0	0.8
Anorthite	16.8	4.0	0.0	1.2	19.6	9.6	28.0	4.4
Albite	0.0	0.4	0.0	0.0	0.0	0.0	0.0	0.0
Pyroxene	0.0	0.4	0.0	0.0	0.8	0.0	0.8	0.4
Calcium Silicate	0.0	0.0	0.0	0.0	2.0	1.6	0.0	0.0
Calcium Aluminate	0.0	0.0	0.0	1.2	0.0	0.0	0.0	0.0
Quartz	5.6	11.2	2.4	12.4	4.0	14.0	2.0	4.8
Iron Oxide	4.0	2.0	0.0	1.6	1.6	3.2	0.8	1.2
Calcium Oxide	0.0	0.0	0.0	0.8	0.4	0.8	0.0	0.0
Anhydrite	0.0	1.2	0.0	2.8	6.4	6.4	1.2	4.4
Pyrrhotite	0.0	1.6	0.0	1.6	0.0	0.0	0.0	0.0
Pure Kaolinite	0.0	2.4	0.0	2.4	0.4	0.8	0.0	0.8
Kaolinite Derived	0.4	3.2	0.0	5.6	2.4	3.6	2.0	7.6
Illite (Amorp)	0.0	1.2	0.0	0.4	3.2	3.2	0.0	3.2
Montmorillonite	44.8	2.8	97.2	3.2	15.6	7.2	35.6	4.4
Unclassified	28.4	65.2	0.4	65.6	42.4	47.6	68.0	30.8
Bulk Oxide Composition (Wt%)								
SiO ₂	61.3	35.0	59.7	36.9	46.4	42.3	58.5	39.9
Al ₂ O ₃	17.0	21.0	18.3	22.8	16.4	20.1	15.2	23.6
Fe ₂ O ₃	10.4	6.4	10.3	5.9	8.6	9.2	9.1	7.8
TiO ₂	0.9	1.8	1.0	2.3	1.2	1.1	1.1	1.4
P ₂ O ₅	0.3	0.9	0.1	1.1	0.6	0.6	0.3	1.1
CaO	6.3	26.1	7.3	22.5	19.0	15.2	10.9	17.9
MgO	2.0	5.5	1.6	5.0	3.4	3.8	2.5	3.3
Na ₂ O	0.8	1.5	0.8	1.8	1.4	1.7	0.9	1.8
K ₂ O	0.6	0.7	0.8	1.6	2.4	5.0	1.4	2.9
ClO	0.0	0.0	0.0	0.0	0.0	0.0	0.0	0.0
BaO	0.3	0.7	0.0	0.0	0.4	0.8	0.0	0.0
SO ₃ (added for comparison)	0.1	14.3	0.0	16.0	6.9	13.6	0.1	13.2
Major Minerals (XRD)								
	<u>100% WY</u>		<u>90/10 Blend</u>		<u>70/30 Blend</u>		<u>70/30 CLN Blend</u>	
Outer Layer	Plagioclase Cristobalite Hematite		Plagioclase Al Diopside		Plagioclase Anhydrite Augite		Plagioclase Hematite	
Inner Layer	Quartz Anhydrite		Anhydrite Quartz Hematite Fe Spinel		Anhydrite Quartz		Hematite Quartz	
Minor Minerals (XRD)								
	<u>100% WY</u>		<u>90/10 Blend</u>		<u>70/30 Blend</u>		<u>70/30 CLN Blend</u>	
Outer Layer	Maghemite Quartz		Quartz Hematite Fe Spinel		Quartz Melilite Hematite		Quartz Diopside Fe Spinel	
Inner Layer	Maghemite Hematite				Plagioclase Augite Hematite		Plagioclase Diopside Fe Spinel	

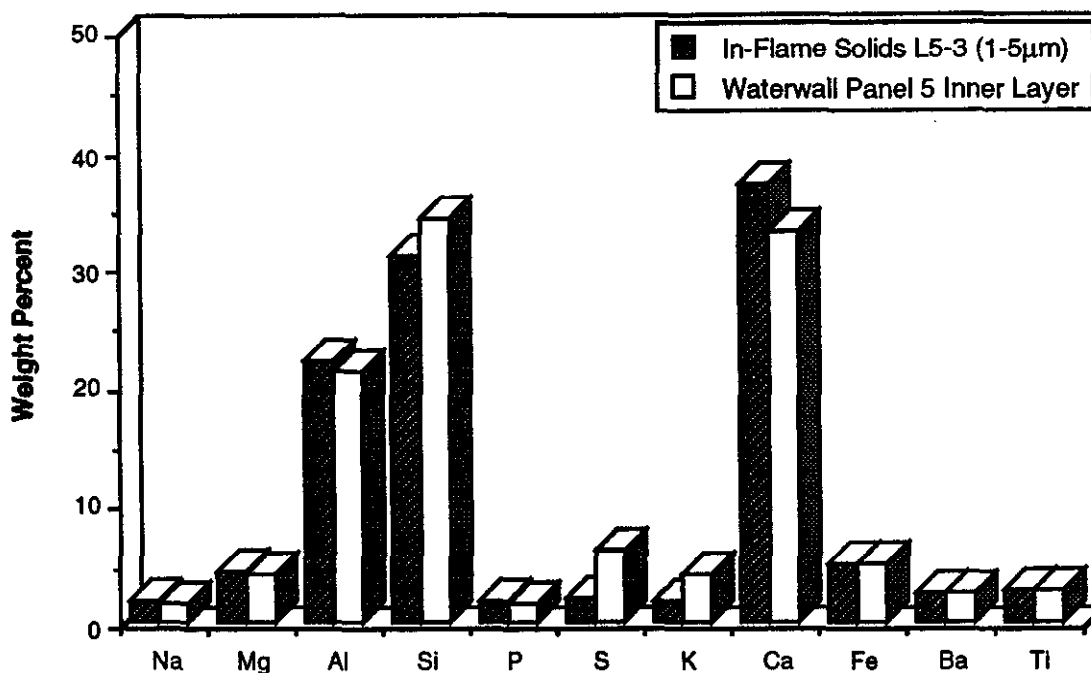


Figure 3.31 Comparison of In-Flame Solids (L5-3) with Waterwall Panel 5 Inner layer (100% WY)

Viscosity distributions of silicate liquid phase in the waterwall deposit inner layers are given in Figure 3.32. The 100% Wyoming, 90/10 blend, and 70/30 cleaned blend have the lowest viscosity values and largest quantity of liquid phase that is less than 250 poise. This large amount of inner layer liquid phase for the 100% Wyoming originated from the large amount of small in-flame solid particles (Figure 3.7). These particles are responsible for producing the low viscosity captive surface. In theory, these deposits may show strong relative adhesive strength and poorer heat flux recovery after soot blowing.

Generally, outer deposits contain more silica (SiO_2) (Table 3.6), which appears to be originating from quartz and clay particles impacting and sticking. Viscosity distributions of silicate liquid phase in the waterwall deposit outer layers are given in Figure 3.33. The 90/10 blend has the largest quantity of low viscosity liquid phase. The dominant phase in the outer deposits for all the fuels is the phase classified as montmorillonite, which is not actually the mineral montmorillonite but is a high Si/Al

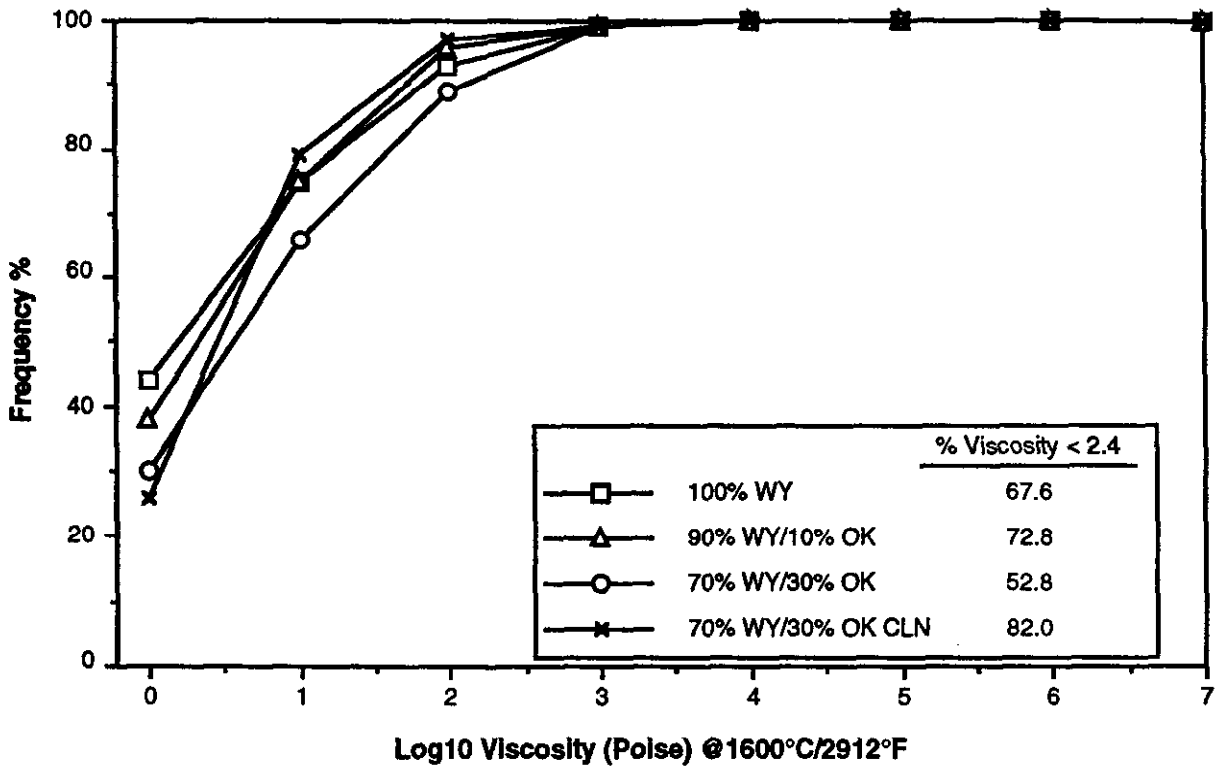


Figure 3.32 Viscosity Distribution Comparison -- Waterwall Panel 1 Inner Layers

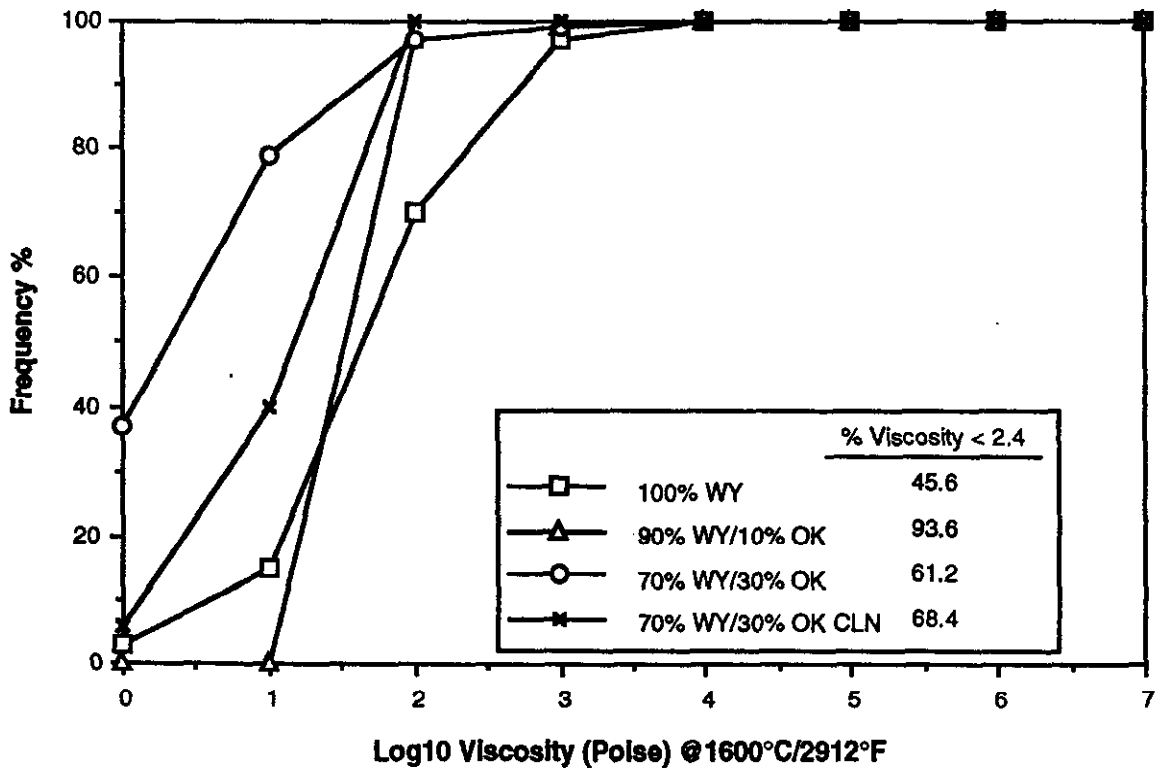


Figure 3.33 Viscosity Distribution -- Waterwall Panel 1 Outer Layer

ratio calcium, iron, or potassium-rich aluminosilicate. This amorphous phase is a product of the assimilation of impacting quartz particles into the reactive captive surface. Another major phase in the outer layer is anorthite (SEMPC) or plagioclase (XRD).

Examination of relevant field data has substantiated the results from pilot-scale testing with regard to lower furnace ash deposit effects. Figure 3.34 shows the furnace outlet temperatures (FOTs) as a function of the location across the width of the commercial unit at similar loads and firing conditions for the different field-tested fuels as indicated. The gas temperatures reported in Figure 3.34 were taken at the furnace outlet plane parallel to the furnace nose as shown in Figure 3.35. Because the furnace is fifty-two feet wide, half of the measurements were taken from the north (left) side and the other half from the south (right) side. Space limitations precluded temperature measurement for the middle twelve feet of the furnace.

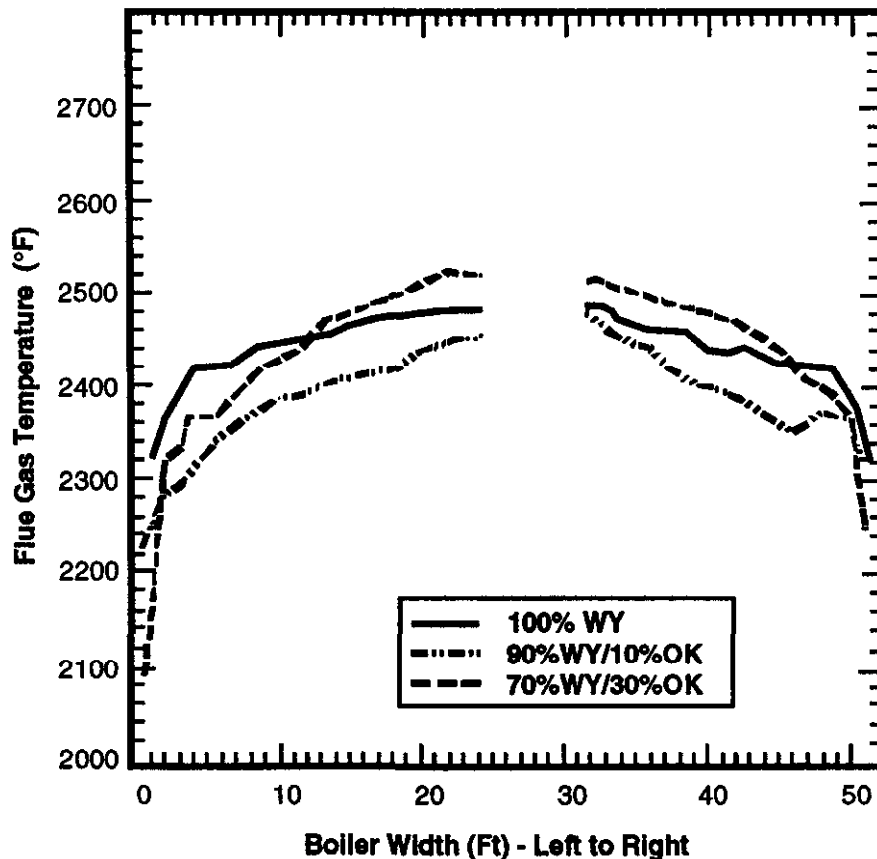


Figure 3.34 A Comparison of Furnace Outlet Gas Temperatures Under Similar Furnace Loads for the Coal/Coal Blends Tested in the Field (EER)

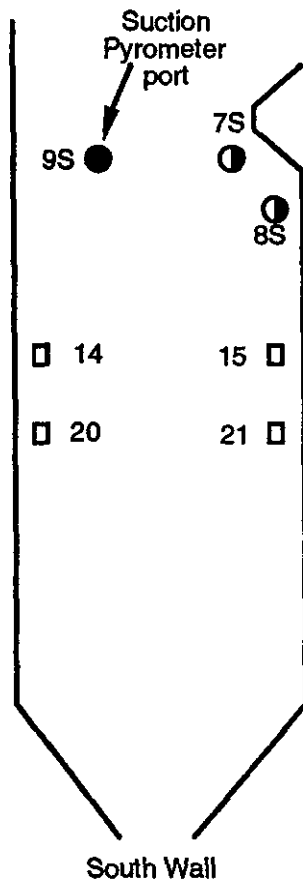


Figure 3.35 Schematic Elevational View of Northeastern Unit 4 Showing the Location of the Furnace Outlet Temperature Measurements

As expected, average gas temperatures dropped off near the side walls for each test case (this is probably due to cooling from the open port as well as cooling from the furnace walls). The average gas temperatures across the width of the furnace were approximately the same for the 100% WY and the 70% WY/30% OK fuel tests and somewhat higher than for the 90% WY/10% OK fuel test. Furnace outlet temperatures at the same firing rate and excess air were determined primarily by lower furnace heat absorption and to a lesser extent by the fuel reactivity. In the case of the 100% WY and the blended fuels, the fuel reactivities, reported in Section 2.2, are very similar. Therefore, differences in FOT can be ascribed to the differences in deposit characteristics, specifically the resistance to heat transfer.

3.2.3.3 Sacrificial Probe Evaluations

It is difficult to analyze the composition of the various layers of ash deposits, particularly the initial and inner layers, if they must first be removed from the collecting surface. Hence, sacrificial (single-use) probes were developed to allow removal of the entire deposit; the deposit and probe are then cross-sectioned to permit analysis of each deposit layer.

Air-cooled sacrificial probes were used to collect slag deposits in the radiant sections of the FPTF. Sacrificial probe surface temperatures were controlled at 700 °F to simulate field waterwall tube conditions, and enabled study of the entire continuum of wall deposits, from the powdery initial layer outward through the deposit thickness to the outer deposit surface. The probes were constructed of one-inch mild carbon steel seamless pipe, and consisted of a five-inch section that was mounted flush with the refractory surface and parallel to the furnace gas flow. A simplified probe schematic is presented in Figure 3.36. Two probes were used for each fuel tested, one at the Panel 1 elevation and the other at the Panel 3 elevation. A control valve regulated air flow

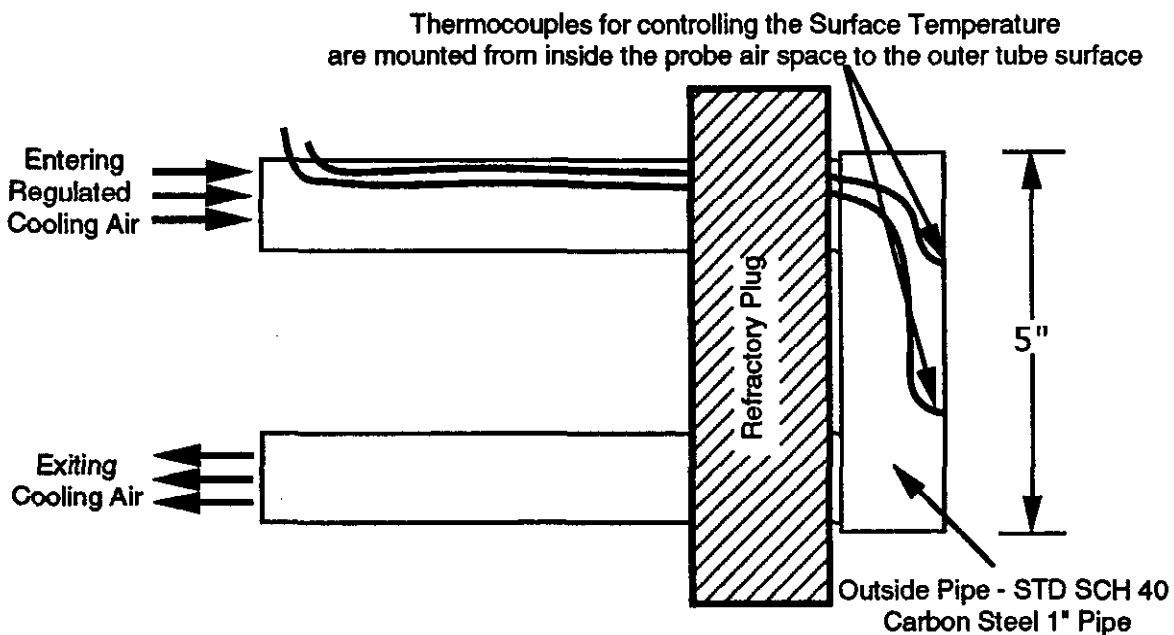


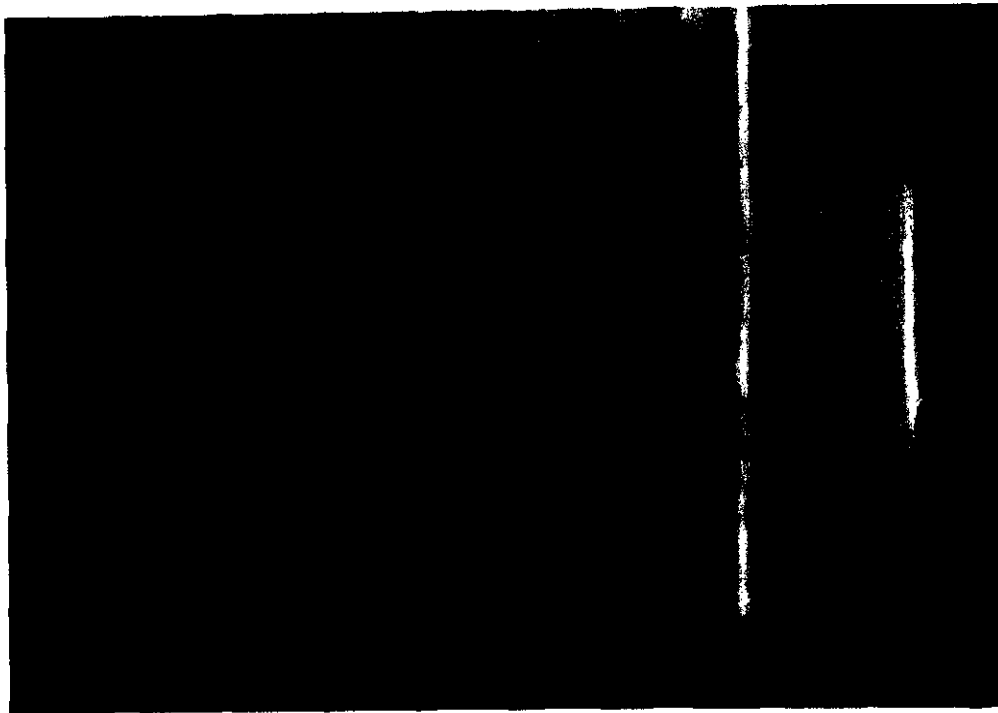
Figure 3.36 A Simplified Schematic of the Sacrificial Probe through the probe to maintain constant surface temperature. Visual observations of

the probes in the FPTF confirmed that the sacrificial probe deposits were representative of those that were forming simultaneously on the waterwall panels. A photograph of an on-line probe is shown in Figure 3.37. It was possible to remove the sacrificial probe assemblies on-line to quench deposition reactions. A deposit-laden probe following removal from the furnace is also shown in Figure 3.37.

SEMP analysis of the various layers of the sacrificial probe deposits was conducted by UNDEERC to determine particle size distribution as well as elemental composition, concentration and phase. These data are presented in Table 3.7. Physically, the 100% WY deposit was 4-6 mm thick and appeared more dense, vitreous and sintered than the deposits resulting from burning the coal blends, which were more porous and friable, and only 2-4 mm thick. The outer layers of the sacrificial probe deposits were typically rich in anorthite, quartz and amorphous montmorillonite phases. They also had higher SiO_2 and lower CaO, MgO and SO_3 contents than the inner layer deposits. The 100% WY and 90% WY/10% OK blend deposits were very similar in crystalline and amorphous phase composition and in elemental chemistry. The 70% WY/30% OK blend showed a pronounced increase in amorphous montmorillonite, SiO_2 and Fe_2O_3 . The increase in montmorillonite and SiO_2 was due to the added illite (K-aluminosilicate) and the increase in Fe_2O_3 was due to the added pyrite from the Oklahoma coal. The 70% WY/30% OK CLN blend showed reduced CaO, most likely from removal of calcite from the Oklahoma coal fraction.

In regard to slagging propensity, 100% WY coal has the greatest slagging potential for the following reasons:

- 1) Heat flux measurements were the lowest and FOT's were very close to the highest for the 100% WY, indicating deposit buildup and/or reflective ash.
- 2) Low viscosity liquid phases, which are generally an indication of higher deposition potential, were high for the 100% WY and 90% WY/10% OK blend based on SEMPC analysis of the sacrificial probe and waterwall deposits.



Sacrificial Probe In-situ



Upon removal from the furnace, the deposit accumulation is rapidly quenched

Figure 3.37 Pictures of the Sacrificial Probe After Deposit Accumulation

- 3) The 100% WY had the largest amount of small sized ash particulate which may have contributed to a low viscous inner layer. This sticky inner layer may have produced a efficient captive surface for the larger non-sticky impacting particles.
- 4) Initial slagging temperature, derived from the EERC DTF, also revealed the 100% WY as having a greater slagging tendency than the other fuels. Crushing strength for the DTF slagging deposits revealed less strength for the 100% WY and 90% WY/10% OK blend. This correlated with the heat flux recovery measurements in the CE-FPTF which showed better recovery for the 100% WY and 90% WY/10% OK blend (82% and 87%, respectively) compared to the 70% WY/30% OK blend (15%). Strong crushing strength *does not necessarily imply resistance to soot blowing.*

Table 3.7 SEMPC Compositions of L1 Sacrificial Probe Deposits

Mineral Phases	100% WY		90/10 Blend		70/30 Blend		70/30 CLN Blend	
	Outer	Inner	Outer	Inner	Outer	Inner	Outer	Inner
Gehlenite	0.4	1.2	0.0	0.0	0.0	0.0	0.0	0.0
Anorthite	27.6	1.2	28.4	2.3	11.6	20.0	18.0	30.0
Pyroxene	0.0	0.4	0.4	0.0	0.0	2.0	0.0	0.4
Calcium Silicate	0.0	0.0	0.0	0.0	0.0	1.6	0.0	0.0
Dicalcium Silicate	0.0	0.0	0.0	0.0	0.0	0.4	0.0	0.0
Quartz	9.2	5.6	1.6	6.9	7.2	2.4	3.2	4.0
Iron Oxide	3.6	2.4	0.8	1.5	0.8	0.4	6.4	4.0
Calcium Oxide	0.0	0.0	0.0	0.0	0.0	0.0	0.0	0.0
Anhydrite	0.0	3.6	0.0	3.8	0.0	1.2	0.0	0.0
Pure Kaolinite	2.0	0.8	1.2	0.0	0.4	0.4	0.0	0.0
Kaolinite Derived	0.8	1.6	0.0	3.1	0.8	2.4	0.0	1.2
Illite (Amorp)	0.0	0.4	0.0	0.8	0.0	0.0	0.0	1.6
Montmorillonite	33.2	2.8	20.8	2.3	22.0	10.4	44.8	15.6
Unclassified	23.2	80.0	46.8	79.3	57.2	58.8	27.6	43.2
Bulk Oxide Composition (Wt%) SO₃-free								
SiO ₂	60.6	33.6	60.0	33.3	67.5	57.6	62.3	61.8
Al ₂ O ₃	16.3	19.1	12.9	19.7	13.9	12.2	14.8	12.6
Fe ₂ O ₃	8.7	10.1	8.8	6.9	6.5	9.1	9.2	8.2
TiO ₂	1.3	1.8	1.5	1.6	0.8	1.1	1.0	1.4
P ₂ O ₅	0.3	1.0	0.3	1.1	0.2	0.2	0.3	0.4
CaO	8.2	24.7	11.0	28.4	7.5	15.2	7.4	10.1
MgO	2.5	5.9	2.8	5.8	2.1	2.4	2.0	2.9
Na ₂ O	1.1	2.5	1.2	1.7	1.3	0.8	1.3	0.8
K ₂ O	0.9	1.3	1.4	1.5	2.1	1.4	1.7	1.8
ClO	0.0	0.0	0.0	0.0	0.0	0.0	0.0	0.0
Cr ₂ O ₃	0.0	0.1	0.1	0.1	0.1	0.1	0.1	0.1
SO ₃ (added for comparison)	0.2	16.7	0.0	22.5	0.1	0.9	0.1	0.1

3.2.3.4 Lower Furnace Deposit Thermal Conductance

Lower furnace deposit thermal conductances were measured on-line in the FPTF at the end of each twelve-hour test period. This measurement is obtained through Fourier's Law of thermal conduction:

$$\frac{Q}{A} = \frac{k}{\Delta x} (T_s - T_p) \quad 3.1$$

Where Q/A is the panel heat flux (Btu/hr/ft²), $k/\Delta x$ is the overall deposit conductance (Btu/hr/ft²/°R), T_s is the fireside deposit surface temperature, and T_p is the panel surface temperature. The deposit surface temperature is measured by placing a platinum/rhodium thermocouple on the deposit surface in several places, as shown in Figure 3.38, to get an average surface temperature. The panel surface temperature is measured with thermocouples embedded in the surface of the panel, and the heat flux is calculated, as described previously, by means of an energy balance on the temperature rise and flow rate of the heat exchanger fluid.

Examination of the ash deposit thermal conductances as measured in the FPTF reveals a direct correlation to the furnace outlet temperatures measured in the field and previously reported in Figure 3.34. Table 3.8 shows the average thermal conductance ($k/\Delta x$) of FPTF-generated deposits at various elevations, as well as an overall average $k/\Delta x$ of the three elevations.

Furnace outlet temperatures measured during the 90% WY/10% OK field test were lower than the furnace outlet temperatures for the other two coals (Figure 3.34); correspondingly, the $k/\Delta x$ measured for the 90% WY/10% OK fuel was 48 Btu/hr/ft²/°R (better heat transfer) compared to the other two fuels which had average $k/\Delta x$ values of 36 Btu/hr/ft²/°R.

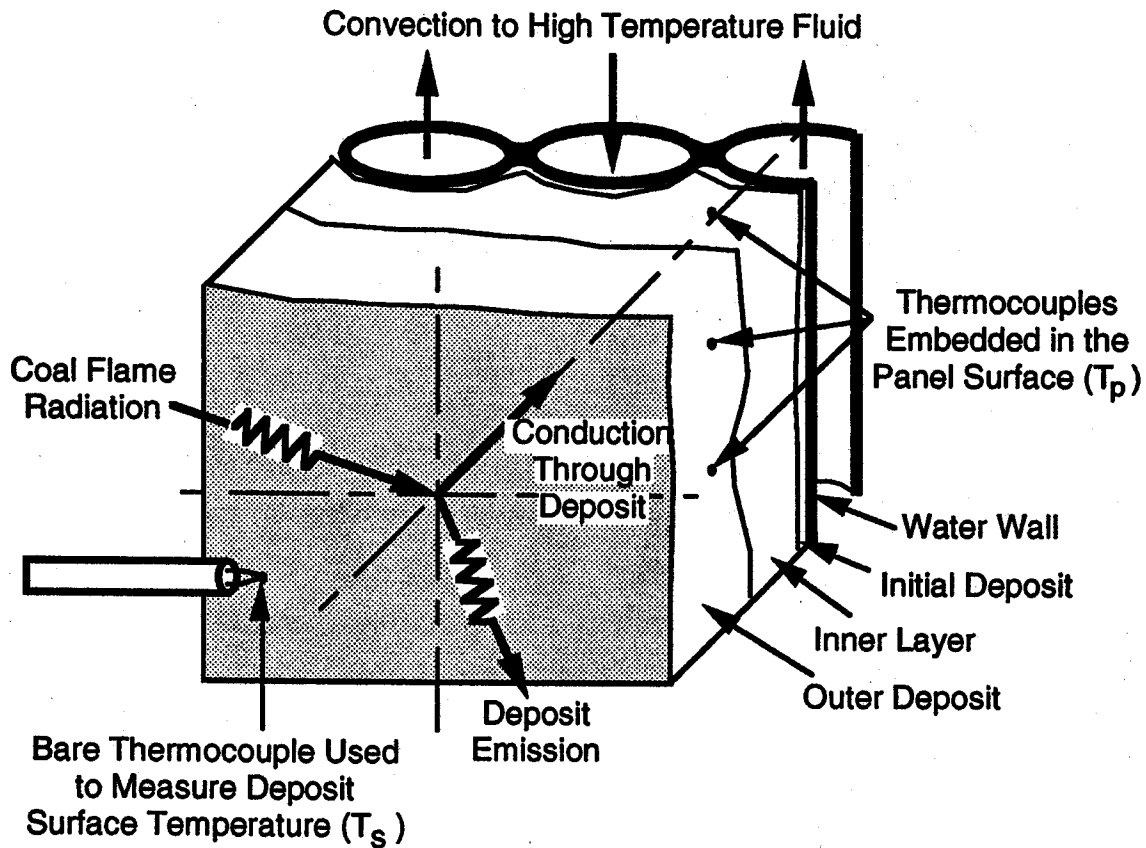


Figure 3.38 Panel Deposit Heat Balance and Thermal Conductance Measurement Technique

Table 3.8 Thermal Conductance of Deposits Generated at Various Elevations in the FPTF (Btu/hr-ft² °F)

Fuel	100% WY	90% WY/10% OK	70% WY/30% OK	70% WY/30% OK CLN
Panel 1	38	49	42	44
Panel 3	32	48	32	40
Panel 4	37	48	35	42
Average $k/\Delta x$	36	48	36	42

3.2.3.5 Effects of Excess Air

Changing excess air in a commercial unit has two possible influences on deposit formation characteristics: 1) the chemical effects of lower oxygen partial pressures on deposit properties, and 2) the thermal effects on the furnace environment. As oxygen partial pressures are decreased, mineral matter transformations to fly ash can be affected. For example, iron compounds with lower oxidation states (resulting from this low oxygen environment) have lower melting temperatures and can promote more fluid, running slag deposit formation. When excess air is decreased, gas temperatures will increase because of the decreased thermal diluent effects; the opposite is true when excess air is increased. Testing in the FPTF has the advantage of separating these two effects, i.e., excess air can be varied while maintaining the same gas temperature at the first elevation in the furnace. Figure 3.39 shows the effect of excess air on lower furnace deposit formation for the 100% WY fuel. Because the gas temperatures are relatively constant, the chemical, rather than thermal, effects of variable oxygen partial pressures are being evaluated. Figure 3.39 also shows that at 20% and 30% excess air, the heat fluxes before soot blowing and heat flux recoveries for the 100% WY coal are very similar. The 12.5% excess air test showed a modest decrease in heat flux before soot blowing and a significant decrease in the heat flux recovery after soot blowing compared to the 20% excess air case. These data strongly suggest that the chemical effect of excess air on the 100% WY fuel will alter the nature of the deposit and its cleanability, despite the relatively low pyritic and total iron contents.

Results of the excess air testing conducted on the 90% WY/10% OK and the 70% WY/30% OK fuels are reported in Figures 3.40 and 3.41 respectively. As can be seen, the 90% WY/10% OK and the 70% WY/30% OK fuels did not show the same lower furnace deposit characteristics as the 100% WY fuel. Pilot-scale data suggests that increasing the excess air resulted in little or no effect on deposit cleanability. The average gas temperatures at the first panel elevation for the 90% WY/10% OK and the 70% WY/30% OK excess air tests were not sufficiently similar to permit an interpretation of chemical versus thermal effects.

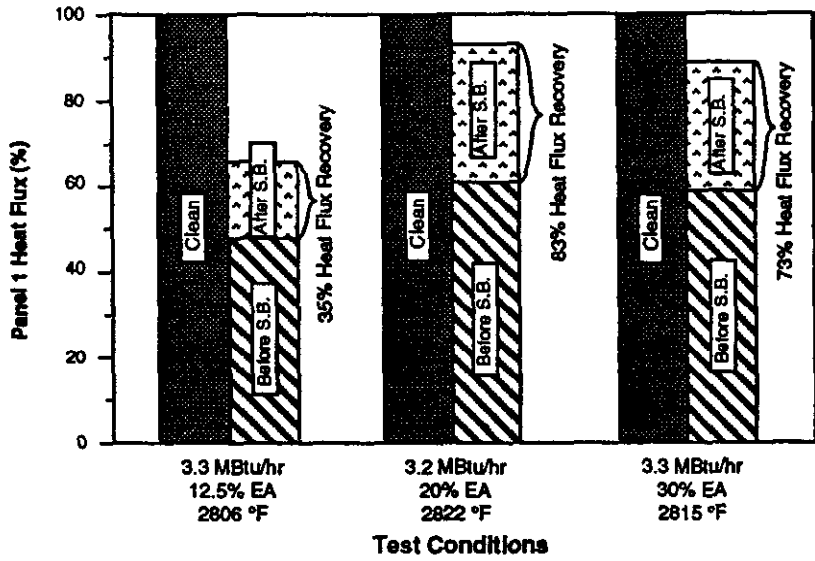


Figure 3.39 PSO 100% WY - Effects of Excess Air

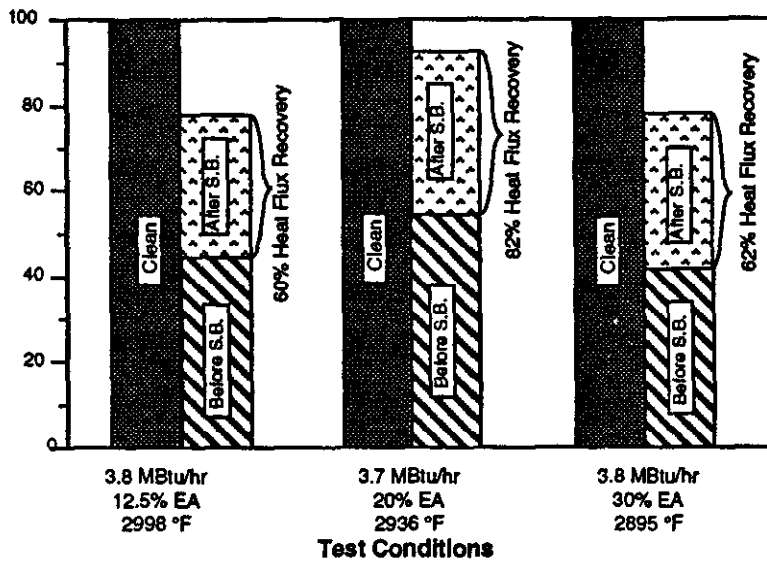


Figure 3.40 90% WY / 10% OK - Effects of Excess Air

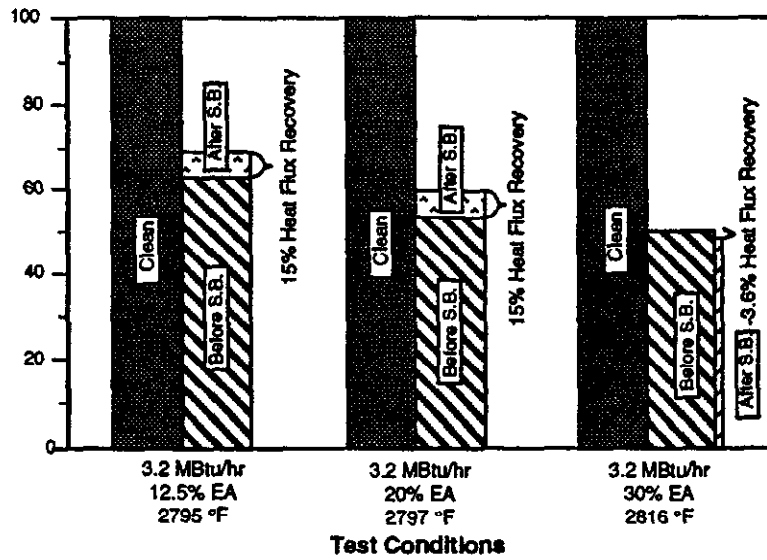


Figure 3.41 70% WY / 30% OK - Effects of Excess Air

A plot of average furnace outlet temperature (FOT) versus oxygen concentration from field testing shows increasing FOT with decreasing oxygen for the three fuels tested (Figure 3.42). Interestingly, the slope of the 100% WY data is much steeper than that of the 90% WY/10% OK and the 70% WY/30% OK data, suggesting a greater chemical effect in the 100% WY case (compared with the other fuels which show a lesser sensitivity). The suggestion of a greater chemical effect in the case of the 100% WY fuel is consistent with data/interpretations from the pilot-scale testing.

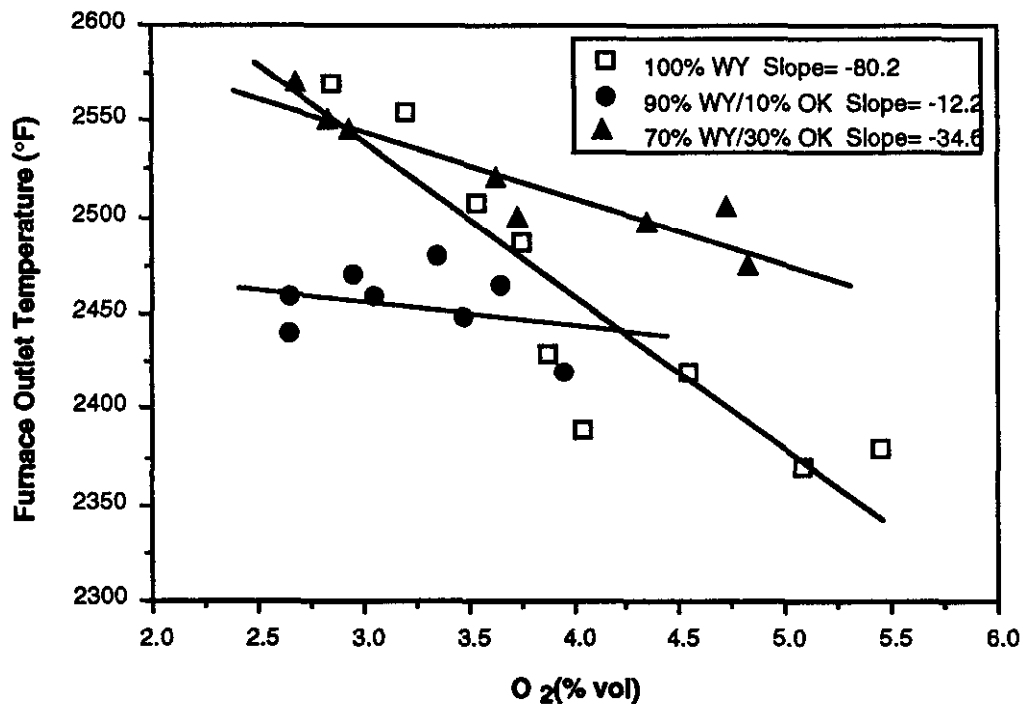


Figure 3.42 Furnace Outlet Temperatures as a Function of Excess Air for Fuels Tested in Northeastern Unit 4 (EER)

3.2.4 Convective Pass Fouling

Fouling characteristics, specifically bonding strengths found during pilot-scale testing, are summarized in Figure 3.43. In general, the bonding strength increased with increasing furnace outlet gas temperatures and increasing blended quantities of the OK coal. There were no significant differences between the 70% WY/30% OK blend and its cleaned counterpart at temperatures which were above 2200 °F. Deposits which formed on simulated superheater tube surfaces in the convective section of the furnace were generally sintered at gas temperatures in the 2100 to 2300 °F range and developed a molten outer surface at higher gas temperatures (above 2300 °F). Deposit bonding strength increased significantly with increasing gas temperature for each coal/coal blend fired, resulting in deposits which exceeded the cleanability level in the blended coal cases. Based on previous data from field tests and pilot-scale evaluations, it is generally considered that bonding strengths of 15 or lower are indicative of deposits which are cleanable with conventional soot blowers.

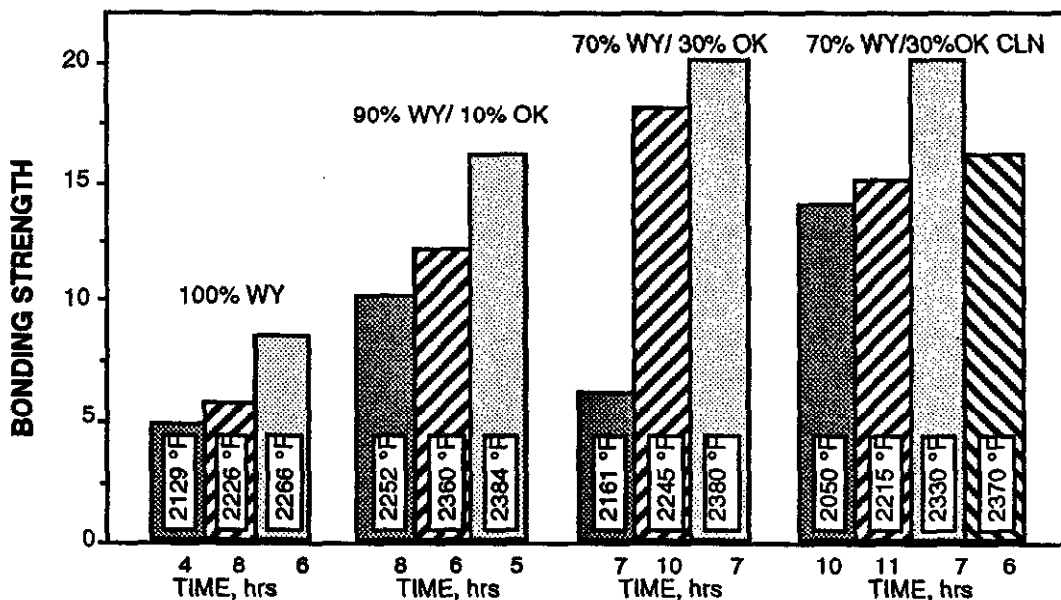


Figure 3.43 Convection Pass Deposit Bonding Strength Summary

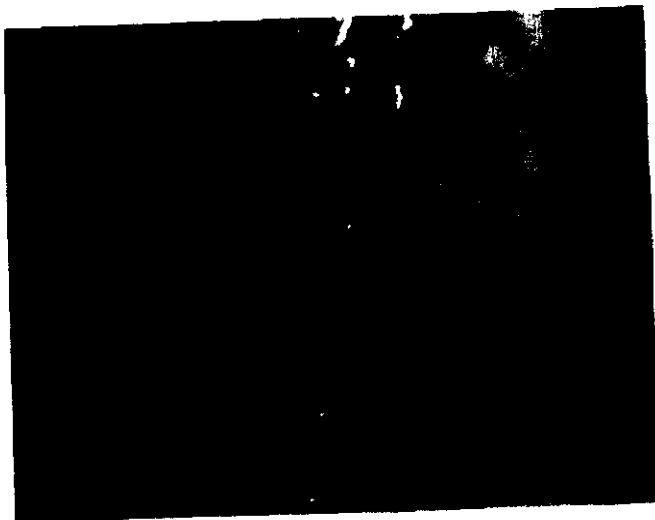
Photographs shown in Figure 3.44 illustrate typical superheater tube initial deposition for the 100% WY and the 90% WY/10% OK fuels. Time-sequenced photographs of

superheater tube depositions for the four fuels tested appear in Figures 3.45 to 3.56. Both the first (IA) and second (IIC) superheater probe banks are depicted, and the firing rate and local gas temperature are provided for each series. These photographs document qualitative deposit buildup rates and deposit physical characteristics.

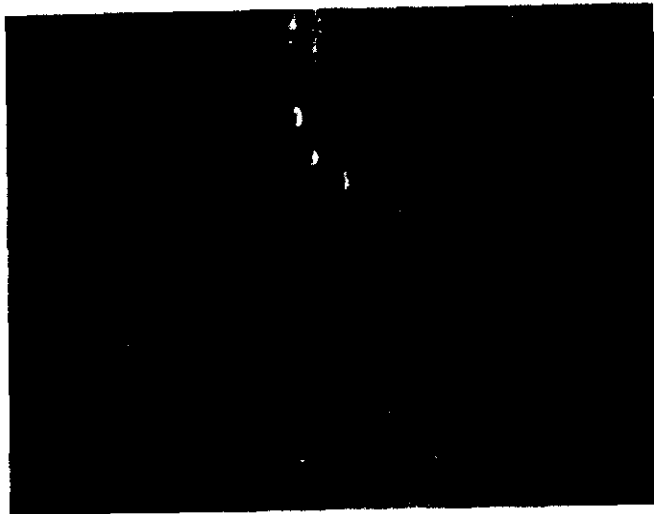
As shown in Figure 3.44, the 100% WY and 90% WY/10% OK fuels exhibited roughly similar initial superheater tube deposition characteristics. It is apparent from the first photographs of these series (taken after fifteen minutes of firing) that the start-of-test probe surface is not clean bare metal, but rather is coated with a powdery dust layer. This coated condition more accurately simulates seasoned superheater tubing than does bare metal. It is also apparent from this series of photographs that once tube deposition initiates at specific sites, these deposited sticky particles retain additional impacting particles. Deposit growth thus proceeds in both a lateral direction (covering additional tube surface) and an outward direction (developing deposit thickness on a given tube surface).

Figures 3.45 and 3.46 illustrate superheater deposit formation for the 100% WY fuel. Figure 3.45 depicts the second probe bank (Probe Bank IIC), and shows that due to its lower local gas temperature (*more than 100 °F lower than the temperature at Probe Bank IA, shown in Figure 3.46*), deposition on the second probe bank is much less severe than that on the first bank. This trend was found to be true for all four fuels tested.

Figure 3.47 shows superheater deposition for the 90% WY/10% OK fuel. Compared to the 100% WY fuel fired at the same load (Fig. 3.46), the 90% WY/10% OK fuel formed more molten deposits. Bonding strength measurements showed the 90% WY/10% OK deposits to be more tenaciously bonded to the tube surface compared to the 100% WY coal. This higher bonding strength is attributed to both the more molten state of the deposits, and the fact that, as documented in Figures 3.44 and 3.46, sometime after the first hour of firing the 100% WY fuel, the deposits on the first probe bank sloughed off and began to reform.



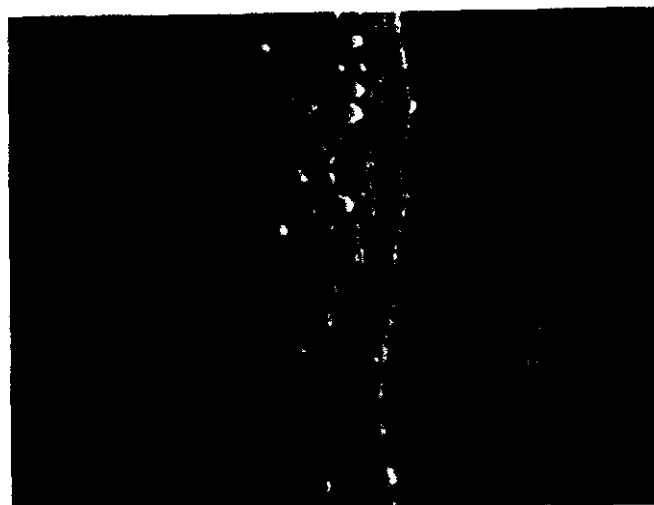
15 MINUTES



15 MINUTES



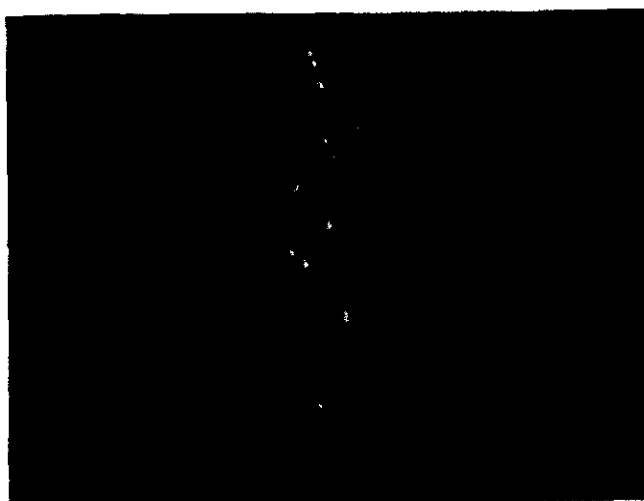
30 MINUTES



30 MINUTES

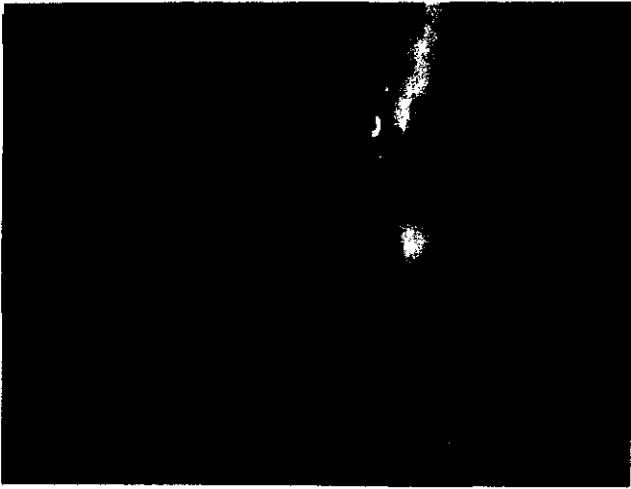


1 HOUR
100% WY Test 5 2258 °F
Probe Bank IA



1 HOUR
90% WY/10% OK Test 3 2384 °F
Probe Bank IA

Figure 3.44 Typical Superheater Tube Initial Deposition for Two Fuels



1 HOURS



1.5 HOURS



2 HOURS



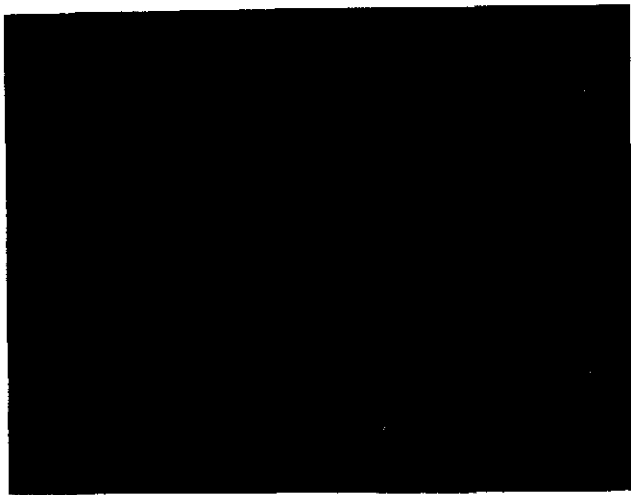
4 HOURS

Probe Bank IIC

Figure 3.45 Superheater Tube Deposit Buildup Rates

100% WY

Test 4 3.3 MBtu/hr 2122 °F



2 HOURS



4 HOURS



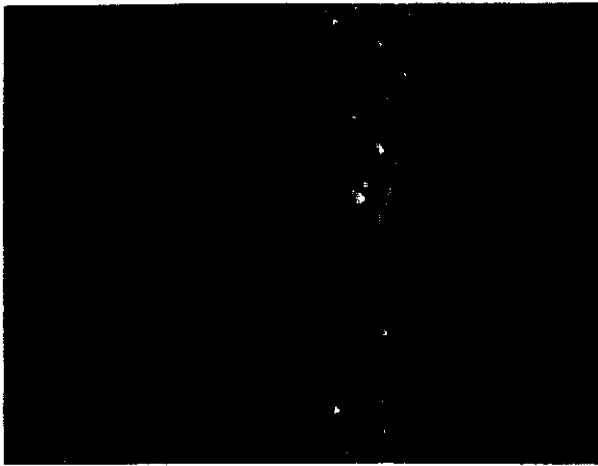
6 HOURS



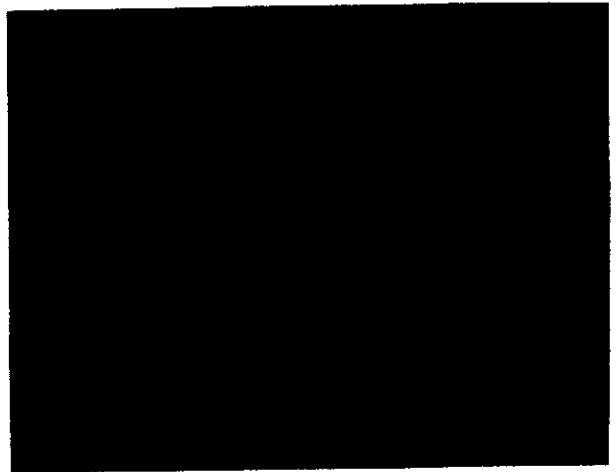
8 HOURS

Probe Bank IA

Figure 3.46 Superheater Tube Deposit Buildup Rates
100% WY
Test 5 3.3MBtu/hr 2258 °F



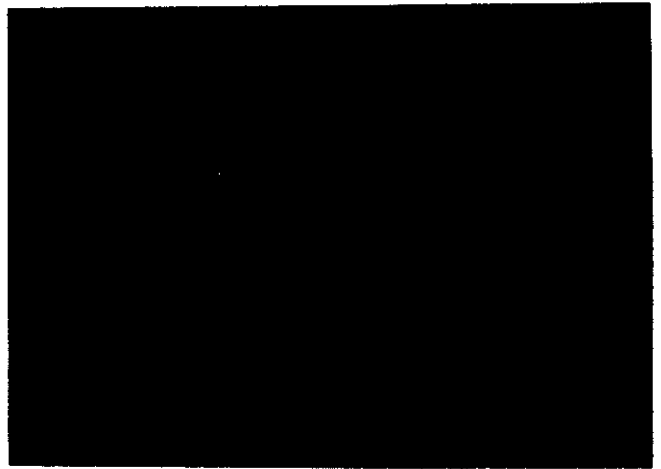
2 HOURS



4 HOURS



6 HOURS



8 HOURS

Probe Bank IA

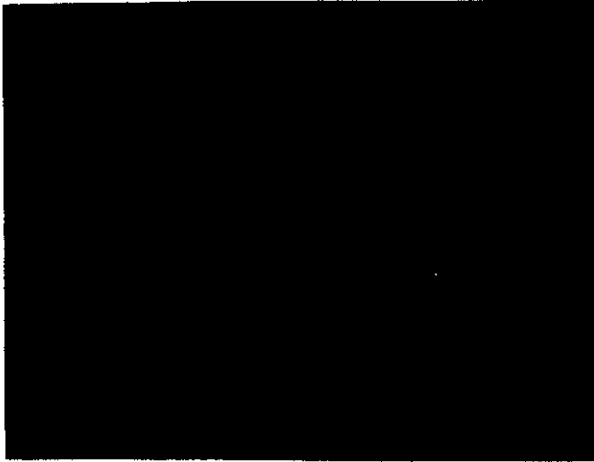
Figure 3.47 Superheater Tube Deposit Buildup Rates
90% WY/10% OK
Test 1 3.3MBtu/hr 2253 °F

Figures 3.48 and 3.49 show deposition characteristics for the second probe bank during firing of the 90% WY/10% OK fuel. Figure 3.48 shows that at a thermal load lower than the critical conditions (as determined by soot blower effectiveness in the radiant furnace), deposition on the second probe bank is negligible. Figure 3.49, however, indicates that at a thermal load higher than critical conditions, even furnace zones at a relatively low temperature are subject to significant and potentially problematic deposition.

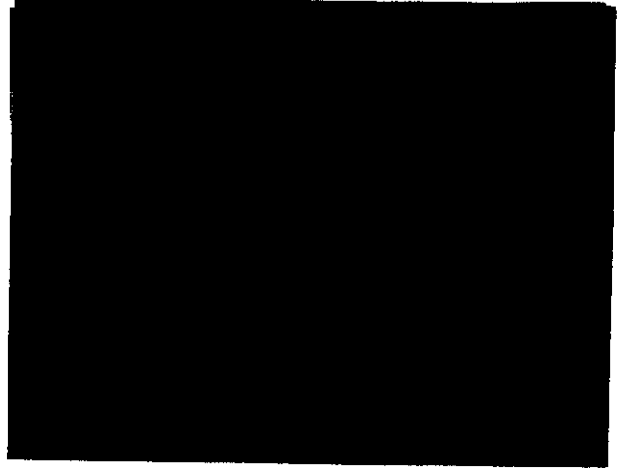
Figure 3.50 substantiates the bonding strength data indicating that firing the 90% WY/10% OK fuel results in more tenaciously bonded superheater deposits compared to the 100% WY fuel. These photographs indicate that when firing the fuel at critical thermal load, superheater deposits left unchecked for eight hours will obstruct the convective pass duct with molten deposit.

Figures 3.51 and 3.52 show deposition characteristics for the 70% WY/30% OK fuel. From Figure 3.51 it is readily apparent that the structure of the deposits on the first probe bank is different than that of the 100% WY and 90% WY/10% OK fuels. The 70% WY/30% OK deposits appear to be more compact and less sintered. Figure 3.52 depicts deposition on the second, lower temperature probe bank, and shows that these deposits are similar in growth rate and physical appearance to the other two fuels.

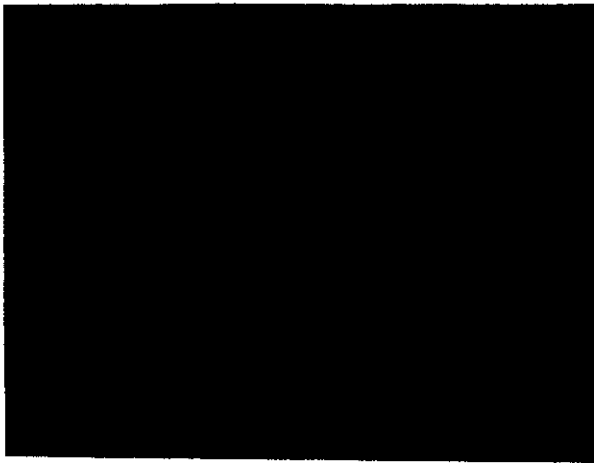
Figures 3.53 through 3.55 present photographs of superheater (Probe Bank IA) deposition for the 70% WY/30% OK CLN fuel. The first two figures show deposition sequences while firing at thermal loads lower than critical conditions, while the third figure shows deposition while firing at a thermal load higher than critical conditions. At very low thermal loading (Fig. 3.53), deposition after six hours of firing is minimal. When the load is increased (Fig. 3.54), deposition is also visibly increased. At a thermal load higher than critical conditions (Fig. 3.55), probe deposits are significantly heavier and more molten. Bonding strength measurements indicated that when deposits formed while firing the 70% WY/30% OK CLN fuel, at temperatures above 2200°F, fouling deposits were uncleanable by normal soot blowing techniques.



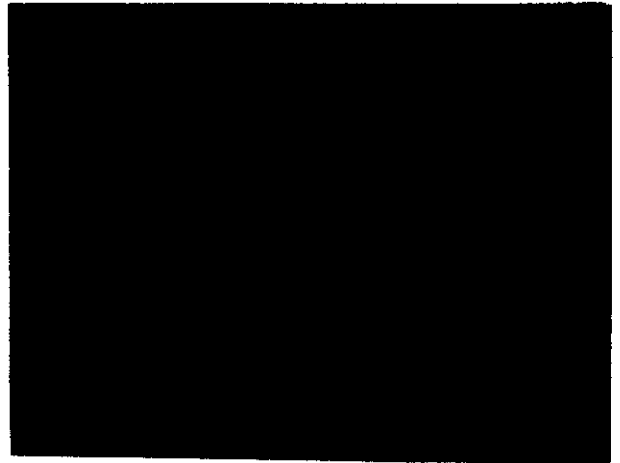
1 HOURS



2 HOURS



4 HOURS



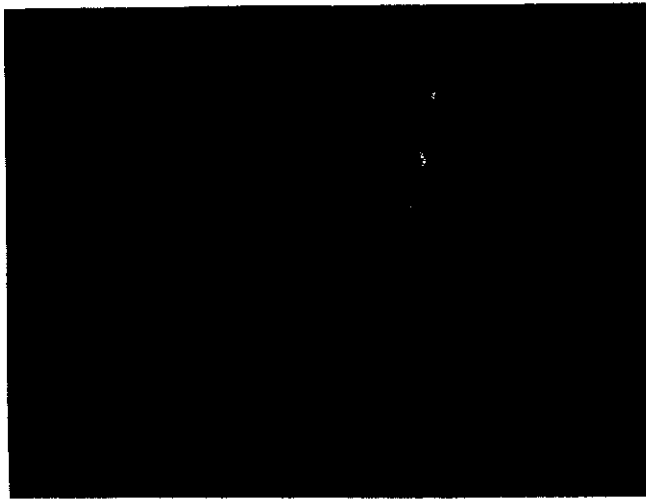
6 HOURS

Probe Bank IIC

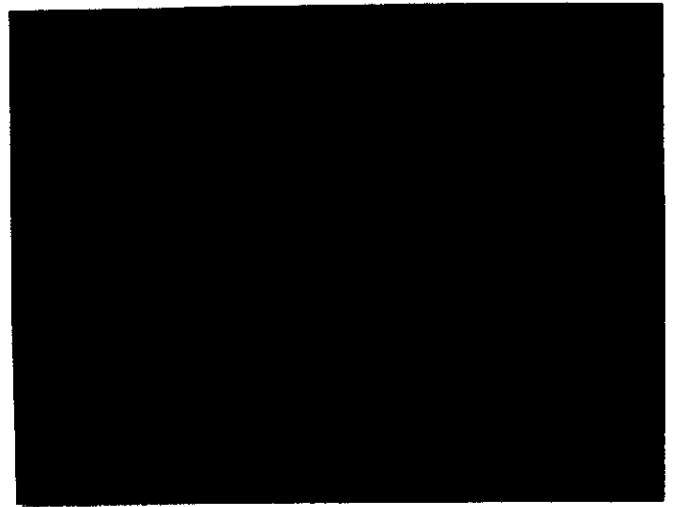
Figure 3.48 Superheater Tube Deposit Buildup Rates

90% WY/10% OK

Test 1 3.3 MBtu/hr 2142 °F



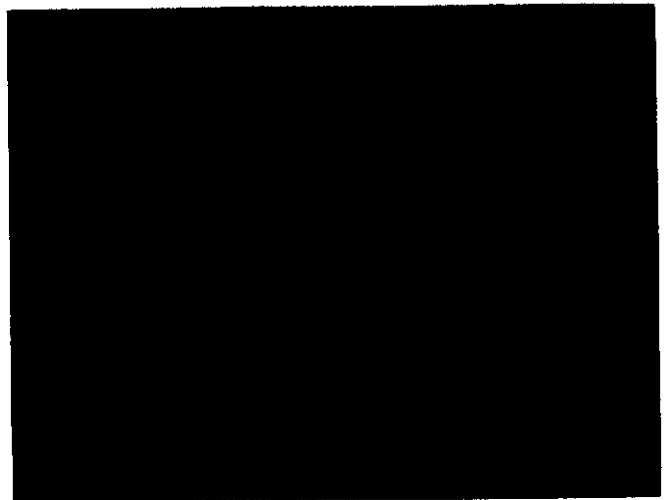
1 HOURS



2 HOURS



4 HOURS



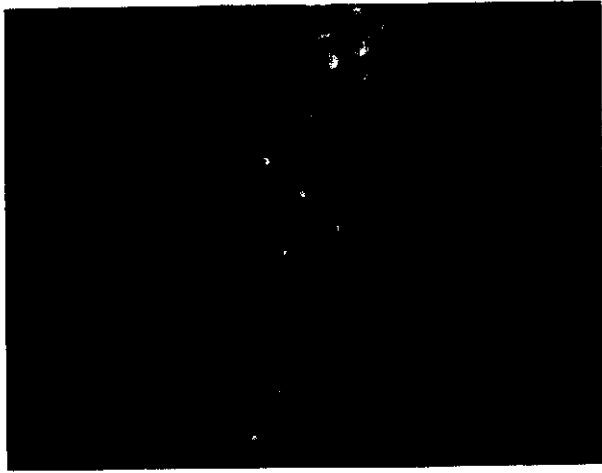
6 HOURS

Probe Bank IIC

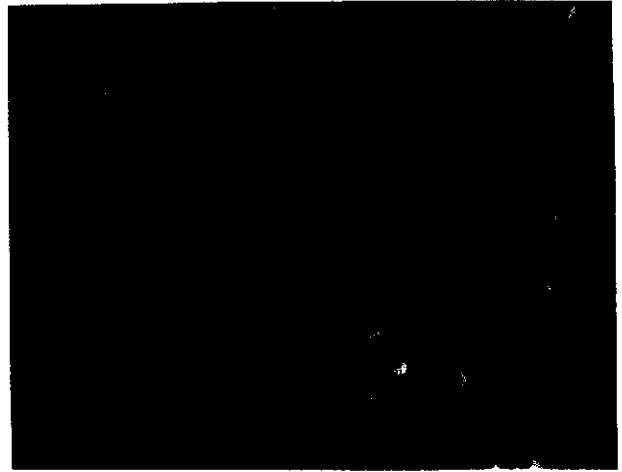
Figure 3.49 Superheater Tube Deposit Buildup Rates

90% WY/10% OK

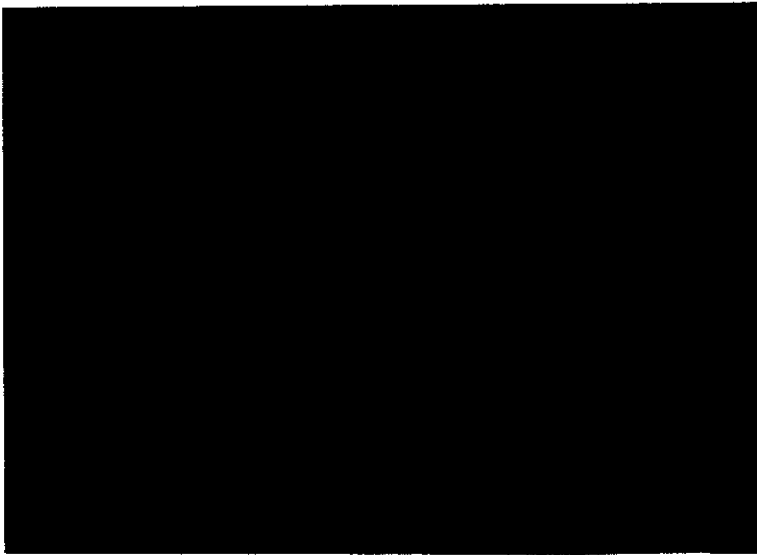
Test 3 4.0 MBtu/hr 2228 °F



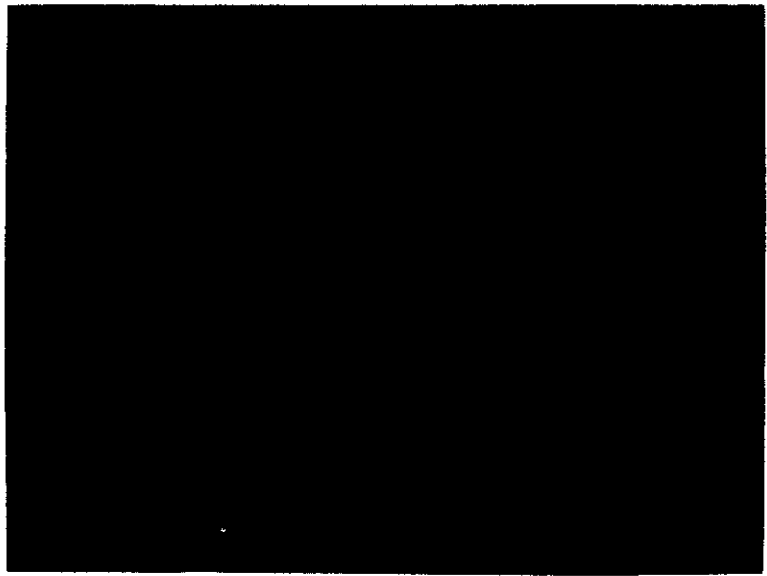
2 HOURS



4 HOURS



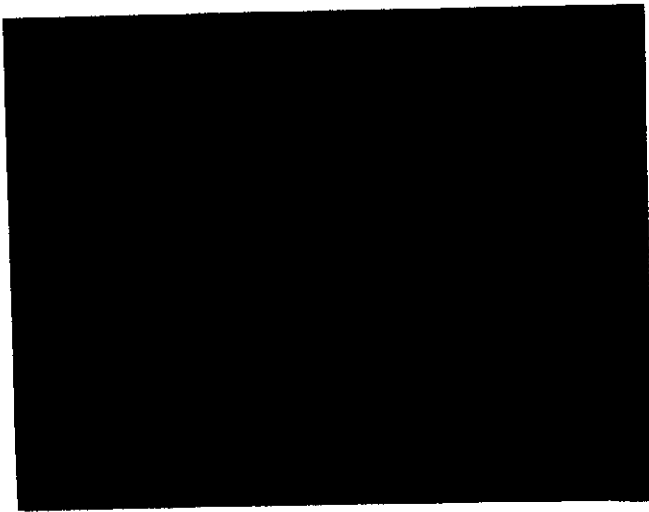
6 HOURS



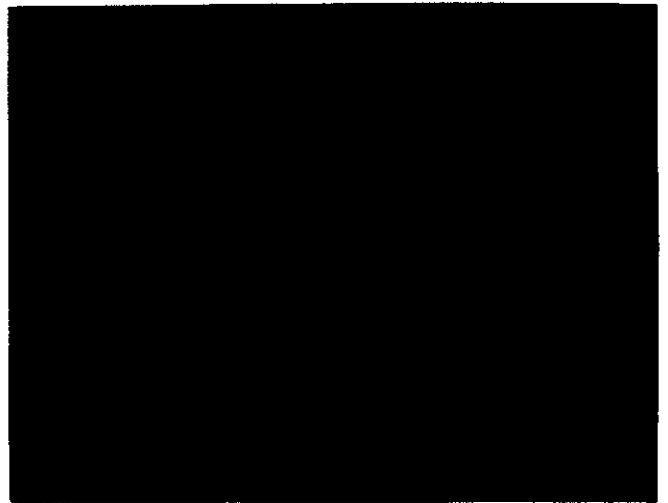
8 HOURS

Probe Bank IA

Figure 3.50 Superheater Tube Deposit Buildup Rates
90% WY/10% OK
Test 5 3.8 MBtu/hr 2253 °F



2 HOURS



4 HOURS



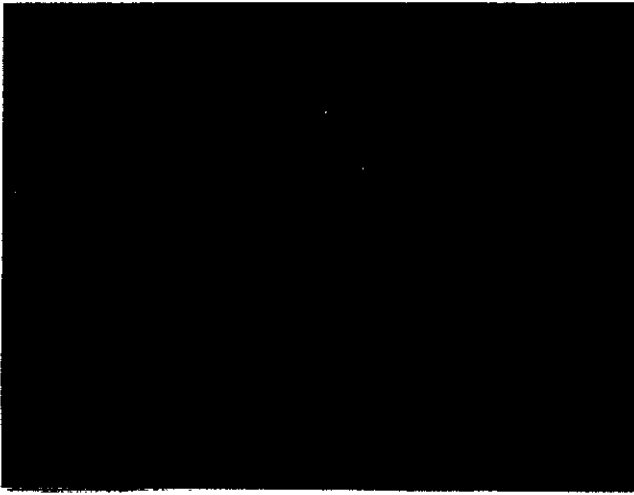
6 HOURS



8 HOURS

Probe Bank IA

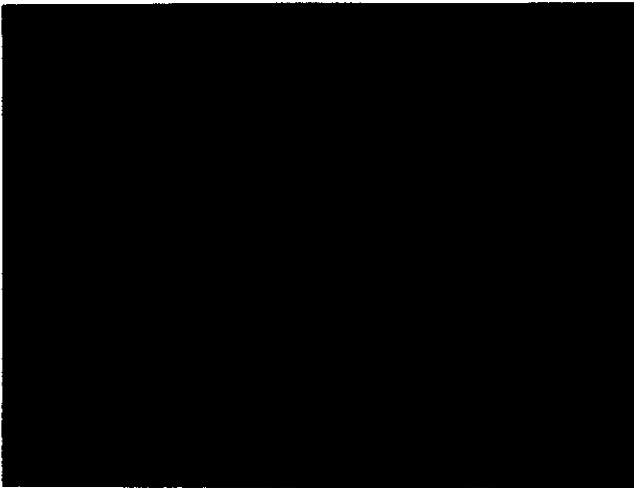
Figure 3.51 Superheater Tube Deposit Buildup Rates
70% WY/30% OK
Test 5 3.3 MBtu/hr 2279 °F



2 HOURS



4 HOURS



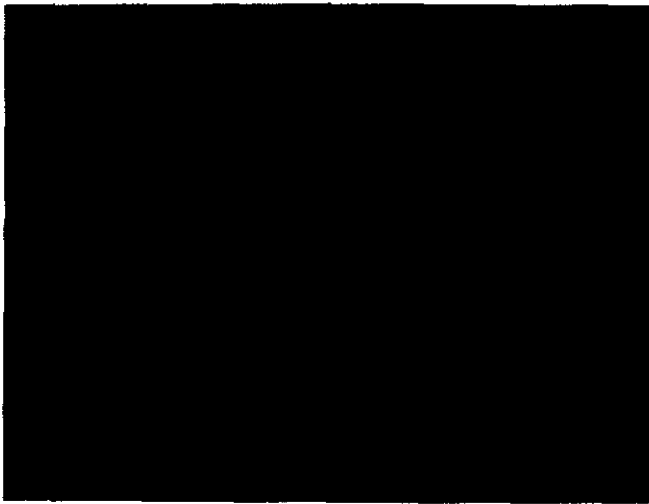
6 HOURS



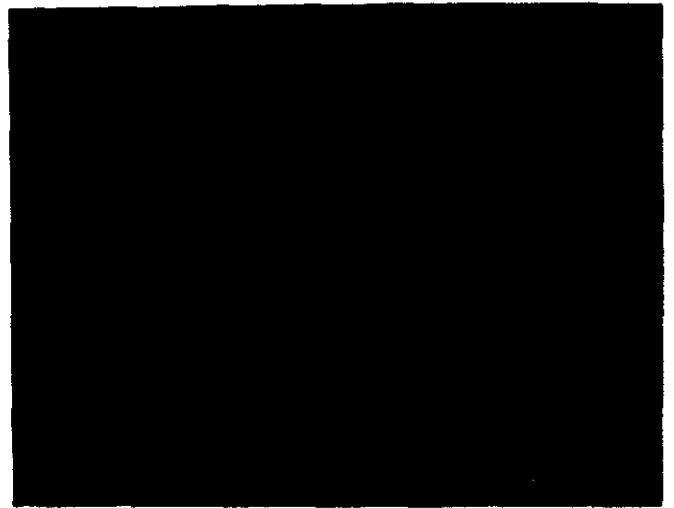
8 HOURS

Probe Bank IIC

Figure 3.52 Superheater Tube Deposit Buildup Rates
70% WY/30% OK
Test 5 3.2 MBtu/hr 2206 °F



2 HOURS



4 HOURS



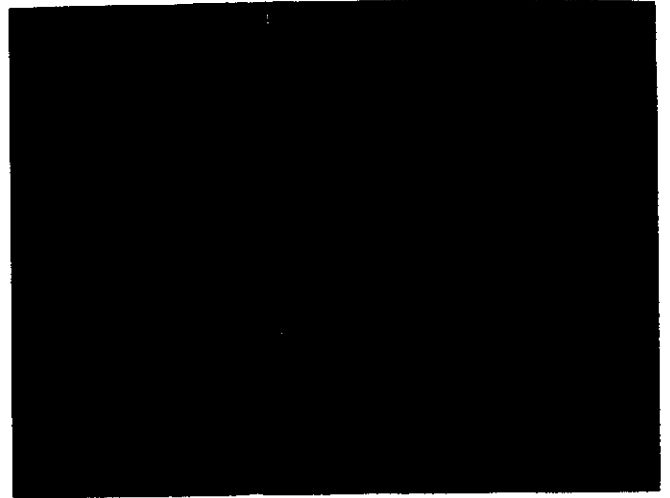
6 HOURS

Probe Bank IA

Figure 3.53 Superheater Tube Deposit Buildup Rates
70% WY/30% OK CLN
Test 1 3.3 MBtu/hr 2090 °F



2 HOURS



4 HOURS



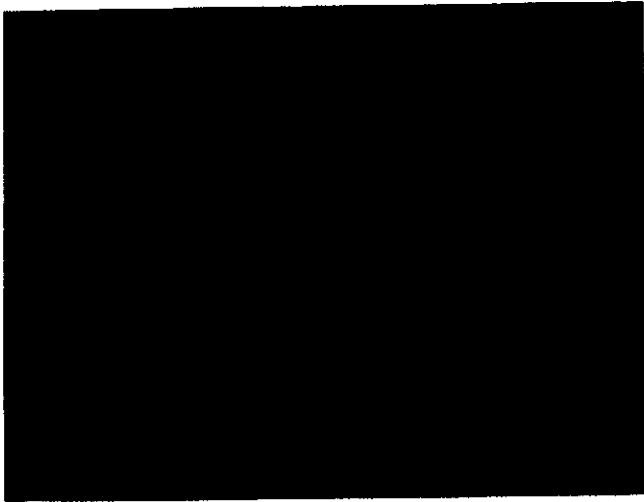
6 HOURS

Probe Bank IA

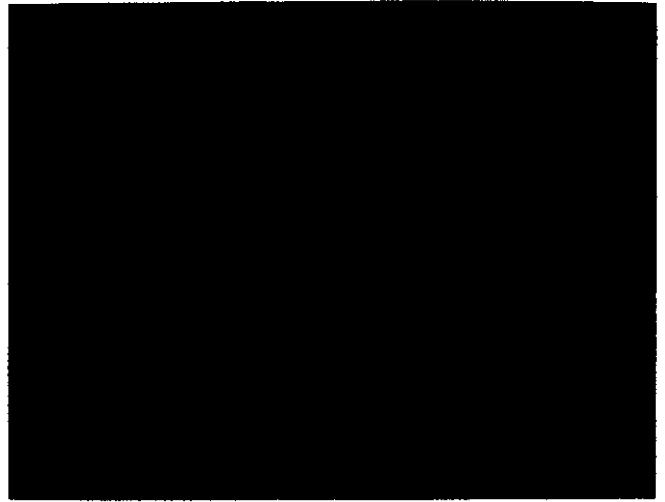
Figure 3.54 Superheater Tube Deposit Buildup Rates

70% WY/30% OK CLN

Test 2 3.6 MBtu/hr 2360 °F



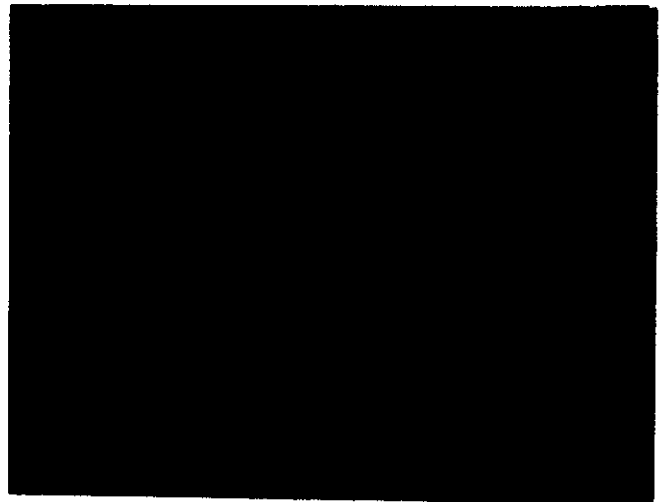
2 HOURS



4 HOURS



6 HOURS



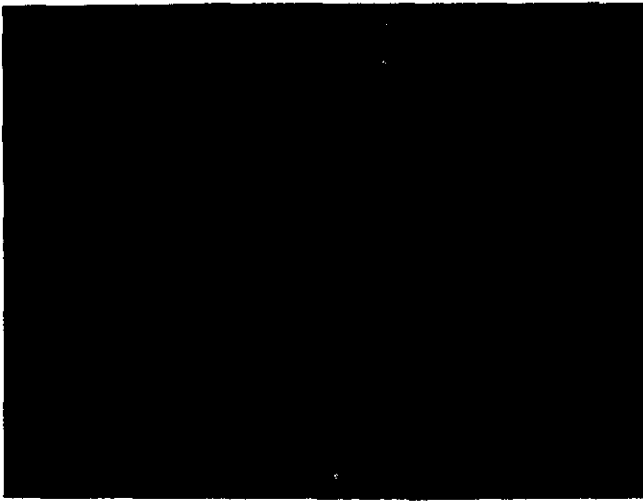
6 HOURS, Opposite Side

Probe Bank IA

Figure 3.55 Superheater Tube Deposit Buildup Rates

70% WY/30% OK CLN

Test 3 4.0 MBtu/hr 2437 °F



1 HOURS



2 HOURS



4 HOURS



6 HOURS

Probe Bank IIC

Figure 3.56 Superheater Tube Deposit Buildup Rates

70% WY/30% OK CLN

Test 3 4.0 MBtu/hr 2285 °F

Figure 3.56 shows Probe Bank IIC tube deposition while firing the 70% WY/30% OK CLN fuel at a thermal load greater than the critical conditions. These deposits also were more tenacious than those generated from the other three fuels.

With regard to performance limitations, the 100% WY coal produced deposits which were cleanable under all conditions tested, i.e., up to a temperature of 2260 °F. In the case of the 90% WY/10% OK fuel, non-cleanable deposits developed when temperatures exceeded 2360 °F. There did not appear to be a significant difference between the 70% WY/30% OK and the 70% WY/30% OK CLN blends in terms of critical fouling temperatures; for both fuels the critical temperature is probably slightly above 2200 °F. Significantly, the blend with the cleaned coal showed higher bonding strengths at lower gas temperatures than did blends with the uncleaned coal. However, because of the lower ash content in the cleaned coal blend the deposition rate (under equivalent firing conditions) was lower and soot blowing frequency could be commensurately decreased.

3.2.4.1 Description of Super Heater Fouling Deposition and Deposits

The fouling deposits usually contain low levels of liquid phases consisting of a combination of silicates and sulfates that binds the particles together. Two types of fouling problems typically occur in utility boilers (Hurley et al., 1991): high-temperature and low-temperature fouling. In high-temperature fouling, the bonding of particles is due to silicate liquid phases; and in low-temperature fouling, the bonding mechanism is a result of the formation of sulfates. Condensed sulfur species, principally in the form of CaSO_4 , are stable and are the matrix or bonding material in the low-temperature deposits.

Convective pass fouling is significantly aggravated by the condensation of flame-volatilized elements. The increase in abundance of P_2O_5 , Na_2O , and K_2O which are vaporized during combustion and subsequently condense upon cooling can contribute to the formation of fouling deposits.

High-temperature fouling deposits consist of easily distinguishable layers. Initial layers are rich in small particles that have high levels of flame-volatilized species such as sodium and sulfur. The transport mechanisms for these initial layers are due primarily to small particle and vapor phase diffusion and thermophoresis. At the same time, larger particles are impacting the surface. The initial deposit layers consist of condensed flame-volatilized species that may provide a sticky surface for trapping inertially impacting larger non-sticky particles. In addition, the initial layers may provide fluxing materials that will cause larger particles to melt. These particles provide sites for the formation of particle islands. These initial islands are the precursors of the more massive upstream deposits that form in the secondary superheater and reheater sections of a utility boiler. Coatings form on the surfaces of entrained ash particles as a result of the condensation and reaction of flame-volatilized species. The condensates react with the surface of the particles to form a molten or plastic surface. Condensation on surfaces of deposited ash particles can also occur. These "puddles" of liquid phase material contribute to the thickening of bonds between particles.

Low-temperature fouling deposits are sometimes produced from subbituminous coals that contain high levels of organically associated calcium. The formation of these deposits is dependent upon the availability of small calcium oxide particles and the process of sulfation. Based on detailed field testing to determine the mechanism by which low-temperature deposits form, Hurley et al., 1991 identified that the deposit characteristics are related to the entrained ash size and composition. Samples were collected that represent the upstream and downstream deposits. The upstream deposits are those that form on leading edge of the tube. The downstream deposits form on the backside of the tube. In all cases, the sulfation process occurred when the particles were deposited; very little sulfation took place while the particles were entrained in the gas stream.

The upstream reheater deposits that form in the range of temperature between 1170 and 1370°C accumulate on the heat-transfer surface as a result of initial impaction of particles >10 µm. Once the particles are deposited, sulfation occurs resulting in

deposit strength development. The upstream deposits are larger and begin as islands that continued to enlarge. This result is based on work conducted using probes that could be cross-sectioned in order to determine how the initial layer was formed. The initial layer is called an upstream enamel. This layer formed on the upstream side of the sacrificial probes in a temperature range between 1060°-1370°C. Microscopic examination of this enamel layer indicates that it consists mainly of particles <3 μm aerodynamic diameter that were highly sulfated. This layer results from thermophoresis/electrophoresis or simple diffusion of small particles. The downstream deposits form on all banks of tubes in the convective pass. Detailed examination of these deposits indicates that the aerodynamic particle sizes that contribute to their formation are the <10-μm particles. The mechanism most significant in deposit buildup for these particles is eddy impaction.

CCSEM analysis conducted by UNDEERC indicated that superheater fouling deposits had the greatest sulfate and iron contents in the inner layers. The sulfur was associated with vapor phase condensation during early formation of the inner white layers. The high iron content was probably an artifact of the steel tube iron oxide layer rather than deposited Fe-rich ash from the fuels. SEM analysis of the tube-deposit interfaces did reveal spalling of steel tube iron oxide layers. Table 3.9 shows that the calcium aluminosilicate species, which include anorthite, gehlenite (a melilite group mineral) and quartz, were more abundant in the outer layer. X-ray diffraction confirmed the presence of crystalline anorthite (plagioclase), gehlenite and quartz in the outer layer. The iron and sulfur species in the inner layer were also confirmed by XRD to be hematite and anhydrite, respectively. The deposits for the different fuels were somewhat similar except that the 90% WY/10% OK blend deposits were higher in quartz, clay-derived aluminosilicates, and anorthite. The 70% WY/30% OK CLN blend had much reduced calcium and iron contents compared to the uncleaned blend.

Table 3.9 Comparisons of Superheater Probe 1A Deposit Composition

Minerals Phases	100% WY		90/10 Blend		70/30 Blend		70/30 CLN Blend	
	Outer	Inner	Outer	Inner	Outer	Inner	Outer	Inner
Akermanite	1.6	1.2	0.4	0.4	0.0	0.8	0.0	0.0
Gehlenite	24.2	8.4	12.4	3.6	24.8	1.6	0.4	2.4
Anorthite	5.6	0.4	17.6	0.0	7.6	0.4	32.4	1.2
Pyroxene	0.8	0.4	0.4	0.8	0.0	0.4	0.8	0.4
Calcium Silicate	5.2	0.0	0.8	0.0	0.0	0.0	0.0	0.0
Calcium Aluminate	0.0	1.2	0.0	1.2	0.0	0.0	0.0	0.4
Quartz	7.2	4.8	11.6	0.8	0.8	2.4	7.6	4.4
Iron Oxide	0.4	32.4	0.4	16.8	0.4	26.0	1.6	14.8
Ankerite	0.0	0.8	0.0	3.2	0.0	3.2	0.0	0.4
Barite	0.0	0.4	0.0	0.0	0.0	0.4	0.0	0.0
Anhydrite	0.8	4.8	0.4	0.0	0.0	1.6	0.4	3.2
Pure Kaolinite	2.0	0.0	0.8	0.0	0.0	0.0	0.4	3.2
Kaolinite Derived	1.2	0.8	2.4	0.0	0.0	0.0	3.6	3.2
Illite (Amorp)	0.8	0.0	1.6	0.4	0.4	0.8	2.8	1.6
Montmorillonite	6.0	0.4	9.2	0.4	2.0	0.8	15.6	0.8
Unclassified	42.6	42.8	64.4	72.4	63.6	61.2	34.0	66.0
Bulk Oxide Composition (Wt%)								
SiO ₂	41.0	21.6	44.1	18.0	39.1	25.9	53.9	30.9
Al ₂ O ₃	20.0	17.3	20.1	13.5	21.0	16.8	18.7	18.7
Fe ₂ O ₃	6.4	16.7	5.0	26.2	6.7	21.4	6.5	13.2
TiO ₂	1.5	1.7	1.8	4.0	1.5	1.7	1.2	1.8
P ₂ O ₅	0.5	0.9	0.8	1.4	0.6	0.9	0.3	1.1
CaO	22.9	31.7	21.8	29.9	23.0	24.0	14.0	22.1
MgO	5.1	7.2	3.9	5.6	4.6	4.8	2.4	4.9
Na ₂ O	1.3	0.9	1.2	0.9	1.1	1.1	0.9	1.7
K ₂ O	0.8	0.3	1.3	0.4	1.8	1.6	1.6	2.5
ClO	0.0	0.0	0.0	0.0	0.0	0.0	0.4	0.0
BaO	0.5	1.5	0.0	0.0	0.3	1.4	0.0	0.0
SO ₃ (added for comparison)	1.1	8.2	0.7	9.5	0.5	8.9	0.1	12.3
Major Minerals (XRD)								
Outer Layer	<u>100% WY</u>	<u>90/10 Blend</u>		<u>70/30 Blend</u>		<u>70/30 CLN Blend</u>		
	Melilite	Melilite		Melilite		Diopside		
	Plagioclase	Quartz		Diopside		Alumina		
	Diopside	Anhydrite		Plagioclase		Plagioclase		
Inner Layer	Quartz							
	Hematite	Anhydrite		Hematite		Anhydrite		
	Anhydrite	Hematite		Anhydrite		Quartz		
Minor Minerals (XRD)								
Outer Layer	<u>100% WY</u>	<u>90/10 Blend</u>		<u>70/30 Blend</u>		<u>70/30 CLN Blend</u>		
	Anhydrite	Hematite		Anhydrite		Quartz		
	Hematite			Quartz		Hematite		
						Fe Spinel		
Inner Layer	Quartz	Quartz		Quartz		Hematite		
		Periclase		Periclase		Fe Spinel		
		Fe Spinel						

Comparisons of the inner and outer layer deposit compositions to those of the in-flame solids samples (just prior to the superheater duct) and the ASTM have revealed some very interesting results. Figure 3.57 is an elemental oxide comparison between the inner layer of a superheater deposit, the small size fraction (0 - 2 μm) of the in-flame solids analysis just prior to the superheater duct, and the ASTM ash analysis. The inner layer composition reported here, as well as the ASTM ash, were measured by X-Ray Fluorescence (XRF) and the in-flame solids compositions were measured through a method which corrects the CCSEM for oxide compositions. As can be seen in the figure, the deposit inner layer composition is very similar to the 0 - 2 μm (actual size, not aerodynamic diameter) in-flame solid sample composition, particularly the CaO, indicating that small particle/vapor phase diffusion and thermophoresis dominate the inner layer formation and growth. Another result drawn from Figure 3.57 is that the inner layer composition does not match the ASTM ash composition; notably the ASTM ash shows lower CaO and higher SiO₂, Al₂O₃ and Fe₂O₃ than the other two samples.

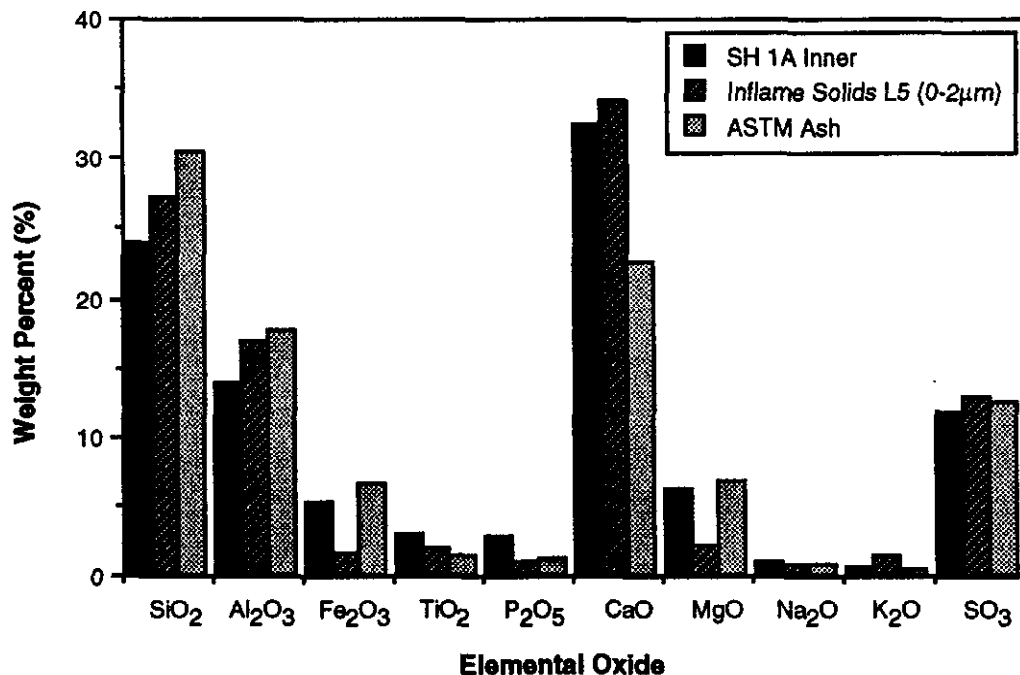


Figure 3.57 Comparison Between Compositions of Inner Deposit, In-flame and ASTM Ash Samples for 100% WY Coal

Transport mechanisms responsible for the fouling deposit outer layer growth is inertial impaction. The similarity in compositions of the 15 to 25 μm in-flame solids and the

superheater outer ash layer is shown in Figure 3.58. This indicates that the larger size particles were impacting the outer surface and sticking. The outer viscous layer is a nonreactive material, such that it does not assimilate the impacting particles in to the melt. The temperature is too high in the outer layer of the deposit to allow sulfation to occur. The calcium aluminosilicate species (which includes anorthite and gehlenite, melilite group minerals) and quartz were more abundant in the outer layer than in the inner layer. XRD confirmed the presence of crystalline anorthite (plagioclase), gehlenite (melilite), and quartz in the outer layer.

Figure 3.58 also shows in comparison the ASTM ash with those of the outer deposit layer, and the in-flame solids sample. Once again, it is noted that the outer layer composition does not match the ASTM ash composition as well; notably the ASTM ash shows lower CaO and higher SiO₂, Al₂O₃ and Fe₂O₃ than the other two samples.

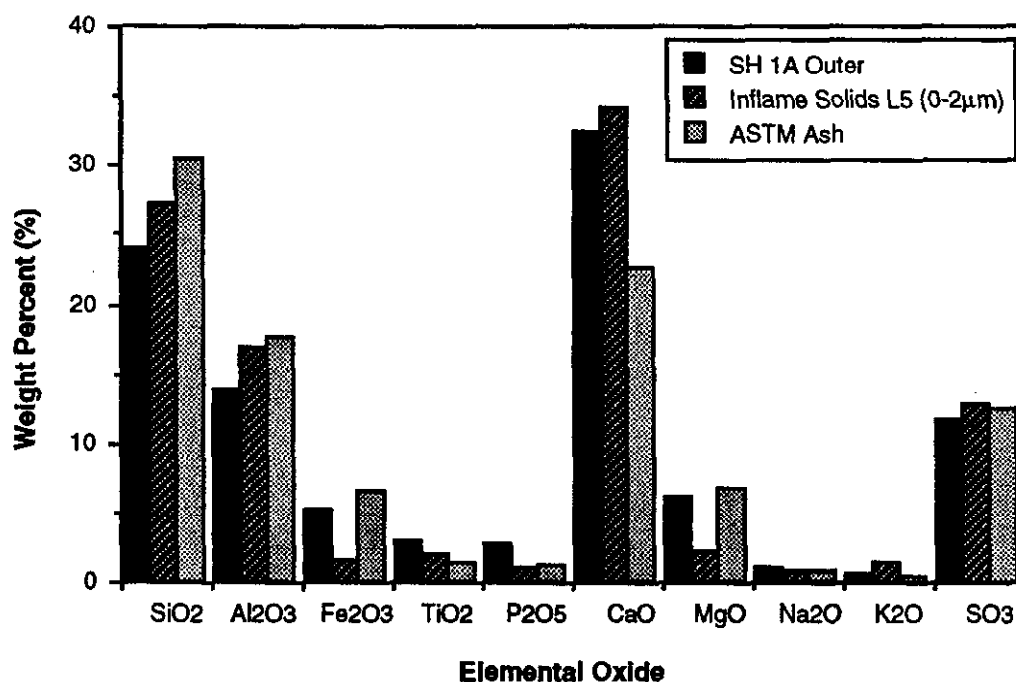


Figure 3.58 Comparison of Outer Deposit, In-flame and ASTM Ash Samples for 100% WY Coal

Liquid phase viscosity distributions calculated for the inner layer superheater deposits showed the 90% WY/10% OK blend deposits to have the lowest viscosities and the largest quantity of low viscosity (less than 250 poise) liquid phase, as shown in Figure

3.59. It is not clear if these data suggest a greater adhesive strength and/or poorer heat flux recovery after soot blowing. However, in light of pilot-scale testing, variations in combustion temperatures dominate most differences in deposit viscosities.

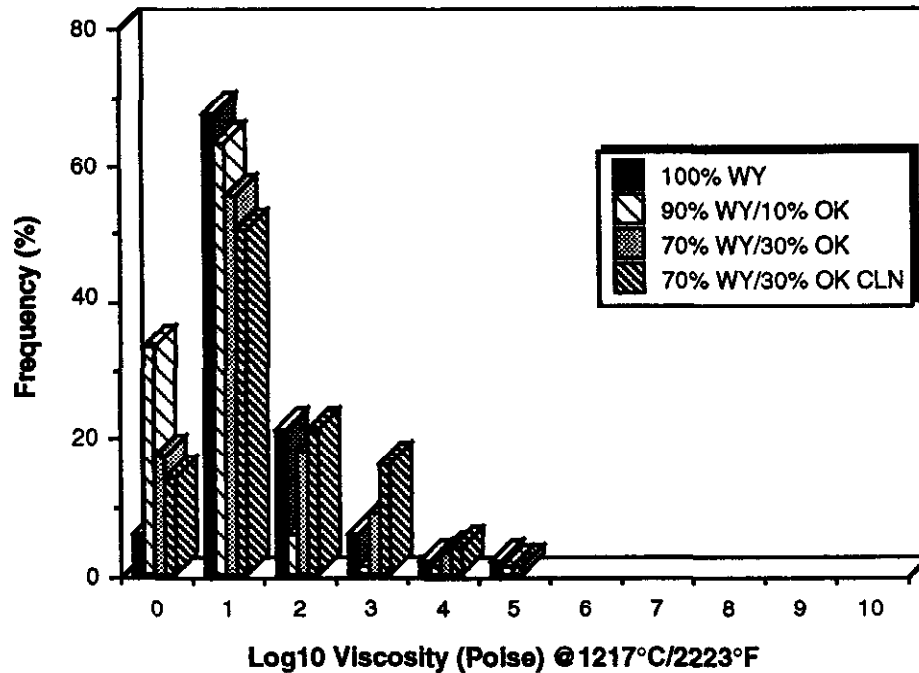


Figure 3.59 Comparison of Viscosity Distributions For Superheater Probe 1A Deposit Inner Layers

Discussions with plant personnel revealed that the main load-limiting factor for Northeastern Unit 4 was deposit formation in the convection pass of the furnace. It is clear from Figure 3.43 that from a fouling deposit standpoint alone, the 100% WY would have the best performance. However, in the full-scale furnace application, the temperatures at which convective pass deposits are formed are largely a function of excess air and lower furnace wall conditions (i.e., slagging and heat absorption), both of which have a direct impact on FOT. Full-scale operating data, shown previously in Figures 3.34 and 3.42, indicate that the 100% WY coal must be fired at greater than 4.0% excess O₂ or the temperatures in the convection pass will be sufficiently high to form deposits which cannot be removed. As the deposition continues, sections of the convection pass which have limited spacing will become plugged, causing a large

pressure drop and flow pattern disturbance. Firing the 100% WY fuel requires maintaining the lower furnace heat absorption, such that lower furnace outlet temperatures do not go in excess of the critical temperature (2825°F). Control of wall conditions is achieved by controlling excess O₂, wall blower operation, and load shedding.

Test results indicate that the 90% WY/10% OK fuel was not very sensitive to O₂ levels and field results also did not show a significant change in the FOT with changes in the excess O₂ fired. This fuel also had the highest furnace heat absorption, resulting in the lower average FOT's that the other fuels fired in the field. The lower average FOT's also provide better conditions for control of upper furnace fouling deposits. In evaluating all of these effects, it can be stated that the 90% WY/10% OK fuel could be fired under conditions similar to the those of the 100% WY fuel.

The 70% WY/30% OK fuel also did not display a large change in the FOT with excess O₂. However, due to the fuel's slagging tendencies in the lower furnace, it caused the highest overall FOT's. Results from the FPTF indicated that the fouling tendencies of the 70% WY/ 30% OK fuel would produce convection pass deposits which could not be removed at temperatures higher than 2200 °F (150 to 200 °F lower than the other fuels tested). Firing this fuel would demand increased lower furnace wall blowing and increased upper furnace retractable soot blowing to remove deposits before they become large and uncleanable. It is not probable that the furnace could be operated at MCR for extended periods of time without major fan-related load-limiting problems occurring.

3.2.5 Fly Ash Characterization and Erosion

FPTF fly ash (dust loading) samples were taken just upstream of the erosion probe during all of the tests. These samples were analyzed at UNDEERC and the results are presented in Table 3.10. A direct comparison between these samples and the previously reported in-flame solid samples should reveal information pertaining to the

Table 3.10 SEMPC and XRD Comparisons of Fly Ash (Dust Loading Samples)

	<u>100% WY</u>	<u>90%WY/10% OK</u>	<u>70%WY/30%OK</u>	<u>70%WY/30%OK CLN</u>
Minerals Phases				
Quartz	8.5	11.5	15.4	9.7
Iron Oxide	0.8	2.0	0.7	0.5
Calcite	0.1	0.7	4.0	0.2
Kaolinite	0.8	1.3	2.2	2.9
Montmorillonite	0.7	0.5	0.6	1.9
K Al-Silicate	0.3	0.3	12.3	4.7
Ca Al-Silicate	16.8	23.5	16.5	18.4
Mixed Al-Silica	0.8	1.5	4.7	4.0
Fe Silicate	0.0	0.0	0.0	1.7
Ca Silicate	3.7	4.1	0.9	2.4
Ca Aluminate	9.5	2.7	4.1	6.7
Gypsum/Al-Silic.	3.7	5.5	0.7	4.9
Si-Rich	1.0	2.2	2.8	2.5
Ca-Rich	4.9	4.3	1.7	0.8
Ca-Si Rich	1.0	2.5	0.6	0.9
Bulk Oxide Composition (Wt%)				
SiO ₂	38.9	41.1	44.0	39.0
Al ₂ O ₃	20.0	19.8	21.4	20.0
Fe ₂ O ₃	4.1	6.4	6.3	7.7
TiO ₂	1.0	1.4	1.2	1.5
P ₂ O ₅	1.1	0.9	0.8	1.2
CaO	27.1	32.1	19.3	23.1
MgO	6.6	5.5	5.1	5.9
Na ₂ O	0.8	0.8	0.7	0.6
K ₂ O	0.5	0.7	1.3	0.9
SO ₃	0.0	0.0	0.0	0.0
Major Minerals (XRD)				
	Lime Periclase Ca ₃ Al ₂ O ₆ Quartz	Quartz Melilite Ca ₃ Al ₂ O ₆	Quartz Lime Periclase	Anhydrite Hematite Periclase Ca ₃ Al ₂ O ₆ Quartz, Calcite Melilite
Minor Minerals				
	Magnesioferrite Anhydrite Dicalcium Silicate	Anhydrite Lime Periclase Fe Spinel Hematite		Fe Spinel

particle sizes deposited on the radiant and convective surfaces, and mineral phase transformations. Some of the entrained ash material is collected on deposition surfaces or simply falls out as bottom ash due to gravitational forces before it can be collected as fly ash. Increases in quartz and SiO₂ were observed in the fly ash as a function of increasing blended OK coal content. Figure 3.60 shows that the 90% WY/10% OK had the smallest PSD followed by, in order of increasing PSD, 100% WY, 70% WY/30% OK, and the 70% WY/30% OK CLN fuels.

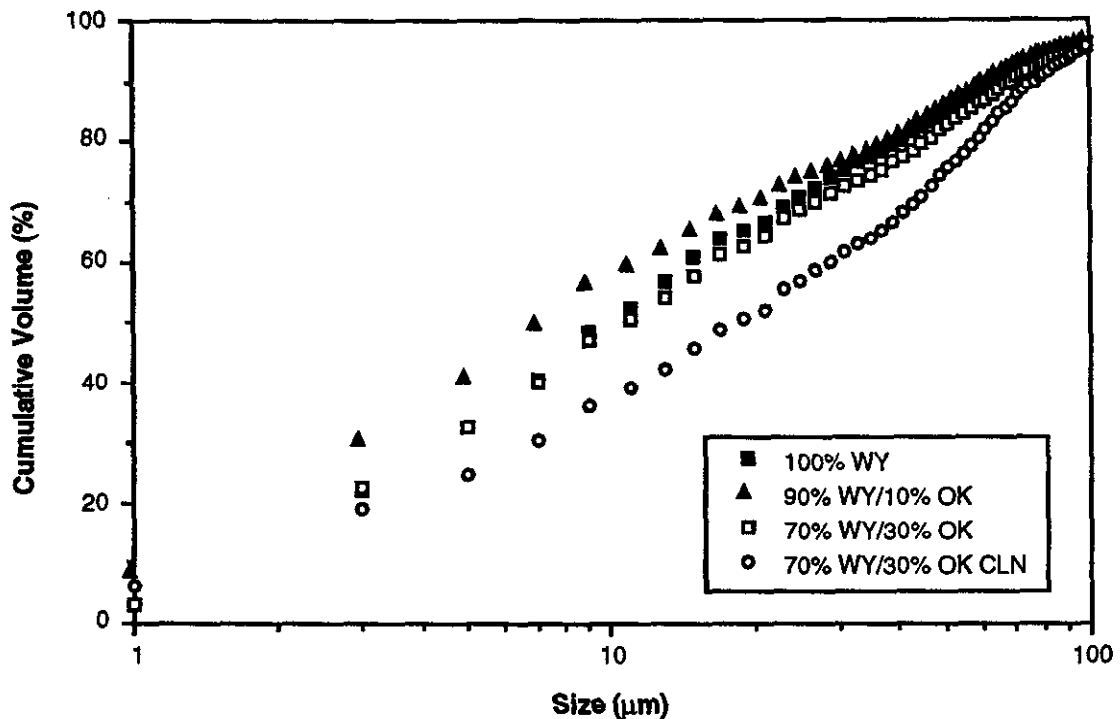


Figure 3.60 Comparison of Fly Ash Particle Size Distributions

Fly ash erosion rates were also measured in the FPTF for the 90% WY/10% OK and the 70% WY/30% OK CLN blends. Though the erosion rate of the former blend was three times that of the latter (see Figure 3.61), both values of 0.9 and 0.3 mils/10,000 hrs are very low. It is generally considered that an erosion rate of 2 mils/10,000 hrs is typical for U.S. coals. Thus, the values measured for the subject fuels indicate a low potential for tube wastage due to fly ash erosion.

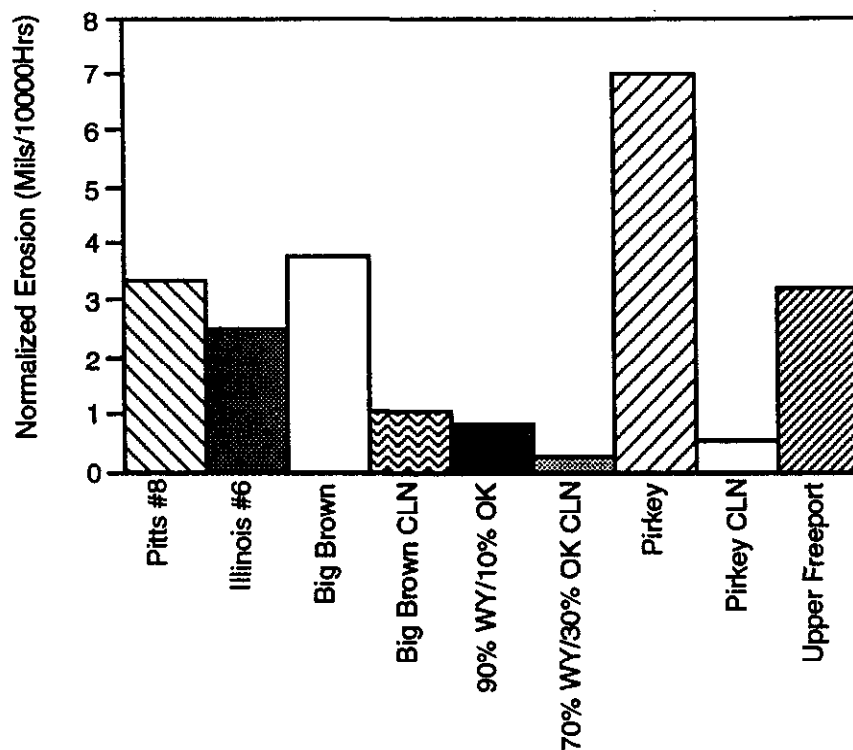


Figure 3.61 Erosion Comparison between PSO Northeastern Unit 4 Coal Blends and Other Coals/Coal Blends

SEMP and XRD analyses performed on the fly ash (dust loading) samples collected in the FPTF showed that the concentration of quartz increased as the Oklahoma coal content increased. However, the cleaning process used for the cleaned portion of the 70% WY/30% OK CLN blend lowered the quartz content to a value only slightly higher than that of the 100% WY fuel, as reported in Table 3.10. Results of the erosion measurements are consistent with the quartz content of the ashes, a logical trend since quartz is generally considered to be one of the most erosive fly ash constituents. However, the overall magnitude of the erosion rates for the fuels tested, as stated earlier, should not present a problem in extended boiler operation.

Section 4

BOILER PERFORMANCE MODELING

The purpose of ABB boiler performance modeling was threefold. Firstly, the model was used to calculate data points not thoroughly measured during field testing due to economic or physical limitations. For example, the furnace gas temperature profile from the burner elevation to the economizer is important for interpretation of performance and deposit behavior. However, due to economic restraints, large boiler dimensions and the availability of access ports, it is generally not possible to “map” gas temperatures for the entire boiler. The boiler performance model, through the use of mass and energy balances, uses data available from the plant data logging systems to back-calculate an average gas temperature at the furnace outlet plane, and at the inlet of each convective section. Additionally, model outputs can be used to assess field test data quality and resolve inconsistencies between measurements.

The second purpose of the boiler performance model was to provide information on performance parameters not measured during field testing. Certain values, such as lower furnace thermal conductance and maximum flame temperature, are not directly measured in the field because of the technical difficulty in obtaining reliable data. These parameters are essentially for correction with laboratory data for algorithm development.

Lastly, the boiler performance model supports the CQE model development through the resolution of the boiler performance. ABB model results provide a basis for comparison of CQE boiler model predictions. This may help to identify specific areas of the CQE model requiring additional development and aid in validating other aspects.

Data from the Northeastern Unit 4 computer system, the pilot-scale test furnace (FPTF) and special bench-scale tests were used as quantitative and qualitative inputs to an in-

house computer model of the boiler and auxiliary equipment. Included in the boiler island are the pulverizers, air heaters and steam generator. Once the information was processed through the model, the impacts of firing the 100% WY, 90% WY/10% OK and 70% WY/30% OK fuels in Northeastern Unit 4 were evaluated. Comparisons were then made between the commercial boiler performance when firing the 100% WY and the blended fuels. Specific performance areas that were evaluated include:

- Overall boiler efficiency
- Boiler capacity (load limitations due to slagging, fouling, erosion or other factors)
- Lower furnace performance (heat release, heat absorption distributions, outlet temperature)
- Convection pass performance (heat absorption rates, exit gas temp.)
- Air heater performance (air temperature rise, gas side efficiency)
- Pulverization (power consumption and capacity)

The consequences and anticipated advantages of firing the 100% WY, 90% WY/10% OK and 70% WY/30% OK fuels in the Northeastern Unit 4 are discussed herein.

4.1 DESCRIPTION OF NORTHEASTERN UNIT 4

The Northeastern Unit 4 Station of Public Service of Oklahoma is a CE-designed radiant-reheat, supercritical pressure combined circulation, single cell balanced draft boiler. The furnace is designed to fire sub-bituminous coal through five elevations of tilting tangential fuel nozzles. It has a design maximum continuous rating (MCR) of 3,200,000 lb/hr main steam flow and 2,825,000 lb/hr reheat steam flow; main and reheat outlet conditions are 1005 °F/3500 psig and 1005 °F/618 psig, respectively. Superheat outlet steam temperature is controlled at 1005 °F for superheat steam flows from 1,483,000 lb/hr to 2,472,000 lb/hr by means of superheat desuperheater spray. Reheat outlet steam is controlled from 1,425,000 lb/hr to 2,825,000 lb/hr by means of fuel nozzle tilt and reheat spray. Outlet conditions at control load (60% of MCR) are 1005 °F/3500 psig for main steam and 1005 °F/305 psig for reheat steam. The unit

provides steam to a turbine which powers a 430 MW (441 MW gross) generator. A side elevation view of the unit is shown in Figure 4.1.

The radiant furnace is 52.1 feet wide and 47.0 feet deep. Eighty-four wall blowers have been installed in the lower furnace to control slag buildup.

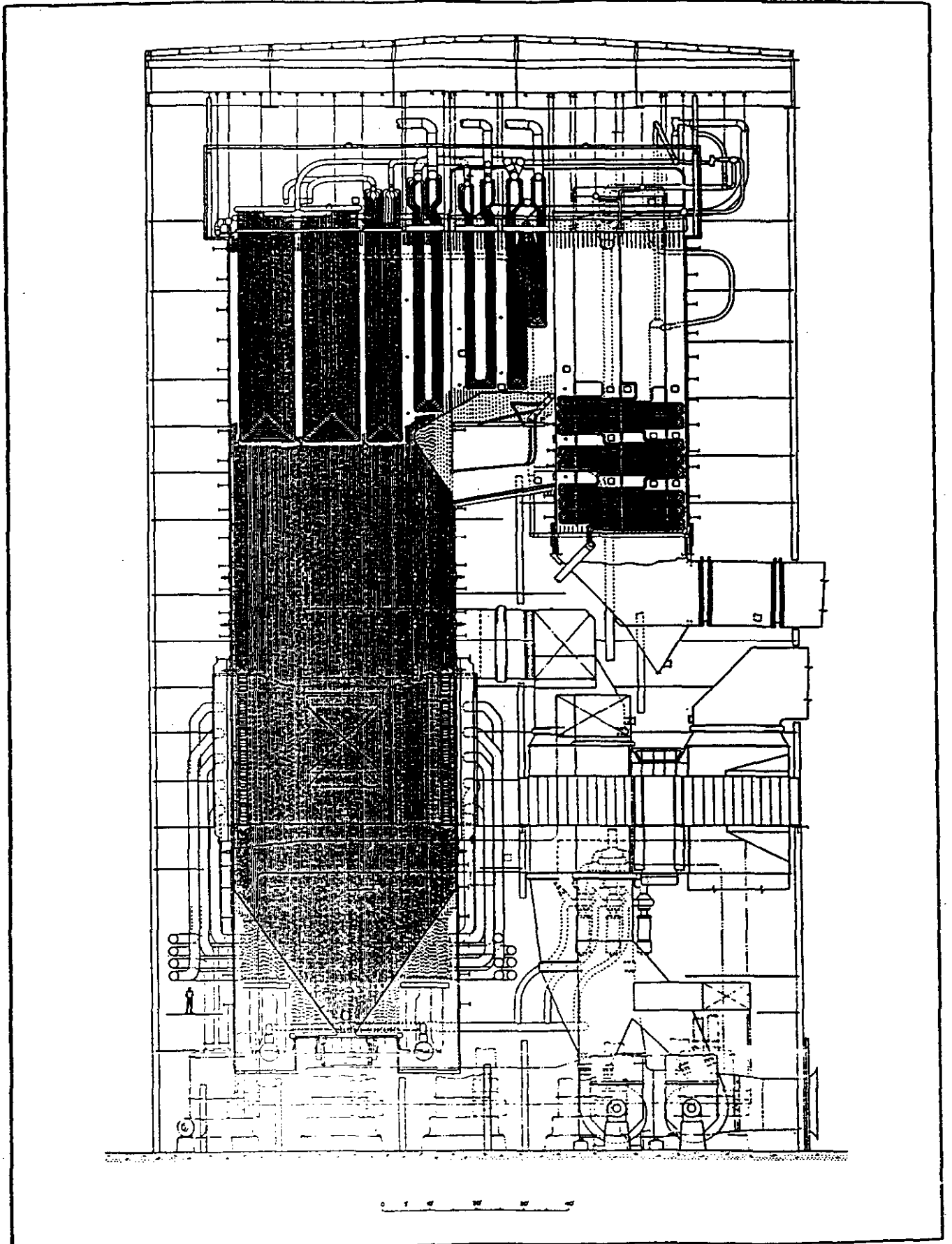
The superheater train consists of, in order, (1) radiant roof, (2) division panels, (3) desuperheaters, (4) pendant platen assemblies and (5) pendant finishing sections. The reheater arrangement utilizes two pendant convective sections, one after the finishing superheat and the second at the furnace vertical outlet plane. The economizer is constructed of staggered continuous fin in-line tubing with a total surface area of 217,000 square feet.

Coal is pulverized in five CE Raymond RP1003 pulverizers, each having a base capacity of 150,000 lb/hr, given a Hardgrove coal grindability index of 55 and a pulverized fineness of 70% through 200 mesh sieve. The pulverized coal is admitted to the furnace through five elevations of concentric-firing tilting tangential burners in the corners. Combustion air is preheated in a Ljungstrom 34 VI 96 trisector air preheater.

4.2 BOILER OPERATION

Unit 4 first went into commercial operation in August of 1980. The unit is currently base loaded, and has a name plate turbine rating of 441 MW gross at 3334 psig. Public Service of Oklahoma, as a member of the Southwest Power Pool, has been given a "continuous dependable full load" rating of 455 MW net/470 MW gross. Typical operation is at 5% over-pressure (3500 psig) to produce 455 MW (net). It operates at full load (455 MW net) during the day and cycles down at night to deslag and/or meet system electrical needs. The unit may cycle down from 455 to 250 MW (net) for a normal deslag; however, removal of particularly tenacious slags may require a further load drop to as low as 150 to 185 MW (net). Typically, when operating in a cycling mode, the lower furnace wall blowers are cycled continuously day and night.

Figure 4.1 Northeastern Unit 4 Side Elevation View



The eight-four (84) wall blowers are initiated sequentially, and after the cycle is completed the sequence is immediately started again. Upper furnace and convection pass soot blowers are typically blown three times per shift, when the unit is in a cycling mode. When operating over MCR for extended periods during peak load demand or when firing a coal which aggravates slagging, the retractable soot blowers can be initiated up to five times per shift.

Northeastern Unit 4 was originally equipped with twenty retractable soot blowers; two more were added immediately following startup. Six additional soot blowers were installed in 1989 at the vertical plane in front of the rear pendant reheater to improve section performance, which was inhibited by fouling deposit buildup. Figure 4.2 illustrates wall and soot blower placement. Two soot blowers have also been added to the air heater to relieve an ash buildup problem. These air heater blowers run in sequence continuously, each for 30 minutes.

4.3 COAL SOURCE

ASTM analyses of composite samples taken during field testing indicate that the Wyoming and Oklahoma fuels used for this study are very similar to those used when Unit 4 was initially put into service. Standard ASTM fuel analysis results for the as-received 100% WY fuel (sample from Unit 4) are given in Table 4.1. The field coal analyses were used for field combustion performance modeling to maximize the accuracy of the model predictions. The small differences between the field and pilot-scale analyses are attributed to variations in laboratory techniques and normal fluctuations in fuel supply, since the fuel for pilot-scale testing was a composite blend taken from the feed belt during field testing. The analyses for the two blended fuels are given on an as-fired (plant) basis in Table 4.1.

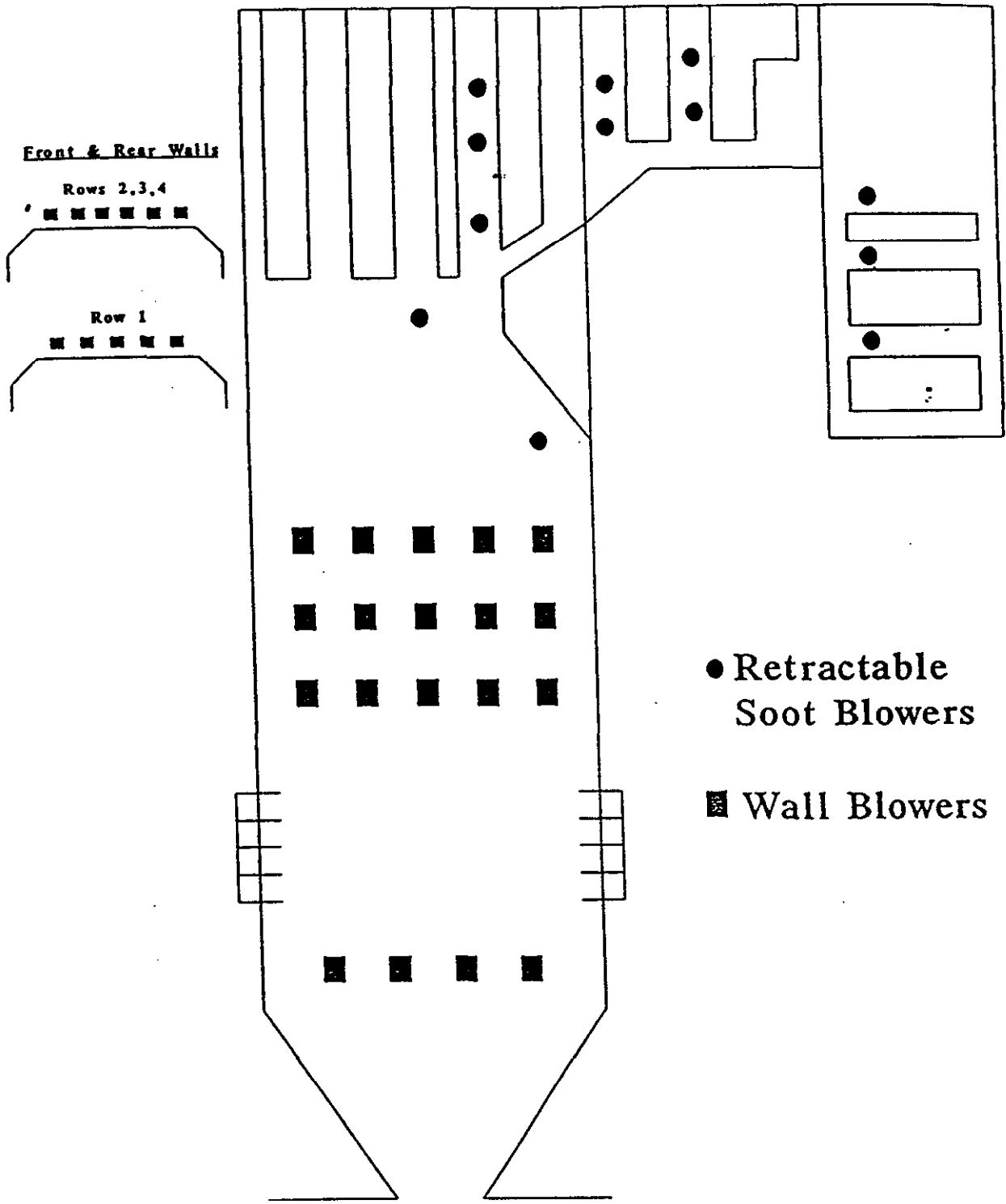


Figure 4.2 Northeastern Unit 4 Wall and Soot Blower Locations

Table 4.1 Analyses of PSO Field-Tested Fuels

	<u>100% WY</u>	<u>90%WY/10%OK</u>	<u>70%WY/30%OK</u>
Proximate Analysis (%)			
Moisture	29.04	26.91	24.05
Ash	4.82	5.00	6.83
Volatile	30.24	30.92	30.62
Fixed Carbon	<u>35.91</u>	<u>37.17</u>	<u>38.52</u>
Total	100.00	100.00	100.01
Ultimate Analysis (%)			
Carbon	48.12	49.45	50.36
Hydrogen	3.49	3.67	3.91
Nitrogen	0.38	0.50	0.87
Sulfur	0.43	0.45	0.46
Oxygen	13.72	14.03	13.54
Moisture	<u>29.04</u>	<u>26.91</u>	<u>24.05</u>
Total	100.00	100.00	100.00
HHV (Btu/lb)	8375	8772	9134
Grindability	54.0	52.6	56.0
Total Moisture (%)	17.8	15.3	8.7

4.4 BOILER PERFORMANCE PROGRAM DESCRIPTION

CE's Boiler Performance Program (BPP) was used to model the Northeastern Unit 4 boiler island. The BPP is a computational tool that was developed to select various boiler components for new boiler designs and predict the performance of the system. Calculations are performed for the steam generator envelope and related auxiliary equipment to generate information required for detailed component design. The program is structured in a modular fashion to perform the calculations in a predetermined sequence. Many of the calculated outputs from the nine modules are passed back to preceding modules for iterative solution.

The calculations begin with the Boiler Efficiency Module, which is dependent on the fuel analysis, and the Turbine Heat Balance Module, which in turn is dependent on the steam turbine design. The calculations continue in the same sequence as the flue gas flows through the boiler. Lower furnace performance is calculated first, followed by the convective pass, and then the air heater. The control volumes of the five modules that

actually model the boiler envelope are shown in Figure 4.3. The major heat absorption surfaces in the study unit associated with these modules are also identified.

The Efficiency Module calculates overall boiler efficiency using the ASME Power Test Code method (PTC 4.1-1964). Inputs such as carbon heat loss (from the Lower Furnace Program-Slice Kinetic Model, described below), radiation loss (from CE standards), and air heater exit gas temperature (from the Air Heater Module) are updated as the program iteratively converges on a solution.

The purpose of the Heat Balance Module is to determine the heat duty for the boiler from the turbine heat balance data. Air and gas flows are calculated based on the total heat duty required and the boiler efficiency. The module has provisions for main steam, two reheats, and auxiliary steam.

The objective of the Pulverizer Module is to determine primary air temperature requirements so that the heat input to the lower furnace may be calculated in the next module. A heat balance is performed around the mill so that either the amount of moisture evaporated, the air temperature entering the mill, or the mixture temperature leaving the mill is calculated. Mill performance (maximum capacity, mill loading, power input, air quantity and temperature) is also calculated.

The Net Heat Input Module determines the thermal energy available for absorption by the furnace above the selected reference temperature of 80 °F. This information is passed to the Lower Furnace Module.

The Lower Furnace Program-Slice Kinetic Model (LFP-SKM) simulates the combustion region of the furnace. The LFP-SKM develops a flame and burn-out profile from fundamental data on the coal combustion kinetics and calculates carbon heat loss (Bueters and Habelt, 1974). The program then determines, through a series of heat balance calculations, the heat transfer from the combustion products to the waterwalls, the corresponding gas temperatures, and the furnace outlet temperature.

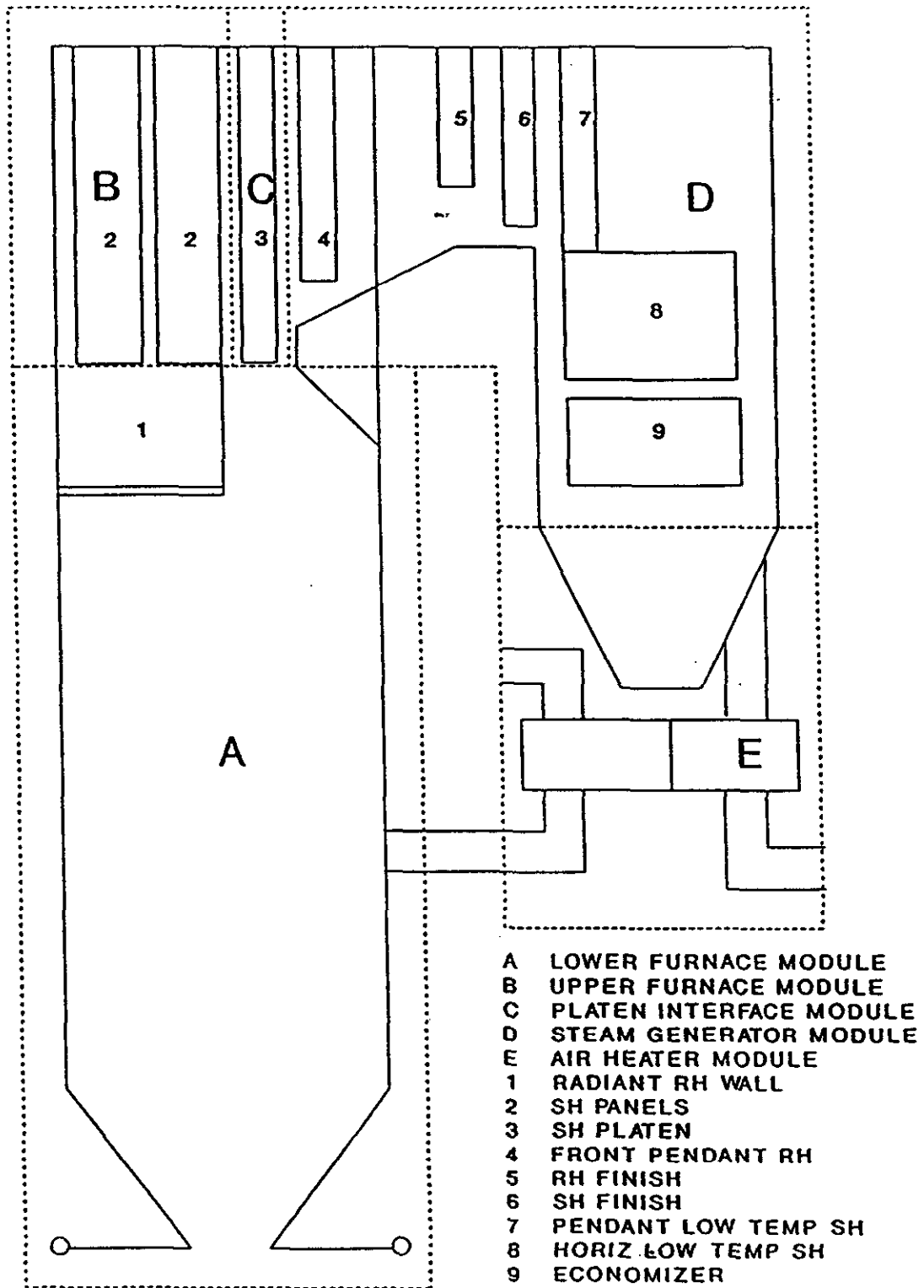


Figure 4.3 Boiler Performance Program Domain

The purpose of the Upper Furnace Module is to calculate the heat transfer in the upper furnace, the resultant gas temperature, and the radiation to the platens and the convective pass of the boiler. The upper furnace outlet values are utilized in the subsequent convection pass calculations. The Platen Interface Module determines the radiant heat absorption of the radiant walls and platens (if applicable) to establish the link between the Upper Furnace and Steam Generator Modules.

The Steam Generator Module determines heat absorption in the convective pass of the boiler. Turbine heat balance data, direct radiation absorptions, and economizer exit gas temperatures are passed automatically to this module during the iteration process. The Steam Generator Module will solve for gas and working fluid temperatures not included in the input. Conversely, given the steam and gas temperature constraints from field test data, the module will back-calculate the heating surfaces required.

The Air Heater Module predicts the performance for Ljungstrom bisector and trisector air heaters. During the boiler performance iteration, the steam temperature increase and uncorrected exit gas temperature (calculated) are passed to the Boiler Efficiency Module. The iteration is completed when the values generated in the Air Heater Module and those used in the efficiency calculation are in agreement.

4.5 BOILER PERFORMANCE PROGRAM CALIBRATION PROCEDURE

The BPP was calibrated with 100% WY coal field test data prior to the 90% WY/10% OK and 70% WY/30% OK fuel performance calculations. The program calibration runs were made to: (1) improve the accuracy and confidence level of the BPP predictions by reducing the number of assumptions about the fireside heat transfer characteristics of the boilers and; (2) develop laboratory-to-field scale-up factors specific to Northeastern Unit 4. The calibration procedure began with the input of field data from Unit 4 into the BPP. These included all known temperatures, pressures and flow rates from both steam and gas sides. The BPP was then used to back-calculate, in a

reverse step-by-step manner, several unknown parameters that affect boiler heat transfer and efficiency. The most important unknown parameters included:

- Furnace gas and wall/deposit radiative properties
- Lower furnace average slag properties (chemical, physical and thermal)
- Tube surface effectiveness
- Maximum gas temperature for soot blower effectiveness
- Air preheater leakage and gas side efficiency

The schematic logic of the calibration procedure is outlined in Figure 4.4. Once values for the above unknown parameters were determined, they were compared to the laboratory data. Additional special measurements and observations were also made during field testing at Northeastern Unit 4 using some of the same procedures used in the laboratory, as follows:

- Radiant and total (convective plus radiant) heat flux to furnace walls (heat flux probes)
- Furnace wall blower effectiveness (photographs)
- Fouling deposit bonding strength (force meter)

These measurements enabled determination of key operating parameters that impact performance, and allowed direct laboratory-to-field comparisons to be made in areas not usually covered by conventional boiler instrumentation.

The results of the calibration are summarized in Table 4.2. As can be seen from the table, the model calibration was quite good. Field test data used for calibration were obtained in August 1990 from the ACUREX 1050 and System 140 plant data loggers and other available operator board instrumentation. Table 4.2 indicates whether data values were back-calculated, obtained directly from the test data sheets, or interpolated from test data. The back-calculated values are those shown as "not available" from the field data. Erroneous or questionable data were replaced by interpolated values or those calculated from heat balance calculations, where appropriate.

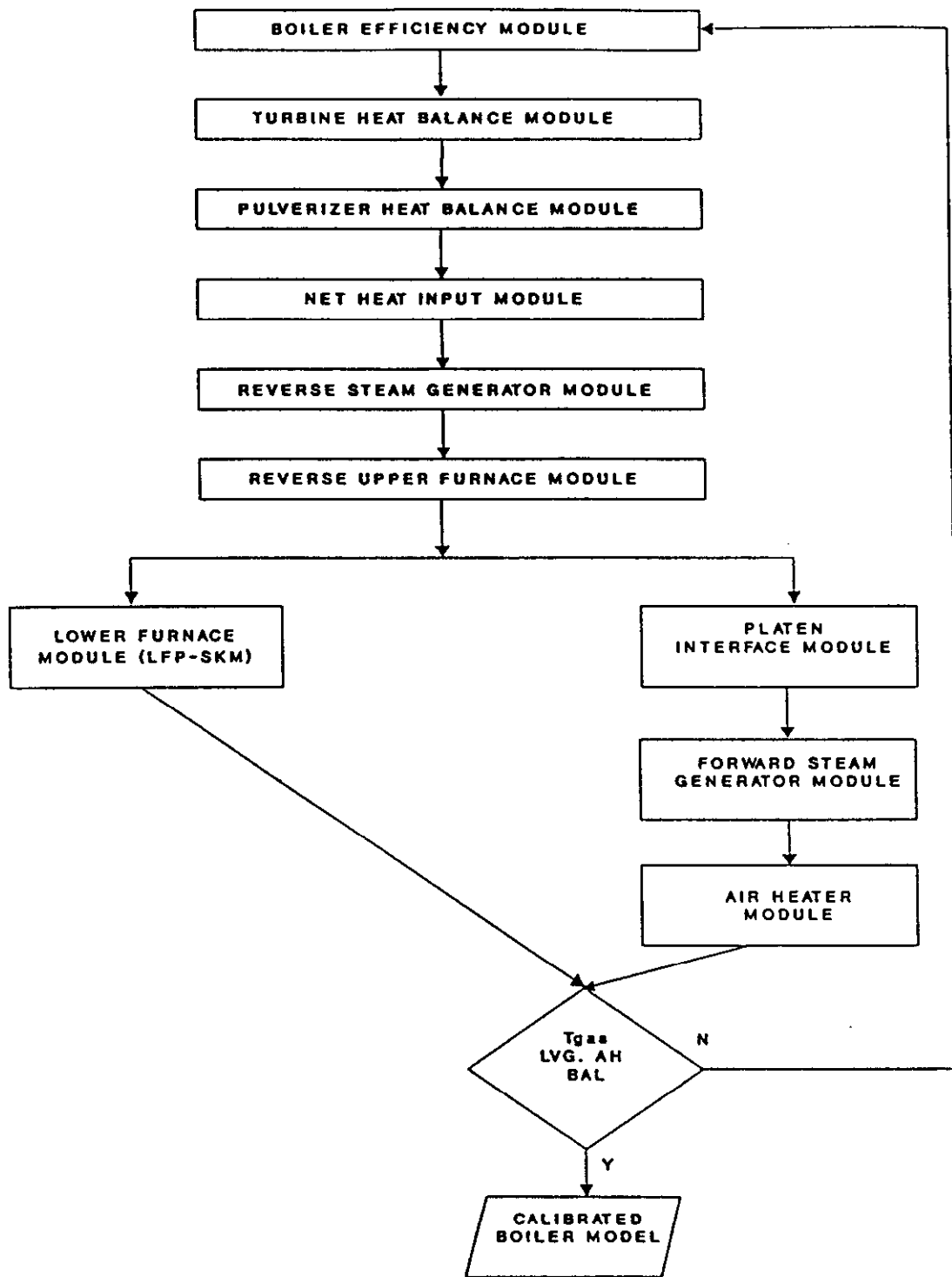


Figure 4.4 Boiler Performance Program Flowchart For 100% WY Coal Calibration

Table 4.2 Northeastern Unit 4 - Calibration of Field Test Data for 100% WY Coal

<u>General Data</u>	<u>Field Test Data</u>	<u>Reverse Calibration Value</u>	<u>Source</u>
Date	8/15/90	891	*
Gross Generator Output, MW	469	469	*
Excess Air (@ FOP), %	24.8	28.4	b
Excess Air (@ ECON OUT), %	32.3	28.4	b
Burner Tilt, Degrees	-10	-10	*
Elevations in Service	4	4	*
Boiler Efficiency, %	86.2	86.43	a
<u>Steam and Water Flows, 10³ lb/hr</u>			
Feedwater	--	3057.8	a
Superheat Spray	59.8	93.5	a
Main Steam	3151.3	3151.3	*
Turbine Seal & Misc. Leakage	98.4	98.4	*
HTR #7 Extraction	277.2	277.2	a
Reheat Spray	4.6	18.1	a
Reheat Steam	2780.3	2793.8	a
<u>Boiler Fluid Temp/Press, °F/PSIG</u>			
Feedwater	478.5/-	478.5/4000	*b
Economizer Outlet	676.6/-	676.6/3983	*b
Panel Inlet	786.5/3851	786.5/3851	*f
Desuperheater Inlet	821.6/-	821.6/3787	*b
SH Spraywater	478.5/-	478.5/4000	*b
Desuperheater Outlet	805.2/-	805.2/3754	*b
SH Platen Outlet	899.6/-	899.6/3678	*b
SH Finishing Outlet	1000.3/3500	1000.3/3500	*f
RH Desuperheat Inlet	545.9/-	545.9/596	*b
RH Spraywater	398.3/1200	398.3/1200	*f
RH Desuperheat Outlet	538.2/596	538.2/596	*f
RH Cross-Over	775.6/-	775.6/581	*b
RH Finishing Outlet	990.0/566	990.0/566	*f
<u>Pulverizer Performance</u>			
Coal Flow, lb/hr	518,708	521,921	a
Air Flow, lb/hr	--	869,644	a
Fineness, % - 200 mesh	79.3	79.3	*
Grinding Capacity	--	91.6	a
Pulverizer Outlet Temperature, °F	152.6	152.6	b
Grinding Power, KW	--	1784	a
<u>Furnace Performance</u>			
Net Heat Input, MBtu/H	--	4620.0	a
Heat Release Rate, MBtu/hr ft ²	--	1.89	a
Furnace Outlet Temperature, °F	2451	2548	a
Convection Pass Inlet Temperature, °F	--	2095	a
Economizer Outlet Temperature, °F	731	731	*
<u>Air Heater Performance</u>			
Ambient Air Temperature, °F	81.3	81.3	*
Avg. Air Inlet Temperature, °F	--	96.4	b
Primary Air Outlet Temperature, °F	745.0	745.0	*
Secondary Air Outlet Temperature, °F	713.9	713.9	*
Gas Inlet Temperature, °F	783.9	783.9	*
Gas Outlet Temperature, °F (uncon) ¹	305.4	305.4	*
Air Side Efficiency, %	89.8	89.8	*
Gas Side Efficiency, %	69.6	69.6	*
* Data is obtained directly from test data unless otherwise noted			
a) Back-calculated			
b) Interpolated from test or prior data			
1) Gas temperature is not corrected for air in-leakage			

Main steam flow was determined by adding feedwater and superheat desuperheater spray flows and subtracting blowdown and auxiliary steam flows. Seal leakages and miscellaneous extractions from the high pressure turbine were obtained from turbine manufacturer diagrams. Reheat flow before the reheat desuperheater was calculated by subtracting extractions and seal leakages. Reheat flow to the boiler was obtained by adding in reheat desuperheater spray flows.

4.5.1 Calibration of Northeastern Unit 4

Generally the field test data were considered to be accurate and reliable with few exceptions. One area open to data interpretation was the O_2 value in the convection pass. O_2 measurements were taken at the horizontal furnace outlet plane (HFOP) and at the economizer outlet. The difference between these two sampling points was substantial enough to suspect significant air in-leakage in the convection section. As no data was acquired throughout the backpass, specific gas weights could not be assigned to tube sections based on percent in-leakage. The approach to calibrating gas weight was to average the two measured values and apply a uniform gas weight over the entire backpass.

The second area open to interpretation was the horizontal furnace outlet temperature (HFOT). Due to the narrow deck around the boiler, the longest probe which was able to be handled was twenty feet in length, operable from both sides of the furnace. This left the middle twelve feet of the boiler unreachable and thus unmeasured. Only one line in the HFOT plane was measured, putting another limit on the usefulness of the available data as furnace averages. Typically a five-shield system with a lengthy data collection time is required to approach the true gas temperature. For this testing a two-shield system was used, and due to radiation losses, the measured temperatures are most likely lower than the true gas temperatures.

The third area open to interpretation was the superheat and reheat desuperheater flows. Discrepancies were found between the orifice-measured flows and the calculated flows which were based on thermocouple data and a heat balance around

the desuperheater station. Discrepancies in superheater desuperheater spray flow values were considerable (59,800 lb/hr measured versus 93,498 lb/hr calculated). Reheat desuperheater spray flows had a discrepancy of 4,600 lb/hr (measured) versus 18,148 lb/hr (calculated). Thermocouple steam temperature measurements are typically more accurate than calibrated orifice mass flow measurements; therefore, the superheat desuperheater values based on thermocouple readings and heat balance calculations were used in the program calibration.

Deposit bonding strength measurements, surface effectiveness factors, thermal conductance calculations, and HFOT and heat flux measurements provided a method for comparison of FPTF data and field data, and also provided a secondary check for the validity of field-acquired data. Field bonding strength measurements (BSM's) taken in the division panel and platen area next to the nose had values of 12.5 to 14.8 (100% WY fuel). The field bonding strength data are presented in Figure 4.5 using gas temperatures measured by the EERC testing team, approximately 15 feet away at the suction pyrometer port location. The field BSM's were taken approximately two feet from the furnace wall, where deposits were within reach of the force meter. Figure 4.5 illustrates bonding strength measurements (field and pilot-scale) versus local gas temperatures for the 100% WY fuel, and indicates the expected trend of increasing deposit tenacity with increasing gas temperature.

The convective pass performance is frequently characterized by tube section surface effectiveness factors (SEF's). Surface effectiveness factors are simply a ratio of the back-calculated tube surface areas to the actual installed tube surface areas assuming a constant heat transfer coefficient. Table 4.3 lists the SEF's calculated for Northeastern Unit 4 during the August 1990 field trip. The boiler had been operating at 469 MW (gross) in a cycling mode for more than one week. The tube section types as shown in Table 4.3 are in the same sequential order as the direction of gas flow. Results from several days of testing were examined and various data sets were processed to check for SEF variability due to the cycling nature of the unit. The data set presented in Table 4.3 reflect the average SEF's.

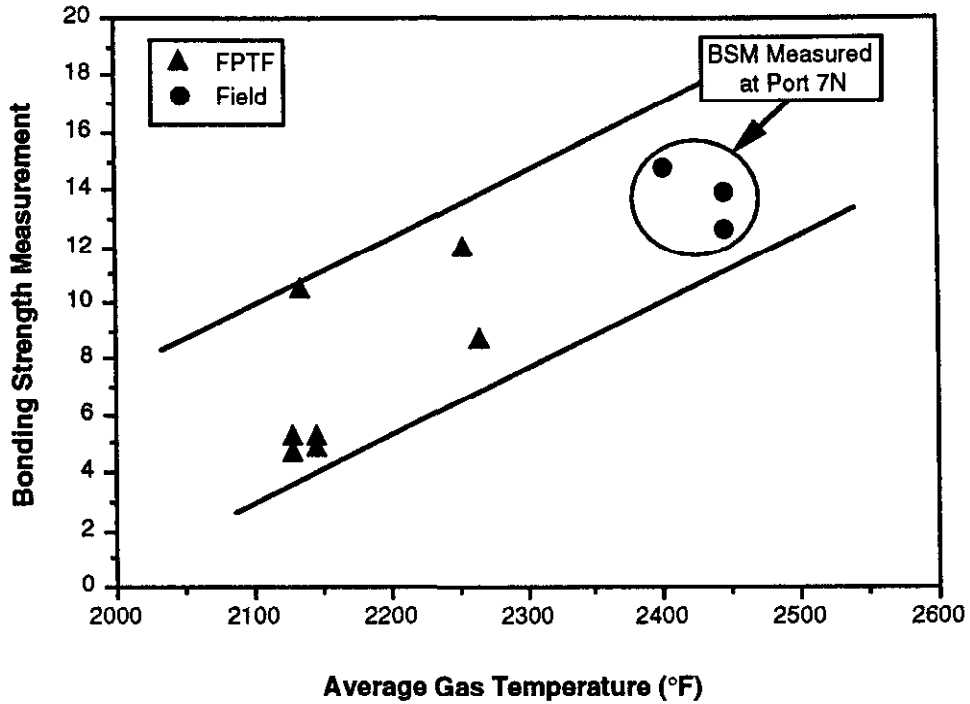


Figure 4.5 Bonding Strength Measurements vs. Gas Temperature for FPTF and Field Data (100% WY)

Table 4.3 Northeastern Unit 4 Surface Effectiveness Factors (SEF's)

Convective Surface		Back-Calculated	
Section Type	Actual Surface (ft ²)	Effective Surface (ft ²)	SEF
SH Platen	14850	15705	1.06
RH Front Pendant	21738	21295	0.98
SH Finish	24282	24765	1.02
RH Rear Pendant	41450	36718	0.89
Economizer	217000	209560	0.97

The energy in the gas stream entering the convection pass, as well as the section absorptions, were used to back-calculate an HFOT (horizontal furnace outlet temperature). The calculated HFOT (2548 °F) differed from the field measured value (2451 °F) by 97 °F. This difference is attributed in part to radiation losses from the thermocouple and inadequate temperature measurement coverage of the HFOT plane, discussed earlier in this section. To further support the higher calculated HFOT, the radiation heat flux measurements calculated in the model are directly in line with those measured in the field, as shown in Figure 4.6. The radiation and total heat flux readings were taken approximately two feet below and six feet above the HFOT plane. The ports used, their locations and the radiation heat flux readings (with the probe face flush with the tube crowns) are illustrated in Figure 4.7. The heat flux distribution across the furnace (ports 1 through 6) was fairly uniform.

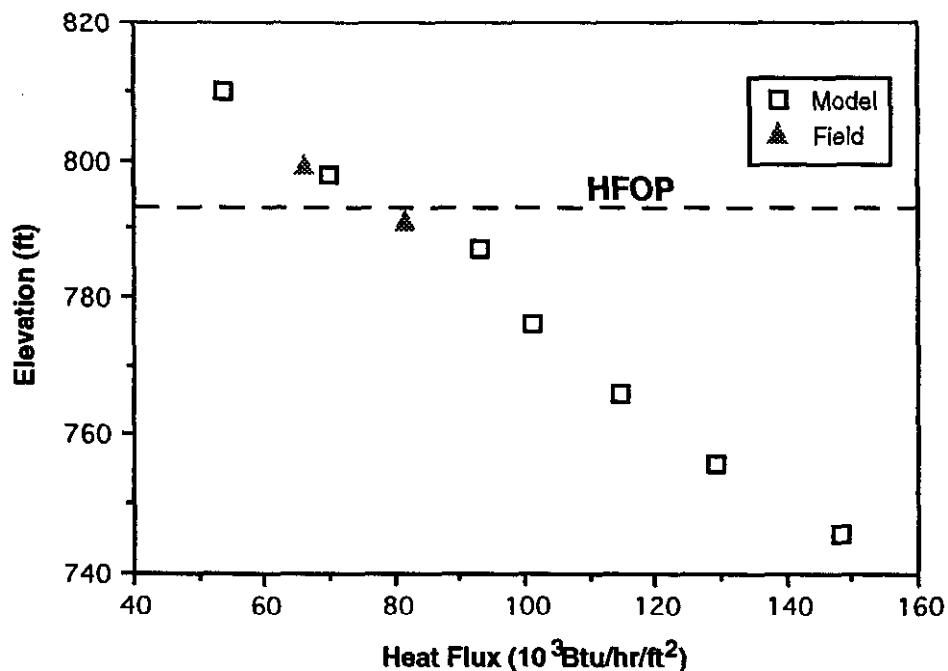


Figure 4.6 Comparison of Field Test Data: Model of Generated vs. Measured Heat Flux Radiation at the Furnace Wall

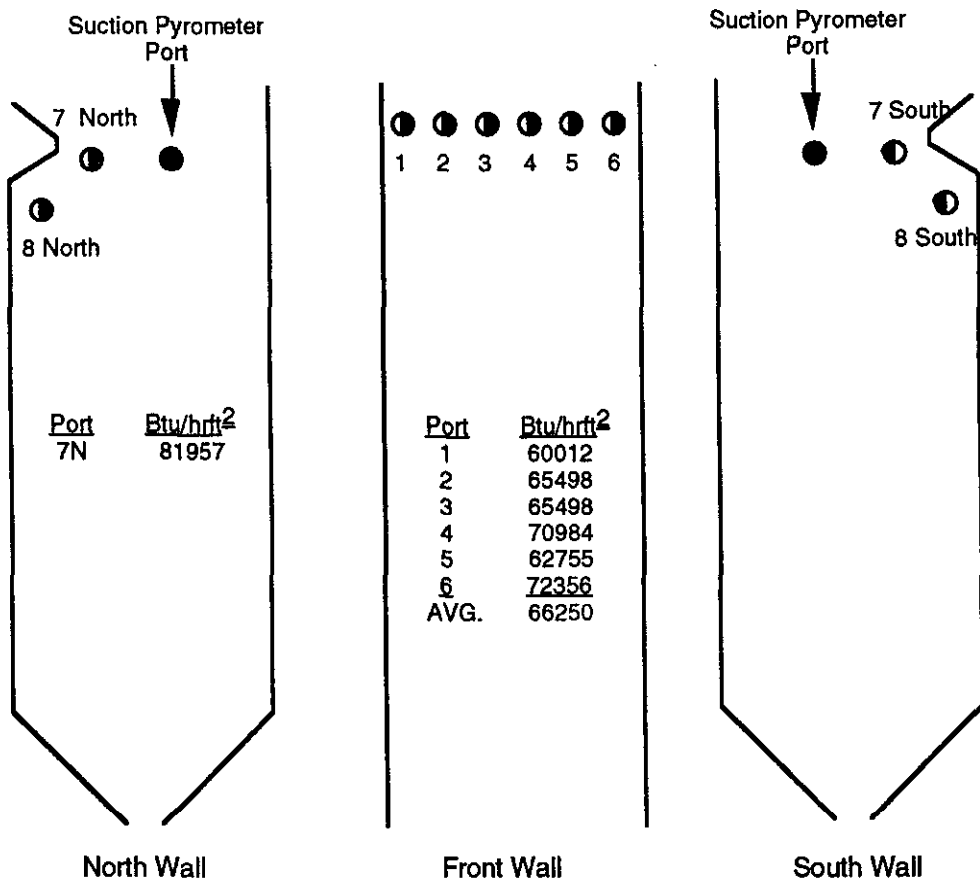


Figure 4.7 Northeastern Unit 4 - Port Arrangement and Radiation Heat Flux Values

The lower furnace performance is characterized by the local thermal conductance of the deposit ($K/\Delta X$). The LFP-SKM is run in an iterative mode until the predicted HFOT and the sensible and radiative energies match the back-calculated HFOT value. The major iteration variable is $K/\Delta X$. Figure 4.8 presents the thermal conductance versus local flame temperature for the FPTF 100% WY data and the back-calculated $K/\Delta X$ values from field data, calculated from the burner zone up through the furnace outlet. Based on this good agreement, correlations were considered unnecessary for scale-up purposes.

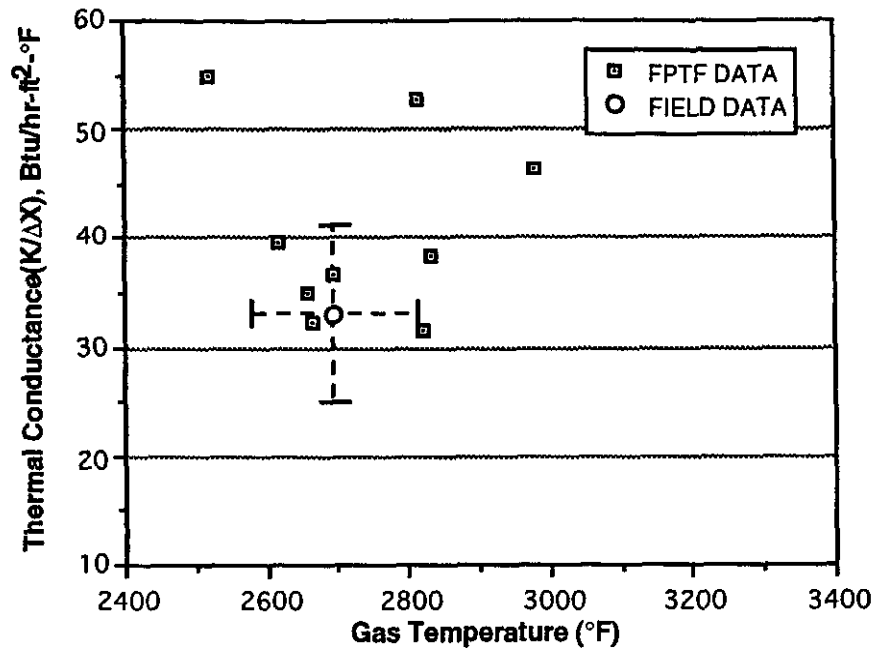


Figure 4.8 Thermal Conductance vs. Gas Temperature for 100% WY

4.6 BOILER PERFORMANCE WITH BLENDED FUELS

4.6.1 Performance Prediction Procedure

Generally, the approach to predicting boiler performance has been fundamentally based on existing bench- and pilot-scale data. Bench and pilot-scale performance "indicators" provided relative comparisons of the 100% WY and blended coal behavior in seven major areas: abrasion, pulverization, combustion, ash slagging, ash fouling, ash erosion, and gaseous emissions. The coal quality/performance indicators have been derived from the laboratory test results in each of these areas and are presented in Table 4.4. The indicators included conventional ASTM coal analysis indices (base/acid ratio, ash fusion temperature, etc.), the special parameters developed from the FPTF and the special bench-scale-derived indices described in Section 2. The ASTM indices were calculated primarily as familiar reference points which are widely understood in the utility industry. However, recent investigations have shown them to have limited reliability in their prediction of coal quality and its relationship to utility

steam generator p
data in conjunctor
which agree quite

ASTM derived coe
the following three
empirical correlat
equipment. All ot
the relative quality

Table 4.4 Bench and Pilot-Scale Coal Quality Indicators

INDICATOR	TEST	100% WYOMING	90% WY/10% OK	70% WY/30% OK
<u>Abrasion</u>				
Ash Content, %MF	ASTM	6.8	6.8	9.0
Alpha- Quartz content, %	Special	20	19	20
<u>Pulverization</u>				
Hardgrove Index	ASTM	62.5	62.5	56.0
Coal HHV, Btu/lb MF	ASTM	11802	12002	12026
<u>Combustion</u>				
Carbon in Ash, %	FPTF	0.24	0.42	0.55
Carbon Conversion, %	FPTF	99.98	99.97	99.96
<u>Ash Slagging</u>				
Base/Acid Ratio (B/A)	ASTM	0.82	0.80	0.52
Slagging Index (B/A x % Sulfur)	ASTM	0.35	0.36	0.24
Fe ₂ O ₃ in Ash, %	ASTM	7.7	7.6	11.0
Max. Gas Temp. for Blower Effectiveness, °F	FPTF	2950	3050	2925
<u>Ash Fouling</u>				
Fouling Index (B/A x % Na ₂ O)	ASTM	0.55	0.45	0.31
Na ₂ O + K ₂ O in Ash, %	ASTM	1.19	1.29	1.77
Weak Acid Leaching, % Active	Special	0.84	0.74	0.53
Max. Gas Temp. for Blower Effectiveness, °F	FPTF	2260	2360	2200
Deposit Bonding Strength @ 2250°F	FPTF	8.0	10.0	18.0
Deposit Buildup Rate/Sootblowing Frequency, hr. @ 2250°F	FPTF	6	8	10
<u>Erosion</u>				
SiO ₂ + Al ₂ O ₃ in Ash, %	ASTM	43.5	44.6	55.1
Ash Content, % MF	ASTM	6.8	6.8	9.0
Erosion Rate @ 60ft/s (Mils/10 ⁴ hr)	FPTF	NA	0.9	0.3
MF = Moisture Free				

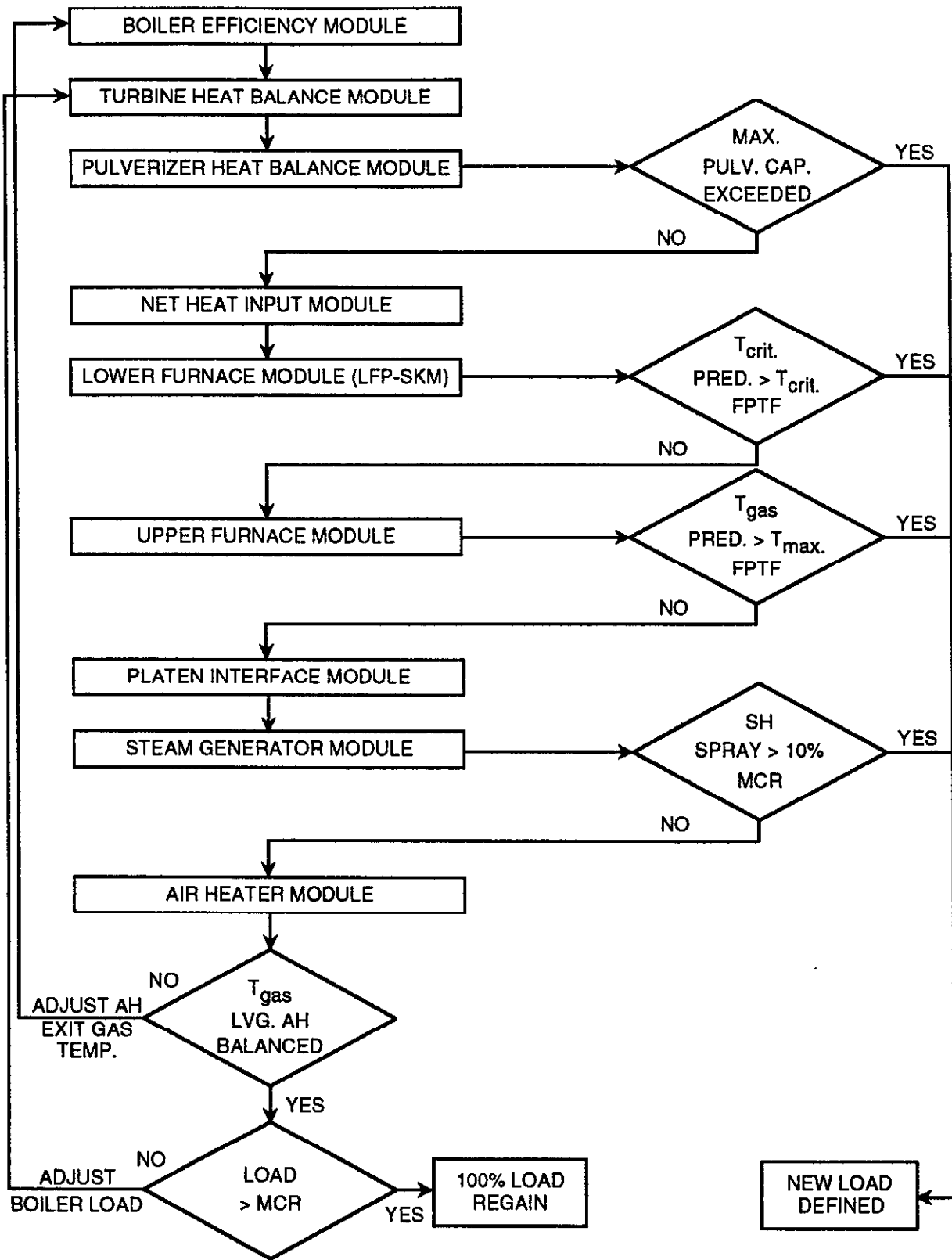


Figure 4.9 Boiler Performance Program Flowchart For Boiler Performance Prediction

The pulverizer capacity was obtained from standard performance curves for a new Raymond RP 1003 pulverizer given the Hardgrove Grindability Index (55), the coal moisture (15.0%), and a standard fineness (70% through 200 mesh). These limits were considered to be absolute maximums for the pulverizers, since wear reduces capacity and not all mill parts are replaced regularly. The actual coal mill capacities were not available from the field test data. Operating a pulverizer beyond its rated capacity results in coal spillage from the bowl and a corresponding heat loss. The ability to maintain coal fineness also becomes difficult. As a result, incomplete carbon burnout of oversize particles can become a problem that further contributes to carbon heat loss.

Lower furnace slagging potential was incorporated into the modeling process by using the maximum furnace temperature data and the effective thermal conductance ($K/\Delta X$) from the FPTF. Pilot-scale determination of the slagging limitation for the 100% WY fuel required firing at a low excess air level. Since a slagging limitation was not reached with the 100% WY fuel at normal excess air levels, a correlation to maximum furnace temperature could not be verified from data attained at Northeastern Unit 4; however, data obtained from previous testing (Levasseur, et al., 1987) indicates that the laboratory data can be applied with a 100 °F field correction factor (i.e., 100% WY coal had an FPTF critical temperature of 2850 °F while in the field this could correlate to a 2950 °F average slice temperature). Lower furnace gas temperatures above the maximum furnace temperature would probably cause deposits to be unremovable and exhibit a lower $K/\Delta X$ value, creating a higher resistance to the transfer of heat from the gas to the water side. Gas temperatures would then be higher than normal, possibly causing slag carry-over into the upper furnace area. Back-calculated data from the 100% WY testing show a clear correlation of the thermal conductance in the field to that obtained in the FPTF, as shown in Figure 4.8. No correction factor was necessary in interpreting the $K/\Delta X$ data for the blended coals. The average $K/\Delta X$'s used for the blends were 42 for the 90% WY/10% OK fuel and 38 for the 70% WY/30% OK fuel, as presented in Figures 4.10 and 4.11. These limits were incorporated into the model to portray the effects of the coal ash deposits on the lower furnace walls.

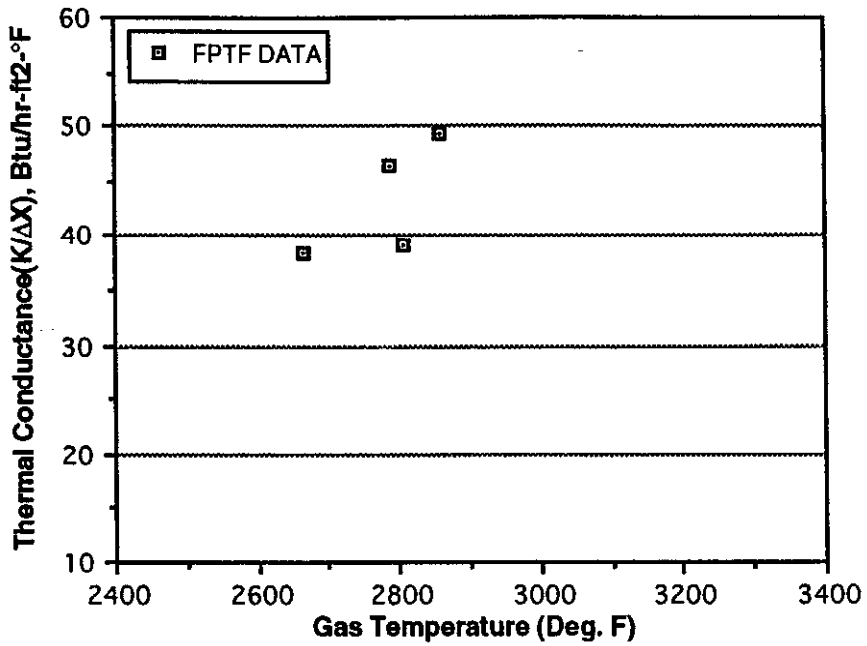


Figure 4.10 Thermal Conductance vs. Gas Temperature for 90% WY/10% OK Blend
FPTF Tests

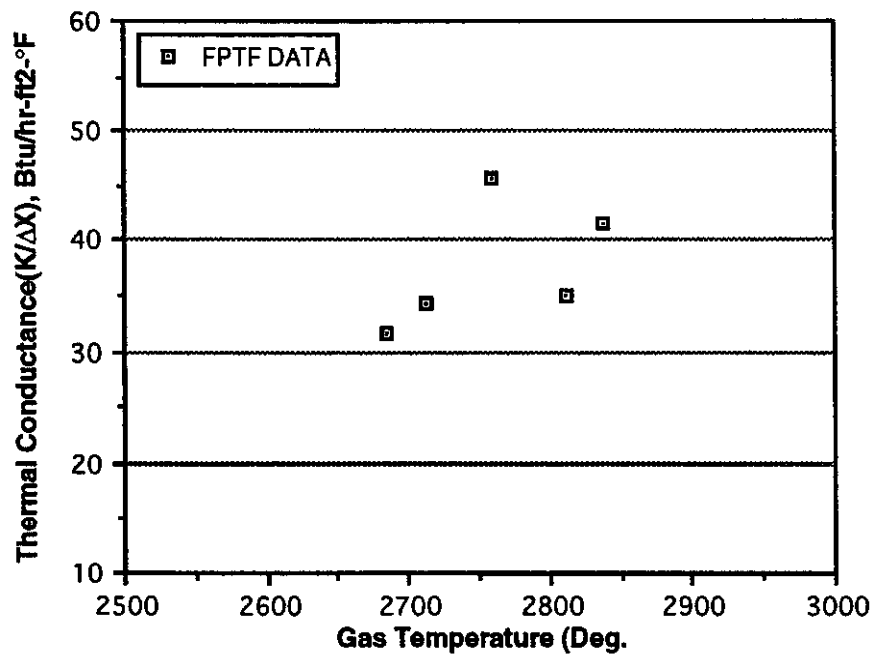


Figure 4.11 Thermal Conductance vs. Gas Temperature for 70% WY/30% OK Blend
FPTF Tests

The 100% WY fuel demonstrated controllable convective section fouling in the FPTF at gas temperatures up to 2260 °F. The 100% WY calibration for the bonding strength/local gas temperature relationship indicated that the laboratory data could be directly applied, as illustrated in Figure 4.5. Therefore, the maximum allowable local convective gas temperature was established at 2260 °F for the 100% WY fuel. Backpass temperature (fouling) limitations were similarly set at 2360 °F and 2200 °F for the 90% WY/10% OK and 70% WY/30% OK fuels, respectively. Above these limits, uncontrollable fouling was observed and measured. In the field, uncontrollable fouling causes a progressive rise in backpass gas temperatures, which can ultimately lead to metal overheating and possible tube failures. Excessive fouling can also cause partial blockages of the gas pass.

Unit 4 is equipped with direct-contact spray desuperheaters for main steam temperature control (located between the division panels and platen sections). Since Unit 4 is a supercritical pressure unit, the superheater outlet steam temperature is controlled by the firing rate. The maximum desuperheater spray flow limit was set at 10% (315,139 lb/hr) of primary steam flow. Limits were established to address the problem of steam flow loss in the low temperature sections, which can drive up steam temperatures and tube metal temperatures beyond their original design values. Reheat steam temperature can be controlled by fuel nozzle tilts and/or with the desuperheater spray system. However, even a small quantity of spray is undesirable from a heat rate standpoint, because the steam generated from the reheat spray water bypasses the high-pressure section of the turbine. The reheat spray limitation was set at 120,000 lb/hr.

The fly ash erosion rate was measured for the 90% WY/10% OK fuel and projected to be 0.9 mils/10,000 hrs at a velocity of 60 ft/s. It is generally considered that an erosion rate of 2.0 mils/10,000 hrs is the maximum allowable rate from a design standpoint. Erosion in excess of this value does not normally affect boiler performance but can contribute to increases in boiler operational and maintenance costs. Erosion rate was therefore not a boiler performance-limiting factor.

4.6.2 Boiler Island Performance of the 90% WY/10% OK and 70% WY/30% OK Fuels

The results of the 90% WY/10 % OK and 70% WY/30 % OK fuel performance evaluations are summarized in Table 4.5. Boiler island performance of the 100% WY coal was compared to that of the blends at an equivalent heat duty. Main and reheat steam flows and pressures were held constant while the coal feed rate was allowed to vary to achieve similar steam outlet temperatures. This analysis is based upon the present wall blower and retractable soot blower operation and coverage in Unit 4 and interpretation of FPTF results. Analyses indicate that superheater performance will be acceptable with both blends. The MCR boiler performance data indicate superheater and reheater steam temperatures are achievable with -10° burner tilt and 3.0% and 0.14% superheat and reheat spray flows, respectively, for the 90% WY/10% OK fuel. Calculations for the 70% WY/30% OK fuel indicate superheater and reheater steam temperatures are achievable with 3.0% and 0.69% superheat and reheat spray flows at -10° burner tilt.

Boiler efficiency improved slightly for the 90% WY/10% OK fuel (86.58%) and remained approximately the same for the 70% WY/30% OK blend (86.39%), compared to the 100% WY coal (86.43%), as shown in Table 4.6. These differences can be attributed to changes in fuel moisture, excess air, air heater exit gas temperature and average air inlet temperature.

Carbon heat losses at Northeastern Unit 4 were calculated using the LFP-SKM program. They were 0.3% for the 100% WY and 0.2% for the 90% WY/10% OK and 70% WY/30% OK fuels.

Pulverizer performance is typically described in terms of maximum capacity (MBtu/h or tons/h), the power consumption (kWh/MBtu), and the outlet coal fineness (% through 200 mesh). Capacity and power consumption were calculated for an equivalent outlet coal fineness of approximately 80% through 200 mesh using CE design performance curves for new (or newly rebuilt) mills. This approach provided somewhat optimistic results in lieu of more detailed information on the working condition of the mills.

Table 4.5 Northeastern Unit 4 Comparison of 90% WY/10% OK and 70% WY/30% OK Blends to Calibrated 100% WY Results

<u>General Data</u>	<u>100% WY Calibrated Results</u>	<u>90%WY/10%OK Projected Performance</u>	<u>70%WY/30%OK Projected Performance</u>
Date	8/91	9/91	9/91
Gross Generator Output, MW	469	469	469
Excess Air (@ FOP), %	28.4	28.6	27.0
Excess Air (@ ECON OUT), %	28.4	28.6	27.0
Burner Tilt, Degrees	-10	-10	-10
Elevations in Service	4	4	4
Boiler Efficiency, %	86.43	86.58	86.39
<u>Steam and Water Flows, 10³ LB/H</u>			
Feedwater	3057.8	3057.8	3057.8
Superheat Spray	93.5	93.5	93.5
Main Steam	3153.3	3153.3	3153.3
Turbine Seal & Misc. Leakage	98.4	98.4	98.4
HTR #7 Extraction	277.2	277.2	277.2
Reheat Spray	18.1	3.9	19.2
Reheat Steam	2793.8	2779.6	2794.9
<u>Boiler Fluid Temp/Press. °F/PSIG</u>			
Feedwater	478.5/4000	478.5/4000	478.5/4000
Economizer Outlet	676.6/3983	674.6/3983	674.5/3983
Panel Inlet	786.5/3851	786.3/3851	786.4/3851
Desuperheater Inlet	821.6/3787	820.6/3787	823.0/3787
SH Spraywater	478.5/4000	478.5/4000	478.5/4000
Desuperheater Outlet	805.2/3754	803.9/3754	806.0/3754
SH Platen Outlet	899.6/3678	895.4/3678	903.0/3678
SH Finishing Outlet	1000.3/3500	1000.3/3500	1000.3/3500
RH Desuperheater Inlet	545.9/596	545.9/596	545.9/596
RH Spraywater	398.3/1200	398.3/1200	397.8/1200
RH Desuperheater Outlet	538.2/596	544.3/596	538.0/596
RH Cross-Over	775.6/581	780.0/581	744.2/581
RH Finishing Outlet	990.0/566	990.9/566	989.6/566
<u>Pulverizer Performance</u>			
Coal Flow, LB/H	521,921	493,542	477,232
Air Flow, LB/H	869,644	857,082	862,569
Fineness, % -200 mesh	79.3	82.8	77.8
Grinding Capacity	91.6	88.1	89.6
Pulverizer Outlet Temperature, °F	152.6	152.6	152.6
Grinding Power, KW	1784	1732	1784

Table 4.5 (Continued) Northeastern Unit 4 Comparison of 90% WY/10% OK and 70% WY/30% OK Blends to Calibrated 100% WY Results

<u>Furnace Performance</u>	<u>100% WY Calibrated Results</u>	<u>90%WY/10%OK Projected Performance</u>	<u>70%WY/30%OK Projected Performance</u>
Net Heat Input, MBtu/H	4620.0	4579.0	4639.0
Heat Release Rate, MBtu/H FT ²	1.89	1.87	1.89
Furnace Outlet Temperature, °F	2548	2523	2577
Convection Pass Inlet Temperature, °F	2095	2081	2108
Economizer Outlet Temperature, °F	731	728	728
<u>Air Heater Performance</u>			
Ambient Air Temperature, °F	81.3	88.7	50.0
Air Inlet Temperature, °F	96.4	103.5	64.7
Primary Air Outlet Temperature, °F	745.0	748.0	749.0
Secondary Air Outlet Temperature, °F	713.9	718.0	718.0
Gas Inlet Temperature, °F	783.9	780.9	780.9
Gas Outlet Temperature, °F*	305.4	320.0	302.0
Air Side Efficiency, %	89.8	90.7	91.2
Gas Side Efficiency, %	69.6	68.0	66.9
* Gas temperature is not corrected for air in-leakage			

Table 4.6 Projected Efficiency Losses (Based on Reverse Calibration of 100% WY) for 90% WY/10% OK and 70% WY/30% OK Fuels

Heat Source Loss	Reverse Calibrated 100% WY	Forward Projected 90% WY/10% OK	Forward Projected 70% WY/30% OK
• Dry Gas	5.01	5.21	5.63
• Carbon	0.3	0.2	0.2
• Other*	8.26	8.01	8.01
• Total Losses	13.57	13.42	13.61
Boiler Efficiency	86.43	86.58	86.39
*Other losses: radiation, moisture (from coal, water in air and hydrogen), combustion and unaccounted for.			

Pulverizer power consumption was reduced by 2.9% with the 90% WY/10% OK fuel at a plant load of 469 MW (gross). This was primarily due to the reduced moisture and higher calorific content of the 90% WY/10% OK fuel, which reduced the fuel tonnage throughput (493,542 lb/hr for the 90% WY/10% OK fuel versus 521,921 lb/hr for the 100% WY fuel at MCR).

Pulverizer power consumption remained unchanged for the 70% WY/30% OK fuel at a plant load of 469 MW (gross). The reduced moisture and higher calorific content of the 70% WY/30% OK fuel would normally indicate a reduction in pulverizer energy requirements; however, these effects were offset by the lower grindability index, indicative of increased difficulty in pulverization. Thus, while the mill throughput was reduced (477,232 lb/hr for the 70% WY/30% OK fuel versus 521,921 lb/hr for the 100% WY fuel), the energy required to grind each fuel was the same due to the decrease in the grindability of the 70% WY/30% OK fuel.

The Northeastern Unit 4 boiler should be capable of its typical cycling operation with normal excess air levels when firing the 90% WY/10% OK fuel. The main limiting factor in maintaining MCR is the wall blower effectiveness and coverage. The critical furnace temperature as defined by field correlations with FPTF data is 3075 °F. The maximum furnace temperature as determined in the furnace modeling procedure is 2833 °F. Therefore a 242 °F differential exists between the operating maximum furnace temperature and the critical temperature. Provided that wall blower maintenance is consistent, the critical furnace temperature would not be exceeded.

The average thermal conductance (as determined from FPTF data) for the 90% WY/10% OK fuel was 42.0 Btu/hr-ft² °F. If the wall blower frequency is increased and wall cleaning made more effective, the reheater performance could become marginal. As wall blower effectiveness increases, lower furnace cleanliness increases, resulting in higher thermal conductances and greater heat absorption through the waterwall. This will lower gas temperatures and reduce energy available for absorption in the reheat sections, which already require very little spray (0.14% of main reheat flow).

The Northeastern Unit 4 unit should similarly be capable of its typical cycling operation with the 70% WY/30% OK fuel. As with the 90% WY/10% OK fuel, the main limiting factor in maintaining MCR with the 70% WY/30% OK fuel is the wall blower effectiveness and coverage. The critical furnace temperature as defined by field correlations with FPTF data is 2925 °F. The maximum furnace temperature as determined in the furnace model is 2892 °F, using an FPTF-derived thermal conductance of 40 Btu-in/hr-ft²-°F. Thus, only a 32 °F buffer exists between the predicted operating maximum furnace temperature and the critical temperature. Careful, continuous removal of waterwall deposits will be required to keep the lower furnace below its slagging-limited temperature of 2925 °F. By keeping the wall deposits to a reduced level, the waterwall heat absorption can be maintained and the temperature profile will facilitate typical MCR operation.

4.6.3 Evaluation of Full-Scale and Pilot-Scale Data for the Blended Fuels

In assessing the impact of firing the 100% WY and blended fuels, the boiler island performance is projected from data provided by bench-scale and pilot-scale testing. For this particular series of tests both the 90% WY/10% OK and 70% WY/30% OK fuels were field tested on Northeastern Unit 4. The usefulness and validity of employing bench- and pilot-scale data can be evaluated relative to actual blended fuel performance. The results of each evaluation can then be used to extend the existing data base for predicting fuel slagging and fouling performance.

Results for the 90% WY/10% OK blend are presented in Table 4.7. The first column lists the actual field test data; the second lists the "calibrated" test data (see Section 4.5.1 for procedure); the last lists the performance projections based on the 100% WY calibration. The calibrated field test data and the performance projection values are quite close.

The results presented in Table 4.8 were expected, based on the similarity in operating conditions between the two sets of tests. Test data in the FPTF were obtained under controlled conditions using a standardized set of test procedures. Therefore, the

Table 4.7 Northeastern Unit 4 90% WY/10% OK Boiler Performance Results

<u>General Data</u>	<u>Field Test Data</u>	<u>Adjusted Field Test Data</u>	<u>Performance Projection</u>
Date	9/8/90	10/91	9/91
Gross Generator Output, MW	465	465	469
Excess Air (@ FOP), %	26.8	28.6	28.6
Excess Air (@ ECON OUT), %	30.4	28.6	28.6
Burner Tilt, Degrees	-11	-11	-10
Elevations in Service	4	4	4
Boiler Efficiency, %	86.3	86.27	86.58
<u>Steam and Water Flows, 10³ LB/H</u>			
Feedwater	3043.2	3043.2	3057.8
Superheat Spray	61.3	86.2	93.5
Main Steam	-	3129.4	3153.3
Turbine Seal & Misc. Leakage	-	98.4	98.4
HTR #7 Extraction	273.9	273.9	277.2
Reheat Spray	5.7	5.6	3.9
Reheat Steam	2768.9	2762.6	2796.3
<u>Boiler Fluid Temp/Press. °F/PSIG</u>			
Feedwater	477.8/--	477.8/4000	478.5/4000
Economizer Outlet	665.9/--	665.9/3985	674.6/3983
Panel Inlet	788.9/3847	788.6/3847	786.3/3851
SH Desuperheater Inlet	826.1/--	826.1/3787	820.6/3787
SH Spraywater	477.8/--	477.8/4000	478.5/4000
SH Desuperheat Outlet	809.2/--	809.2/3754	803.9/3754
SH Platen Outlet	903.2/--	903.2/3678	895.4/3678
SH Finishing Outlet	1000.3/3500	1000.3/3500	1000.3/3500
RH Desuperheater Inlet	544.6/--	544.6/590	545.9/596
RH Spraywater	397.8/1200	397.8/1200	398.3/1200
RH Desuperheat Outlet	542.2/590	542.2/590	544.3/596
RH Cross-Over	762.0/--	762.0/575	780.0/581
RH Finishing Outlet	977.9/560	977.9/560	990.9/566

Table 4.7(Cont.) Northeastern Unit 4 90% WY/10% OK Boiler Performance Results

	<u>Field Test Data</u>	<u>Adjusted Field Test Data</u>	<u>Performance Projection</u>
<u>Pulverizer</u>			
Coal Flow, LB/H	509,080	490,014	493,542
Air Flow, LB/H	-	873,781	857,082
Fineness,% -200 mesh	82.8	82.8	82.8
Grinding Capacity, %	-	92.7	88.1
Pulverizer Outlet Temperature, ° F	154.2	154.2	152.6
Grinding Power, KW	-	1804	1732
<u>Furnace Performance</u>			
Net Heat Input, MBtu/H	-	4546.0	4579.0
Heat Release Rate, MBtu/H FT ²	-	1.86	1.87
Furnace Outlet Temperature, °F	2446	2500	2523
Convection Pass Inlet Temperature, °F	-	2044	2081
Economizer Outlet , °F	742	742	728
<u>Air Heater Performance</u>			
Ambient Air Temperature, °F	88.7	88.7	88.7
Air Inlet Temperature, °F	99.7	99.7	103.5
Primary Air Outlet Temperature, °F	-	-	748.0
Secondary Air Outlet Temperature, °F	712.0	712.0	718.0
Gas Inlet Temperature, °F	778.0	778.0	780.9
Gas Outlet Temperature, °F	303.0	303.0	320.0
Air Side Efficiency,%	90.3	90.3	90.7
Gas Side Efficiency,%	70.0	70.0	68.0

Table 4.8 Data Summary for the 90% WY/10% OK Fuel

<u>Boiler Operating Parameter</u>	<u>Adjusted Field Data</u>	<u>Performance Projection</u>	<u>Percent Difference</u>
Boiler Efficiency, %	86.27	86.58	+0.36
SH Outlet Temp, °F	1000.3	1000.3	0.00
RH Outlet Temp, °F	977.9	990.9	+1.33
Furnace Outlet Temp, °F	2500	2523	+0.92
Economizer Outlet Temp, °F	742	728	-1.89

differences observed between the 100% WY and blended fuel performance are based exclusively on the fuels. For example, the 100% WY thermal conductance ($K/\Delta x$) back-calculated from the field testing fell within the range of values obtained during corresponding pilot-scale testing, as shown in Figure 4.12. Therefore, the slagging effects in the lower furnace could be accurately modeled using the 100% WY calibrated model in conjunction with the pilot-scale data for the 90% WY/10% OK blend.

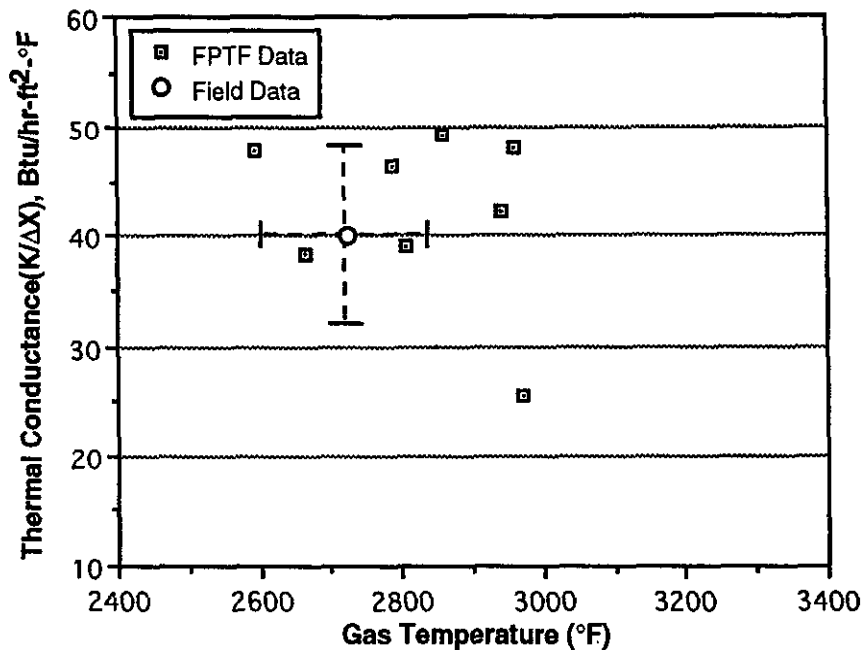


Figure 4.12 Thermal Conductance vs. Gas Temperature for the 90% WY/10% OK Fuel

The differences which exist in Table 4.8 are most likely due to the effects of mass flow differences (gas and steam side) and surface effectiveness factors (SEF's). Surface effectiveness factors increased by an average of 2.12% across superheat sections and 0.91% across reheat sections for the 90% WY/10% OK fuel. This increase in surface area available for heat transfer is supported by the lower superheater deposit buildup rates for the 90% WY/10% OK fuel determined during pilot-scale testing.

Results for the 70% WY/30% OK field test data calibration are presented in Table 4.9. The performance prediction results summarized in Table 4.10 are also close to the calibrated field test data.

Table 4.9 Northeastern Unit 4 70% WY/30% OK Fuel Performance Results

General Data	Field Test Data	Field Test Data	Calibrated Performance Projection
Date	12/5/91	10/91	9/91
Gross Generator Output, MW	468.1	468.1	469.0
Excess Air (@ FOP), %	20.3	27.0	27.0
Excess Air (@ ECON OUT), %	33.7	27.0	27.0
Burner Tilt, Degrees	-9	-9	-10
Elevations in Service	4	4	4
Boiler Efficiency, %	86.3	86.04	86.39
Steam and Water Flows, 10³ LB/H			
Feedwater	3031.5	3031.5	3057.8
Superheat Spray	60.6	104.7	93.5
Main Steam	--	3136.2	3151.3
Turbine Seal & Misc. Leakage	--	98.4	98.4
HTR #7 Extraction	275.4	275.4	277.2
Reheat Spray	7.9	7.6	19.2
Reheat Steam	--	2770.0	2794.9
Boiler Fluid Temp/Press, °F/PSIG			
Feedwater	478.2/-	478.2/4000	478.5/4000
Economizer Outlet	665.1/-	665.1/3983	674.5/3983
Panel Inlet	791.1/-	791.1/3847	786.4/3851
SH Desuperheater Inlet	827.1/-	827.1/3787	823.0/3787
SH Spraywater	478.1/-	478.2/4000	478.5/4000
SH Desuperheater Outlet	807.8/-	807.8/3754	806.0/3754
SH Platen Outlet	902.6/-	902.6/3678	903.0/3678
SH Finishing Outlet	1004.5/3500	1004.5/3500	1000.3/3500
RH Desuperheater Inlet	546.9/-	546.9/590	545.9/596
RH Spraywater	397.8/1200	397.8/1200	397.8/1200
RH Desuperheater Outlet	543.6/590	543.6/590	538.0/596
RH Cross-Over	772.1/-	772.1/575	744.2/581
RH Finishing Outlet	986.4/560	986.4/560	989.6/566
Pulverizer Performance			
Coal Flow, LB/H	464,525	475,241	477,232
Air Flow, LB/H	--	834,190	862,569
Fineness, % - 200 mesh	77.8	77.8	77.8
Grinding Capacity	--	81.7	89.6
Pulverizer Outlet Temperature	153.8	153.8	152.6
Grinding Power, KW	--	1636	1784
Furnace Performance			
Net Heat Input, MBtu/H	--	4529.0	4639.0
Heat Release Rate, MBtu/H ft ²	--	1.85	1.89
Furnace Outlet Temperature, °F	2464	2489	2577
Convection Pass Inlet Temperature, °F	--	2037	2108
Economizer Outlet Temperature, °F	716	716	728
Air Heater Performance			
Ambient Air Temperature, °F	52	52	52
Air Inlet Temperature, °F	63	63	63
Primary Air Outlet Temperature, °F	--	--	749.0
Secondary Air Outlet Temperature, °F	--	--	718.0
Gas Inlet Temperature, °F	--	--	780.9
Gas Outlet Temperature, °F	286.5	286.5	302.0
Air Side Efficiency, %	--	--	91.2
Gas Side Efficiency, %	--	--	66.9

Table 4.10 Data Summary for the 70% WY/30% OK Fuel

<u>Boiler Operating Parameter</u>	<u>Adjusted Field Data</u>	<u>Performance Projection</u>	<u>Percent Difference</u>
Boiler Efficiency, %	86.04	86.39	+0.41
SH Outlet Temp, °F	1004.5	1000.3	-0.42
RH Outlet Temp, °F	986.4	989.6	+0.32
Furnace Outlet Temp, °F	2489	2577	+3.54
Economizer Outlet Temp, °F	716	728	+1.68

data were obtained three months after the testing of the 100% WY and 90% WY/10% OK fuels and after numerous repairs had been made to the wall and soot blower systems. Although a similar soot blowing sequence was used for all testing, there were many more wall and soot blowers in service for the 70% WY/30% OK blend tests. Thus, furnace cleanliness was not constant for all tests. Changes in the furnace cleanliness directly impacted the lower furnace absorptions, and were reflected in changes in furnace outlet temperatures and steam temperatures. Thus, the back-calculated thermal conductance ($K/\Delta x$) values and surface effectiveness factors (SEF's) were higher than expected from pilot-scale testing.

The pilot-scale testing for the 70% WY/30% OK blend was conducted under the same standardized set of test procedures used for the 100% WY and 90% WY/10% OK fuels. Results from the pilot-scale testing indicate that the average $K/\Delta x$ for the lower furnace should have been approximately 36 Btu/hr-ft²°F if the level of furnace cleanliness had been consistent with the other fuels field tested. Back-calculated $K/\Delta x$ values from field data give the thermal conductance a value of 57 Btu/hr-ft²°F, as shown in Figure 4.13. Similarly, the back-calculated SEF's for the 70% WY/30% OK fuel were significantly higher than those for the 100% WY fuel, by an average of 7.75% for the superheat sections and 6.22% for the reheat sections. These differences are consistent with results from pilot-scale testing, which indicate lower superheater deposit buildup rates for the 70% WY/30% OK fuel.

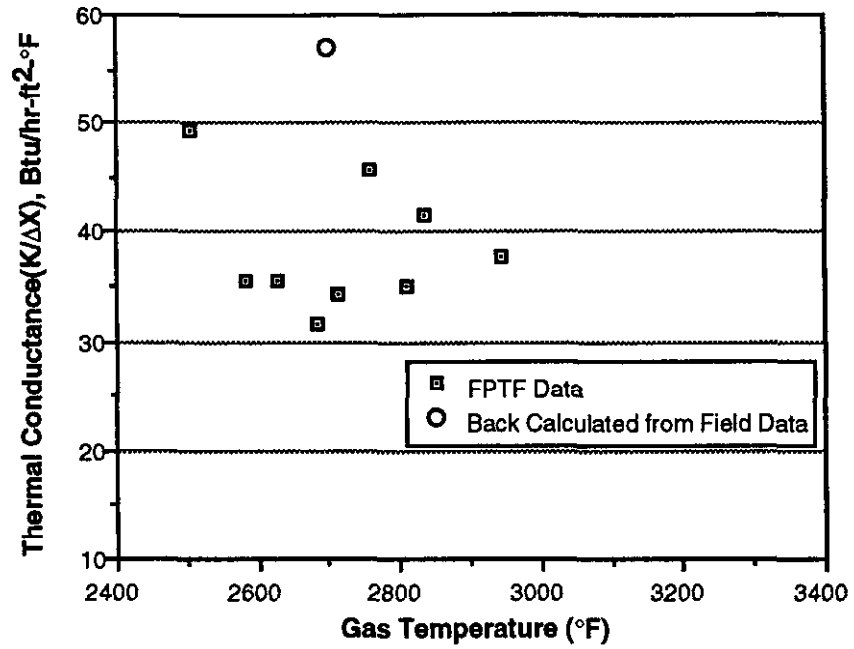


Figure 4.13 Thermal Conductance vs. Gas Temperature for 70% WY/30% OK Fuel in FPTF and Field Tests

Section 5

CONCLUSIONS

The effect of coal quality on boiler performance is ultimately determined by a combination of the specific coal properties and the conditions or operating parameters under which the coal is utilized. Information reported in this document can be broken into three broad categories: (1) bench-scale analyses wherein the objective has been to measure any and all properties of coal which can help to elucidate how a particular coal will affect performance within the combustor/boiler and associated handling equipment (e.g. pulverizers), (2) pilot-scale and drop tube furnace analyses wherein the objective has been to measure end-result effects which are not currently possible to predict reliably from the more basic bench-scale results. The manifestations of coal properties on coal reactivity and fireside performance (i.e. slagging, fouling and erosion) are examples of end-result effects which will ultimately be determined with the Coal Quality Expert (CQE). Input to the CQE will be (ideally) primarily derived through bench-scale analyses, scanning electron microscopy (SEM) being a good example of a more sophisticated bench-scale derived input. Pilot-scale testing is the only source of "end-result" information such as ash deposit thermal properties and bonding strengths which are needed for development of the Coal Quality Expert. Such information is required to develop algorithms which will translate bench-scale measurements into the required CQE inputs relative to fuel reactivity and fireside performance, and (3) boiler performance modeling wherein the objective has been to provide a means of validating the pilot- and bench-scale results by determining whether a prediction of commercial boiler performance through use of bench- and pilot-scale information is, indeed, corroborated by actual commercial boiler performance.

Bench-scale results clearly indicate the impact of coal properties on its combustion and fireside performance in a pulverized coal-fired application. As such, coal quality dictates the behavior of a given coal or coal blend if suspension-fired in a boiler operating under specific conditions. Specific conclusions follow:

- Wyoming subbituminous and Oklahoma bituminous coals differ significantly in chemical characteristics (volatility contents, calorific values, ash loadings, etc.). They are, however, similar in ash chemistry (compositions, fusibility temperatures, etc.). The impact of coal quality is evident when comparing the Oklahoma coal with its CQ, Inc. cleaned counterpart. The calorific value of the cleaned product is 10% higher than that of its run-of-mine parent coal, and its ash loading is reduced by a factor of three. The chemical analyses and ash characteristics of the WY/OK and WY/OK CLN blends are commensurate with the various mixture ratios of the individual constituents.
- Analysis of the coal minerals using CCSEM revealed major differences between the Wyoming and Oklahoma coals, their ash chemistry similarity notwithstanding. The major minerals in the Wyoming coal were kaolinite, quartz, montmorillonite, and Ca-Al-phosphate mineral, while the major minerals in the Oklahoma coal were quartz, calcite, and illite (K Al-silicate). The 90% WY/10% OK and 70% WY/30% OK blends show intermediate mineral quantities between the mineral contents of the parent coals. The 70% WY/30% OK CLN blend was similar to the uncleaned 70% WY/30% OK blend, with the exception of a lower level of illite in the cleaned blend.
- The TGA burn-off curves of the 200x400-mesh char test results indicate that: (1) The Wyoming coal char is much more reactive than the Oklahoma coal char; (2) the reactivities of the coal blend chars fall in a narrow band, and in between those of the Wyoming and Oklahoma coal chars; (3) the reactivities of the run-of-mine and CQ Inc.-cleaned Oklahoma coal chars are close to one another; (4) The reactivity of both Oklahoma coal chars are slightly lower than that of the West Virginia high volatile A bituminous coal char (from Pittsburgh #8 Coal Seam); and (5) most importantly, all PSO chars prepared from the parent coals and coal blends are much higher in reactivity than a char prepared from a West Virginia medium volatile bituminous coal, which is used as a marginal coal reactivity bench-mark at ABB CE, and is successfully burned in pulverized form in a tangentially-fired utility boiler.

- The apparent activation energies are 19.2, 22.9 and 24.3 kcal/mole for the 100% WY, 70% WY/30% OK CLN and Oklahoma coal chars, respectively. The corresponding frequency factors are 17.7, 55.6 and 70.1 g/cm² sec. (O₂ atm.). These results indicate a significant variability in temperature sensitivity between the three coal chars. These reaction kinetic parameters imply the Wyoming coal char is much less sensitive to temperature than the Oklahoma coal char; i.e., at relatively lower temperatures, it would react more rapidly and completely than the Oklahoma coal char.
- A solid fuels combustion kinetic database (i.e., apparent activation energies, frequency factors, mercury densities and BET surface areas of fuel chars, and swelling factors of parent fuels), encompassing virtually all the fuels evaluated to date by ABB CE under the DOE/PETC and EPRI auspices, has been established. This constitutes a first step towards the development of an algorithm which will enable the CQE to use, in some cases, this type of information on a surrogate basis.

Pilot-scale results serve two purposes: (1) quantitative ranking of the fireside performance of the specific coal/coal blends tested and (2) the determination of specific physical and thermal properties of coal ash deposits as a function of furnace operating parameters for slagging and fouling algorithm development as part of the Coal Quality Expert. Importantly, pilot-scale testing has been carried out in concert with field testing conducted at Public Service of Oklahoma's Northeastern Station. The correspondence of data from pilot-scale and field testing is very good. Specific conclusions from the pilot-scale testing are as follows:

- The blend of 70% WY/30% OK CLN coal resulted in lower furnace deposits which remained cleanable at temperatures up to 2975 to 3000 °F. Deposits in the lower furnace from the 90% WY/10% OK blend were cleanable up to temperatures only slightly below the 70% WY/30% OK CLN blend. The 100% WY and 70% WY/30% OK fuels, by contrast, produced lower furnace deposits which were cleanable only up to 2800 to 2850°F. Interestingly, of the three coals which were field tested, the

90% WY/10% OK coal blend resulted in the lowest furnace outlet temperature, implying that resistance to heat transfer (due to deposits) was less in this case. Thermal conductance ($k/\Delta x$), as measured in the FPTF, was indeed significantly higher for the 90% WY/10% OK case as compared to the 100% WY and 70% WY/30% OK cases.

- Low excess air was shown to have a more significant effect on the nature of lower furnace deposits in the 100% WY case; this was corroborated by field data. Specifically, low excess air reduced the critical temperature for adequate deposit cleanability to a greater extent in the 100% WY case than for the other fuel blends tested.
- It should be noted that Northeastern Unit 4 operates at MCR (maximum continuous rating) during the day, when load demand is high, and typically drops load by 40 percent or more as load demand decreases. This type of operation is conducive to "slag shedding," an incompletely-understood process involving thermal forces attributed to differential thermal contraction between deposit and tube and which ultimately weaken the deposit bond. Load-cycling operation would generally permit the unit to operate for finite periods of time at conditions that could be considered to be above the critical conditions for either the lower furnace or convective pass regions.
- Bonding strength of deposits in the convective pass generally increased with increasing concentrations of the OK coal. However, only with the 70% WY/30% OK and the 70% WY/30% OK cleaned coal blends did the deposit bonding strength clearly begin to exceed the ability of conventional soot blowers to remove deposits; such conditions generally occurred at gas temperatures of 2250°F or higher.
- Though erosion rates of fly ashes from the 90% WY/10% OK fuel were three times that of the 70% WY/30% OK CLN fuel, both blends showed very low erosion relative to most other U.S. coals.

- Pilot-scale testing affords an opportunity to obtain bonding strength and thermal properties of ash deposits over a wide range of thermal conditions. Furnace heat inputs can be increased until limiting conditions, termed critical conditions, are achieved at which deposits can no longer be removed with conventional soot blowers; this type of determination is usually not possible to obtain during field testing. In the pilot-scale facility, the coal or coal blend is tested without the concerns of uncontrollable operational problems associated with full-scale plant operation, allowing the fireside characteristics to be assessed as a function of known, consistent operating conditions.
- Superheater deposit inner layer composition (measured by CCSEM) was shown to be very similar to the composition of the 0 - 2 μm (actual size, not aerodynamic diameter) fraction of the in-flame solid samples, indicating that small particle/vapor phase diffusion and thermophoresis dominate the inner layer formation and growth. ASTM coal ash composition did not match the superheater inner layer composition.
- Superheater deposit outer layer composition (measured with XRD) is very similar to the composition of the 15 - 25 μm (actual size) size fraction of the L-5 in-flame solids sample (taken just prior to the superheater duct). From these analyses, it is concluded that the inertial impaction of large particles dominates deposit growth after the initial layer has been formed. Once again, it is also noted that the outer layer composition does not match the ASTM coal ash composition.
- A sound set of cause and effect relationships, both fundamentally and empirically based, which requires the intelligent integration/use of data from bench, pilot, and field testing, will provide the foundation for slagging and fouling algorithm formulation for the CQE.

Results from the Boiler Performance Modeling are as follows:

- Northeastern Unit 4 should be capable of typical cycling operation while firing the 90% WY/10% OK fuel. The main controlling factor in maintaining MCR is the wall blower effectiveness and coverage. The maximum peak flame temperature as defined by field correlations with FPTF data is 3075 °F. The peak flame temperature as determined in the furnace modeling procedure is 2833 °F. Therefore a 242 °F differential exists between the operating peak flame temperature and the critical temperature. Provided that wall blower maintenance is consistent, the critical peak flame temperature would not be exceeded.
- The average thermal conductance (as determined from FPTF data) for the 90% WY/10% OK blend was 42.0 Btu/hr-ft²-°F. If the wall blower frequency is increased and wall blowing made more effective, the reheater performance could be marginal. As wall blower effectiveness increases, lower furnace cleanliness increases, resulting in higher thermal conductances and greater heat absorption through the waterwall. This will lower gas temperature and decrease the energy available for absorption in the reheat sections, which already have very little spray (0.14%) in service.
- Northeastern Unit 4 should similarly be capable of typical cycling operation with the 70% WY/30% OK fuel. As with the 90% WY/10% OK fuel, the main controlling factor in maintaining MCR is the wall blower effectiveness and coverage. The maximum peak flame temperature as defined by field correlations with FPTF data is 2925 °F. The peak flame temperature as determined in the furnace model is 2892 °F. The FPTF-derived thermal conductance was 40 Btu/hr-ft²-°F. Thus, only a 32 °F buffer exists between the operating peak flame temperature and the critical temperature. Careful, continuous removal of waterwall deposits will be required to keep the lower furnace below its slagging-limited temperature of 2925 °F. By keeping the wall deposits to a reduced level, the waterwall heat absorption can be maintained and the temperature profile will facilitate typical MCR operation.

- The boiler island performance is projected from data provided by bench-scale and pilot-scale testing. Both of the blended fuels in this evaluation were field tested in Northeastern Unit 4. The results from the "calibrated" field test data and the "performance projection" values indicate that the overall performance for the 90% WY/10% OK fuel is fairly close. The close results were expected based on the similarity in operating conditions between the baseline 100% WY tests (used for calibration) and the 90% WY/10% OK tests. Results for the 70% WY/30% OK are not quite as close as the 90% WY/10% OK. This is attributed to a higher level of cleanliness during the 70% WY/30% OK field testing, which was caused by a greater number of wall and soot blowers in service.

BIBLIOGRAPHY

- Badzioch, S. and Hawksley, P.G.W., "Kinetics of Thermal Decomposition of Pulverized Coal Particles," *Ind. Eng. Chem. Process Des. Develop.*, **9**, 521, 1970.
- Beer, J.M., *Proc. Anthracite Conference, Bull. 75, Mineral Industries Experiment Station, The Pennsylvania State University, September 1961.*
- Borio, R.W. and Levasseur, A.A., "Overview of Coal Ash Deposition to Boilers," *American Chemical Society Annual Meeting, August 1984.*
- Brunauer, S., Emmett, P.H. and Teller, E., "Adsorption of Gases in Multi-layers,:" *J. Am. Chem. Soc.*, **60**, 309, 1938.
- Bueters, K.A. and Habelt, W.W., "Performance Prediction of Tangentially Fired Utility Furnaces by Computer Model," *Fifteenth International Symposium on Combustion, Tokyo, Japan, August 25-31, 1974.*
- EER, EPT, FERCo team, from a preliminary internal report, 1991.
- Field, M.A., Gill, D.W., Morgan, B.B., and Hawksley, P.G.W., "The Surface Reaction Rate of Carbon with Oxygen," *Combustion of Pulverised Coal*, p. 329, BCURA, Leatherhead, England, 1967.
- Field, M.A., Gill, D.W., Morgan, B.B., and Hawksley, P.G.W., "The Fineness of Pulverised Fuel," *Combustion of Pulverised Coal*, p. 245, BCURA, Leatherhead, England, 1967.
- Field, M.A., Gill, D.W., Morgan, B.B., and Hawksley, P.G.W., "Reaction Rate of Carbon Particles," *Combustion of Pulverised Coal*, p. 186, BCURA, Leatherhead, England, 1967.
- Godridge, A.M. and Morgan, E.S., "Emissivities of Materials from Coal and Oil Fired Water Boilers," *Journal of the Institute of Fuel*, **44**, 207., 1971.
- Goetz, G.J., Nsakala, N., and Patel, R.L., "Combustion and Gasification Kinetics of Chars from Four Commercially Significant Coals of Varying Rank," *Proc. International Conf. on Coal Science*, p. 571, 1983.
- Gregg, S.J. and Sing, K.S.W., *Adsorption. Surface Area and Porosity*, Academic Press, London and New York, p. 123, 1969.
- Levasseur, A.A., et al., "Combustion Characterization of EPRI Cleaned Coals," Co-author, *Engineering Foundation Conference on "Fine Coal Cleaning," Santa Barbara, CA, February 1987.*

- Levasseur, A.A., et al., "Combustion Characterization of the Kentucky No. 9 Cleaned Coals," EPRI CS-4994, February 1987.
- Mitchell, R.E., "Experimentally Determined Overall Burning Rates of Coal Chars," *Combustion Science and Technology*, **53**, 165, 1987.
- Mulcahy, M.F., Boow, J. and Goard, P.R., "Fireside Deposits and Their Effect on Heat Transfer in a Pulverized-Fuel-Fired Boiler. Part 1: The Radiant Emittance and Effective Thermal Conductance of the Deposits. Part 2: The Effect of the Deposit on Heat Transfer from the Combustion Chamber Considered as a Continuous Well-Stirred Reactor," *J. Institute of Fuel*, **39** (308), 385-398, 1966.
- Nsakala, N., Goetz, G.J., Patel, R.L., Lao, T.C., Hickerson, J.D., and Ritz, H.J., "Pyrolysis and Combustion Characterization of Pulverized Coals for Industrial Applications," 189th ACS National Meeting, Miami, Florida, April 28-May 3, 1985. CE Pub. TIS-7877.
- Nsakala, N., Patel, R.L., and Borio, R.W., "An Advanced Methodology for Prediction of Carbon Loss in Commercial Pulverized Coal-Fired Boilers," 1986 JPGC, Portland, Oregon, October 19-23, 1986. CE Publication TIS-8211.
- Nsakala, N., Patel, R.L., Hargrove, M.J., Hurley, J. and Benson, S.A., "Effects of Coal Natures and Cleaning Processes on the Physicochemical and Reactivity Characteristics of Beneficiated Coal-Based Products," 16th International Conf. on Coal and Slurry Technologies, Clearwater, Florida, April 22-25, 1991.
- Raask, E., Erosion Wear in Coal Utilization, Hemisphere Publishing Corp., New York, 1988.

APPENDIX A
FACILITY DESCRIPTIONS

ABB CE BENCH-SCALE FACILITIES

Drop Tube Furnace System-1 (DTFS-1)

The Drop Tube Furnace System-1 (Figures A-1 and A-2) is comprised of a 1-inch inner-diameter horizontal-tube gas preheater and a 2-inch inner-diameter vertical-tube test furnace for providing controlled temperature conditions. Both tubes are electrically heated with silicon carbide elements (SiC) and are rated at 2800°F.

The principle of operation of the DTFS is as follows: Size-graded fuel is introduced with a small amount of carrier gas into the hot reaction zone of the test furnace through a water-cooled fuel injector. A pre-heated secondary gas stream is introduced around the primary stream. Injection of fuel particles into the hot gas stream results in a rapid heating of the particles to the prevailing gas temperature (at rates greater than 10^4 °C/sec.). Following the rapid heating period, pyrolysis, gasification and/or combustion of particles occur for a specific time. Then all reactions are rapidly quenched in a water-cooled sampling probe. Solid products are separated from the gaseous products in a small filter housing, and an aliquot of the effluent gas sample is sent to a pre-calibrated gas analysis system for on-line determination of NO_x, SO₂, O₂, CO₂, CO and THC (total hydrocarbons) concentrations using the principles given in Table A-1. A Data Acquisition System (DAS) records, on demand, all relevant test data for subsequent retrieval and processing.

The solid products collected at various locations along the axis of the DTFS-1 reaction zone can be analyzed to determine solid conversion efficiencies. An ash tracer method, which is based on the assumption that ash remains inert during combustion, is used to calculate the fuels' pyrolysis, gasification or combustion efficiencies.

Flammability Index Apparatus

The Flammability Index Apparatus (Figure A-3) is a device used to determine the ignition temperatures of pulverized solid fuels under specific conditions. About 0.2 g of sample sized to 200x0 mesh is placed in a sample holder. The furnace is preheated to a desired temperature, then a solenoid-operated valve is opened, allowing oxygen from a 2-liter storage reservoir to suspend and convey the sample through the

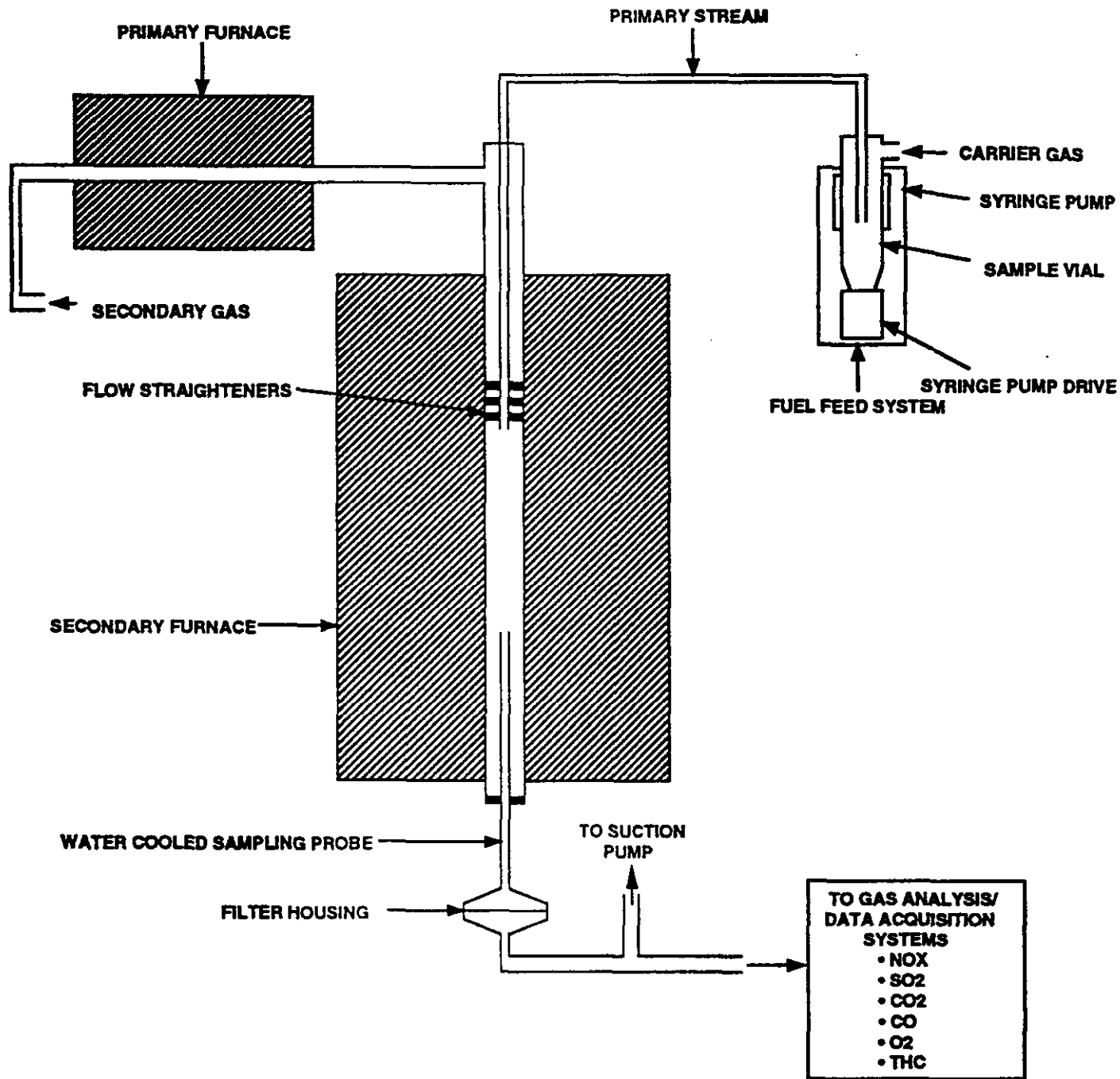


Figure A.1 Schematic of Drop Tube Furnace System (DTFS-1)

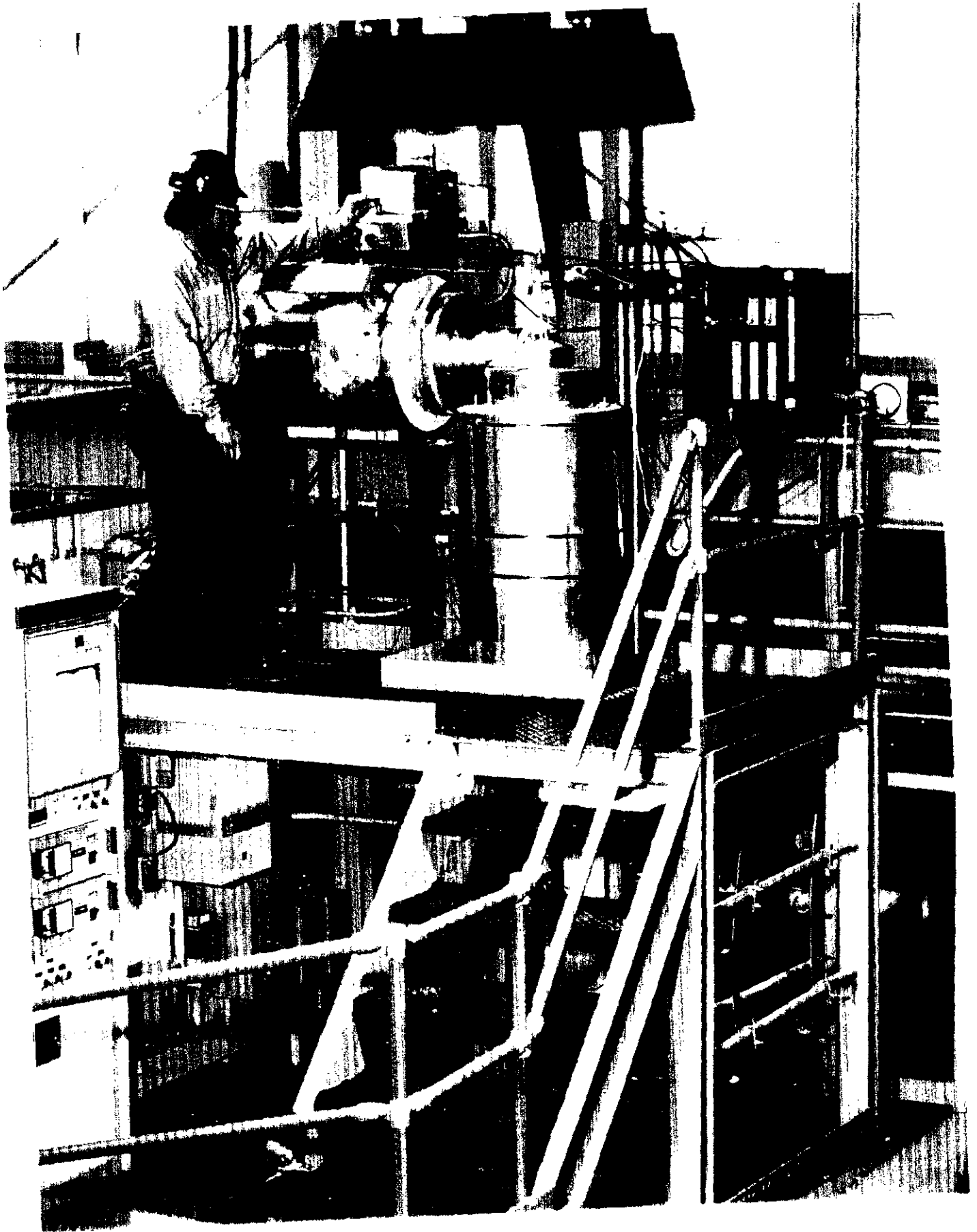


Figure A.2 Overview of Drop Tube Furnace System

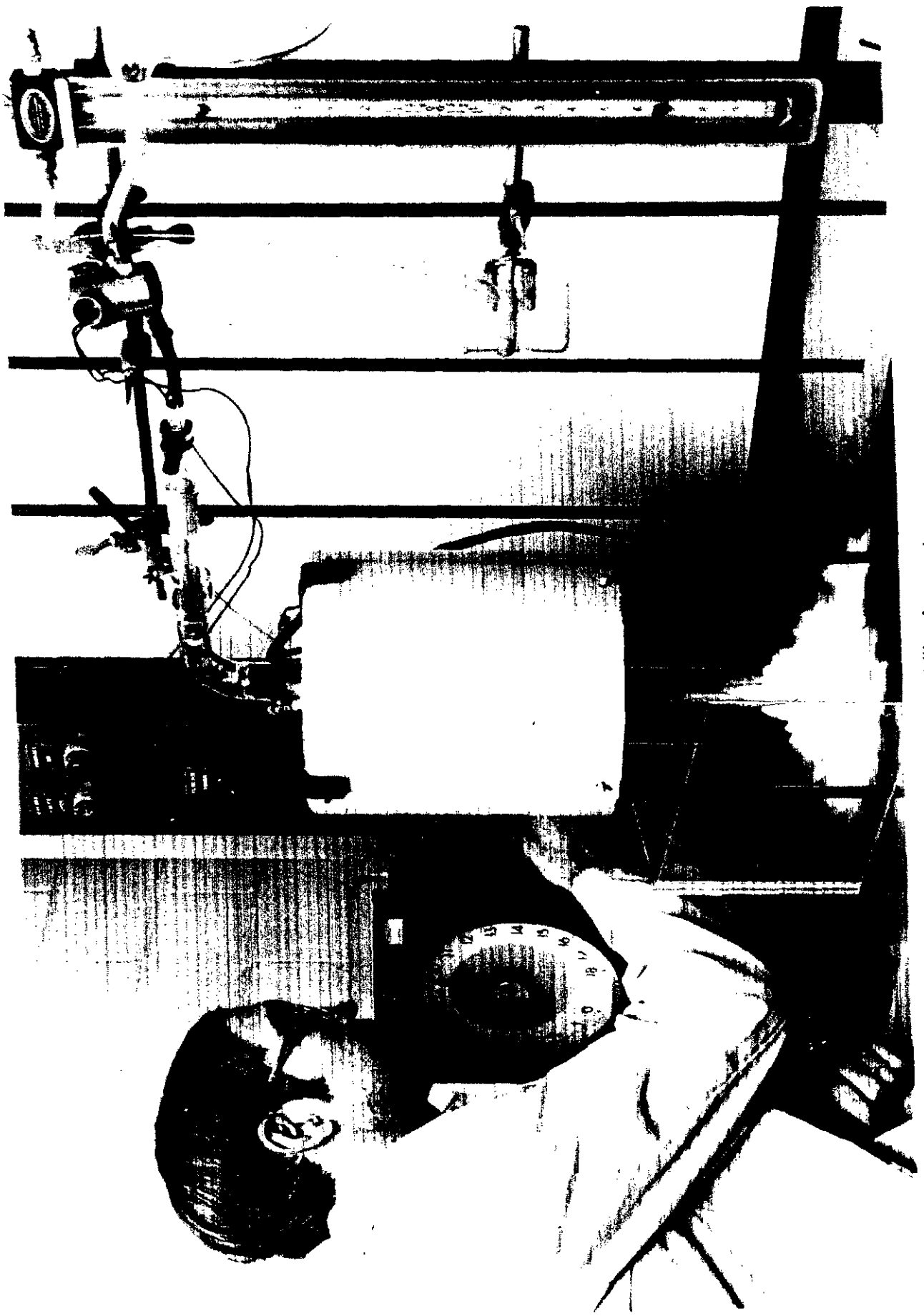


Figure A.3 Flammability Apparatus

furnace. If ignition does not occur, the procedure is repeated at higher temperatures, in 50 °F increments, until ignition occurs. If ignition does

Table A-1
**DIAGNOSTIC EQUIPMENT ASSOCIATED WITH
 THE DROP TUBE FURNACE SYSTEM**

COMPONENT	PRINCIPLE	ANALYZER
Nitrogen Oxides (NO _x)	Chemiluminescence	Thermo-Electron Model 10AR
Oxygen (O ₂)	Fuel Cell	Teledyne Model 326A
Sulfur Dioxide (SO ₂)	Photometric	DuPont Instruments Model 400 :
Carbon Monoxide (CO)	IR Spectroscopy	IR Industries Model 703-021
Carbon Dioxide (CO ₂)	IR Spectroscopy	IR Industries Model 702-074
Total Hydrocarbons (THC)	Flame Ionization	Beckman Model 400A

occur in the first trial, then the procedure is repeated to determine the temperature below which ignition does not occur. In either case, fine tuning is necessary to further narrow the error margin. This ignition temperature is called the Flammability Index. The value of the Flammability Index compared to other fuels indicates the ignition temperature/flame stability on a relative basis.

TGS-2 Thermo-Gravimetric Analysis System

The Perkin-Elmer Model TGS-2 (Figure A-4) is a complete, second-generation system for accurately recording the weight loss or weight gain or rate of weight change of a sample as it is subjected to a precisely controlled temperature environment. It is a completely modular system consisting of the following independently packaged units:

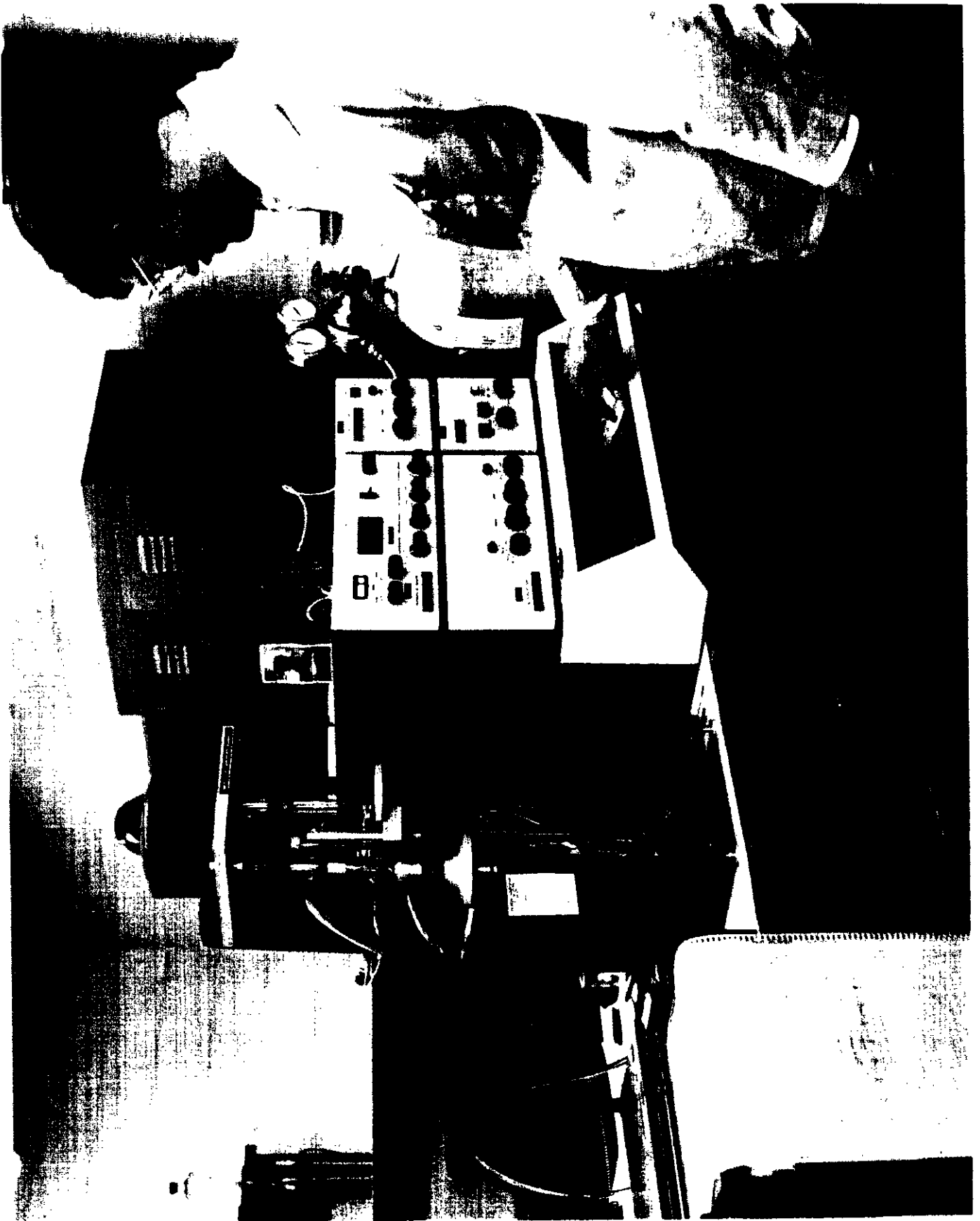


Figure A.4 Thermo-Gravimetric Analysis System

the Thermo-balance Analyzer, the Electronic Balance Control, the programmable Temperature Microprocessor Controller, the Heater Control Unit, the First Derivative Computer (FDC), and the Recorder.

This apparatus uses a small solid sample to determine either its micro-proximate analysis using the general procedure established by the American Society for Testing and Materials (ASTM) or its thermo-gravimetric reactivity under specific experimental conditions (heating rate, reaction medium, and reaction temperature).

The micro-proximate analysis is determined as follows: A 4-6 mg sample is purged with nitrogen to remove trace oxygen. The moisture loss is obtained by heating in nitrogen to 105°C and holding for three minutes. Subsequently, the sample is heated at 100°C/min to 950°C and held at this temperature for five minutes to determine volatile matter content. After this, the temperature is lowered to 750°C and a switching valve is used to introduce oxygen for the combustion of fixed carbon at this temperature. The residue represents the ash content.

The isothermal char reactivity test is determined as follows: A 4-6 mg sample of specific size grade is placed in the TGS-2 System and heated in the presence of nitrogen at 50°C/min to the reactivity temperature (700°C). After stabilization at this temperature, the reaction medium (air) is introduced. The percent weight of the unburned char and rate of weight loss are recorded on a strip chart as a function of time. These thermo-grams are subsequently used to determine the char combustion efficiency history and reactivity parameter (which indicates the maximum rate of weight loss per unit weight of the original sample in the TGS-2 System).

Quantasorb Surface Area Analyzer

The principle of operation of the Quantasorb Surface Area Analyzer (Figure A-5) involves passing a mixture of helium (used as a carrier) and adsorbate (N₂ or CO₂) through a small, U-shaped cell containing the dry sample (i.e., out-gassed a priori in the Quantasorb for one hour at 200 °C using nitrogen as the sweeping gas). The amount of adsorbate physically adsorbed at various partial pressures on the sample (adsorbent) surface can then be used to calculate the sample's surface area.

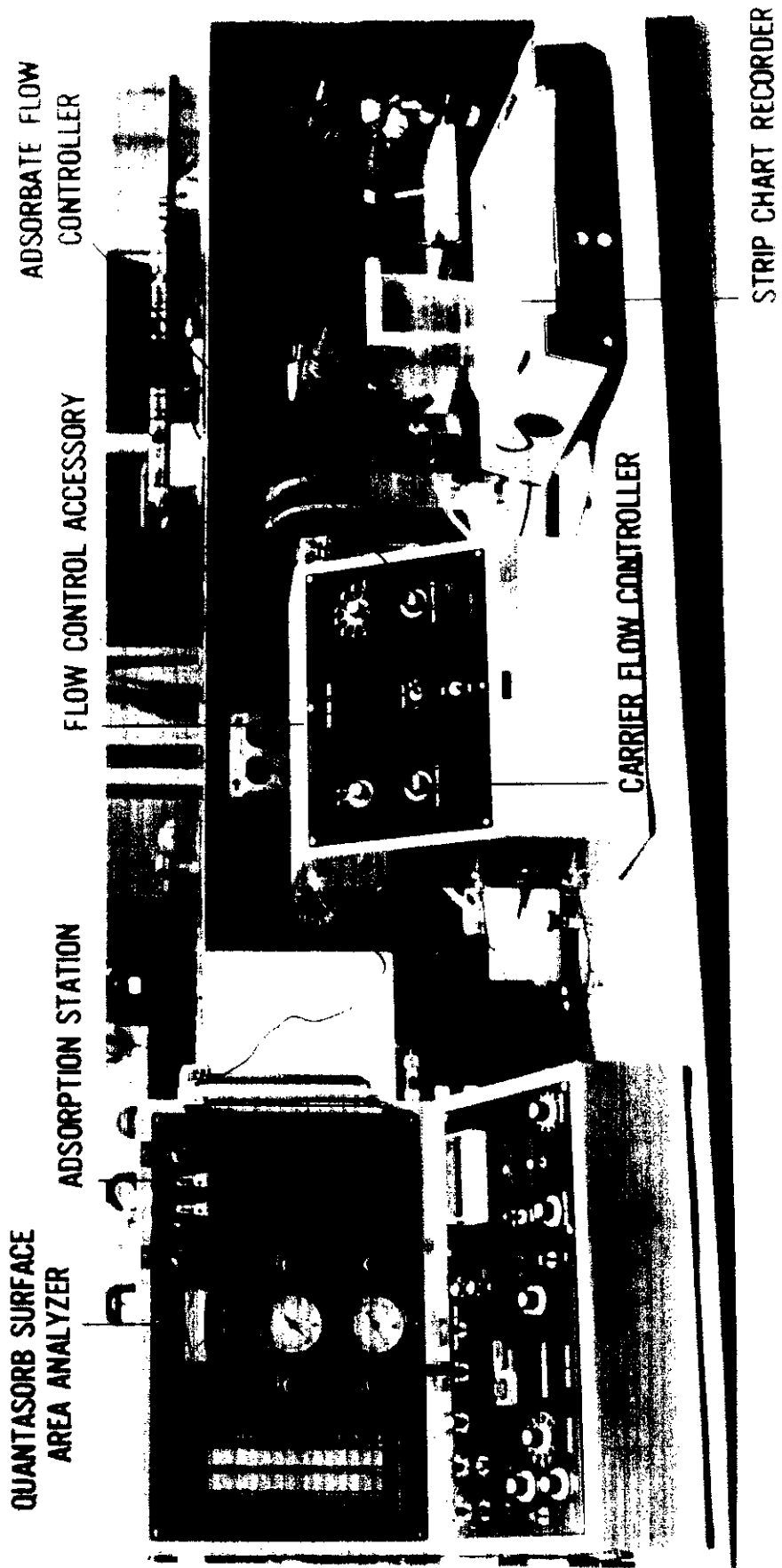


Figure A.5 Surface Area Analysis Equipment

Adsorption and desorption occur when the sample is immersed into and then withdrawn from the liquid controlling the adsorption temperature. Liquid nitrogen and room-temperature (25 °C) water are used for nitrogen adsorption and desorption, respectively.

Room temperature (25 °C) and hot (60 °C) water are used for carbon dioxide adsorption and desorption, respectively. Changes in the ratio of helium to adsorbate in the flowing stream, due to adsorption and desorption, are sensed by a specially designed thermal conductivity detector. The signals delivered by the detector are nearly Gaussian in shape. The instantaneous signal height is proportional to the rate of adsorption or desorption and the total integrated area under the curve is proportional to the quantity of gas adsorbed. As such, the function of the Quantasorb Surface Area Analyzer is to measure the quantity of gas adsorbed at a given temperature and partial pressure.

A BET (Brunauer, Emmett and Teller, 1938) single point method is used in conjunction with N₂ adsorption at -196 °C to determine the samples' BET specific surface areas. A Dubinin-Kaganer method (Gregg and Sing, 1969) is used in conjunction with CO₂ adsorption at 25 °C to determine the samples' CO₂ specific surface area.

UNDEERC BENCH-SCALE FACILITIES

Drop Tube Furnace (DTF)

UNDEERC's DTF is a laboratory-scale, entrained flow, vertical down-fired tube furnace with the ability to combust coal and produce ash under closely controlled conditions. Combustion parameters such as initial hot zone temperature, residence time, and gas cooling rates can be closely controlled and monitored.

The furnace system is housed in a laboratory that provides a clean environment for operation of the system. The furnaces are mounted on a common furnace bar and can be reconfigured to accommodate specific applications. The furnace system is designed for gas flow rates of 5 standard liters per minute. Oxygen and nitrogen mass flow controllers vary the oxygen concentration of the primary and secondary gas from 0-21%. Flowmeters split the gas mixture from the flow controllers between

primary and secondary air. Approximately one liter/minute of the gas mixture is used for primary air, and the remainder is introduced into the furnace as preheated secondary air. The unheated primary air (used as the sample carrier gas) entrains the coal from the sample feeder and carries it through the injector into the furnace. The secondary air is preheated before entering the furnace through the top of the reactor tube.

The furnace assembly consists of a 2-1/2" ID alumina reaction tube heated externally by a series of tube furnaces illustrated in Figure A-6. These furnaces possess a total of five independently controlled, electrically heated zones. This provides maximum flexibility and precise control over combustion conditions. An initial preheat furnace warms the gas that will be used as secondary air. A secondary preheat furnace further heats the secondary air before it enters the reaction tube. A split shell, two-zone furnace provides the heat for obtaining the desired reaction zone temperature. A bottom furnace is utilized to maintain the temperature of the collection zone located in the optical access section.

Coal and primary air are introduced into the furnace system by means of a traversing water-cooled injector (Figure A-7). This system injects ambient temperature primary air and coal into the furnace at the center of the tube. Secondary air is typically heated to 1000°C and introduced into the furnace through the top of the alumina tube and travels down through the tube around the injector. The traversing injection probe permits the residence time to be varied while allowing the ash deposition point to remain fixed. Thus the material to be combusted is introduced into the furnace with the primary air through the injector and combines with the preheated secondary air. The coal and gas travel down the furnace in a laminar flow regime and pass through an accelerator just above where the deposition probe is located. The ash not adhering to the probe is carried with the combustion gases into a water-cooled particulate collection probe.

The fly ash quenching probe shown in Figure A-8 is attached to the bottom of the drop-tube furnace to cool the fly ash before collection. This system is reliable and versatile. Ash collection devices can be added to the probe, such as a multicyclone

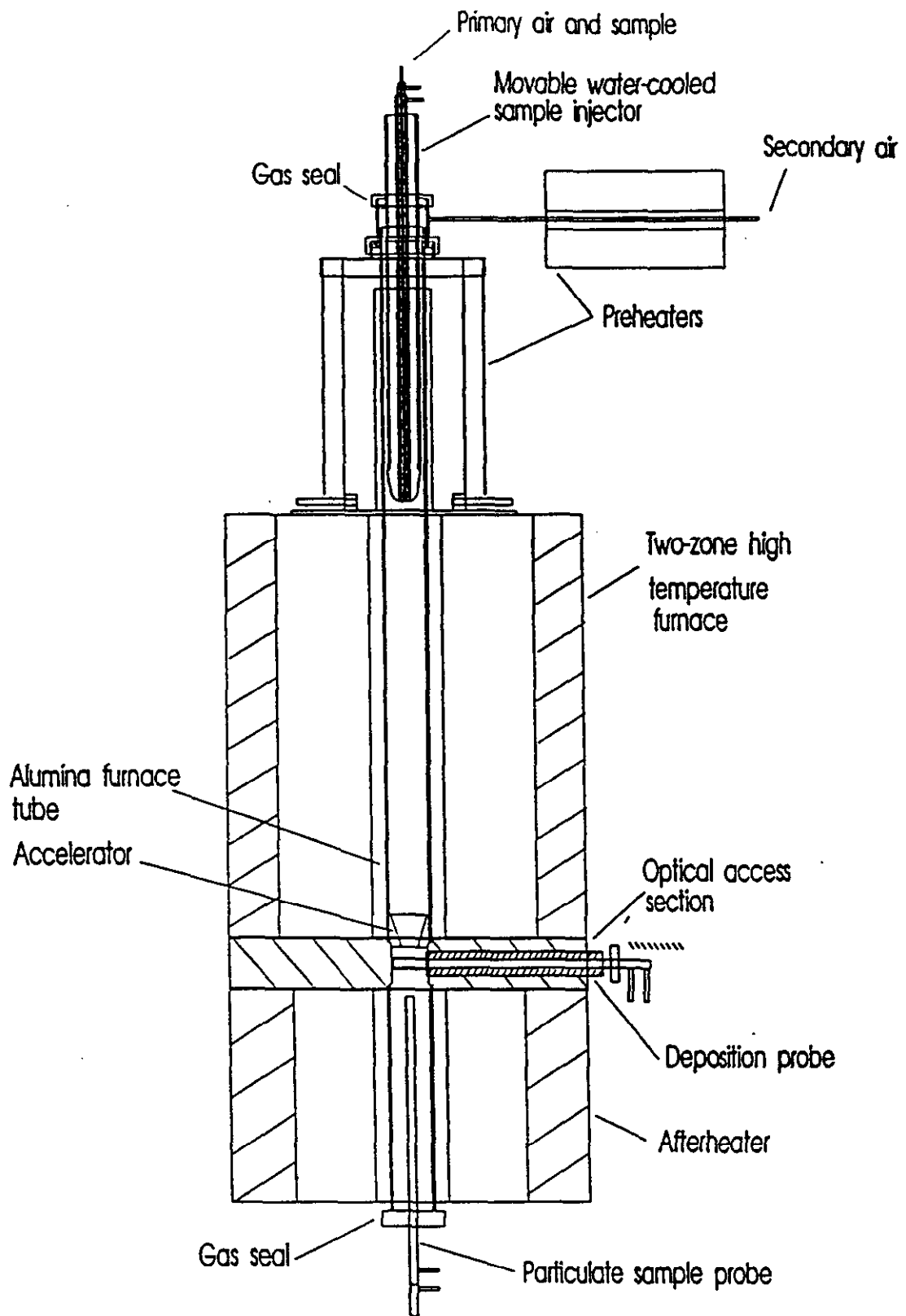


FIGURE A-6 CROSS SECTION OF UNDEERC DROP TUBE FURNACE (DTF)

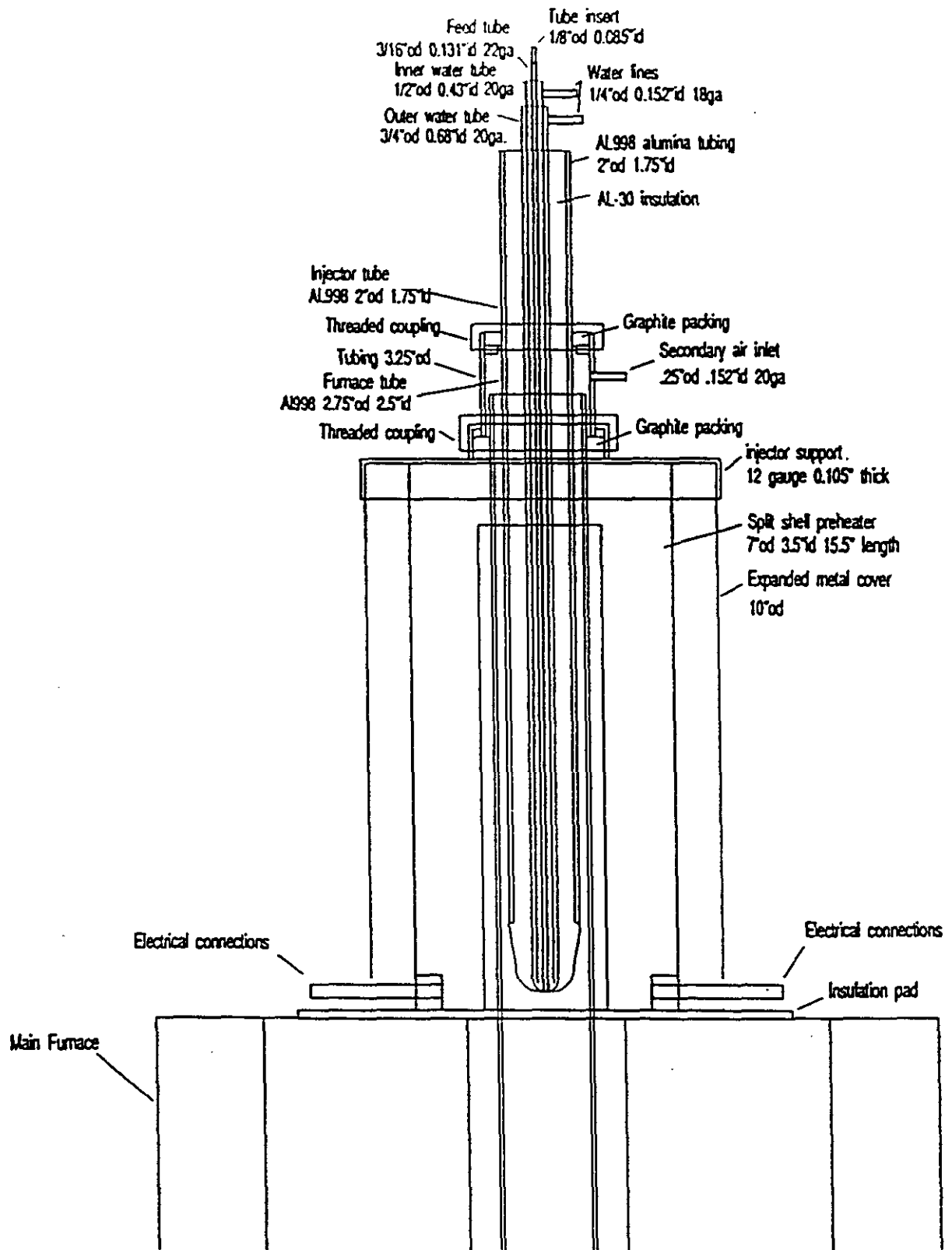


FIGURE A-7 DTF MOVABLE WATER-COOLED SAMPLE INJECTOR CONFIGURATION

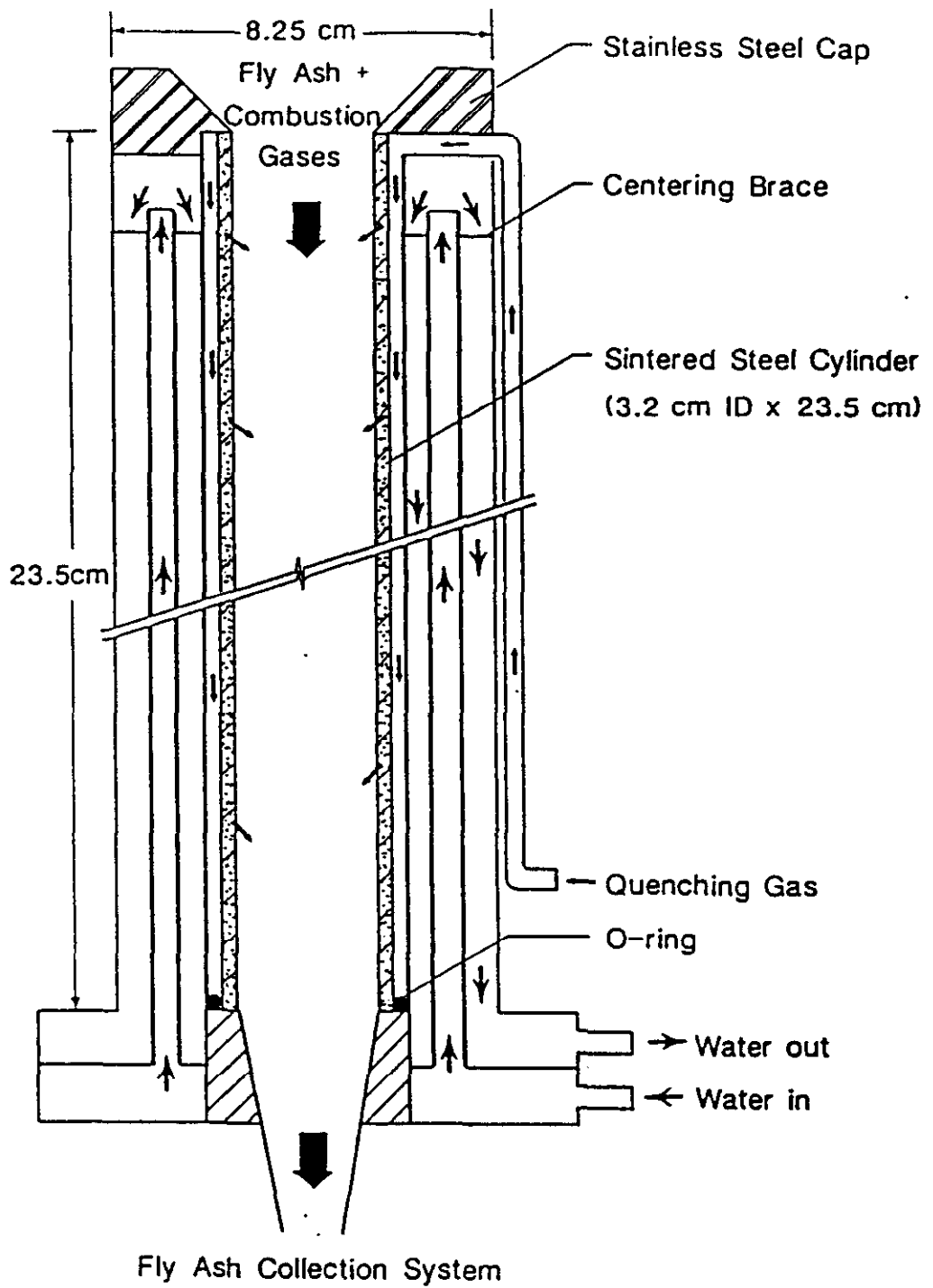


FIGURE A-8 DTF FLY ASH QUENCHING PROBE

and an impactor, to size segregate the ash. Bulk ash is collected on a Magna Nylon 66 filter placed in a 2-1/2" filter holder.

Downstream of the sampling probe and collection filter, the combustion gas is cooled and passes through a filter before entering an airtight diaphragm pump. The gas leaving the positive pressure side of the pump is passed through a flowmeter which measures the volume of gas being pulled through the probe. After the flowmeter, part of the gas is directed through carbon monoxide, carbon dioxide, and oxygen analyzers. The concentrations of these gases can then be read directly from the digital readouts of the analyzers or a chart recorder. The analyzers also send voltage signals to a computer which records the gas concentrations. The computer allows real-time comparisons of gas concentrations with coal feed rates. The configuration of this system is shown in Figure A-9.

The coal feed system is designed to feed particles of various sizes in the pulverized coal range at rates of 0.05 to 0.5 g per minute and at primary carrier gas rates of approximately one liter per minute. The basic apparatus shown in Figure A-10 consists of a pressurized cylinder in which a container filled with coal is placed. A rotating brush and stirrer attached to a variable speed motor feeds the coal from the container into a funnel where it is transported through the feed tubing into the furnace injector by the carrier gas. The coal feeder is mounted on a Sartorius top-loading balance which monitors real-time coal feed rates. The balance is connected via a RS232 to a computer which records the feed rate.

A ceramic constrictor is used to accelerate the gas flow to approximately 3-5 m/sec before it impinges on the coupon. The flow accelerator is made of Zircar AL-30 machined to fit the inside of the alumina reactor tube and coated with alumina cement. The top has a 1.27-cm hole drilled through the center and beveled at approximately 60 degrees to form the nozzle. The coupon is placed 1" (2.5 cm) below the constrictor.

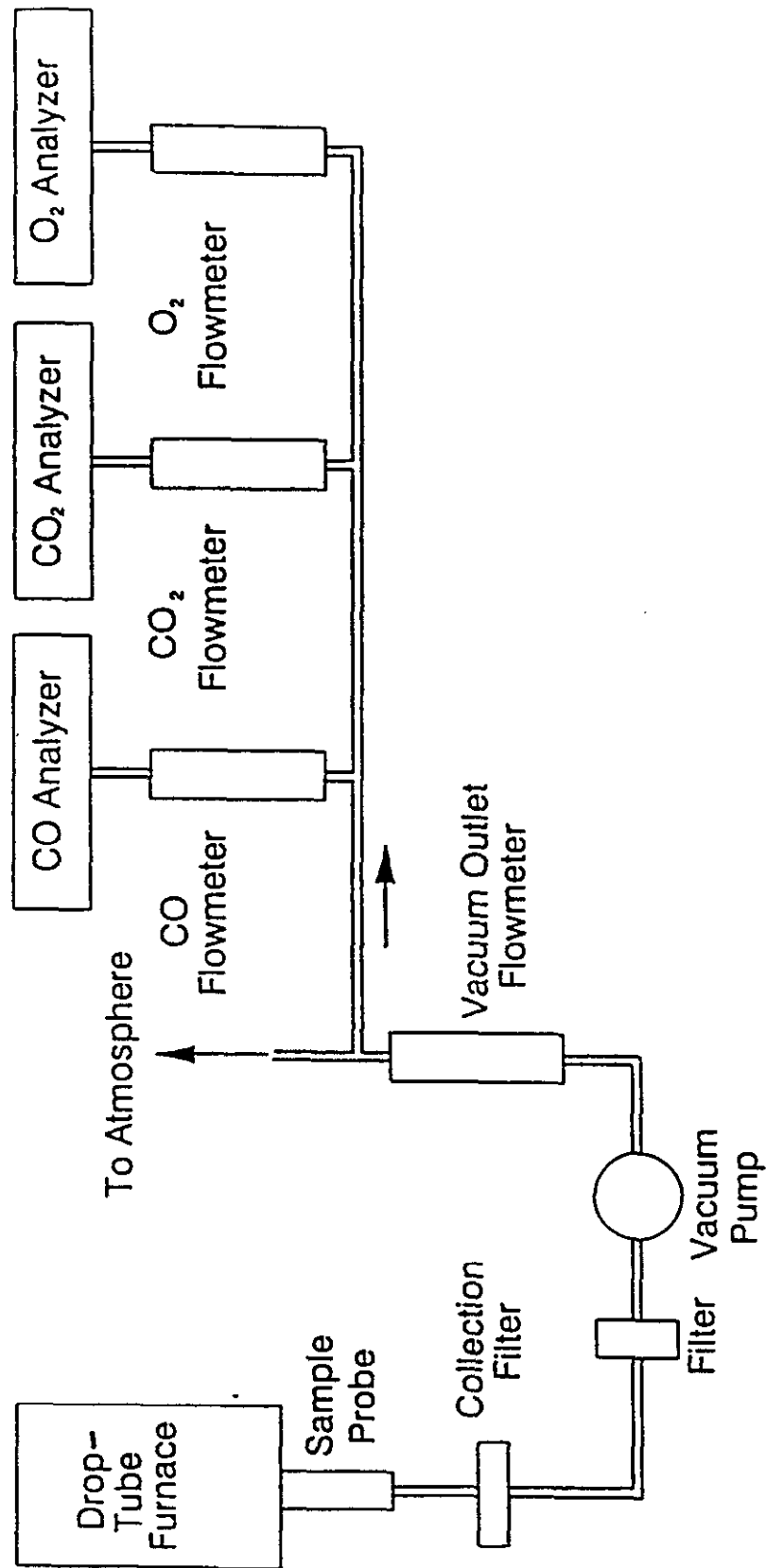


FIGURE A-9 DTF GAS SAMPLING SYSTEM

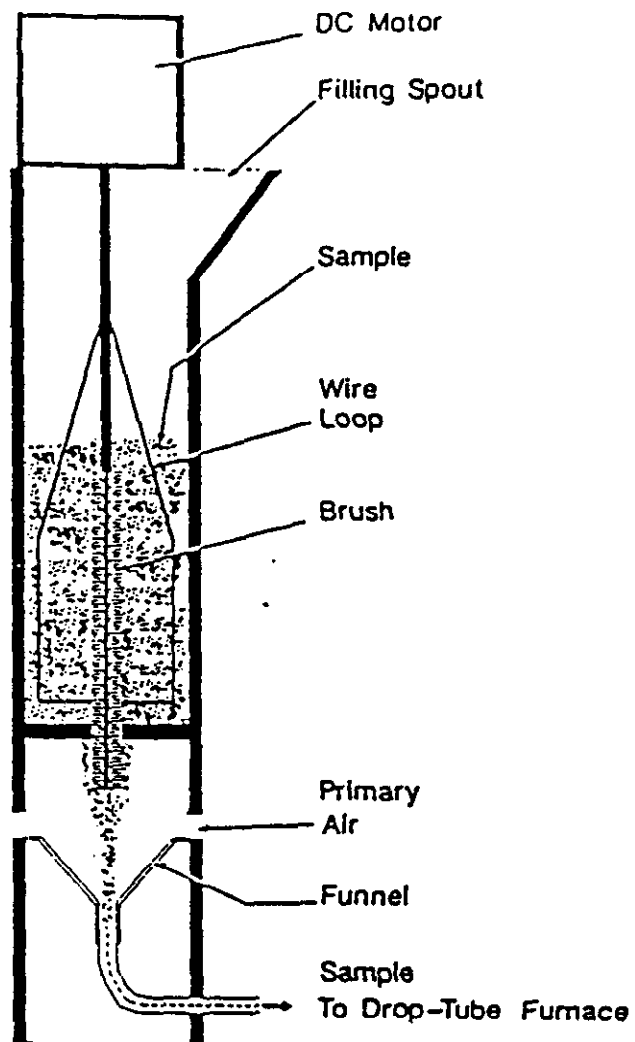


FIGURE A-10 DTF COAL FEEDER

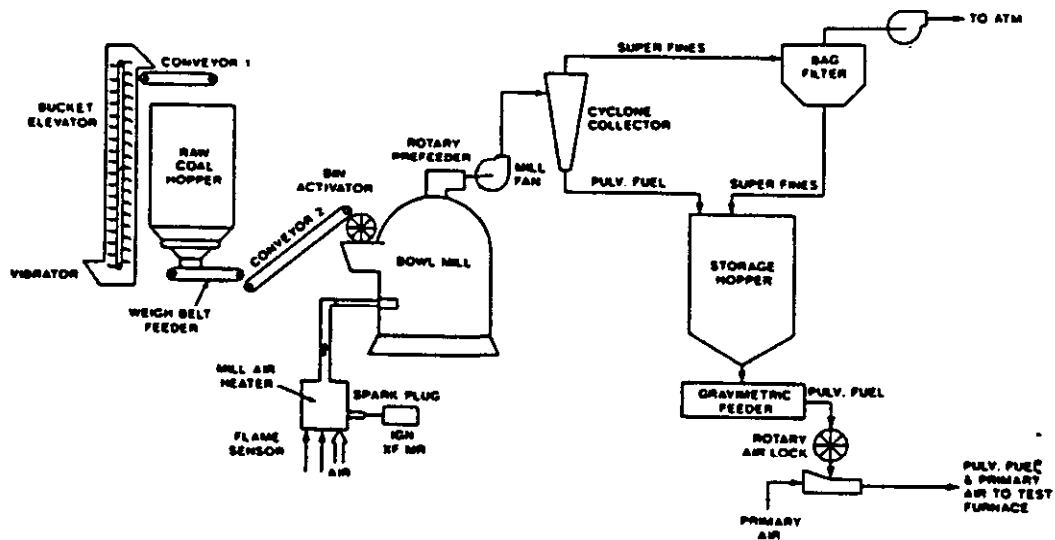
PILOT-SCALE TEST FACILITY

CE's Fireside Performance Test Facility (FPTF) is a pilot-scale combustion facility used primarily to assess fuel properties (such as ash deposition and fly ash erosion) which influence boiler performance. It is composed of a complete fuel handling system (for both solid and liquid fuels), including a pulverizer, air preheater and an upward-fired test furnace. Schematics of these facilities are shown in Figures A-11 and A-12.

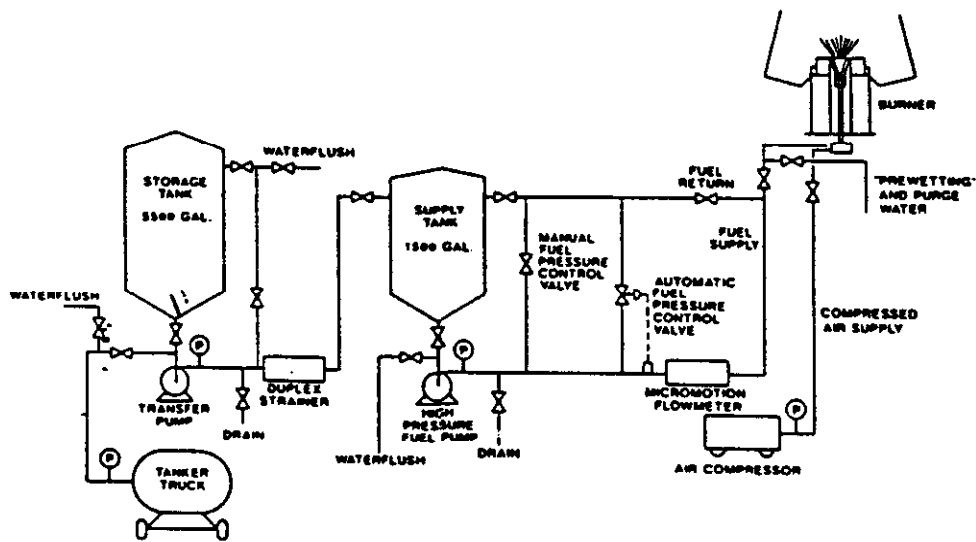
Evaluation of pulverization characteristics of solid fuels is accomplished using a CE Raymond Model 271 bowl mill. This pulverizer utilizes one spring-loaded grinding roll in a 27-inch diameter bowl driven by an external motor. The roller is positioned in the bowl so that there is no metal-to-metal contact between the roller and the bowl. When fuel is fed into the pulverizer, it is directed to the small gap between the bowl and the roller, causing the roller to turn and the material to be ground.

Crushed coal (1 in. to 1-1/2 in. top size) is fed from a large storage hopper to the pulverizer by a gravimetric belt feeder. The feeder is used to control the feed rate of the coal going into the bowl mill. The pulverizer is equipped with a direct gas-fired air heater to provide mill drying air. The coal is dried by heated air entering below the bowl. The hot air carries the pulverized coal up through the classifier and into the fuel transport piping. The particle size of the coal is controlled by adjustable vanes in the mill classifier, while the over-sized particles are returned to the mill. The outlet temperature of the pulverizer is held at a constant $140 \pm 10^\circ\text{F}$. The grinding roll to grinding ring distance and the spring compression can be varied as necessary to obtain the desired fuel fineness.

The pulverized coal is pneumatically transported to a cyclone collector where it is separated from the transport gases and stored in a three-ton storage hopper. The air is then passed through a bag filter which removes any remaining coal particles before venting to the atmosphere. Pulverized coal is fed by a belt-type gravimetric feeder from the hopper into a rotary air lock, from which it is pneumatically transported into the



SOLID FUEL HANDLING SYSTEM



LIQUID FUEL HANDLING SYSTEM

Figure A-11 Fireside Performance Test Facility Fuel Handling Systems

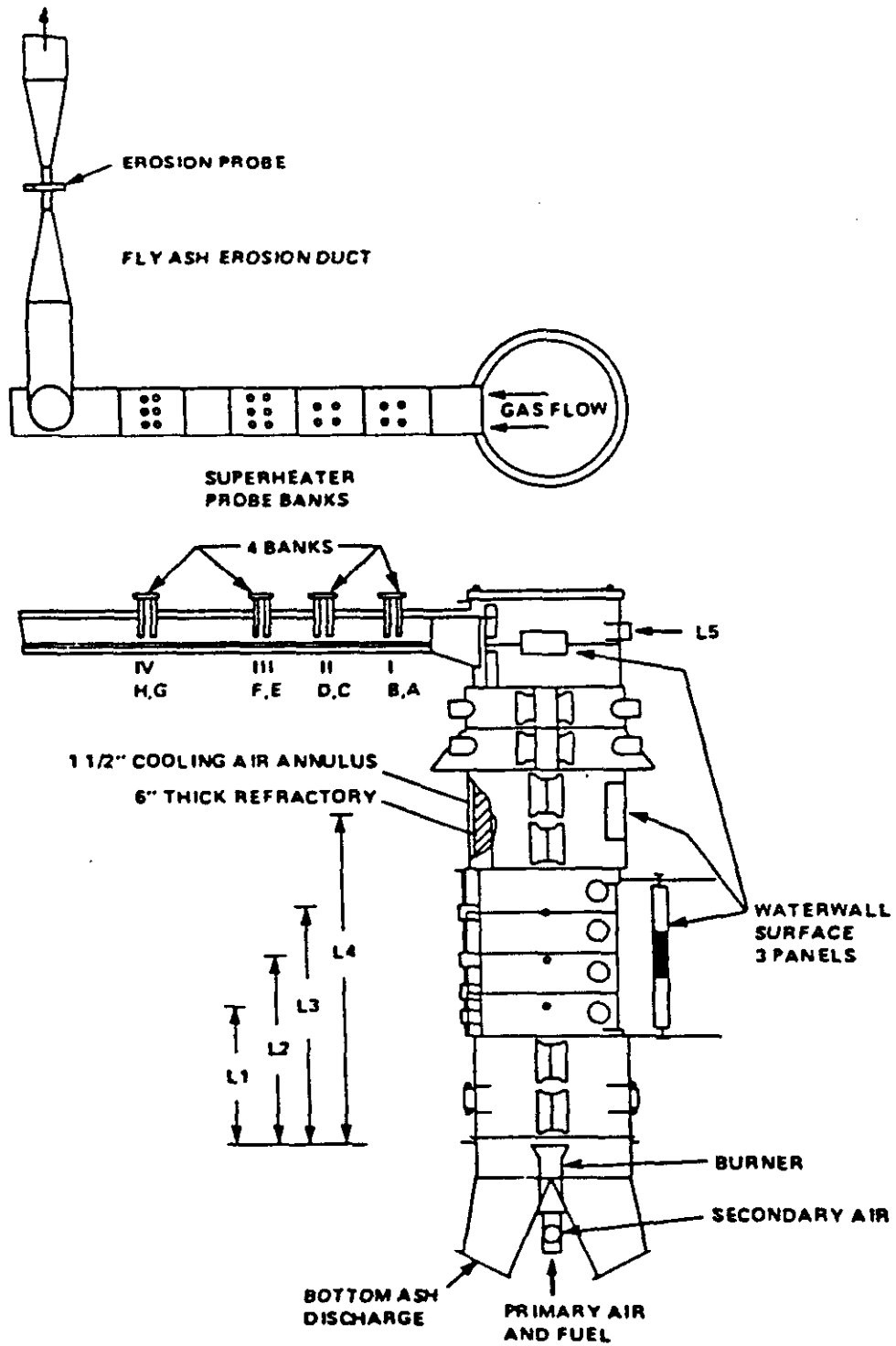


Figure A-12 Fireside Performance Test Facility (FPTF)

furnace. For pulverizer testing, the bowl mill is allowed to grind coal for fifteen minutes at the desired fuel feed rate before a test is started. A test point consists of a five-minute mill reject sample, a pulverized coal sample and a reading from the recording wattmeter for power consumption. The pulverized coal sample is then screened for size (normally percent through 200 mesh). The mill classifier vanes are adjusted as necessary to obtain the required fuel fineness.

The test furnace consists of an 18-foot high, refractory-lined 36-inch diameter cylinder. The six-inch thick refractory lining minimizes the potential heat losses associated with the large surface-to-volume ratio inherent with small furnaces. Cooling air is drawn through the 1-1/2 inch annulus surrounding the refractory lining, which provides cooling for the furnace structural shell as well as control of the heat absorption and temperature in the lower furnace.

The furnace is bottom-fired through a single swirl-type burner. Either a conventional burner for pulverized coal or a specially-designed burner for coal-water slurries can be used. The maximum firing capacity of the FPTF is approximately 5.0 MBtu/hr. Firing in this test facility is designed to simulate commercial boiler time-temperature history. The firing rate can be varied to obtain a wide range of conditions, with flame temperatures from 1900 °F to 3000 °F, and residence times from 1.0 to 2.5 seconds.

Located in the radiant section of the furnace (starting approximately three feet above the burner) are waterwall test panels, as shown in Figure A-12. These panels are used to study lower furnace ash deposition and to provide a detailed assessment of the slagging and heat transfer characteristics of the test fuel. A water-cooled frame surrounds the panels to reduce interference from molten slag generated on the hot refractory surfaces. The test panels have a total surface of approximately 4.7 square feet, and are used to model the waterwall surfaces in the lower furnace of commercial boilers. The metal temperature of the panel is typically controlled at 700 °F. Syltherm, a high boiling point organic liquid, is used as the coolant and flows through the serpentine tubing of the panels. The heat absorption rate of the panel is continuously

recorded by measuring the coolant flow rates and inlet and outlet temperatures.

Flue gas exits the lower furnace at a right angle through a horizontal water-cooled superheater duct, as shown in Figure A-12. This test section consists of five sub-sections of duct, each containing two rows of probes. This section of the FPTF can be configured to simulate the convection sections of a commercial unit. Air-cooled probes are used to simulate boiler superheater tubes. Probe metal temperatures are typically controlled at 1100 °F. Gas temperatures and velocities through these probe banks range from 1600 to 2300 °F and 30 to 70 ft/sec.

A high-velocity section is located downstream of the convection superheater duct and is used for fly ash erosion characterization. A specially-prepared test probe made of removable coupons is installed in this section. Probe metal temperatures are controlled at 800 °F. A surface activation technique is used to determine metal loss from the test probe after exposure to ash-laden flue gas. This method measures the change in the intensity of emitted radiation to determine the depth of metal erosion. The test probe is made slightly radioactive by impinging a particle beam onto its surface. As the metal surface is eroded, the level of emitted gamma radiation decreases. At the end of each test, the tube is removed and the level of emitted radiation is measured and compared to pre-test levels. Changes in radioactivity are related to the amount of metal loss due to fly ash erosion. Tube erosion from each test coal can then be accurately compared to determine the relative metal wear.

The FPTF is fully instrumented and uses a computer-controlled data acquisition system to accurately monitor and record all fuel and air inputs. Cooling flows and temperatures are measured to obtain mass and energy balances around the furnace. A gas analysis system allows for periodic on-line measurement of O₂, CO₂, CO, NO_x and SO₂ concentrations in the flue gas. The flue gas sample is obtained downstream of the FPTF convective pass probes, and is conditioned to remove fly ash and water vapor before being introduced into the individual gas analyzers.

APPENDIX B
UND SEM PROCEDURE

STANDARD OPERATING PROCEDURE FOR COAL/ASH MINERAL ANALYSIS BY COMPUTER-CONTROLLED SCANNING ELECTRON MICROSCOPY

INTRODUCTION

This appendix describes a procedure employed at the Energy and Environmental Research Center (EERC) for sizing, identifying, and quantifying mineral constituents in coal and coal combustion products (fly ash and bottom ash) using a computer-controlled scanning electron microscopy (CCSEM) technique (Lee and Kelly, 1980; Huggins et al., 1980, 1982). Quantitative coal/ash mineral analysis and mineral size analysis is useful in characterizing the physical and chemical properties of coal, predicting the inorganic transformations that occur during combustion, understanding the deposition, slagging, and fouling characteristics of combusted materials, and determining the potential utilization or disposal of ash by-products. The reader is referred to Zygarlicke and Steadman (1990), Zygarlicke and others (1990), and Jones and others (1992) for additional information and examples of specific CCSEM applications.

SUMMARY OF PROCEDURE

Coals and coal combustion products to be analyzed are mounted in epoxy resin or caruba wax, cross sectioned, and polished according to ASTM Standard Practice D2797 (ASTM, 1991), or ultrasonically dispersed and mounted on filter paper. The sample is sputter coated with carbon to minimize electron-beam charging artifacts. A JEOL JSM-35 analytical SEM equipped with a Noran (formally Tracor Northern, TN) Micro-Z ultrathin window x-ray detector, TN-5500 x-ray analyzer, TN-5600 stage automation system, TN-8502 image analyzer, and a GW Electronics annular solid-state back-scattered electron (BSE) detector, is used for coal/ash mineral analysis. The automated analytical SEM, operating at a beam voltage of 15 kV and current of 0.6 nA in the BSE imaging mode, is programmed to scan preselected areas of the sample.

A modified version of Noran's Particle Recognition and Characterization (PRC) program is used to locate, size, and chemically analyze coal/ash mineral particles. Mineral particles are automatically detected by an increase in the BSE signal above a preset video threshold. The electron microbeam performs an iterative bisection of

chords to locate the detected particle's center. Eight diameters are measured to determine the particle's minimum, maximum, and average diameter. The particle's area, perimeter, and shape factor are also calculated. After the size analysis, an energy-dispersive x-ray spectrum (0-10keV) is acquired from the particle's center for a period of five seconds. Spectral regions-of-interest (ROI) are defined and the characteristic x-ray emission intensities of 12 common, mineral-forming, major and minor elements (Na, Mg, Al, Si, P, S, Cl, K, Ca, Ti, Fe, and Ba) are measured. Relative intensities are calculated by dividing the net counts for each element by the total ROI counts for all elements. X-ray intensity data and location, size, and shape parameters for approximately 2000 particles are collected at two magnifications: 50X for 10 to 100 micron and 240X for 1 to 10 micron diameter particles. These data are transferred on-line to a personal computer where they are tabulated and stored to disk for subsequent manipulation, report generation, and archiving. The modified PRC program also has the capability to acquire and store BSE images for additional analysis.

A fortran program called PARTCHAR classifies the PRC analyses based on elemental relative intensities, relative-intensity ratios, and stoichiometric criteria into one of 33 mineral/chemical and mineral association categories (Table 1). Analyses that do not conform to any of the specified criteria are termed unclassified. The CCSEM analysis cannot distinguish polymorphous minerals (e.g., quartz versus cristobalite) or crystalline from amorphous phases because it identifies solely by chemical composition. Therefore, qualitative crystalline phase analysis data are obtained by x-ray powder diffraction and referred to for confirmation of CCSEM phase identifications whenever possible. The program allocates the classified particles according to average diameter into six intervals (1.0-2.2 μm , 2.2-4.6 μm , 4.6-10 μm , 10-22 μm , 22-46 μm , 46-100 μm) so that the size distribution of mineral/chemical types can be determined. The particle-diameter intervals are a geometric progression based on the cube root of ten. A geometric size distribution is used to lessen sectioning effects that cause the measured cross-sectional diameters of the particles to be less than or equal to the maximum diameter of the particles (Hurley, 1990). A report is generated that summarizes the results in a series of tables containing information on the number and proportions of minerals in their respective size intervals. Mineral weight percentages are calculated assuming that particle areas are proportional to volumes (DeHoff and Rhines, 1968) and mineral densities are constants (Table 1). The CCSEM analysis generates two PRC raw data files, a PARTCHAR data output file, and a summary report output file that are achieved on tape via a computer network system.

Summary Page

1. Percent Epoxy Used Average area percent of epoxy or carnauba wax mounting medium for an analyzed coal sample. Value is estimated by creating binary images of representative areas on the sample and performing an area mode histogram analysis of each image. An average value is calculated.
2. Total Mineral Area Analyzed at High Mag. - Summation of the cross-sectional areas (μm^2) measured at 240x for the 1 to 10 μm diameter particles.
3. Normalized Area Analyzed at High Mag. The total mineral area analyzed at 240x is normalized by multiplying by $(F^1N^1)/(F^2N^2)$ where F^1 and F^2 are the field sizes (μm^2) at 50x and 240x, respectively; and N^1 and N^2 are the number of frames collected on the sample at 50x and 240x, respectively. The actual sample area scanned by the electron microbeam at high magnification (240x) for the 1 to 10 μm size particles is smaller than the sample area scanned at low magnification (50x) for the 10 to 100 μm size particles. Therefore, the total mineral area analyzed at 240x is normalized so that the 1 to 10 μm size particles have equal statistical representation.
4. Total Mineral Area Analyzed at Low Mag. Summation of the cross-sectional areas (μm^2) measured at 50x for the 10 to 100 μm diameter particles.
5. Field Size Used at High Mag. and Low Mag. Total area imaged (μm^2) per frame on the sample at 240x and 50x, respectively.
6. Number of Frames at High Mag. and Low Mag. Total number of frames collected on the sample at 240x and 50x, respectively.
7. total Mineral Area on a Coal Basis - The total mineral area analyzed is expressed on a coal basis, M_i^c , by

$$M_i^c = \left(\frac{M}{C} \right) 100$$

where M is the total mineral area analyzed (M = normalized area analyzed at high mag. + total mineral area analyzed at low mag.) and C is the total coal area imaged (μm^2). C is determined from

$$C = \frac{A(100 - E)}{100}$$

where A is the total area (μm^2) imaged on the sample ($A - F^1N^1$), and E is the estimated area percent of mounting medium (percent epoxy used value).

8. Total Mineral Weight Percent on a Coal Basis. The total mineral content by weight on a coal basis, W_i^c , is calculated from

$$W_i^c = \left(\frac{\sum_{j=1}^{NP} A_j d_j^i}{d_c(C - M) + \sum_{j=1}^{NP} A_j d_j^i} \right) 100$$

where A_j is the area for particle j, d_{ji} is the density of mineral/chemical classification category i (Table 1) assigned to particle j, NP is the total number of particles analyzed, C is the total coal area imaged, M is the total mineral area analyzed, and d_c is the density of coal ($d_c = 1.4 \text{ g/cm}^3$).

9. Total Number of Points Analyzed Total number of mineral/ash particles detected and analyzed.

10. Number of Points Under Threshold Number of particle analyses excluded from the PARTCHAR mineral classification routine because of an insufficient x-ray signal for chemical characterization. Particles that emit < 600 total x-ray counts are excluded.

11. Weight Percent on a Mineral Basis The weight proportions of each mineral/chemical classification category i on a mineral basis, W_i^m are calculated from

$$W_i^m = \left(\frac{(A_i d_i)}{\sum_{j=1}^{NP} A_j d_j^i} \right) 100$$

where A_1 is the total area of the particles assigned to mineral/chemical classification category i, d^1 is the density (g/cm^3) for mineral/chemical classification category i

(Table 1), A_j is the area of particle j , d_{ji} is the density of mineral/chemical classification category i assigned to particle j , and NP is the total number of particles analyzed. This table of mineral weight percentages is also presented on page 4. The average diameter interval values in this and subsequent tables are in microns.

12. Area in Each Size Range Summation of the measured cross-sectional areas (μm^2) for each mineral/chemical and mineral association category in each diameter interval. The values for the 1 to 10 μm diameter particles are not normalized.

13. Normalized Area in Each Size Range Essentially the same data as in #12, except that the cross-sectional areas for the 1 to 10 μm diameter particles have been normalized.

14. Area Percent Mineral Basis The total area of the particles assigned to each mineral/chemical classification category, A_i , (#13) is converted to area percent by

$$\left(\frac{A_i}{M}\right)100$$

where M is the total mineral area analyzed.

15. Weight Percent Mineral Basis Refer to summary page, item 11 for an explanation

16. Mineral Area Percent Coal Basis The area percent on a mineral basis values from page 3 are converted to a coal basis by multiplying by (M / C) where M is the total mineral area analyzed and C is the total coal area imaged. These values are equivalent to volume percent assuming that a representative planar section of the coal was analyzed.

17. Weight Percent Coal Basis The weight percent of each mineral/chemical classification category i on a coal basis, W_i^c , is determined by

$$W_i^c = \left(\frac{A_i d_i}{d_c(C - M) + \sum_{j=1}^{NP} A_j d_j^i} \right) 100$$

where A_i is the total area of the particles assigned to mineral/chemical classification category i , d_i is the density (g/cm^3) of mineral/chemical classification category i , A_j is the area of particle j , d_{ji} is the density of mineral/chemical category i assigned to particle j , NP is the total number of particles analyzed, C is the total coal area imaged, M is the total mineral area analyzed, and d_c is the density of coal ($d_c = 1.4 \text{ g/cm}^3$).

18. Distribution by Percent of Each Mineral Phase The distribution percent, D_i , of mineral/chemical phase i is determined by

$$D_i = \left(\frac{W'_i}{W_i} \right) 100$$

where W'_i is the weight percent of mineral/chemical classification category i in the average particle diameter interval s , and W_i is the total weight percent of mineral/chemical classification category i .

19. Number of Particles in Each Size Range Actual number of particles detected and analyzed in their respective diameter intervals.

20. Distribution of Mineral Phases (Frequency Percent) The total number of particles analyzed for each mineral/chemical classification category (#19) are converted to frequency percent by dividing by the total number of points analyzed and multiplying by 100.

REFERENCES

- American Society for Testing and Materials (ASTM). "Standard Practice for Preparing Coal Samples for Microscopical Analysis by Reflected Light (D2797)," Annual Book of ASTM Standards: 1991, Vol. 5.05, p. 308-311.
- DeHoff, R.T.; Rhines, F.N. Quantitative Microscopy. Materials Science and Engineering Series, McGraw Hill Book Company, 1968.
- Huggins, F.E.; Kosmack, D.A.; Huffman, G.P.; Lee, R.J. "Coal Mineralogies by SEM Automatic Image Analysis," Scanning Electron Microscopy; 1980, I, 531-540.
- Huggins, F.E.; Huffman, G.P.; Lee, R.J. "Scanning Electron Microscope-Based Automated Image Analysis (SEM-AIA) and Mössbauer Spectroscopy: Quantitative Characterization of Coal Minerals," In Coal and Coal Products: Analytical Characterization Techniques; Fuller, E.L., Jr., Ed.; American Chemical Society Symposium Series 205; 1982, Chapter 12, p. 239-258.
- Hurley, J.P. A Pilot-Scale Study of the Formation of Ash During Pulverized Low-Rank Coal Combustion, University of North Dakota, Ph.D. Dissertation, 1990, 247 pp.
- Jones, M.L.; Kalmanovitch, D.P.; Steadman, E.N.; Zygarlicke, C.J.; Benson, S.A. "Application of SEM Techniques to the Characterization of Coal and Coal Ash Products," Advances in Coal Spectroscopy; Meuzelaar, M.L.C., Ed.; Plenum Publishing Corp.: New York, 1992; Chapter 1, p. 1-27.
- Lee, R.J.; Kelly, J.F. "Overview of SEM-Based Automated Image Analysis," Scanning Electron Microscopy; 1980, I, p. 303-310.
- Zygarlicke, C.J.; Steadman, E.N. "Advanced SEM Techniques to Characterize Coal Minerals," Scanning Microscopy; 1990, Vol. 4, No. 3, p. 579-590.
- Zygarlicke, C.J.; Steadman, E.N.; Benson, S.A. "Studies of Transformations of Inorganic Constituents in a Texas Lignite During Combustion," Prog. Energy Combust. Sci.; 1990, Vol. 16, p. 195-204.

TABLE 1

CCSEM Phase Classification Definitions

Classification Number	Mineral/Chemical & Mineral Association Categories	Density (g/cm ³)	Compositional Criteria (relative EDX intensity)
1	Quartz	2.65	Al \leq 5, Si \geq 80
2	Iron Oxide	5.30	Mg \leq 5, Al \leq 5, Si $<$ 10, S \leq 5, Fe \geq 80
3	Periclase	3.61	Mg \geq 80, Ca \leq 5
4	Rutile	4.90	S \leq 5, Ti+Ba \geq 80
5	Alumina	4.00	Al \geq 80
6	Calcite	2.80	Mg \leq 5, Si \leq 5, P \leq 5, S $<$ 10, Ca \geq 80, Ti \leq 5, Ba \leq 5
7	Dolomite	2.86	Mg \geq 5, Ca $>$ 10, Ca+Mg \geq 80
8	Ankerite	3.00	Mg $<$ Fe, S $<$ 15, Ca $>$ 20, Fe $>$ 20, Ca+Mg+Fe \geq 80
9	Kaolinite	2.65	Al+Si \geq 80, K \leq 5, Ca \leq 5, 0.8 $<$ Si/Al $<$ 1.5, Fe \leq 5
10	Montmorillonite	2.50	Al+Si \geq 80, K \leq 5, Ca \leq 5, 1.5 $<$ Si/Al $<$ 2.5, Fe \leq 5
11	K-Al Silicate	2.60	Na \leq 5, Al \geq 15, Si $>$ 20, K \leq 5, K+Al+Si \geq 80, Ca \leq 5, Fe \leq 5
12	Fe-Al Silicate	2.80	Na \leq 5, Al \geq 15, Si $>$ 20, S \leq 5, K \leq 5, Ca \leq 5, Fe \geq 5, Fe+Al+Si \geq 80
13	Ca-Al Silicate	2.65	Na \leq 5, Al \geq 15, Si $>$ 20, S \leq 5, K \leq 5, Ca \leq 5, Ca+Al+Si \geq 80, Fe \leq 5
14	Na-Al Silicate	2.60	Na \geq 5, Al \geq 15, Si $>$ 20, Na+Al+Si \geq 80, S \leq 5, K \leq 5, Ca \leq 5, Fe \leq 5
15	Aluminosilicate	2.65	Na \leq 5, Al $>$ 20, Si $>$ 20, Si+Al \geq 80, K \leq 5, Ca \leq 5, Fe \leq 5
16	Mixed Silicate	2.65	Na $<$ 10, Al $>$ 20, Si $>$ 20, S \leq 5, K $<$ 10, Ca $<$ 10, Fe $<$ 10, Na+Al+Si+K+Ca+Fe \geq 80
17	Fe Silicate	4.40	Na \leq 5, Al \leq 5, Si $>$ 20, S \leq 5, K \leq 5, Ca \leq 5, Fe $>$ 10, Fe+Si \geq 80

(continued)

TABLE 1
CCSEM Phase Classification Definitions (continued)

Classification Number	Mineral/Chemical & Mineral Association Categories	Density (g/cm ³)	Compositional Criteria (relative EDX [*] intensity)
18	Ca Silicate	3.09	Na \leq 5, Al \leq 5, Si $>$ 20, S \leq 5, K \leq 5, Ca $>$ 10, Ca+Si \geq 80, Fe \leq 5
19	Ca Aluminate	2.80	Al $>$ 15, Si \leq 5, P \leq 5, S \leq 5, Ca $>$ 20, Ca+Al \geq 80
20	Pyrite	5.00	S $>$ 40, Ca $<$ 10, 10 \leq Fe \leq 40, Fe+S \geq 80
21	Pyrrhotite	4.60	10 \leq S $<$ 40, Fe $<$ 40, Fe+S \geq 80
22	Oxidized Pyrrhotite	5.30	S $>$ 5, Ca $<$ 10, Fe $>$ 40, Fe/S $>$ 1.5, Fe+S $>$ 80, Ba $<$ 5
23	Gypsum	2.50	Si $<$ 10, S $>$ 20, Ca $>$ 20, Ca+S \geq 80, Ti $<$ 10, Ba $<$ 10
24	Barite	4.50	S $>$ 20, Ca \leq 5, Fe $<$ 10, Ba+Ti $>$ 20, Ba+S+Ti \geq 80
25	Apatite	3.20	Al \leq 5, P \geq 20, S \leq 5, Ca \geq 20, Ca+P \geq 80
26	Ca-Al-P	2.80	Al $>$ 10, Si \leq 5, P $>$ 10, S \leq 5, Ca $>$ 10, Al+P+Ca \geq 80
27	KCl	1.99	K \geq 30, Cl \geq 30, K+Cl \geq 80
28	Gypsum/Barite	3.50	S $>$ 20, Ca \leq 5, Ti \leq 5, Fe \leq 5, Ba \geq 5, S+Ca+Ti+Ba \geq 80
29	Gypsum/Al Silicate	2.60	Al \geq 5, Si \geq 5, S \leq 5, Ca \geq 5, Al+Si+S+Ca \geq 80
30	Si Rich	2.65	65 \leq Si $<$ 80
31	Ca Rich	2.60	Al $<$ 15, 65 \leq Ca $<$ 80
32	Ca-Si Rich	2.60	Si $>$ 20, Ca $>$ 20, Si+Ca $>$ 80
33	Unknown	2.70	Unclassified Compositions

*Energy-dispersive x-ray.

APPENDIX C

DETAILED CCSEM AND

CHEMICAL FRACTIONATION RESULTS

Appendix C-1. Detailed Particle Distributions (CCSEM)

100% Wyoming

MINERAL/PHASE	Particle Size Categories (microns)						Wt. % Mineral Basis	Wt. % Coal Basis
	<2.2	2.2-4.6	4.6-10	10-22	22-46	>46		
Quartz	1.7	2.7	5.9	5.9	6.8	1.5	24.4	1.50
Iron Oxide	0.0	0.0	0.8	0.1	0.2	0.0	1.1	0.07
Rutile	0.1	0.0	0.0	0.1	0.0	0.0	0.1	0.01
Calcite	0.0	0.0	0.0	0.0	0.0	0.0	0.0	0.00
Kaolinite	1.4	1.9	3.3	5.8	4.5	0.9	17.8	1.10
Montmorillonite	1.2	3.2	1.3	2.5	2.8	0.0	11.0	0.67
K Al-Silicate	0.3	0.7	0.6	0.5	1.4	0.0	3.5	0.21
Fe Al-Silicate	0.0	0.0	0.0	0.0	0.0	0.0	0.0	0.00
Ca Al-Silicate	0.2	0.3	0.0	1.0	0.4	0.0	1.8	0.11
Na Al-Silicate	0.0	0.0	0.0	0.0	0.0	0.0	0.0	0.00
Aluminosilicate	0.3	1.2	0.8	1.0	0.6	0.4	4.3	0.27
Mixed Al-Silicate	0.0	0.1	0.0	0.2	0.4	0.0	0.7	0.04
Pyrite	0.4	0.6	0.0	2.1	1.4	0.7	5.2	0.32
Gypsum	0.0	0.0	0.0	0.0	0.0	0.0	0.0	0.00
Ca Al-Phosphate	1.3	4.4	5.5	1.8	0.8	0.5	14.2	0.88
Gypsum\Al-Silicate	0.0	0.0	0.0	0.9	0.6	0.0	1.6	0.10
Si-Rich	0.2	1.0	0.1	1.4	2.9	0.9	6.5	0.40
Unknown	1.0	0.4	0.1	1.7	2.6	1.0	6.8	0.42
Totals	8.2	16.5	18.6	25.0	26.0	5.8	100.0	6.15

Appendix C-1. Detailed Particle Distributions (CCSEM) Cont.

90/10 Blend

MINERAL/PHASE	Particle Size Categories (microns)						Wt. % Mineral Basis	Wt. % Coal Basis
	<2.2	2.2-4.6	4.6-10	10-22	22-46	>46		
Quartz	0.0	4.9	6.5	3.1	3.5	3.2	24.1	1.38
Iron Oxide	0.0	0.0	0.0	0.2	0.1	0.4	0.7	0.04
Rutile	0.0	0.0	0.0	0.0	0.0	0.0	0.0	0.00
Calcite	0.1	0.3	0.0	0.2	0.6	0.6	1.7	0.10
Kaolinite	2.0	3.1	2.3	3.3	2.9	2.6	16.3	0.93
Montmorillonite	1.5	2.0	4.4	0.9	0.4	0.0	9.2	0.53
K Al-Silicate	1.4	3.2	3.1	1.0	0.6	0.7	10.0	0.57
Fe Al-Silicate	0.2	0.0	0.0	0.1	0.0	0.0	0.2	0.01
Ca Al-Silicate	0.8	0.4	0.5	0.1	0.0	0.0	1.6	0.09
Na Al-Silicate	0.0	0.0	0.0	0.0	0.0	0.0	0.0	0.00
Aluminosilicate	0.4	1.2	0.7	0.4	0.3	0.0	3.1	0.18
Mixed Al-Silicate	0.2	0.1	0.0	0.1	0.0	0.0	0.4	0.02
Pyrite	1.0	0.9	0.0	1.9	2.4	2.4	8.5	0.49
Gypsum	0.1	0.0	0.0	0.0	0.1	0.0	0.2	0.01
Ca Al-Phosphate	1.0	3.2	2.9	0.1	0.4	0.0	7.6	0.43
Gypsum\Al-Silicate	0.1	0.2	0.0	0.0	0.0	0.0	0.4	0.02
Si-Rich	0.5	1.0	3.6	0.6	0.2	0.8	6.9	0.39
Unknown	2.3	2.7	0.5	0.6	0.5	1.2	7.7	0.44
Totals	14.8	23.7	24.4	13.0	12.3	11.8	100.0	5.71

Appendix C-1. Detailed Particle Distributions (CCSEM) Cont.

70/30 Blend

MINERAL/PHASE	Particle Size Categories (microns)						Wt. % Mineral Basis	Wt. % Coal Basis
	<2.2	2.2-4.6	4.6-10	10-22	22-46	>46		
Quartz	2.3	3.2	3.1	3.4	1.2	0.2	13.4	0.72
Iron Oxide	0.0	0.0	0.0	0.0	0.0	0.0	0.0	0.00
Rutile	0.3	1.6	0.0	0.0	0.0	0.0	1.9	0.05
Calcite	0.0	0.0	0.0	1.6	1.2	0.0	2.8	0.14
Kaolinite	1.9	7.8	1.1	2.5	0.8	0.4	14.5	0.77
Montmorillonite	0.9	2.8	1.3	0.5	0.3	0.2	5.9	0.34
K Al-Silicate	3.8	6.2	6.2	1.8	0.5	0.0	18.5	1.01
Fe Al-Silicate	0.8	0.3	2.2	0.2	0.0	0.0	3.5	0.18
Ca Al-Silicate	0.4	0.9	0.0	0.1	0.0	0.0	1.4	0.07
Na Al-Silicate	0.0	0.0	2.6	0.1	0.1	0.0	2.9	0.16
Aluminosilicate	0.0	0.3	0.0	0.2	0.3	0.0	0.8	0.04
Mixed Al-Silicate	0.9	1.6	2.4	0.1	0.0	0.0	4.9	0.66
Pyrite	0.6	0.7	2.7	1.6	0.1	0.0	5.6	0.16
Gypsum	0.0	0.0	0.0	0.0	0.0	0.0	0.0	0.00
Ca Al-Phosphate	0.0	0.8	0.0	0.3	0.0	0.0	1.1	0.06
Gypsum\Al-Silicate	0.2	2.0	0.0	0.0	0.0	0.0	2.2	0.12
Si-Rich	0.5	1.7	1.5	0.5	0.5	0.0	4.7	0.25
Unknown	5.2	8.8	0.0	0.9	0.5	0.0	15.4	0.81
Totals	18.0	38.5	23.1	14.1	5.5	0.7	100.0	5.16

Appendix C-1. Detailed Particle Distributions (CCSEM) Cont.

70/30 Cleaned Blend

MINERAL/PHASE	Particle Size Categories (microns)						Wt. % Mineral Basis	Wt. % Coal Basis
	<2.2	2.2-4.6	4.6-10	10-22	22-46	>46		
Quartz	2.4	4.5	6.0	3.2	4.2	2.8	23.1	0.88
Iron Oxide	0.1	0.0	0.0	0.6	1.0	0.0	1.7	0.06
Rutile	0.1	0.0	0.0	0.0	0.0	0.0	0.2	0.01
Calcite	0.1	0.1	0.4	0.5	1.6	2.4	5.1	0.19
Kaolinite	1.1	2.8	3.7	3.3	2.8	1.6	15.3	0.58
Montmorillonite	2.1	2.2	0.5	0.9	0.4	0.0	6.2	0.24
K Al-Silicate	2.7	4.5	2.3	1.2	0.8	0.0	11.6	0.44
Fe Al-Silicate	0.4	0.3	0.2	0.1	0.0	0.0	1.1	0.04
Ca Al-Silicate	0.3	0.4	0.4	0.1	0.1	0.0	1.2	0.05
Na Al-Silicate	0.0	0.0	0.0	0.0	0.0	0.0	0.0	0.00
Aluminosilicate	0.4	0.8	0.5	0.5	0.0	0.0	2.2	0.08
Mixed Al-Silicate	0.1	0.3	0.0	0.0	0.0	0.0	0.5	0.02
Pyrite	1.4	1.0	0.0	2.0	2.5	1.1	8.0	0.30
Gypsum	0.2	0.8	0.3	0.3	0.7	0.0	2.3	0.09
Ca Al-Phosphate	0.7	1.6	1.5	0.5	0.0	0.0	4.4	0.17
Gypsum\Al-Silicate	0.2	0.1	0.0	0.0	0.0	0.0	0.2	0.01
Si-Rich	0.7	0.8	0.5	0.6	0.5	0.5	3.7	0.14
Unknown	2.8	2.1	0.5	1.4	1.4	0.0	8.2	0.31
Totals	16.2	23.0	19.9	15.9	16.5	8.5	100.0	3.81

Appendix C-1. Detailed Particle Distributions (CCSEM) Cont.

100% Oklahoma

MINERAL/PHASE	Particle Size Categories (microns)						Wt. % Mineral Basis	Wt. % Coal Basis
	<2.2	2.2-4.6	4.6-10	10-22	22-46	>46		
Quartz	0.8	2.0	2.6	1.5	2.5	0.0	9.3	1.27
Iron Oxide	0.0	0.0	0.0	0.3	0.2	0.0	0.5	0.08
Rutile	0.0	0.1	0.0	0.0	0.0	0.0	0.1	0.01
Calcite	0.0	0.2	0.2	2.3	8.0	4.3	15.1	2.05
Kaolinite	0.4	0.8	0.4	0.9	1.3	1.1	4.9	0.66
Montmorillonite	0.3	0.6	0.2	0.3	0.0	0.0	1.4	0.19
K Al-Silicate	2.4	7.0	11.5	6.7	7.9	4.8	40.3	5.48
Fe Al-Silicate	0.2	0.4	0.6	0.3	0.5	0.0	2.0	0.27
Ca Al-Silicate	0.1	0.6	0.3	0.0	0.0	0.0	1.1	0.15
Na Al-Silicate	0.0	0.3	0.0	0.1	0.0	0.0	0.4	0.05
Aluminosilicate	0.1	0.4	0.3	0.3	0.4	0.0	1.5	0.20
Mixed Al-Silicate	0.3	0.5	0.9	0.3	0.0	0.0	2.1	0.28
Pyrite	0.4	0.5	0.0	1.2	0.8	0.0	2.8	0.39
Gypsum	0.0	0.0	0.0	0.2	0.4	0.0	0.6	0.08
Ca Al-Phosphate	0.0	0.0	0.0	0.0	0.0	0.0	0.0	0.00
Gypsum\Al-Silicate	0.1	0.0	0.0	0.1	0.0	0.0	0.2	0.02
Si-Rich	0.5	0.9	1.1	1.3	1.2	0.0	4.9	0.67
Unknown	2.5	2.9	3.3	1.4	0.8	0.6	11.6	1.57
Totals	8.5	17.6	21.7	17.3	24.1	10.8	100.0	13.58

Appendix C-2. Detailed Chemical Fractionation Results

100% Wyoming

	Initial (ppm)	Removed by H ₂ O (%)	Removed by NH ₄ Ac (%)	Removed by HCL (%)	Remaining (%)
Silicon	12506	0	0	0	100
Aluminum	8198	3	0	28	69
Iron	432	7	20	35	39
Titanium	702	15	9	14	61
Phosphorus	472	8	0	83	9
Calcium	14224	16	50	32	3
Magnesium	3586	14	68	13	5
Sodium	468	35	45	0	20
Potassium	299	8	0	0	92

90/10 Blend

	Initial (ppm)	Removed by H ₂ O (%)	Removed by NH ₄ Ac (%)	Removed by HCL (%)	Remaining (%)
Silicon	15009	0	0	0	100
Aluminum	7511	0	0	25	75
Iron	4072	6	0	53	41
Titanium	587	0	0	0	100
Phosphorus	384	0	0	89	11
Calcium	11498	0	62	34	4
Magnesium	2788	0	79	17	4
Sodium	484	38	38	10	14
Potassium	378	0	0	0	100

70/30 Blend

	Initial (ppm)	Removed by H ₂ O (%)	Removed by NH ₄ Ac (%)	Removed by HCL (%)	Remaining (%)
Silicon	192886	2	0	0	100
Aluminum	9039	0	0	2	98
Iron	4611	6	0	49	45
Titanium	539	0	0	25	75
Phosphorus	349	0	0	84	16
Calcium	11706	0	72	27	1
Magnesium	2531	0	74	6	20
Sodium	445	33	25	0	42
Potassium	829	0	0	32	68

Appendix C-2. Detailed Chemical Fractionation Results Cont.

70/30 Blend Cleaned

	Initial (ppm)	Removed by H ₂ O (%)	Removed by NH ₄ Ac (%)	Removed by HCL (%)	Remaining (%)
Silicon	13838	0	0	0	100
Aluminum	7091	0	0	26	74
Iron	4150	6	0	53	41
Titanium	467	0	0	100	0
Phosphorus	361	0	0	90	10
Calcium	9086	0	64	31	5
Magnesium	2416	5	70	14	11
Sodium	345	40	29	2	29
Sum	477	0	0	0	100

100% Oklahoma

	Initial (ppm)	Removed by H ₂ O (%)	Removed by NH ₄ Ac (%)	Removed by HCL (%)	Remaining (%)
Silicon	31329	0	0	0	100
Aluminum	12437	0	0	2	98
Iron	7890	9	0	57	34
Titanium	483	1	0	36	63
Phosphorus	117	1	16	46	37
Calcium	15067	8	87	2	3
Magnesium	1701	6	39	5	50
Sodium	498	21	0	8	71
Potassium	2118	7	0	0	93

APPENDIX D

CE PILOT-SCALE (FPTF) DATA

Table D.1 Residence Time and Corresponding Gas Temperatures as a Function of Location

Location	Test 1		Test 2		Test 3		Test 4		Test 5		Test 6		
	Distance From Burner (ft.)	Avg. Gas Temp. (°F)	Time (Sec.)										
Suction Port L1	38	2977	0.264	2832	0.295	2822	0.308	2808	0.319	2815	0.274	2865	0.292
Suction Port L2	53	2908	0.376	2781	0.420	2731	0.440	2754	0.455	2712	0.391	2752	0.417
Suction Port L3	69	2815	0.484	2684	0.541	2656	0.567	2697	0.584	2678	0.503	2714	0.537
Suction Port L4	99	2651	0.712	2595	0.793	2521	0.834	2543	0.858	2591	0.735	2608	0.786
Suction Port L5	156	2511	1.158	2428	1.278	2340	1.354	2436	1.381	2430	1.184	2373	1.275
S.H. Duct IA	209	2329	1.362	2178	1.508	2140	1.600	2236	1.628	2258	1.394	2195	1.508
S.H. Duct IIC	242	2215	1.399	2083	1.548	1993	1.644	2122	1.667	2110	1.428	2082	1.547
S.H. Duct IIIE	272	2102	1.435	1939	1.588	1834	1.688	2001	1.687	1999	1.462	1943	1.585
S.H. Duct IVG	322	1923	1.498	1711	1.658	1641	1.767	1738	1.780	1811	1.522	1782	1.653

100% WY

Location	Test 1		Test 2		Test 3		Test 4		Test 5		Test 6		
	Distance From Burner (ft.)	Avg. Gas Temp. (°F)	Time (Sec.)										
Suction Port L1	38	2850	0.300	2935	0.257	2990	0.236	2998	0.264	2895	0.238	2960	0.257
Suction Port L2	53	2777	0.428	2858	0.387	2905	0.337	2900	0.378	2838	0.338	2840	0.367
Suction Port L3	69	2708	0.551	2786	0.472	2815	0.434	2799	0.485	2780	0.432	2738	0.474
Suction Port L4	99	2593	0.807	2661	0.693	2738	0.638	2703	0.713	2678	0.632	2701	0.696
Suction Port L5	156	2419	1.308	2503	1.120	2597	1.023	2507	1.158	2500	1.018	2665	1.119
S.H. Duct IA	209	2253	1.539	2314	1.320	2384	1.204	2311	1.364	2253	1.201	2379	1.316
S.H. Duct IIC	242	2142	1.574	2180	1.349	2228	1.230	2189	1.394	2139	1.226	2291	1.344
S.H. Duct IIIE	272	1979	1.609	2041	1.378	2032	1.256	2039	1.432	2063	1.250	2112	1.372
S.H. Duct IVG	322	1789	1.670	1877	1.429	1896	1.302	1819	1.475	1856	1.292	1915	1.422

90% WY/10% OK

Table D.1 (Cont.) Residence Time and Corresponding Gas Temperatures as a Function of Location

70% WY/30% OK

Location	Distance From Burner (In.)	Test 1		Test 2		Test 3		Test 4		Test 5		Test 6	
		Avg. Gas Temp. (°F)	Time (Sec.)										
Suction Port L1	38	2851	0.261	2838	0.305	2752	0.342	2797	0.335	2812	0.286	2792	0.312
Suction Port L2	53	2865	0.372	2746	0.435	2611	0.490	2675	0.479	2699	0.409	2692	0.445
Suction Port L3	69	2804	0.479	2685	0.580	2577	0.632	2637	0.617	2633	0.527	2663	0.573
Suction Port L4	99	2703	0.701	2630	0.819	2479	0.927	2563	0.903	2561	0.773	2565	0.837
Suction Port L5	156	2524	1.131	2454	1.318	2317	1.499	2387	1.456	2475	1.240	2410	1.349
S.H. Duct IA	209	2329	1.333	2256	1.552	2114	1.768	2178	1.717	2279	1.457	2213	1.589
S.H. Duct IIC	242	2143	1.369	2172	1.595	2034	1.816	2082	1.784	2208	1.498	2107	1.631
S.H. Duct IIIE	272	1866	1.406	2012	1.635	1897	1.862	1908	1.810	2066	1.537	1962	1.672
S.H. Duct IVG	322	1799	1.471	1827	1.709	1729	1.944	1717	1.892	1897	1.606	1787	1.745

70% WY/30% OK CLN

Location	Distance From Burner (In.)	Test 1		Test 2		Test 3	
		Avg. Gas Temp. (°F)	Time (Sec.)	Avg. Gas Temp. (°F)	Time (Sec.)	Avg. Gas Temp. (°F)	Time (Sec.)
Suction Port L1	38	2821	0.305	2911	0.267	2984	0.237
Suction Port L2	53	2724	0.435	2801	0.381	2910	0.338
Suction Port L3	69	2640	0.561	2722	0.491	2798	0.435
Suction Port L4	99	2569	0.823	2665	0.720	2765	0.637
Suction Port L5	156	2335	1.334	2496	1.160	2587	1.024
S.H. Duct IA	209	2090	1.580	2360	1.364	2437	1.205
S.H. Duct IIC	242	2022	1.623	2151	1.399	2285	1.235
S.H. Duct IIIE	272	1886	1.664	2097	1.434	2160	1.264
S.H. Duct IVG	322	1674	1.739	1902	1.494	1990	1.315

Table D.2 Gas Analyses from Pilot-Scale Tests

COAL	TEST ID	O ₂ (%) (CALC.)	E.A. (%) (CALC.)	CO (ppm) (@ 3% O ₂)	CO ₂ (%) (@ 3% O ₂)	SO ₂ (ppm) (@ 3% O ₂)	NO _x (ppm) (@ 3% O ₂)	COAL (lb/hr)	PRIM. AIR (lb/hr)	SEC. AIR (lb/hr)
100% Wyoming	TEST 1	3.6	20.9	N/A	13.6	460	692	352	312	2936
	TEST 2	3.4	19.6	N/A	14.0	476	440	332	306	2729
	TEST 3	3.8	21.9	N/A	14.0	447	540	312	308	2603
	TEST 4	2.6	14.2	247	14.1	475	480	323	316	2498
	TEST 5	5.4	34.3	257	11.9	347	1065	323	309	2999
	TEST 6	4.0	23.4	239	13.0	452	877	323	306	2734
90% Wyoming/ 10% Oklahoma	TEST 1	3.6	20.7	N/A	12.4	363	510	310	321	2660
	TEST 2	3.9	22.5	105	13.0	353	666	348	321	3072
	TEST 3	3.7	21.5	147	12.8	350	582	375	320	3319
	TEST 4	2.5	13.8	132	13.1	394	470	355	294	2944
	TEST 5	5.1	32.3	85	11.9	327	966	355	293	3470
	TEST 6	3.8	21.9	77	13.8	401	1217	340	295	3082
70% Wyoming/ 30% Oklahoma	TEST 1	3.6	21.0	141	13.4	416	1484	329	315	3051
	TEST 2	3.5	19.8	132	15.8	437	1565	295	315	2658
	TEST 3	3.6	20.8	163	15.1	415	1134	267	319	2405
	TEST 4	2.5	13.7	150	16.1	518	892	286	321	2414
	TEST 5	5.3	33.5	144	14.7	412	1579	287	315	2897
	TEST 6	3.9	22.8	51	15.1	473	1259	285	319	2636
70% Wyoming/ 30% Oklahoma Cl.	TEST 1	4.1	24.0	406	14.9	486	1316	287	306	2684
	TEST 2	3.9	22.6	439	14.1	471	1358	319	322	3004
	TEST 3	3.7	21.5	450	15.6	481	1243	355	316	3346

PSO 100%WYOMING COAL TEST 1

COMBUSTION DATA

FUEL FEED RATE (LB/HR)	351.74
ADDITIVE FEED/RATE (LB/HR)	.00
FUEL HHV (BTU/LB)	10225.00
TOTAL HEAT INPUT (MBTU/HR)	4.18
PRIMARY AIR FLOW (LB/HR)	311.95
PRIMARY AIR TEMP. (F)	75.81
SECONDARY AIR FLOW (LB/HR)	2935.63
SECONDARY AIR TEMP. (F)	841.24
TRANSPORT AIR FLOW (LB/HR)	.00
OXYGEN IN FLUE GAS (PCT)	4.40
PERCENT EXCESS AIR	22.88
LOWER FURNACE PEAK FLAME TEMP. (F)	2977.00
LOWER FURNACE RESIDENCE TIME (SEC)	1.16

WATERWALL TEST PANELS

PANEL P1 SURFACE TEMP. (F)	685.20
PANEL P2 SURFACE TEMP. (F)	594.56
PANEL P3 SURFACE TEMP. (F)	703.61
PANEL P4 SURFACE TEMP. (F)	688.06

SUPERHEATER PROBES

DUCT 1 GAS TEMPERATURE (F)	2329.00
DUCT 2 GAS TEMPERATURE (F)	2215.00
DUCT 3 GAS TEMPERATURE (F)	2102.00
DUCT 4 GAS TEMPERATURE (F)	1923.00
EROSION DUCT GAS TEMP. (F)	1200.00
DUCT 1 GAS VELOCITY (FT/SEC)	70.82
DUCT 2 GAS VELOCITY (FT/SEC)	67.93
DUCT 3 GAS VELOCITY (FT/SEC)	65.06
DUCT 4 GAS VELOCITY (FT/SEC)	60.51
ER.DUCT GAS VEL. [1] (FT/SEC)	196.71
ER.DUCT GAS VEL. [2] (FT/SEC)	205.42

ASH

INPUT (LB/HR)	24.27
DUST LOADING (LB/HR)	14.00
CARBON CONVERSION (PCT)	100.000
CARBON HEAT LOSS (PCT)	.000

METHOD 1-----		
FLUE GAS FLOW RATE (LB/HR)	3575.675	
COMPOSITION (MOLES/HR), (PERCENT)		
OXYGEN	4.472	3.67
CARBON DIOXIDE	16.971	13.94
WATER	12.493	10.26
SULFUR DIOXIDE	.055	.05
NITROGEN	87.766	72.08

METHOD 2-----		
FLUE GAS FLOW RATE (LB/HR)	3730.147	
COMPOSITION (MOLES/HR), PERCENT		
OXYGEN	5.595	4.40
CARBON DIOXIDE	16.971	13.35
WATER	12.594	9.91
SULFUR DIOXIDE	.055	.04
NITROGEN	91.935	72.30

	KBTU/HR	PCT
HEAT OUT		
HEAT LOSS FROM REFRACTORY	220.955	5.29
HEAT LOSS FROM PANELS	309.782	7.41
HEAT LOSS FROM WATER COOLED FRAME	143.459	3.43
HEAT LOSS FROM FLY ASH	7.886	.19
HEAT LOSS FROM UNBURNT CARBON	.000	.00
HEAT LOSS FROM ROOF	49.156	1.18
HEAT LOSS FROM S.H. TRANSITION	123.409	2.95
HEAT LOSS FROM S.H. FRAME	129.344	3.09
HEAT LOSS FROM S.H. DUCT	141.029	3.37
HEAT LOSS FROM OBS. PORT	68.714	1.64
HEAT LOSS FROM BURNER	89.346	2.14
HEAT LOSS FROM FURNACE BOTTOM LEFT	101.505	2.43
HEAT LOSS FROM FURNACE BOTTOM RIGHT	98.429	2.35
HEAT LOSS FROM FLUE GAS, [METHOD 1]	2463.004	58.91
HEAT LOSS FROM FLUE GAS, [METHOD 2]	2570.146	61.48

METHOD 1-----TOTAL MATERIAL INPUT (LB/HR)	3599.32
TOTAL MATERIAL OUTPUT (LB/HR)	3598.68
MATERIAL UNACCOUNTED FOR	.02
TOTAL HEAT INPUT (MBTU/HR)	4.18
TOTAL HEAT OUTPUT (MBTU/HR)	4.03
HEAT UNACCOUNTED FOR (PCT)	3.54

METHOD 2-----TOTAL MATERIAL INPUT (LB/HR)	3754.42
TOTAL MATERIAL OUTPUT (LB/HR)	3753.15
MATERIAL UNACCOUNTED FOR (PCT)	.03

TOTAL HEAT OUTPUT (MBTU/HR)	4.14
HEAT UNACCOUNTED FOR (PCT)	.98

RESIDENCE TIME ALONG GAS STREAM

LOCATION	TEMP. (F)	TIME, SEC.
SUCTION PORT L1	2977.	.264
SUCTION PORT L2	2908.	.376
SUCTION PORT L3	2815.	.484
SUCTION PORT L4	2651.	.712
SUCTION PORT L5	2511.	1.155
S.H DUCT 1A	2329.	1.362
S.H DUCT 2C	2215.	1.399
S.H DUCT 3E	2102.	1.435
S.H DUCT 4G	1923.	1.499
DUST LOADING PORT	1200.	1.755

PSO 100% WYOMING COAL TEST 2

COMBUSTION DATA

FUEL FEED RATE (LB/HR)	331.92
ADDITIVE FEED/RATE (LB/HR)	.00
FUEL HHV (BTU/LB)	10225.00
TOTAL HEAT INPUT (MBTU/HR)	3.75
PRIMARY AIR FLOW (LB/HR)	306.37
PRIMARY AIR TEMP. (F)	74.78
SECONDARY AIR FLOW (LB/HR)	2728.77
SECONDARY AIR TEMP. (F)	578.33
TRANSPORT AIR FLOW (LB/HR)	.00
OXYGEN IN FLUE GAS (PCT)	4.93
PERCENT EXCESS AIR	21.69
LOWER FURNACE PEAK FLAME TEMP. (F)	2831.95
LOWER FURNACE RESIDENCE TIME (SEC)	1.28

WATERWALL TEST PANELS

PANEL P1 SURFACE TEMP. (F)	672.03
PANEL P2 SURFACE TEMP. (F)	586.02
PANEL P3 SURFACE TEMP. (F)	697.77
PANEL P4 SURFACE TEMP. (F)	691.56

SUPERHEATER PROBES

DUCT 1 GAS TEMPERATURE (F)	2178.25
DUCT 2 GAS TEMPERATURE (F)	2082.53
DUCT 3 GAS TEMPERATURE (F)	1938.83
DUCT 4 GAS TEMPERATURE (F)	1710.60
EROSION DUCT GAS TEMP. (F)	1302.00
DUCT 1 GAS VELOCITY (FT/SEC)	62.65
DUCT 2 GAS VELOCITY (FT/SEC)	60.38
DUCT 3 GAS VELOCITY (FT/SEC)	56.97
DUCT 4 GAS VELOCITY (FT/SEC)	51.55
ER.DUCT GAS VEL.[1] (FT/SEC)	195.27
ER.DUCT GAS VEL.[2] (FT/SEC)	212.62

ASH

INPUT (LB/HR)	22.90
DUST LOADING (LB/HR)	14.25
CARBON CONVERSION (PCT)	100.000
CARBON HEAT LOSS (PCT)	.000

METHOD 1-----

FLUE GAS FLOW RATE (LB/HR)	3344.735	
COMPOSITION (MOLES/HR), (PERCENT)		
OXYGEN	4.005	3.52
CARBON DIOXIDE	16.015	14.06
WATER	11.770	10.34
SULFUR DIOXIDE	.052	.05
NITROGEN	82.026	72.04

METHOD 2-----

FLUE GAS FLOW RATE (LB/HR)	3634.646	
COMPOSITION (MOLES/HR), PERCENT		
OXYGEN	6.113	4.93
CARBON DIOXIDE	16.015	12.92
WATER	11.960	9.65
SULFUR DIOXIDE	.052	.04
NITROGEN	89.849	72.47

	KBTU/HR	PCT
HEAT OUT		
HEAT LOSS FROM REFRACTORY	207.042	5.52
HEAT LOSS FROM PANELS	292.095	7.79
HEAT LOSS FROM WATER COOLED FRAME	135.068	3.60
HEAT LOSS FROM FLY ASH	7.494	.20
HEAT LOSS FROM UNBURNT CARBON	.000	.00
HEAT LOSS FROM ROOF	43.201	1.15
HEAT LOSS FROM S.H. TRANSITION	115.167	3.07
HEAT LOSS FROM S.H. FRAME	117.179	3.12
HEAT LOSS FROM S.H. DUCT	144.421	3.85
HEAT LOSS FROM OBS. PORT	57.287	1.53
HEAT LOSS FROM BURNER	54.665	1.46
HEAT LOSS FROM FURNACE BOTTOM LEFT	76.116	2.03
HEAT LOSS FROM FURNACE BOTTOM RIGHT	76.116	2.03
HEAT LOSS FROM FLUE GAS, [METHOD 1]	2125.691	56.67
HEAT LOSS FROM FLUE GAS, [METHOD 2]	2309.772	61.58

METHOD 1-----TOTAL MATERIAL INPUT (LB/HR)	3367.05
TOTAL MATERIAL OUTPUT (LB/HR)	3366.98
MATERIAL UNACCOUNTED FOR	.00
TOTAL HEAT INPUT (MBTU/HR)	3.75
TOTAL HEAT OUTPUT (MBTU/HR)	3.53
HEAT UNACCOUNTED FOR (PCT)	6.00

METHOD 2-----TOTAL MATERIAL INPUT (LB/HR)	3657.55
TOTAL MATERIAL OUTPUT (LB/HR)	3656.90
MATERIAL UNACCOUNTED FOR (PCT)	.02

TOTAL HEAT OUTPUT (MBTU/HR)	3.71
HEAT UNACCOUNTED FOR (PCT)	1.10

RESIDENCE TIME ALONG GAS STREAM

LOCATION	TEMP. (F)	TIME, SEC.
SUCTION PORT L1	2832.	.295
SUCTION PORT L2	2761.	.420
SUCTION PORT L3	2664.	.541
SUCTION PORT L4	2595.	.793
SUCTION PORT L5	2428.	1.278
S.H DUCT 1A	2178.	1.508
S.H DUCT 2C	2083.	1.549
S.H DUCT 3E	1939.	1.588
S.H DUCT 4G	1711.	1.658
DUST LOADING PORT	1302.	1.928

PSO 100%WYOMING COAL TEST 3

COMBUSTION DATA

FUEL FEED RATE (LB/HR)	311.76
ADDITIVE FEED/RATE (LB/HR)	.00
FUEL HHV (BTU/LB)	10225.00
TOTAL HEAT INPUT (MBTU/HR)	3.53
PRIMARY AIR FLOW (LB/HR)	308.19
PRIMARY AIR TEMP. (F)	79.01
SECONDARY AIR FLOW (LB/HR)	2602.90
SECONDARY AIR TEMP. (F)	577.78
TRANSPORT AIR FLOW (LB/HR)	.00
OXYGEN IN FLUE GAS (PCT)	4.81
PERCENT EXCESS AIR	24.27
LOWER FURNACE PEAK FLAME TEMP. (F)	2822.33
LOWER FURNACE RESIDENCE TIME (SEC)	1.36

WATERWALL TEST PANELS

PANEL P1 SURFACE TEMP. (F)	689.58
PANEL P2 SURFACE TEMP. (F)	566.95
PANEL P3 SURFACE TEMP. (F)	674.27
PANEL P4 SURFACE TEMP. (F)	674.02

SUPERHEATER PROBES

DUCT 1 GAS TEMPERATURE (F)	2139.81
DUCT 2 GAS TEMPERATURE (F)	1993.29
DUCT 3 GAS TEMPERATURE (F)	1834.31
DUCT 4 GAS TEMPERATURE (F)	1640.85
EROSION DUCT GAS TEMP. (F)	1200.00
DUCT 1 GAS VELOCITY (FT/SEC)	59.13
DUCT 2 GAS VELOCITY (FT/SEC)	55.80
DUCT 3 GAS VELOCITY (FT/SEC)	52.18
DUCT 4 GAS VELOCITY (FT/SEC)	47.78
ER.DUCT GAS VEL.[1] (FT/SEC)	176.19
ER.DUCT GAS VEL.[2] (FT/SEC)	186.74

ASH

INPUT (LB/HR)	21.51
DUST LOADING (LB/HR)	12.00
CARBON CONVERSION (PCT)	100.000
CARBON HEAT LOSS (PCT)	.000

METHOD 1-----		
FLUE GAS FLOW RATE (LB/HR)	3201.906	
COMPOSITION (MOLES/HR), (PERCENT)		
OXYGEN	4.201	3.85
CARBON DIOXIDE	15.043	13.79
WATER	11.095	10.17
SULFUR DIOXIDE	.049	.04
NITROGEN	78.671	72.14

METHOD 2-----		
FLUE GAS FLOW RATE (LB/HR)	3388.902	
COMPOSITION (MOLES/HR), PERCENT		
OXYGEN	5.560	4.81
CARBON DIOXIDE	15.043	13.01
WATER	11.217	9.70
SULFUR DIOXIDE	.049	.04
NITROGEN	83.717	72.43

	KBTU/HR	PCT
HEAT OUT		
HEAT LOSS FROM REFRACTORY	192.740	5.47
HEAT LOSS FROM PANELS	278.474	7.90
HEAT LOSS FROM WATER COOLED FRAME	119.301	3.38
HEAT LOSS FROM FLY ASH	6.182	.18
HEAT LOSS FROM UNBURNT CARBON	.000	.00
HEAT LOSS FROM ROOF	33.479	.95
HEAT LOSS FROM S.H. TRANSITION	107.778	3.06
HEAT LOSS FROM S.H. FRAME	75.925	2.15
HEAT LOSS FROM S.H. DUCT	132.523	3.76
HEAT LOSS FROM OBS. PORT	42.265	1.20
HEAT LOSS FROM BURNER	57.083	1.62
HEAT LOSS FROM FURNACE BOTTOM LEFT	68.529	1.94
HEAT LOSS FROM FURNACE BOTTOM RIGHT	68.529	1.94
HEAT LOSS FROM FLUE GAS, [METHOD 1]	1988.349	56.40
HEAT LOSS FROM FLUE GAS, [METHOD 2]	2104.154	59.69

METHOD 1-----TOTAL MATERIAL INPUT (LB/HR)	3222.86
TOTAL MATERIAL OUTPUT (LB/HR)	3220.91
MATERIAL UNACCOUNTED FOR	.06
TOTAL HEAT INPUT (MBTU/HR)	3.53
TOTAL HEAT OUTPUT (MBTU/HR)	3.24
HEAT UNACCOUNTED FOR (PCT)	8.01

METHOD 2-----TOTAL MATERIAL INPUT (LB/HR)	3410.42
TOTAL MATERIAL OUTPUT (LB/HR)	3407.90
MATERIAL UNACCOUNTED FOR (PCT)	.07

TOTAL HEAT OUTPUT (MBTU/HR)	3.36
HEAT UNACCOUNTED FOR (PCT)	4.72

RESIDENCE TIME ALONG GAS STREAM

LOCATION	TEMP. (F)	TIME, SEC.
SUCTION PORT L1	2822.	.308
SUCTION PORT L2	2731.	.440
SUCTION PORT L3	2656.	.567
SUCTION PORT L4	2521.	.834
SUCTION PORT L5	2340.	1.354
S.H DUCT 1A	2140.	1.600
S.H DUCT 2C	1993.	1.644
S.H DUCT 3E	1834.	1.688
S.H DUCT 4G	1641.	1.767
DUST LOADING PORT	1200.	2.070

PSO 100% WYOMING COAL TEST 4

COMBUSTION DATA

FUEL FEED RATE (LB/HR)	322.70
ADDITIVE FEED/RATE (LB/HR)	.00
FUEL HHV (BTU/LB)	10225.00
TOTAL HEAT INPUT (MBTU/HR)	3.55
PRIMARY AIR FLOW (LB/HR)	315.88
PRIMARY AIR TEMP. (F)	74.25
SECONDARY AIR FLOW (LB/HR)	2497.73
SECONDARY AIR TEMP. (F)	462.30
TRANSPORT AIR FLOW (LB/HR)	.00
OXYGEN IN FLUE GAS (PCT)	4.64
PERCENT EXCESS AIR	16.03
LOWER FURNACE PEAK FLAME TEMP. (F)	2805.64
LOWER FURNACE RESIDENCE TIME (SEC)	1.38

WATERWALL TEST PANELS

PANEL P1 SURFACE TEMP. (F)	702.94
PANEL P2 SURFACE TEMP. (F)	583.02
PANEL P3 SURFACE TEMP. (F)	691.04
PANEL P4 SURFACE TEMP. (F)	684.40

SUPERHEATER PROBES

DUCT 1 GAS TEMPERATURE (F)	2235.84
DUCT 2 GAS TEMPERATURE (F)	2122.00
DUCT 3 GAS TEMPERATURE (F)	2001.15
DUCT 4 GAS TEMPERATURE (F)	1736.28
EROSION DUCT GAS TEMP. (F)	1283.00
DUCT 1 GAS VELOCITY (FT/SEC)	59.55
DUCT 2 GAS VELOCITY (FT/SEC)	57.03
DUCT 3 GAS VELOCITY (FT/SEC)	54.36
DUCT 4 GAS VELOCITY (FT/SEC)	48.51
ER.DUCT GAS VEL.[1] (FT/SEC)	179.67
ER.DUCT GAS VEL.[2] (FT/SEC)	200.82

ASH

INPUT (LB/HR)	22.27
DUST LOADING (LB/HR)	12.90
CARBON CONVERSION (PCT)	100.000
CARBON HEAT LOSS (PCT)	.000

METHOD 1-----		
FLUE GAS FLOW RATE (LB/HR)	3114.581	
COMPOSITION (MOLES/HR), (PERCENT)		
OXYGEN	2.897	2.74
CARBON DIOXIDE	15.570	14.70
WATER	11.353	10.72
SULFUR DIOXIDE	.050	.05
NITROGEN	76.044	71.80

METHOD 2-----		
FLUE GAS FLOW RATE (LB/HR)	3471.775	
COMPOSITION (MOLES/HR), PERCENT		
OXYGEN	5.493	4.64
CARBON DIOXIDE	15.570	13.15
WATER	11.587	9.79
SULFUR DIOXIDE	.050	.04
NITROGEN	85.683	72.38

	KBTU/HR	PCT
HEAT OUT		
HEAT LOSS FROM REFRACTORY	201.928	5.69
HEAT LOSS FROM PANELS	282.745	7.96
HEAT LOSS FROM WATER COOLED FRAME	123.154	3.47
HEAT LOSS FROM FLY ASH	6.971	.20
HEAT LOSS FROM UNBURNT CARBON	.000	.00
HEAT LOSS FROM ROOF	37.515	1.06
HEAT LOSS FROM S.H. TRANSITION	117.199	3.30
HEAT LOSS FROM S.H. FRAME	91.668	2.58
HEAT LOSS FROM S.H. DUCT	122.180	3.44
HEAT LOSS FROM OBS. PORT	47.884	1.35
HEAT LOSS FROM BURNER	46.570	1.31
HEAT LOSS FROM FURNACE BOTTOM LEFT	68.782	1.94
HEAT LOSS FROM FURNACE BOTTOM RIGHT	68.782	1.94
HEAT LOSS FROM FLUE GAS, [METHOD 1]	2043.034	57.52
HEAT LOSS FROM FLUE GAS, [METHOD 2]	2277.831	64.14

METHOD 1-----TOTAL MATERIAL INPUT (LB/HR)	3136.30
TOTAL MATERIAL OUTPUT (LB/HR)	3134.48
MATERIAL UNACCOUNTED FOR	.06
TOTAL HEAT INPUT (MBTU/HR)	3.55
TOTAL HEAT OUTPUT (MBTU/HR)	3.34
HEAT UNACCOUNTED FOR (PCT)	5.88

METHOD 2-----TOTAL MATERIAL INPUT (LB/HR)	3494.04
TOTAL MATERIAL OUTPUT (LB/HR)	3491.67
MATERIAL UNACCOUNTED FOR (PCT)	.07

TOTAL HEAT OUTPUT (MBTU/HR)	3.58
HEAT UNACCOUNTED FOR (PCT)	-.73

RESIDENCE TIME ALONG GAS STREAM

LOCATION	TEMP. (F)	TIME, SEC.
SUCTION PORT L1	2806.	.319
SUCTION PORT L2	2754.	.455
SUCTION PORT L3	2697.	.584
SUCTION PORT L4	2543.	.856
SUCTION PORT L5	2436.	1.381
S.H DUCT 1A	2236.	1.626
S.H DUCT 2C	2122.	1.667
S.H DUCT 3E	2001.	1.707
S.H DUCT 4G	1736.	1.780
DUST LOADING PORT	1283.	2.062

PSO 100% WYOMING COAL TEST 5

COMBUSTION DATA

FUEL FEED RATE (LB/HR)	323.31
ADDITIVE FEED/RATE (LB/HR)	.00
FUEL HHV (BTU/LB)	10225.00
TOTAL HEAT INPUT (MBTU/HR)	4.12
PRIMARY AIR FLOW (LB/HR)	308.88
PRIMARY AIR TEMP. (F)	82.94
SECONDARY AIR FLOW (LB/HR)	2999.18
SECONDARY AIR TEMP. (F)	1126.99
TRANSPORT AIR FLOW (LB/HR)	.00
OXYGEN IN FLUE GAS (PCT)	7.14
PERCENT EXCESS AIR	36.17
LOWER FURNACE PEAK FLAME TEMP. (F)	2814.66
LOWER FURNACE RESIDENCE TIME (SEC)	1.19

WATERWALL TEST PANELS

PANEL P1 SURFACE TEMP. (F)	722.69
PANEL P2 SURFACE TEMP. (F)	581.29
PANEL P3 SURFACE TEMP. (F)	688.77
PANEL P4 SURFACE TEMP. (F)	698.73

SUPERHEATER PROBES

DUCT 1 GAS TEMPERATURE (F)	2257.84
DUCT 2 GAS TEMPERATURE (F)	2109.77
DUCT 3 GAS TEMPERATURE (F)	1999.16
DUCT 4 GAS TEMPERATURE (F)	1811.17
EROSION DUCT GAS TEMP. (F)	1291.00
DUCT 1 GAS VELOCITY (FT/SEC)	69.83
DUCT 2 GAS VELOCITY (FT/SEC)	66.02
DUCT 3 GAS VELOCITY (FT/SEC)	63.18
DUCT 4 GAS VELOCITY (FT/SEC)	58.35
ER.DUCT GAS VEL.[1] (FT/SEC)	209.94
ER.DUCT GAS VEL.[2] (FT/SEC)	239.06

ASH

INPUT (LB/HR)	22.31
DUST LOADING (LB/HR)	12.90
CARBON CONVERSION (PCT)	100.000
CARBON HEAT LOSS (PCT)	.000

METHOD 1-----		
FLUE GAS FLOW RATE (LB/HR)	3609.695	
COMPOSITION (MOLES/HR), (PERCENT)		
OXYGEN	6.458	5.24
CARBON DIOXIDE	15.600	12.66
WATER	11.696	9.49
SULFUR DIOXIDE	.051	.04
NITROGEN	89.389	72.56

METHOD 2-----		
FLUE GAS FLOW RATE (LB/HR)	4099.231	
COMPOSITION (MOLES/HR), PERCENT		
OXYGEN	10.016	7.14
CARBON DIOXIDE	15.600	11.12
WATER	12.017	8.57
SULFUR DIOXIDE	.051	.04
NITROGEN	102.599	73.14

	KBTU/HR	PCT
HEAT OUT		
HEAT LOSS FROM REFRACTORY	202.289	4.91
HEAT LOSS FROM PANELS	290.368	7.05
HEAT LOSS FROM WATER COOLED FRAME	124.720	3.03
HEAT LOSS FROM FLY ASH	7.014	.17
HEAT LOSS FROM UNBURNT CARBON	.000	.00
HEAT LOSS FROM ROOF	32.317	.78
HEAT LOSS FROM S.H. TRANSITION	110.491	2.68
HEAT LOSS FROM S.H. FRAME	91.729	2.23
HEAT LOSS FROM S.H. DUCT	130.147	3.16
HEAT LOSS FROM OBS. PORT	46.559	1.13
HEAT LOSS FROM BURNER	129.070	3.13
HEAT LOSS FROM FURNACE BOTTOM LEFT	80.321	1.95
HEAT LOSS FROM FURNACE BOTTOM RIGHT	80.321	1.95
HEAT LOSS FROM FLUE GAS, [METHOD 1]	2389.720	58.00
HEAT LOSS FROM FLUE GAS, [METHOD 2]	2714.735	65.89

METHOD 1-----	TOTAL MATERIAL INPUT (LB/HR)	3631.37
	TOTAL MATERIAL OUTPUT (LB/HR)	3629.60
	MATERIAL UNACCOUNTED FOR	.05
	TOTAL HEAT INPUT (MBTU/HR)	4.12
	TOTAL HEAT OUTPUT (MBTU/HR)	3.79
	HEAT UNACCOUNTED FOR (PCT)	7.90

METHOD 2-----	TOTAL MATERIAL INPUT (LB/HR)	4121.54
	TOTAL MATERIAL OUTPUT (LB/HR)	4119.13
	MATERIAL UNACCOUNTED FOR (PCT)	.06

TOTAL HEAT OUTPUT (MBTU/HR)	4.12
HEAT UNACCOUNTED FOR (PCT)	.01

RESIDENCE TIME ALONG GAS STREAM

LOCATION	TEMP. (F)	TIME, SEC.
SUCTION PORT L1	2815.	.274
SUCTION PORT L2	2721.	.391
SUCTION PORT L3	2678.	.503
SUCTION PORT L4	2591.	.735
SUCTION PORT L5	2430.	1.184
S.H DUCT 1A	2258.	1.394
S.H DUCT 2C	2110.	1.428
S.H DUCT 3E	1999.	1.462
S.H DUCT 4G	1811.	1.522
DUST LOADING PORT	1291.	1.756

PSO 100%WYOMING COAL TEST 6

COMBUSTION DATA

FUEL FEED RATE (LB/HR)	322.96
ADDITIVE FEED/RATE (LB/HR)	.00
FUEL HHV (BTU/LB)	10225.00
TOTAL HEAT INPUT (MBTU/HR)	3.72
PRIMARY AIR FLOW (LB/HR)	305.87
PRIMARY AIR TEMP. (F)	79.94
SECONDARY AIR FLOW (LB/HR)	2733.58
SECONDARY AIR TEMP. (F)	665.33
TRANSPORT AIR FLOW (LB/HR)	.00
OXYGEN IN FLUE GAS (PCT)	5.70
PERCENT EXCESS AIR	25.25
LOWER FURNACE PEAK FLAME TEMP. (F)	2864.55
LOWER FURNACE RESIDENCE TIME (SEC)	1.28

WATERWALL TEST PANELS

PANEL P1 SURFACE TEMP. (F)	694.29
PANEL P2 SURFACE TEMP. (F)	575.86
PANEL P3 SURFACE TEMP. (F)	694.21
PANEL P4 SURFACE TEMP. (F)	701.39

SUPERHEATER PROBES

DUCT 1 GAS TEMPERATURE (F)	2195.00
DUCT 2 GAS TEMPERATURE (F)	2082.34
DUCT 3 GAS TEMPERATURE (F)	1943.12
DUCT 4 GAS TEMPERATURE (F)	1781.60
EROSION DUCT GAS TEMP. (F)	1239.00
DUCT 1 GAS VELOCITY (FT/SEC)	63.01
DUCT 2 GAS VELOCITY (FT/SEC)	60.34
DUCT 3 GAS VELOCITY (FT/SEC)	57.04
DUCT 4 GAS VELOCITY (FT/SEC)	53.20
ER.DUCT GAS VEL. [1] (FT/SEC)	188.18
ER.DUCT GAS VEL. [2] (FT/SEC)	209.64

ASH

INPUT (LB/HR)	22.28
DUST LOADING (LB/HR)	13.05
CARBON CONVERSION (PCT)	100.000
CARBON HEAT LOSS (PCT)	.000

METHOD 1-----

FLUE GAS FLOW RATE (LB/HR)	3340.705	
COMPOSITION (MOLES/HR), (PERCENT)		
OXYGEN	4.524	3.98
CARBON DIOXIDE	15.583	13.69
WATER	11.509	10.11
SULFUR DIOXIDE	.050	.04
NITROGEN	82.139	72.17

METHOD 2-----

FLUE GAS FLOW RATE (LB/HR)	3712.500	
COMPOSITION (MOLES/HR), PERCENT		
OXYGEN	7.227	5.70
CARBON DIOXIDE	15.583	12.29
WATER	11.753	9.27
SULFUR DIOXIDE	.050	.04
NITROGEN	92.172	72.70

	KBTU/HR	PCT
HEAT OUT		
HEAT LOSS FROM REFRACTORY	215.379	5.79
HEAT LOSS FROM PANELS	300.226	8.07
HEAT LOSS FROM WATER COOLED FRAME	124.836	3.36
HEAT LOSS FROM FLY ASH	6.900	.19
HEAT LOSS FROM UNBURNT CARBON	.000	.00
HEAT LOSS FROM ROOF	33.982	.91
HEAT LOSS FROM S.H. TRANSITION	109.281	2.94
HEAT LOSS FROM S.H. FRAME	91.504	2.46
HEAT LOSS FROM S.H. DUCT	124.050	3.34
HEAT LOSS FROM OBS. PORT	50.442	1.36
HEAT LOSS FROM BURNER	70.612	1.90
HEAT LOSS FROM FURNACE BOTTOM LEFT	75.323	2.03
HEAT LOSS FROM FURNACE BOTTOM RIGHT	75.323	2.03
HEAT LOSS FROM FLUE GAS, [METHOD 1]	2138.923	57.52
HEAT LOSS FROM FLUE GAS, [METHOD 2]	2376.951	63.93

METHOD 1-----TOTAL MATERIAL INPUT (LB/HR)	3362.40
TOTAL MATERIAL OUTPUT (LB/HR)	3360.76
MATERIAL UNACCOUNTED FOR	.05
TOTAL HEAT INPUT (MBTU/HR)	3.72
TOTAL HEAT OUTPUT (MBTU/HR)	3.50
HEAT UNACCOUNTED FOR (PCT)	5.87

METHOD 2-----TOTAL MATERIAL INPUT (LB/HR)	3734.79
TOTAL MATERIAL OUTPUT (LB/HR)	3732.55
MATERIAL UNACCOUNTED FOR (PCT)	.06

TOTAL HEAT OUTPUT (MBTU/HR)	3.74
HEAT UNACCOUNTED FOR (PCT)	-.53

RESIDENCE TIME ALONG GAS STREAM

LOCATION	TEMP. (F)	TIME, SEC.
SUCTION PORT L1	2865.	.292
SUCTION PORT L2	2752.	.417
SUCTION PORT L3	2714.	.537
SUCTION PORT L4	2606.	.786
SUCTION PORT L5	2373.	1.275
S.H DUCT 1A	2195.	1.508
S.H DUCT 2C	2082.	1.547
S.H DUCT 3E	1943.	1.585
S.H DUCT 4G	1782.	1.653
DUST LOADING PORT	1239.	1.916

PSO 90%WY/10%OK BLEND TEST 1

COMBUSTION DATA

FUEL FEED RATE (LB/HR)	309.70
ADDITIVE FEED/RATE (LB/HR)	.00
FUEL HHV (BTU/LB)	10552.00
TOTAL HEAT INPUT (MBTU/HR)	3.94
PRIMARY AIR FLOW (LB/HR)	321.00
PRIMARY AIR TEMP. (F)	80.16
SECONDARY AIR FLOW (LB/HR)	2659.92
SECONDARY AIR TEMP. (F)	1057.36
TRANSPORT AIR FLOW (LB/HR)	.00
OXYGEN IN FLUE GAS (PCT)	4.85
PERCENT EXCESS AIR	23.93
LOWER FURNACE PEAK FLAME TEMP. (F)	2849.75
LOWER FURNACE RESIDENCE TIME (SEC)	1.31

WATERWALL TEST PANELS

PANEL P1 SURFACE TEMP. (F)	704.83
PANEL P2 SURFACE TEMP. (F)	573.79
PANEL P3 SURFACE TEMP. (F)	692.64
PANEL P4 SURFACE TEMP. (F)	698.57

SUPERHEATER PROBES

DUCT 1 GAS TEMPERATURE (F)	2253.06
DUCT 2 GAS TEMPERATURE (F)	2141.93
DUCT 3 GAS TEMPERATURE (F)	1979.13
DUCT 4 GAS TEMPERATURE (F)	1788.90
EROSION DUCT GAS TEMP. (F)	1315.00
DUCT 1 GAS VELOCITY (FT/SEC)	62.85
DUCT 2 GAS VELOCITY (FT/SEC)	60.27
DUCT 3 GAS VELOCITY (FT/SEC)	56.50
DUCT 4 GAS VELOCITY (FT/SEC)	52.09
ER.DUCT GAS VEL.[1] (FT/SEC)	191.88
ER.DUCT GAS VEL.[2] (FT/SEC)	204.05

ASH

INPUT (LB/HR)	22.61
DUST LOADING (LB/HR)	13.50
CARBON CONVERSION (PCT)	100.000
CARBON HEAT LOSS (PCT)	.000

METHOD 1-----		
FLUE GAS FLOW RATE (LB/HR)	3268.593	
COMPOSITION (MOLES/HR), (PERCENT)		
OXYGEN	4.262	3.84
CARBON DIOXIDE	15.433	13.89
WATER	10.753	9.68
SULFUR DIOXIDE	.058	.05
NITROGEN	80.566	72.53

METHOD 2-----		
FLUE GAS FLOW RATE (LB/HR)	3470.345	
COMPOSITION (MOLES/HR), PERCENT		
OXYGEN	5.729	4.85
CARBON DIOXIDE	15.433	13.07
WATER	10.885	9.22
SULFUR DIOXIDE	.058	.05
NITROGEN	86.011	72.82

	KBTU/HR	PCT
HEAT OUT		
HEAT LOSS FROM REFRACTORY	230.204	5.84
HEAT LOSS FROM PANELS	308.916	7.83
HEAT LOSS FROM WATER COOLED FRAME	128.204	3.25
HEAT LOSS FROM FLY ASH	7.334	.19
HEAT LOSS FROM UNBURNT CARBON	.000	.00
HEAT LOSS FROM ROOF	20.309	.51
HEAT LOSS FROM S.H. TRANSITION	109.161	2.77
HEAT LOSS FROM S.H. FRAME	101.058	2.56
HEAT LOSS FROM S.H. DUCT	107.298	2.72
HEAT LOSS FROM OBS. PORT	67.863	1.72
HEAT LOSS FROM BURNER	192.677	4.89
HEAT LOSS FROM FURNACE BOTTOM LEFT	89.924	2.28
HEAT LOSS FROM FURNACE BOTTOM RIGHT	89.924	2.28
HEAT LOSS FROM FLUE GAS, [METHOD 1]	2152.777	54.59
HEAT LOSS FROM FLUE GAS, [METHOD 2]	2286.476	57.98

METHOD 1-----	TOTAL MATERIAL INPUT (LB/HR)	3290.63
	TOTAL MATERIAL OUTPUT (LB/HR)	3290.59
	MATERIAL UNACCOUNTED FOR	.00
	TOTAL HEAT INPUT (MBTU/HR)	3.94
	TOTAL HEAT OUTPUT (MBTU/HR)	3.69
	HEAT UNACCOUNTED FOR (PCT)	6.49

METHOD 2-----	TOTAL MATERIAL INPUT (LB/HR)	3492.96
	TOTAL MATERIAL OUTPUT (LB/HR)	3492.34
	MATERIAL UNACCOUNTED FOR (PCT)	.02

TOTAL HEAT OUTPUT (MBTU/HR)	3.82
HEAT UNACCOUNTED FOR (PCT)	3.10

RESIDENCE TIME ALONG GAS STREAM

LOCATION	TEMP. (F)	TIME, SEC.
SUCTION PORT L1	2850.	.300
SUCTION PORT L2	2777.	.428
SUCTION PORT L3	2708.	.551
SUCTION PORT L4	2593.	.807
SUCTION PORT L5	2419.	1.306
S.H DUCT 1A	2253.	1.539
S.H DUCT 2C	2142.	1.580
S.H DUCT 3E	1979.	1.620
S.H DUCT 4G	1789.	1.693
DUST LOADING PORT	1315.	1.970

PSO 90%WY/10%OK TEST 2

COMBUSTION DATA

FUEL FEED RATE (LB/HR)	348.38
ADDITIVE FEED/RATE (LB/HR)	.00
FUEL HHV (BTU/LB)	10552.00
TOTAL HEAT INPUT (MBTU/HR)	4.37
PRIMARY AIR FLOW (LB/HR)	320.55
PRIMARY AIR TEMP. (F)	79.79
SECONDARY AIR FLOW (LB/HR)	3072.30
SECONDARY AIR TEMP. (F)	945.99
TRANSPORT AIR FLOW (LB/HR)	.00
OXYGEN IN FLUE GAS (PCT)	4.75
PERCENT EXCESS AIR	25.31
LOWER FURNACE PEAK FLAME TEMP. (F)	2934.73
LOWER FURNACE RESIDENCE TIME (SEC)	1.12

WATERWALL TEST PANELS

PANEL P1 SURFACE TEMP. (F)	705.78
PANEL P2 SURFACE TEMP. (F)	578.23
PANEL P3 SURFACE TEMP. (F)	702.51
PANEL P4 SURFACE TEMP. (F)	701.73

SUPERHEATER PROBES

DUCT 1 GAS TEMPERATURE (F)	2314.33
DUCT 2 GAS TEMPERATURE (F)	2180.08
DUCT 3 GAS TEMPERATURE (F)	2040.64
DUCT 4 GAS TEMPERATURE (F)	1877.16
EROSION DUCT GAS TEMP. (F)	1303.00
DUCT 1 GAS VELOCITY (FT/SEC)	73.15
DUCT 2 GAS VELOCITY (FT/SEC)	69.61
DUCT 3 GAS VELOCITY (FT/SEC)	65.94
DUCT 4 GAS VELOCITY (FT/SEC)	61.63
ER.DUCT GAS VEL.[1] (FT/SEC)	216.93
ER.DUCT GAS VEL.[2] (FT/SEC)	226.76

ASH

INPUT (LB/HR)	24.04
DUST LOADING (LB/HR)	14.50
CARBON CONVERSION (PCT)	100.000
CARBON HEAT LOSS (PCT)	.000

METHOD 1-----

FLUE GAS FLOW RATE (LB/HR)	3718.191	
COMPOSITION (MOLES/HR), (PERCENT)		
OXYGEN	5.094	4.03
CARBON DIOXIDE	17.361	13.73
WATER	12.199	9.65
SULFUR DIOXIDE	.054	.04
NITROGEN	91.723	72.55

METHOD 2-----

FLUE GAS FLOW RATE (LB/HR)	3882.189	
COMPOSITION (MOLES/HR), PERCENT		
OXYGEN	6.277	4.75
CARBON DIOXIDE	17.361	13.14
WATER	12.307	9.31
SULFUR DIOXIDE	.054	.04
NITROGEN	96.158	72.76

	KBTU/HR	PCT
HEAT OUT		
HEAT LOSS FROM REFRACTORY	232.560	5.32
HEAT LOSS FROM PANELS	340.295	7.79
HEAT LOSS FROM WATER COOLED FRAME	129.685	2.97
HEAT LOSS FROM FLY ASH	8.100	.19
HEAT LOSS FROM UNBURNT CARBON	.000	.00
HEAT LOSS FROM ROOF	41.404	.95
HEAT LOSS FROM S.H. TRANSITION	121.607	2.78
HEAT LOSS FROM S.H. FRAME	102.434	2.35
HEAT LOSS FROM S.H. DUCT	136.138	3.12
HEAT LOSS FROM OBS. PORT	54.778	1.25
HEAT LOSS FROM BURNER	161.336	3.69
HEAT LOSS FROM FURNACE BOTTOM LEFT	79.027	1.81
HEAT LOSS FROM FURNACE BOTTOM RIGHT	79.027	1.81
HEAT LOSS FROM FLUE GAS, [METHOD 1]	2531.624	57.96
HEAT LOSS FROM FLUE GAS, [METHOD 2]	2644.227	60.54

METHOD 1-----TOTAL MATERIAL INPUT (LB/HR)	3741.23
TOTAL MATERIAL OUTPUT (LB/HR)	3742.19
MATERIAL UNACCOUNTED FOR	-.03
TOTAL HEAT INPUT (MBTU/HR)	4.37
TOTAL HEAT OUTPUT (MBTU/HR)	4.10
HEAT UNACCOUNTED FOR (PCT)	6.11

METHOD 2-----TOTAL MATERIAL INPUT (LB/HR)	3906.23
TOTAL MATERIAL OUTPUT (LB/HR)	3906.19
MATERIAL UNACCOUNTED FOR (PCT)	.00

TOTAL HEAT OUTPUT (MBTU/HR)	4.21
HEAT UNACCOUNTED FOR (PCT)	3.53

RESIDENCE TIME ALONG GAS STREAM

LOCATION	TEMP. (F)	TIME, SEC.
SUCTION PORT L1	2935.	.257
SUCTION PORT L2	2858.	.367
SUCTION PORT L3	2786.	.472
SUCTION PORT L4	2661.	.692
SUCTION PORT L5	2503.	1.119
S.H DUCT 1A	2314.	1.319
S.H DUCT 2C	2180.	1.355
S.H DUCT 3E	2041.	1.390
S.H DUCT 4G	1877.	1.452
DUST LOADING PORT	1303.	1.695

PSO 90%WY/10%OK TEST 3

COMBUSTION DATA

FUEL FEED RATE (LB/HR)	374.96
ADDITIVE FEED/RATE (LB/HR)	.00
FUEL HHV (BTU/LB)	10552.00
TOTAL HEAT INPUT (MBTU/HR)	4.77
PRIMARY AIR FLOW (LB/HR)	319.56
PRIMARY AIR TEMP. (F)	81.79
SECONDARY AIR FLOW (LB/HR)	3319.13
SECONDARY AIR TEMP. (F)	1019.32
TRANSPORT AIR FLOW (LB/HR)	.00
OXYGEN IN FLUE GAS (PCT)	4.75
PERCENT EXCESS AIR	24.95
LOWER FURNACE PEAK FLAME TEMP. (F)	2990.39
LOWER FURNACE RESIDENCE TIME (SEC)	1.03

WATERWALL TEST PANELS

PANEL P1 SURFACE TEMP. (F)	705.82
PANEL P2 SURFACE TEMP. (F)	580.04
PANEL P3 SURFACE TEMP. (F)	704.65
PANEL P4 SURFACE TEMP. (F)	702.64

SUPERHEATER PROBES

DUCT 1 GAS TEMPERATURE (F)	2383.60
DUCT 2 GAS TEMPERATURE (F)	2227.99
DUCT 3 GAS TEMPERATURE (F)	2032.25
DUCT 4 GAS TEMPERATURE (F)	1896.33
EROSION DUCT GAS TEMP. (F)	1380.00
DUCT 1 GAS VELOCITY (FT/SEC)	80.36
DUCT 2 GAS VELOCITY (FT/SEC)	75.97
DUCT 3 GAS VELOCITY (FT/SEC)	70.43
DUCT 4 GAS VELOCITY (FT/SEC)	66.59
ER.DUCT GAS VEL.[1] (FT/SEC)	242.67
ER.DUCT GAS VEL.[2] (FT/SEC)	254.49

ASH

INPUT (LB/HR)	27.37
DUST LOADING (LB/HR)	16.00
CARBON CONVERSION (PCT)	100.000
CARBON HEAT LOSS (PCT)	.000

METHOD 1-----

FLUE GAS FLOW RATE (LB/HR)	3986.975	
COMPOSITION (MOLES/HR), (PERCENT)		
OXYGEN	5.376	3.97
CARBON DIOXIDE	18.685	13.79
WATER	13.038	9.62
SULFUR DIOXIDE	.070	.05
NITROGEN	98.343	72.57

METHOD 2-----

FLUE GAS FLOW RATE (LB/HR)	4176.063	
COMPOSITION (MOLES/HR), PERCENT		
OXYGEN	6.750	4.75
CARBON DIOXIDE	18.685	13.15
WATER	13.162	9.26
SULFUR DIOXIDE	.070	.05
NITROGEN	103.446	72.79

	KBTU/HR	PCT
HEAT OUT		
HEAT LOSS FROM REFRACTORY	237.064	4.97
HEAT LOSS FROM PANELS	367.245	7.71
HEAT LOSS FROM WATER COOLED FRAME	30.422	.64
HEAT LOSS FROM FLY ASH	9.207	.19
HEAT LOSS FROM UNBURNT CARBON	.000	.00
HEAT LOSS FROM ROOF	47.958	1.01
HEAT LOSS FROM S.H. TRANSITION	124.298	2.61
HEAT LOSS FROM S.H. FRAME	110.247	2.31
HEAT LOSS FROM S.H. DUCT	141.910	2.98
HEAT LOSS FROM OBS. PORT	53.628	1.13
HEAT LOSS FROM BURNER	176.284	3.70
HEAT LOSS FROM FURNACE BOTTOM LEFT	79.267	1.66
HEAT LOSS FROM FURNACE BOTTOM RIGHT	81.478	1.71
HEAT LOSS FROM FLUE GAS, [METHOD 1]	2809.732	58.96
HEAT LOSS FROM FLUE GAS, [METHOD 2]	2944.752	61.79

METHOD 1-----TOTAL MATERIAL INPUT (LB/HR)	4013.65
TOTAL MATERIAL OUTPUT (LB/HR)	4012.97
MATERIAL UNACCOUNTED FOR	.02
TOTAL HEAT INPUT (MBTU/HR)	4.77
TOTAL HEAT OUTPUT (MBTU/HR)	4.36
HEAT UNACCOUNTED FOR (PCT)	8.51

METHOD 2-----TOTAL MATERIAL INPUT (LB/HR)	4203.44
TOTAL MATERIAL OUTPUT (LB/HR)	4202.06
MATERIAL UNACCOUNTED FOR (PCT)	.03

TOTAL HEAT OUTPUT (MBTU/HR)	4.50
HEAT UNACCOUNTED FOR (PCT)	5.68

RESIDENCE TIME ALONG GAS STREAM

LOCATION	TEMP. (F)	TIME, SEC.
SUCTION PORT L1	2990.	.236
SUCTION PORT L2	2905.	.337
SUCTION PORT L3	2815.	.434
SUCTION PORT L4	2738.	.636
SUCTION PORT L5	2597.	1.023
S.H DUCT 1A	2384.	1.204
S.H DUCT 2C	2228.	1.237
S.H DUCT 3E	2032.	1.270
S.H DUCT 4G	1896.	1.328
DUST LOADING PORT	1380.	1.548

PSO 70/30 T1

COMBUSTION DATA

FUEL FEED RATE (LB/HR)	329.11
ADDITIVE FEED/RATE (LB/HR)	.00
FUEL HHV (BTU/LB)	11332.00
TOTAL HEAT INPUT (MBTU/HR)	4.50
PRIMARY AIR FLOW (LB/HR)	314.85
PRIMARY AIR TEMP. (F)	77.25
SECONDARY AIR FLOW (LB/HR)	3051.11
SECONDARY AIR TEMP. (F)	1051.66
TRANSPORT AIR FLOW (LB/HR)	.00
OXYGEN IN FLUE GAS (PCT)	4.39
PERCENT EXCESS AIR	21.19
LOWER FURNACE PEAK FLAME TEMP. (F)	2950.75
LOWER FURNACE RESIDENCE TIME (SEC)	1.14

WATERWALL TEST PANELS

PANEL P1 SURFACE TEMP. (F)	708.76
PANEL P2 SURFACE TEMP. (F)	706.02
PANEL P3 SURFACE TEMP. (F)	704.25
PANEL P4 SURFACE TEMP. (F)	702.09

SUPERHEATER PROBES

DUCT 1 GAS TEMPERATURE (F)	2329.00
DUCT 2 GAS TEMPERATURE (F)	2143.00
DUCT 3 GAS TEMPERATURE (F)	1966.00
DUCT 4 GAS TEMPERATURE (F)	1799.00
EROSION DUCT GAS TEMP. (F)	1385.00
DUCT 1 GAS VELOCITY (FT/SEC)	72.21
DUCT 2 GAS VELOCITY (FT/SEC)	67.40
DUCT 3 GAS VELOCITY (FT/SEC)	62.82
DUCT 4 GAS VELOCITY (FT/SEC)	58.49
ER.DUCT GAS VEL.[1] (FT/SEC)	222.94
ER.DUCT GAS VEL.[2] (FT/SEC)	234.49

ASH

INPUT (LB/HR)	26.66
DUST LOADING (LB/HR)	17.50
CARBON CONVERSION (PCT)	100.000
CARBON HEAT LOSS (PCT)	.000

METHOD 1-----

FLUE GAS FLOW RATE (LB/HR)	3669.063	
COMPOSITION (MOLES/HR), (PERCENT)		
OXYGEN	4.393	3.54
CARBON DIOXIDE	17.690	14.25
WATER	11.009	8.87
SULFUR DIOXIDE	.062	.05
NITROGEN	91.001	73.30

METHOD 2-----

FLUE GAS FLOW RATE (LB/HR)	3853.371	
COMPOSITION (MOLES/HR), PERCENT		
OXYGEN	5.733	4.39
CARBON DIOXIDE	17.690	13.55
WATER	11.130	8.52
SULFUR DIOXIDE	.062	.05
NITROGEN	95.974	73.49

	KBTU/HR	PCT
HEAT OUT		
HEAT LOSS FROM REFRACTORY	252.709	5.61
HEAT LOSS FROM PANELS	444.841	9.88
HEAT LOSS FROM WATER COOLED FRAME	193.298	4.29
HEAT LOSS FROM FLY ASH	9.851	.22
HEAT LOSS FROM UNBURNT CARBON	.000	.00
HEAT LOSS FROM ROOF	49.952	1.11
HEAT LOSS FROM S.H. TRANSITION	118.847	2.64
HEAT LOSS FROM S.H. FRAME	106.969	2.38
HEAT LOSS FROM S.H. DUCT	142.446	3.16
HEAT LOSS FROM OBS. PORT	64.650	1.44
HEAT LOSS FROM BURNER	160.580	3.57
HEAT LOSS FROM FURNACE BOTTOM LEFT	110.317	2.45
HEAT LOSS FROM FURNACE BOTTOM RIGHT	110.317	2.45
HEAT LOSS FROM FLUE GAS, [METHOD 1]	2502.535	55.58
HEAT LOSS FROM FLUE GAS, [METHOD 2]	2630.311	58.42

METHOD 1-----TOTAL MATERIAL INPUT (LB/HR)	3695.07
TOTAL MATERIAL OUTPUT (LB/HR)	3691.56
MATERIAL UNACCOUNTED FOR	.09
TOTAL HEAT INPUT (MBTU/HR)	4.50
TOTAL HEAT OUTPUT (MBTU/HR)	4.33
HEAT UNACCOUNTED FOR (PCT)	3.92

METHOD 2-----TOTAL MATERIAL INPUT (LB/HR)	3880.03
TOTAL MATERIAL OUTPUT (LB/HR)	3875.87
MATERIAL UNACCOUNTED FOR (PCT)	.11

TOTAL HEAT OUTPUT (MBTU/HR)	4.45
HEAT UNACCOUNTED FOR (PCT)	1.08

RESIDENCE TIME ALONG GAS STREAM

LOCATION	TEMP. (F)	TIME, SEC.
SUCTION PORT L1	2951.	.261
SUCTION PORT L2	2865.	.372
SUCTION PORT L3	2804.	.479
SUCTION PORT L4	2703.	.701
SUCTION PORT L5	2524.	1.131
S.H DUCT 1A	2329.	1.333
S.H DUCT 2C	2143.	1.369
S.H DUCT 3E	1966.	1.406
S.H DUCT 4G	1799.	1.471
DUST LOADING PORT	1385.	1.717

PSO 70/30 T2

COMBUSTION DATA

FUEL FEED RATE (LB/HR)	294.92
ADDITIVE FEED/RATE (LB/HR)	.00
FUEL HHV (BTU/LB)	11208.00
TOTAL HEAT INPUT (MBTU/HR)	3.92
PRIMARY AIR FLOW (LB/HR)	315.41
PRIMARY AIR TEMP. (F)	78.64
SECONDARY AIR FLOW (LB/HR)	2658.12
SECONDARY AIR TEMP. (F)	961.93
TRANSPORT AIR FLOW (LB/HR)	.00
OXYGEN IN FLUE GAS (PCT)	4.05
PERCENT EXCESS AIR	19.47
LOWER FURNACE PEAK FLAME TEMP. (F)	2838.05
LOWER FURNACE RESIDENCE TIME (SEC)	1.33

WATERWALL TEST PANELS

PANEL P1 SURFACE TEMP. (F)	707.95
PANEL P2 SURFACE TEMP. (F)	708.84
PANEL P3 SURFACE TEMP. (F)	704.40
PANEL P4 SURFACE TEMP. (F)	700.43

SUPERHEATER PROBES

DUCT 1 GAS TEMPERATURE (F)	2256.00
DUCT 2 GAS TEMPERATURE (F)	2172.00
DUCT 3 GAS TEMPERATURE (F)	2012.00
DUCT 4 GAS TEMPERATURE (F)	1827.00
EROSION DUCT GAS TEMP. (F)	1343.00
DUCT 1 GAS VELOCITY (FT/SEC)	62.17
DUCT 2 GAS VELOCITY (FT/SEC)	60.25
DUCT 3 GAS VELOCITY (FT/SEC)	56.59
DUCT 4 GAS VELOCITY (FT/SEC)	52.35
ER.DUCT GAS VEL.[1] (FT/SEC)	192.61
ER.DUCT GAS VEL.[2] (FT/SEC)	201.18

ASH

INPUT (LB/HR)	23.89
DUST LOADING (LB/HR)	15.50
CARBON CONVERSION (PCT)	100.000
CARBON HEAT LOSS (PCT)	.000

METHOD 1-----		
FLUE GAS FLOW RATE (LB/HR)	3245.142	
COMPOSITION (MOLES/HR), (PERCENT)		
OXYGEN	3.626	3.30
CARBON DIOXIDE	15.852	14.44
WATER	9.837	8.96
SULFUR DIOXIDE	.055	.05
NITROGEN	80.393	73.24

METHOD 2-----		
FLUE GAS FLOW RATE (LB/HR)	3385.097	
COMPOSITION (MOLES/HR), PERCENT		
OXYGEN	4.643	4.05
CARBON DIOXIDE	15.852	13.83
WATER	9.929	8.66
SULFUR DIOXIDE	.055	.05
NITROGEN	84.170	73.42

	KBTU/HR	PCT
HEAT OUT		
HEAT LOSS FROM REFRACTORY	240.101	6.13
HEAT LOSS FROM PANELS	394.227	10.07
HEAT LOSS FROM WATER COOLED FRAME	170.976	4.37
HEAT LOSS FROM FLY ASH	8.437	.22
HEAT LOSS FROM UNBURNT CARBON	.000	.00
HEAT LOSS FROM ROOF	41.124	1.05
HEAT LOSS FROM S.H. TRANSITION	102.016	2.61
HEAT LOSS FROM S.H. FRAME	94.172	2.40
HEAT LOSS FROM S.H. DUCT	116.096	2.96
HEAT LOSS FROM OBS. PORT	56.977	1.46
HEAT LOSS FROM BURNER	134.962	3.45
HEAT LOSS FROM FURNACE BOTTOM LEFT	93.143	2.38
HEAT LOSS FROM FURNACE BOTTOM RIGHT	91.825	2.34
HEAT LOSS FROM FLUE GAS, [METHOD 1]	2128.753	54.36
HEAT LOSS FROM FLUE GAS, [METHOD 2]	2221.709	56.74

METHOD 1-----TOTAL MATERIAL INPUT (LB/HR)	3268.46
TOTAL MATERIAL OUTPUT (LB/HR)	3268.14
MATERIAL UNACCOUNTED FOR	.01
TOTAL HEAT INPUT (MBTU/HR)	3.92
TOTAL HEAT OUTPUT (MBTU/HR)	3.73
HEAT UNACCOUNTED FOR (PCT)	4.67

METHOD 2-----TOTAL MATERIAL INPUT (LB/HR)	3408.99
TOTAL MATERIAL OUTPUT (LB/HR)	3408.10
MATERIAL UNACCOUNTED FOR (PCT)	.03

TOTAL HEAT OUTPUT (MBTU/HR)	3.83
HEAT UNACCOUNTED FOR (PCT)	2.30

RESIDENCE TIME ALONG GAS STREAM

LOCATION	TEMP. (F)	TIME, SEC.
SUCTION PORT L1	2838.	.305
SUCTION PORT L2	2746.	.435
SUCTION PORT L3	2685.	.560
SUCTION PORT L4	2630.	.819
SUCTION PORT L5	2454.	1.318
S.H DUCT 1A	2256.	1.552
S.H DUCT 2C	2172.	1.595
S.H DUCT 3E	2012.	1.635
S.H DUCT 4G	1827.	1.709
DUST LOADING PORT	1343.	1.989

PSO 70/30 T3 [first 9.5 hours of t3]

COMBUSTION DATA

FUEL FEED RATE (LB/HR)	267.23
ADDITIVE FEED/RATE (LB/HR)	.00
FUEL HHV (BTU/LB)	11208.00
TOTAL HEAT INPUT (MBTU/HR)	3.41
PRIMARY AIR FLOW (LB/HR)	319.20
PRIMARY AIR TEMP. (F)	76.51
SECONDARY AIR FLOW (LB/HR)	2404.85
SECONDARY AIR TEMP. (F)	734.25
TRANSPORT AIR FLOW (LB/HR)	.00
OXYGEN IN FLUE GAS (PCT)	4.65
PERCENT EXCESS AIR	21.01
LOWER FURNACE PEAK FLAME TEMP. (F)	2752.00
LOWER FURNACE RESIDENCE TIME (SEC)	1.51

WATERWALL TEST PANELS

PANEL P1 SURFACE TEMP. (F)	708.14
PANEL P2 SURFACE TEMP. (F)	698.00
PANEL P3 SURFACE TEMP. (F)	703.58
PANEL P4 SURFACE TEMP. (F)	702.51

SUPERHEATER PROBES

DUCT 1 GAS TEMPERATURE (F)	2114.00
DUCT 2 GAS TEMPERATURE (F)	2034.00
DUCT 3 GAS TEMPERATURE (F)	1897.00
DUCT 4 GAS TEMPERATURE (F)	1729.00
EROSION DUCT GAS TEMP. (F)	1256.00
DUCT 1 GAS VELOCITY (FT/SEC)	53.93
DUCT 2 GAS VELOCITY (FT/SEC)	52.25
DUCT 3 GAS VELOCITY (FT/SEC)	49.38
DUCT 4 GAS VELOCITY (FT/SEC)	45.86
ER.DUCT GAS VEL.[1] (FT/SEC)	167.79
ER.DUCT GAS VEL.[2] (FT/SEC)	179.63

ASH

INPUT (LB/HR)	21.65
DUST LOADING (LB/HR)	14.00
CARBON CONVERSION (PCT)	100.000
CARBON HEAT LOSS (PCT)	.000

METHOD 1-----

FLUE GAS FLOW RATE (LB/HR)	2969.325	
COMPOSITION (MOLES/HR), (PERCENT)		
OXYGEN	3.502	3.49
CARBON DIOXIDE	14.363	14.30
WATER	8.933	8.89
SULFUR DIOXIDE	.050	.05
NITROGEN	73.617	73.28

METHOD 2-----

FLUE GAS FLOW RATE (LB/HR)	3172.621	
COMPOSITION (MOLES/HR), PERCENT		
OXYGEN	4.999	4.65
CARBON DIOXIDE	14.363	13.35
WATER	9.066	8.43
SULFUR DIOXIDE	.050	.05
NITROGEN	79.081	73.52

	KBTU/HR	PCT
HEAT OUT		
HEAT LOSS FROM REFRACTORY	227.865	6.69
HEAT LOSS FROM PANELS	339.150	9.96
HEAT LOSS FROM WATER COOLED FRAME	146.809	4.31
HEAT LOSS FROM FLY ASH	7.131	.21
HEAT LOSS FROM UNBURNT CARBON	.000	.00
HEAT LOSS FROM ROOF	35.323	1.04
HEAT LOSS FROM S.H. TRANSITION	96.104	2.82
HEAT LOSS FROM S.H. FRAME	98.584	2.89
HEAT LOSS FROM S.H. DUCT	103.170	3.03
HEAT LOSS FROM OBS. PORT	51.261	1.50
HEAT LOSS FROM BURNER	96.223	2.82
HEAT LOSS FROM FURNACE BOTTOM LEFT	85.658	2.51
HEAT LOSS FROM FURNACE BOTTOM RIGHT	83.343	2.45
HEAT LOSS FROM FLUE GAS, [METHOD 1]	1802.474	52.92
HEAT LOSS FROM FLUE GAS, [METHOD 2]	1926.571	56.56

METHOD 1-----TOTAL MATERIAL INPUT (LB/HR)	2991.27
TOTAL MATERIAL OUTPUT (LB/HR)	2989.83
MATERIAL UNACCOUNTED FOR	.05
TOTAL HEAT INPUT (MBTU/HR)	3.41
TOTAL HEAT OUTPUT (MBTU/HR)	3.23
HEAT UNACCOUNTED FOR (PCT)	5.21

METHOD 2-----TOTAL MATERIAL INPUT (LB/HR)	3194.27
TOTAL MATERIAL OUTPUT (LB/HR)	3193.12
MATERIAL UNACCOUNTED FOR (PCT)	.04

TOTAL HEAT OUTPUT (MBTU/HR)	3.35
HEAT UNACCOUNTED FOR (PCT)	1.56

RESIDENCE TIME ALONG GAS STREAM

LOCATION	TEMP. (F)	TIME, SEC.
SUCTION PORT L1	2752.	.342
SUCTION PORT L2	2611.	.490
SUCTION PORT L3	2577.	.632
SUCTION PORT L4	2479.	.927
SUCTION PORT L5	2317.	1.499
S.H DUCT 1A	2114.	1.768
S.H DUCT 2C	2034.	1.816
S.H DUCT 3E	1897.	1.862
S.H DUCT 4G	1729.	1.944
DUST LOADING PORT	1256.	2.257

pso 70/30 t4

COMBUSTION DATA

FUEL FEED RATE (LB/HR)	285.93
ADDITIVE FEED/RATE (LB/HR)	.00
FUEL HHV (BTU/LB)	11332.00
TOTAL HEAT INPUT (MBTU/HR)	3.63
PRIMARY AIR FLOW (LB/HR)	320.53
PRIMARY AIR TEMP. (F)	76.77
SECONDARY AIR FLOW (LB/HR)	2413.63
SECONDARY AIR TEMP. (F)	699.62
TRANSPORT AIR FLOW (LB/HR)	.00
OXYGEN IN FLUE GAS (PCT)	3.30
PERCENT EXCESS AIR	13.31
LOWER FURNACE PEAK FLAME TEMP. (F)	2797.00
LOWER FURNACE RESIDENCE TIME (SEC)	1.46

WATERWALL TEST PANELS

PANEL P1 SURFACE TEMP. (F)	708.35
PANEL P2 SURFACE TEMP. (F)	701.36
PANEL P3 SURFACE TEMP. (F)	705.52
PANEL P4 SURFACE TEMP. (F)	702.00

SUPERHEATER PROBES

DUCT 1 GAS TEMPERATURE (F)	2178.00
DUCT 2 GAS TEMPERATURE (F)	2082.00
DUCT 3 GAS TEMPERATURE (F)	1908.00
DUCT 4 GAS TEMPERATURE (F)	1717.00
EROSION DUCT GAS TEMP. (F)	1271.00
DUCT 1 GAS VELOCITY (FT/SEC)	55.69
DUCT 2 GAS VELOCITY (FT/SEC)	53.66
DUCT 3 GAS VELOCITY (FT/SEC)	49.99
DUCT 4 GAS VELOCITY (FT/SEC)	45.96
ER.DUCT GAS VEL.[1] (FT/SEC)	170.53
ER.DUCT GAS VEL.[2] (FT/SEC)	179.25

ASH

INPUT (LB/HR)	23.16
DUST LOADING (LB/HR)	15.00
CARBON CONVERSION (PCT)	100.000
CARBON HEAT LOSS (PCT)	.000

METHOD 1-----

FLUE GAS FLOW RATE (LB/HR)	2997.460	
COMPOSITION (MOLES/HR), (PERCENT)		
OXYGEN	2.434	2.40
CARBON DIOXIDE	15.369	15.18
WATER	9.439	9.33
SULFUR DIOXIDE	.054	.05
NITROGEN	73.928	73.03

METHOD 2-----

FLUE GAS FLOW RATE (LB/HR)	3145.635	
COMPOSITION (MOLES/HR), PERCENT		
OXYGEN	3.511	3.30
CARBON DIOXIDE	15.369	14.44
WATER	9.537	8.96
SULFUR DIOXIDE	.054	.05
NITROGEN	77.927	73.24

	KBTU/HR	PCT
HEAT OUT		
HEAT LOSS FROM REFRACTORY	237.686	6.55
HEAT LOSS FROM PANELS	375.047	10.33
HEAT LOSS FROM WATER COOLED FRAME	160.560	4.42
HEAT LOSS FROM FLY ASH	7.880	.22
HEAT LOSS FROM UNBURNT CARBON	.000	.00
HEAT LOSS FROM ROOF	37.372	1.03
HEAT LOSS FROM S.H. TRANSITION	108.040	2.98
HEAT LOSS FROM S.H. FRAME	9.684	.27
HEAT LOSS FROM S.H. DUCT	112.702	3.10
HEAT LOSS FROM OBS. PORT	55.688	1.53
HEAT LOSS FROM BURNER	99.191	2.73
HEAT LOSS FROM FURNACE BOTTOM LEFT	82.458	2.27
HEAT LOSS FROM FURNACE BOTTOM RIGHT	79.069	2.18
HEAT LOSS FROM FLUE GAS, [METHOD 1]	1885.129	51.92
HEAT LOSS FROM FLUE GAS, [METHOD 2]	1979.131	54.51

METHOD 1-----TOTAL MATERIAL INPUT (LB/HR)	3020.09
TOTAL MATERIAL OUTPUT (LB/HR)	3019.96
MATERIAL UNACCOUNTED FOR	.00
TOTAL HEAT INPUT (MBTU/HR)	3.63
TOTAL HEAT OUTPUT (MBTU/HR)	3.31
HEAT UNACCOUNTED FOR (PCT)	8.88

METHOD 2-----TOTAL MATERIAL INPUT (LB/HR)	3168.80
TOTAL MATERIAL OUTPUT (LB/HR)	3168.13
MATERIAL UNACCOUNTED FOR (PCT)	.02

TOTAL HEAT OUTPUT (MBTU/HR)	3.40
HEAT UNACCOUNTED FOR (PCT)	6.29

RESIDENCE TIME ALONG GAS STREAM

LOCATION	TEMP. (F)	TIME, SEC.
SUCTION PORT L1	2797.	.335
SUCTION PORT L2	2675.	.479
SUCTION PORT L3	2637.	.617
SUCTION PORT L4	2563.	.903
SUCTION PORT L5	2387.	1.456
S.H DUCT 1A	2178.	1.717
S.H DUCT 2C	2082.	1.764
S.H DUCT 3E	1908.	1.810
S.H DUCT 4G	1717.	1.892
DUST LOADING PORT	1271.	2.209

PSO 70/30 CLEANED T1

COMBUSTION DATA

FUEL FEED RATE (LB/HR)	286.99
ADDITIVE FEED/RATE (LB/HR)	.00
FUEL HHV (BTU/LB)	11484.00
TOTAL HEAT INPUT (MBTU/HR)	4.02
PRIMARY AIR FLOW (LB/HR)	305.97
PRIMARY AIR TEMP. (F)	82.62
SECONDARY AIR FLOW (LB/HR)	2683.71
SECONDARY AIR TEMP. (F)	1120.91
TRANSPORT AIR FLOW (LB/HR)	.00
OXYGEN IN FLUE GAS (PCT)	4.84
PERCENT EXCESS AIR	20.89
LOWER FURNACE PEAK FLAME TEMP. (F)	2821.00
LOWER FURNACE RESIDENCE TIME (SEC)	1.34

WATERWALL TEST PANELS

PANEL P1 SURFACE TEMP. (F)	707.75
PANEL P2 SURFACE TEMP. (F)	682.24
PANEL P3 SURFACE TEMP. (F)	701.14
PANEL P4 SURFACE TEMP. (F)	702.35

SUPERHEATER PROBES

DUCT 1 GAS TEMPERATURE (F)	2089.68
DUCT 2 GAS TEMPERATURE (F)	2022.23
DUCT 3 GAS TEMPERATURE (F)	1886.47
DUCT 4 GAS TEMPERATURE (F)	1673.83
EROSION DUCT GAS TEMP. (F)	1267.00
DUCT 1 GAS VELOCITY (FT/SEC)	58.69
DUCT 2 GAS VELOCITY (FT/SEC)	57.13
DUCT 3 GAS VELOCITY (FT/SEC)	54.01
DUCT 4 GAS VELOCITY (FT/SEC)	49.11
ER.DUCT GAS VEL.[1] (FT/SEC)	185.50
ER.DUCT GAS VEL.[2] (FT/SEC)	201.25

ASH

INPUT (LB/HR)	18.94
DUST LOADING (LB/HR)	12.40
CARBON CONVERSION (PCT)	100.000
CARBON HEAT LOSS (PCT)	.000

METHOD 1-----

FLUE GAS FLOW RATE (LB/HR)	3258.309	
COMPOSITION (MOLES/HR), (PERCENT)		
OXYGEN	3.844	3.48
CARBON DIOXIDE	15.665	14.19
WATER	9.987	9.05
SULFUR DIOXIDE	.054	.05
NITROGEN	80.815	73.23

METHOD 2-----

FLUE GAS FLOW RATE (LB/HR)	3526.693	
COMPOSITION (MOLES/HR), PERCENT		
OXYGEN	5.795	4.84
CARBON DIOXIDE	15.665	13.08
WATER	10.163	8.49
SULFUR DIOXIDE	.054	.04
NITROGEN	88.058	73.54

	KBTU/HR	PCT
HEAT OUT		
HEAT LOSS FROM REFRACTORY	235.767	5.86
HEAT LOSS FROM PANELS	368.689	9.17
HEAT LOSS FROM WATER COOLED FRAME	47.019	1.17
HEAT LOSS FROM FLY ASH	6.222	.15
HEAT LOSS FROM UNBURNT CARBON	.000	.00
HEAT LOSS FROM ROOF	43.668	1.09
HEAT LOSS FROM S.H. TRANSITION	107.989	2.69
HEAT LOSS FROM S.H. FRAME	92.642	2.30
HEAT LOSS FROM S.H. DUCT	162.044	4.03
HEAT LOSS FROM OBS. PORT	57.856	1.44
HEAT LOSS FROM BURNER	173.454	4.31
HEAT LOSS FROM FURNACE BOTTOM LEFT	125.194	3.11
HEAT LOSS FROM FURNACE BOTTOM RIGHT	125.194	3.11
HEAT LOSS FROM FLUE GAS, [METHOD 1]	1947.879	48.45
HEAT LOSS FROM FLUE GAS, [METHOD 2]	2108.771	52.45

METHOD 1-----TOTAL MATERIAL INPUT (LB/HR)	3276.67
TOTAL MATERIAL OUTPUT (LB/HR)	3276.71
MATERIAL UNACCOUNTED FOR	.00
TOTAL HEAT INPUT (MBTU/HR)	4.02
TOTAL HEAT OUTPUT (MBTU/HR)	3.53
HEAT UNACCOUNTED FOR (PCT)	12.30

METHOD 2-----TOTAL MATERIAL INPUT (LB/HR)	3545.64
TOTAL MATERIAL OUTPUT (LB/HR)	3545.09
MATERIAL UNACCOUNTED FOR (PCT)	.02

TOTAL HEAT OUTPUT (MBTU/HR)	3.69
HEAT UNACCOUNTED FOR (PCT)	8.30

RESIDENCE TIME ALONG GAS STREAM

LOCATION	TEMP. (F)	TIME, SEC.
SUCTION PORT L1	2821.	.305
SUCTION PORT L2	2724.	.435
SUCTION PORT L3	2640.	.561
SUCTION PORT L4	2569.	.823
SUCTION PORT L5	2335.	1.334
S.H DUCT 1A	2090.	1.580
S.H DUCT 2C	2022.	1.623
S.H DUCT 3E	1886.	1.664
S.H DUCT 4G	1674.	1.739
DUST LOADING PORT	1267.	2.023

pso 70/30 cln t2

COMBUSTION DATA

FUEL FEED RATE (LB/HR)	318.74
ADDITIVE FEED/RATE (LB/HR)	.00
FUEL HHV (BTU/LB)	11484.00
TOTAL HEAT INPUT (MBTU/HR)	4.54
PRIMARY AIR FLOW (LB/HR)	321.96
PRIMARY AIR TEMP. (F)	81.48
SECONDARY AIR FLOW (LB/HR)	3004.20
SECONDARY AIR TEMP. (F)	1210.54
TRANSPORT AIR FLOW (LB/HR)	.00
OXYGEN IN FLUE GAS (PCT)	4.99
PERCENT EXCESS AIR	21.10
LOWER FURNACE PEAK FLAME TEMP. (F)	2911.00
LOWER FURNACE RESIDENCE TIME (SEC)	1.17

WATERWALL TEST PANELS

PANEL P1 SURFACE TEMP. (F)	707.30
PANEL P2 SURFACE TEMP. (F)	696.32
PANEL P3 SURFACE TEMP. (F)	700.41
PANEL P4 SURFACE TEMP. (F)	702.40

SUPERHEATER PROBES

DUCT 1 GAS TEMPERATURE (F)	2360.00
DUCT 2 GAS TEMPERATURE (F)	2151.00
DUCT 3 GAS TEMPERATURE (F)	2097.00
DUCT 4 GAS TEMPERATURE (F)	1902.00
EROSION DUCT GAS TEMP. (F)	1363.00
DUCT 1 GAS VELOCITY (FT/SEC)	72.21
DUCT 2 GAS VELOCITY (FT/SEC)	66.85
DUCT 3 GAS VELOCITY (FT/SEC)	65.47
DUCT 4 GAS VELOCITY (FT/SEC)	60.48
ER.DUCT GAS VEL.[1] (FT/SEC)	217.83
ER.DUCT GAS VEL.[2] (FT/SEC)	238.17

ASH

INPUT (LB/HR)	21.04
DUST LOADING (LB/HR)	13.90
CARBON CONVERSION (PCT)	100.000
CARBON HEAT LOSS (PCT)	.000

METHOD 1-----		
FLUE GAS FLOW RATE (LB/HR)	3624.513	
COMPOSITION (MOLES/HR), (PERCENT)		
OXYGEN	4.312	3.51
CARBON DIOXIDE	17.398	14.17
WATER	11.095	9.04
SULFUR DIOXIDE	.060	.05
NITROGEN	89.911	73.23

METHOD 2-----		
FLUE GAS FLOW RATE (LB/HR)	3952.916	
COMPOSITION (MOLES/HR), PERCENT		
OXYGEN	6.699	4.99
CARBON DIOXIDE	17.398	12.96
WATER	11.311	8.43
SULFUR DIOXIDE	.060	.04
NITROGEN	98.773	73.58

	KBTU/HR	PCT
HEAT OUT		
HEAT LOSS FROM REFRACTORY	253.474	5.58
HEAT LOSS FROM PANELS	425.307	9.36
HEAT LOSS FROM WATER COOLED FRAME	50.920	1.12
HEAT LOSS FROM FLY ASH	7.918	.17
HEAT LOSS FROM UNBURNT CARBON	.000	.00
HEAT LOSS FROM ROOF	49.763	1.10
HEAT LOSS FROM S.H. TRANSITION	123.402	2.72
HEAT LOSS FROM S.H. FRAME	107.965	2.38
HEAT LOSS FROM S.H. DUCT	141.998	3.13
HEAT LOSS FROM OBS. PORT	58.547	1.29
HEAT LOSS FROM BURNER	208.409	4.59
HEAT LOSS FROM FURNACE BOTTOM LEFT	129.921	2.86
HEAT LOSS FROM FURNACE BOTTOM RIGHT	113.681	2.50
HEAT LOSS FROM FLUE GAS, [METHOD 1]	2510.977	55.28
HEAT LOSS FROM FLUE GAS, [METHOD 2]	2742.392	60.37

METHOD 1-----	TOTAL MATERIAL INPUT (LB/HR)	3644.91
	TOTAL MATERIAL OUTPUT (LB/HR)	3644.71
	MATERIAL UNACCOUNTED FOR	.01
	TOTAL HEAT INPUT (MBTU/HR)	4.54
	TOTAL HEAT OUTPUT (MBTU/HR)	4.24
	HEAT UNACCOUNTED FOR (PCT)	6.59

METHOD 2-----	TOTAL MATERIAL INPUT (LB/HR)	3973.96
	TOTAL MATERIAL OUTPUT (LB/HR)	3973.12
	MATERIAL UNACCOUNTED FOR (PCT)	.02

TOTAL HEAT OUTPUT (MBTU/HR)	4.47
HEAT UNACCOUNTED FOR (PCT)	1.49

RESIDENCE TIME ALONG GAS STREAM

LOCATION	TEMP. (F)	TIME, SEC.
SUCTION PORT L1	2911.	.267
SUCTION PORT L2	2801.	.381
SUCTION PORT L3	2722.	.491
SUCTION PORT L4	2665.	.720
SUCTION PORT L5	2496.	1.160
S.H DUCT 1A	2360.	1.364
S.H DUCT 2C	2151.	1.399
S.H DUCT 3E	2097.	1.434
S.H DUCT 4G	1902.	1.494
DUST LOADING PORT	1363.	1.729

PSO 70/30 CLN T3

COMBUSTION DATA

FUEL FEED RATE (LB/HR)	355.13
ADDITIVE FEED/RATE (LB/HR)	.00
FUEL HHV (BTU/LB)	11676.00
TOTAL HEAT INPUT (MBTU/HR)	5.06
PRIMARY AIR FLOW (LB/HR)	316.04
PRIMARY AIR TEMP. (F)	67.34
SECONDARY AIR FLOW (LB/HR)	3345.94
SECONDARY AIR TEMP. (F)	1121.04
TRANSPORT AIR FLOW (LB/HR)	.00
OXYGEN IN FLUE GAS (PCT)	5.30
PERCENT EXCESS AIR	19.66
LOWER FURNACE PEAK FLAME TEMP. (F)	2984.00
LOWER FURNACE RESIDENCE TIME (SEC)	1.03

WATERWALL TEST PANELS

PANEL P1 SURFACE TEMP. (F)	706.77
PANEL P2 SURFACE TEMP. (F)	702.12
PANEL P3 SURFACE TEMP. (F)	701.42
PANEL P4 SURFACE TEMP. (F)	703.41

SUPERHEATER PROBES

DUCT 1 GAS TEMPERATURE (F)	2437.00
DUCT 2 GAS TEMPERATURE (F)	2285.00
DUCT 3 GAS TEMPERATURE (F)	2160.00
DUCT 4 GAS TEMPERATURE (F)	1990.00
EROSION DUCT GAS TEMP. (F)	1372.00
DUCT 1 GAS VELOCITY (FT/SEC)	81.72
DUCT 2 GAS VELOCITY (FT/SEC)	77.43
DUCT 3 GAS VELOCITY (FT/SEC)	73.91
DUCT 4 GAS VELOCITY (FT/SEC)	69.11
ER.DUCT GAS VEL.[1] (FT/SEC)	241.16
ER.DUCT GAS VEL.[2] (FT/SEC)	272.00

ASH

INPUT (LB/HR)	23.44
DUST LOADING (LB/HR)	14.50
CARBON CONVERSION (PCT)	100.000
CARBON HEAT LOSS (PCT)	.000

METHOD 1-----		
FLUE GAS FLOW RATE (LB/HR)	3994.375	
COMPOSITION (MOLES/HR), (PERCENT)		
OXYGEN	4.485	3.32
CARBON DIOXIDE	19.384	14.33
WATER	12.333	9.12
SULFUR DIOXIDE	.067	.05
NITROGEN	98.990	73.19

METHOD 2-----		
FLUE GAS FLOW RATE (LB/HR)	4489.777	
COMPOSITION (MOLES/HR), PERCENT		
OXYGEN	8.085	5.30
CARBON DIOXIDE	19.384	12.71
WATER	12.658	8.30
SULFUR DIOXIDE	.067	.04
NITROGEN	112.358	73.65

	KBTU/HR	PCT
HEAT OUT		
HEAT LOSS FROM REFRACTORY	270.693	5.35
HEAT LOSS FROM PANELS	482.554	9.53
HEAT LOSS FROM WATER COOLED FRAME	60.994	1.20
HEAT LOSS FROM FLY ASH	8.590	.17
HEAT LOSS FROM UNBURNT CARBON	.000	.00
HEAT LOSS FROM ROOF	63.190	1.25
HEAT LOSS FROM S.H. TRANSITION	136.903	2.70
HEAT LOSS FROM S.H. FRAME	126.825	2.50
HEAT LOSS FROM S.H. DUCT	188.761	3.73
HEAT LOSS FROM OBS. PORT	99.064	1.96
HEAT LOSS FROM BURNER	249.730	4.93
HEAT LOSS FROM FURNACE BOTTOM LEFT	127.687	2.52
HEAT LOSS FROM FURNACE BOTTOM RIGHT	127.687	2.52
HEAT LOSS FROM FLUE GAS, [METHOD 1]	2888.330	57.05
HEAT LOSS FROM FLUE GAS, [METHOD 2]	3254.434	64.28

METHOD 1-----	TOTAL MATERIAL INPUT (LB/HR)	4017.11
	TOTAL MATERIAL OUTPUT (LB/HR)	4016.38
	MATERIAL UNACCOUNTED FOR	.02
	TOTAL HEAT INPUT (MBTU/HR)	5.06
	TOTAL HEAT OUTPUT (MBTU/HR)	4.88
	HEAT UNACCOUNTED FOR (PCT)	3.65

METHOD 2-----	TOTAL MATERIAL INPUT (LB/HR)	4513.22
	TOTAL MATERIAL OUTPUT (LB/HR)	4511.78
	MATERIAL UNACCOUNTED FOR (PCT)	.03

TOTAL HEAT OUTPUT (MBTU/HR)	5.24
HEAT UNACCOUNTED FOR (PCT)	-3.58

RESIDENCE TIME ALONG GAS STREAM

LOCATION	TEMP. (F)	TIME, SEC.
SUCTION PORT L1	2984.	.237
SUCTION PORT L2	2910.	.338
SUCTION PORT L3	2798.	.435
SUCTION PORT L4	2765.	.637
SUCTION PORT L5	2587.	1.024
S.H DUCT 1A	2437.	1.205
S.H DUCT 2C	2285.	1.235
S.H DUCT 3E	2160.	1.264
S.H DUCT 4G	1990.	1.315
DUST LOADING PORT	1372.	1.517